NASA TECHNICAL TRANSLATION

NASA TT F-822

NASA TT F-822

STOCHASTIC STRUCTURE OF CLOUD AND RADIATION FIELDS

Yu. R. Mullamaa, M. A. Sulev, V. K. Poldmaa,
H. A. Ohvril, H. J. Niylisk, M. I. Allenov,
L. G. Tchubakov, and A. F. Kuusk

Academy of Sciences of the Estonian SSR
Tartu, 1972

NATIONAL AERONAUTICS AND SPACE ADMINISTRATION • WASHINGTON, D. C. • OCTOBER 1975

1. Report No. NASA TT F-822	2. Government Accession No.
4. Title and Subtitle: Stochastic Structure of Cloud and Radiation Fields	5. Report Date: October 1975
	6. Performing Organization Code
7. Author(s): Yu. R. Mullamaa, M. A. Sulev, V. K. Poldmaa, H. A. Ohvril, H. J. Niylisk, M. I. Allenov, L. G. Tchubakov, A. F. Kuusk	8. Performing Organization Report No.
	10. Work Unit No.
9. Performing Organization Name and Address: National Aeronautics and Space Administration Washington, D.C. 20546	11. Contract or Grant No. NASw-2485
	13. Type of Report and Period Covered: Translation
12. Sponsoring Agency Name and Address: Techtran Corporation P.O. Box 729, Glen Burnie, Md. 21061	14. Sponsoring Agency Code

15. Supplementary Notes

Translation of: "Stokhasticheskaya Struktura Poley Oblachnosti i Radiatsii", Tartu, Academy of Sciences of the Estonian SSR, 1972, pp 1 - 283

16. Abstract

The results are presented of theoretical and experimental studies of the stochastic structure of cloud fields and radiation of the Earth's atmosphere. A description is given of the array of equipment developed by the authors and used to conduct ground and aircraft experimental studies. A survey is made of the measurement methods and the methods of the theory of random processes employed in theoretical analysis. A detailed description is given of the results of the experimental studies and a comparison is made with the theoretical model established.

17. Key Words (Selected by Author(s))	18. Distribution Statement: Unclassified-Unlimited Subject Category 46

19. Security Classif. (of this report)	20. Security Classif. (of this page)	21. No. of Pages	22. Price *
Unclassified	Unclassified	192	$7.00

For sale by the National Technical Information Service, Springfield, Virginia 22161

NASA-HQ

STOCHASTIC STRUCTURE OF CLOUD AND RADIATION FIELDS

Yu. R. Mullamaa, M. A. Sulev, V. K. Poldmaa,
H. A. Ohvril, H. J. Niylisk, M. I. Allenov,
L. G. Tchubakov, A. F. Kuusk[1]

Foreword

Cloudiness is one of the most important factors determining the nature of /5* most processes taking place in the Earth's atmosphere. Cloudiness regulates the radiation balance. The role of cloudiness as a basic element in weather formation feedback is obvious. The instability of the cloud cover, and especially of the cumulus population, which is the most variable, leaves its imprint on the course of these processes. In shielding us from the Sun, cloudiness regulates the arrival of solar radiation. Detection takes place because many natural processes (such as heating of the atmosphere and of the Earth's surface, the melting of snow, photosynthesis, and so forth) are nonlinear relative to radiation. For this reason these processes depend not only on the mean amount of incoming radiation but also on the variation of the latter in space and time, which is largely determined by the structure of cloud fields.

At the same time, we are not thoroughly familiar with the laws governing the transfer of energy (including the conversion of solar radiation) in mesoscale processes under unstable cloudiness conditions, i.e., sufficient study has not yet been made of the physical formation of weather in a real, non-hypothetical atmosphere.

It is now universally acknowledged that from the viewpoint of practical application it is necessary to consider the radiative and optical characteristics not of the individual clouds but of cloudiness in general as a stochastic formation. Even in the relatively recent past there was no way of approaching solution of problems of this nature. It seemed to be impossible even to establish a rigidly scientific formulation of such problems. In particular, in utilizing the transfer theory to study the radiation regime of the real atmosphere investigators were forced to restrict themselves either to clear weather conditions of to uniform continuous stratified clouds. This was due to the circumstance that effective methods of applying the transfer theory to stochastic structures such /6 as a broken cloud cover were virtually non-existent. Obstacles were represented by the mathematical difficulties, which even now have not been fully overcome, in solving the transfer equation for a medium with statistically disturbed optical parameters varying over a very wide range, as well as the lack of methods for experimental determination of the microphysical cloudiness parameters entering into this theory and the variability of these parameters in a given concrete situation.

---

*Numbers in margin indicate pagination from foreign text.

[1]Academy of Sciences of the Estonian SSR, Institute of Physics and Astronomy

Hence emphasis is now being placed on study of the statistical parameters and radiation fields and their interrelations. This field also includes study of the stochastic structure of cloud and radiation fields which has been conducted in recent years at the Department of Atmospheric Physics of the Institute of Physics and Astronomy, Academy of Sciences of the Estonian SSR. The present book is devoted to a systematic presentation of this research.

G. V. Rozenberg promoted this research; he was the initiator of the basic ideas underlying the investigations and took active part in drawing up the program for them.

In 1966 a joint project was instituted among groups of specialists in the radiation energetics of the atmosphere from the Institute of Atmospheric Physics of the Academy of Sciences of the USSR, the Ukrainian Hydrometeorological Scientific Research Institute, and the Institute of Physics and Astronomy of the Academy of Sciences of the Estonian SSR. The project was organized and directed by Prof. G. V. Rozenberg and Ye. M. Feygel'son, Doctor of Physical and Mathematical Sciences. The success of the project was assured by the assistance of Yu. K. Ross, Doctor of Physical and Mathematical Sciences, in formulation of the problem and in organization of the joint studies.

Within the framework of the joint research, which continued until 1970, study was made chiefly of radiative heat transfer. At the same time, research was instituted at the Institute of Atmospheric Physics of the Academy of Sciences of the USSR and the Institute of Atmospheric Physics of the Academy of Sciences of the Estonian SSR on the statitical structure of radiation fields in the atmosphere when clouds are present. The results of these joint studies were published in a collection entitled "Heat Transfer in the Atmosphere." In recent years study of the stochastic structure of radiation and cloud fields has been continued and expanded at both Institutes. /7

For the sake of completeness of presentation, along with previously unpublished results the present study also includes the results of work done within the framework of joint research. Only to a certain extent, however, have comparisons been made with the results of studies by other investigators.

The present study is the result of the joint work of a team consisting of M. I. Allenov, A. E. Kuusk, H. I. Niylisk, Associate in Physical and Mathematical Sciences, H. A. Ohvril, V. K. Põldmaa, Associate in Physical and Mathematical Sciences, M. A. Sulev, Associate in Physical and Mathematical Sciences, L. G. Chubakov, and Yu. R. Mullamaa, Associate in Physical and Mathematical Sciences, who supervised the project group and generalized the data obtained. The present paper was written by Yu. R. Mullamaa, with the exception of Section 4 of Chapter II and Section 4 of Chapter V, which were written by M. I. Allenov, and Section I of Chapter V, written by H. J. Niylisk. The following took part in writing individual sections of the book: V. K. Põldmaa, Section 3 of Chapter I; H. A. Ohvril, Section 4 of Chapter I; M. A. Sulev, Sections 1-3, 5 and 6 of Chapter II; M. I. Allenov, Section 4 of Chapter II; V. K. Põldmaa and M. A. Sulev, Sections 2 and 3 of Chapter 3; H. A. Ohvril, Sections 4-6 of Chapter 3; V. K. Põldmaa, Section 7 of Chapter 3; H. A. Ohvril, Section 1 and 2 of Chapter IV; V. K. Põldmaa and M. A. Sulev, Sections 3-5 of Chapter IV; A. E. Kuusk,

Section 6 of Chapter IV; H. J. Niylisk, Sections 1 and 2 of Chapter V; H. A. Ohvril, Section 3 of Chapter V; and M. I. Allenov and L. G. Chubakov, Section 4 of Chapter V.

The present work consists of five chapters. In the first chapter a general formulation of the problem is given and the possibilities afforded by application of the theory of random processes are considered. The statistical characteristics of random processes utilized to describe and analyze the structure of cloud and radiation fields are presented, possible errors in experimental measurement of such fields are estimated, and information is given on the methods used in conversion of statistical characteristics. A description is given of the cloud model we have constructed, which is employed in theoretical analysis of the results obtained. /8

The array of equipment used in the experimental studies is described in the second chapter. The results of investigation of the stochastic structure of the cloud cover are presented in Chapter III.

The stochastic structures of shortwave and longwave radiation fields and their relationship to the cloud cover structure are considered in Chapters 4 and 5.

A first attempt at systematic presentation of study of the stochastic structure of cloud and radiation fields of the earth's atmosphere must inevitably be imcomplete. At the present time more or less complete experimental data have been obtained only on cumulus clouds. Nor has full use been made of the potential of theoretical analysis of the available experimental data. A convenient form has nevertheless been found for modeling cloud fields on the basis of which theoretical analysis has been performed making it possible to establish the relationship between cloud structure and radiation field structure. The measurements actually performed have confirmed the theoretical assumptions made. The parameters employed in the theory have been determined by way of experiment. A considerable number of important empirical relations have also been established. A more or less complete concept has consequently been fashioned, one which may be used to advantage in consideration of a number of problems of atmospheric physics.

The authors would like to express their great indebtedness to Prof. G. V. Rozenberg for his encouragement toward the conduct of this research, his guidance in the matter of the underlying concept, and his constant support as the work progressed. Thanks are due E. M. Feigelson, Doctor of Physical and Mathematical Sciences for organization and scientific guidance in the process of the joint research, to N. I. Goisa, Associate in Geographic Sciences, for his kind collaboration, to A. I. Furman, Director of the Meteorological Experimental Station of the Ukrainian Hydrometeorological Scientific Research Institute, for his assistance in carrying out joint aircraft research and to R. G. Timanovskaya for her participation in the research.

The authors are grateful to the head of the Department of Atmospheric Physics, J. K. Ross, Doctor of Physical and Mathematical Sciences, for his extensive

support and assistance both in formulation of the problem and in resolving organizational problems, and to all the personnel of the Institute who participated in the studies and in compilation of the present work. /9

CHAPTER I. STATISTICAL DESCRIPTION OF CLOUD AND RADIATION FIELDS /13

Section 1. Introduction

The cloud cover is basically a stochastic formation. Hence in the study of the properties of clouds as a complete formation they must be described statistically. In addition, owing to the influence of the cloud cover on the radiation field, the latter is also stochastic when clouds are present and it must be described by statistical methods. As a result, formulation of the problem itself is of a nature such that it is necessary to seek a relationship between the structural characteristics of radiation fields on the one hand and the cloud cover on the other. All attempts to utilize deterministic methods, including the transfer equation, for this purpose have proved to be ineffective, At the same time, no statistical theory of transfer exists. At the present time only the first steps have been taken toward generalization of the transfer theory to media with statistically distributed paramters. This circumstance is to be ascribed to the mathematical difficulties inherent in solution of the transfer equation for such a medium.

An obstacle of no less importance, and indeed the main one from the viewpoint of the physics of the problem, is the disparity between the transfer theory and actual experimental capabilities. There are virtually no methods of experimental determination of the entire complex of microphysical cloudiness factors entering into this theory, and especially the variability of such factors in the constantly changing concrete situations in the real atmosphere.

In view of the foregoing, there is no sense in proceeding on the basis of the /14
radiative theory, taking all its fine points into account. Theoretical synthesis should not in our opinion strive for excessive precision. It should be approximative in nature. At the same time, due attention must be devoted to adjustment of the structure of the theory to experimental capabilities, since only actual measurements can confirm theoretical expectations and determine the parameters involved in the theory.

Thus formulation of the problem itself depends largely on the scale of the phenomenon in question, and the structure of the theory in turn depends on the formulation of the problem. In addition to the physical nature of the problem, an approach such as this is at the present time dictated by mathematical considerations, since statistical analysis in the general form, without numerical analysis in the form of tables and graphs, simply cannot be accomplished without a convenient and flexible mathematical apparatus.

We are faced with the problem of mesoscale study of cloud and radiation fields and their relationships. The special interest in mesoscale processes is due to the fact that precisely on such scales and over the typical time intervals corresponding to them is the influence of radiation exerted on natural processes and does cloudiness appear in the role of feedback regulator in the formation of weather.

It must be noted that the radiation regime of an individual uniform stratified cloud has now been thoroughly studied within the framework of the deterministic transfer theory. However, under actual conditions the scales of such cloud sections which are horizontally uniform is small, i.e., the radiation regime of plane-parallel cloud formation is insignificant in the array of phenomena under consideration.

In the radiation characteristics of cloudiness as a complete formation the minute details of the structure and radiation properties of individual cloud elements are smoothed out and thus exert only a slight effect, both from the viewpoint of energetics and as regards influence on the atmosphere.

Hence in undertaking to study the optics of the cloud cover as a complete /15
formation it is logical to exclude superfluous details from the analysis and to characterize the cloud cover by a small number of generalized microparameters. In the process the minuteness of detail of the parameters, as was noted earlier, is determined by the physical nature of the problems under consideration and the natural restrictions determining the reproducibility of a concrete measurement. It goes without saying that the introduction of generalizing microparameters entails the need for study of their relationship to the definitive aggregate of microoptical parameters, with allowance made for the variability of the latter.

The minimum scale to which macrocharacteristics are applicable is determined primarily by the possibility of establishing sufficiently stable mean values for the macrooptical parameters, i.e., it is dictated by the physics of cloud formation, but insofar as radiation processes are concerned the minimum scale must considerably exceed the length of the mean free path of a photon in a cloud. In addition, in determination of the minimum cloud structure scale the basis adopted should be the scales of modulation of the radiation field determined by this structure. On the basis of our experimental studies (for further details see Chapter III) in the shortwave region of the spectrum, approximately 100 m should be adopted as the minimum scale. The optical properties of the cloud cover are known to depend largely on the wavelength of radiation. The minimum scale is reduced in the region of thermal radiation, where the length of the mean free path of a photon is substantially shorter.

We give no consideration to the comparatively well known large-scale processes, which determine the climate of our planet and on the theory of which synoptic weather forecasting methods rest.

The maximum scales of the statistical structure of cloud and radiation fields with which we are concerned are determined by the extent of the cloud formations. If the scales were to be larger, we would enter the domain of large-scale nephanalysis. As our experiments demonstrate (for further details see Chapters III and IV), the maximum scales for various types of cloud formations range from 50 to 500 km.

Thus the scale of the processes is determined by the dynamics of the atmos- /16
sphere and should always be verified by experiment. This is one of the key areas in which a theory is untenable without experimentation.

As we know from the theory of random processes, actual processes are never rigorously stationary, if for no other reason than that they are restricted in time or space. This is fully applicable to radiation and cloud fields, which generally speaking are non-homogeneous and especially are non-isotropic. However, the results of experimental research indicate that it is almost always possible to select temporal or spatial scales of adequate extent within the limits of mesoscale processes, in which the processes investigated may be regarded in approximation as being stationary (homogeneous). From the mathematical viewpoint homogeneous fields, and especially isotropic ones, are unquestionably the simplest and for this reason it is advisable to conduct model study to ascertain the typical features of radiation and cloud fields by means of approximation to these fields.

In processing the results of experimental studies we employ two criteria for scale selection: (1) the possibility of formation of mean values and (2) the asymptotic force of the structural function. We accordingly select the spatial or temporal averaging scales which yield minimum dispersion for the statistical characteristics. The statistical characteristics of the radiation and cloud fields determined from the experimental studies involve an error which depends not only on instrument accuracy and the physical nature of the quantities studied, but on the nature of the variability of the latter as well.

Inasmuch as statistical description is involved, and, as we saw earlier, the accuracy is limited, only one-dimensional and two-dimensional probability distribution functions and first-order and second-order factors can be arrived at with acceptable accuracy. From the mathematical viewpoint this means that accurate algorithms are obtained for linear conversions of statistical characteristics, but only approximate ones for nonlinear conversions. At the same time, in the latter case the accuracy is determined to a considerable extent both /17
by the nature of the nonlinear conversion and by the properties of the random process being converted.

Inasmuch as analysis of two interrelated stochastic fields (clouds and radiation) characterized by a large number of parameters is involved, it is necessary to investigate:

(1) the relationship between the statistics of the various parameters of each of these fields separately;

(2) conversion of these relationships on change in the observer's position relative to the cloud cover; and

(3) the relationship between the statistical characteristics of the fields.

The problem is greatly simplified by the circumstance that there is a linear relationship between many of the radiation and cloud parameters. The chief complications occur in study of the relationships between the statistics of radiations fields and the optical macroparameters of the cloud cover. This occasions mathematical difficulties, as well as considerable errors, which are inherent in even the simplest non-linear conversions. Only the first steps have been taken in this field of research and the results obtained are highly tentative in nature.

Let us proceed now to presentation of the algorithms of statistical characteristics employed in description of the cloud and radiation field structures.

Section 2. Basic Characteristics in The Theory of Random Processes

The following statistical characteristics of the theory of random functions have been used to describe the structure of cloud and radiation fields and their relationships:

$\xi(t), \eta(t)$ --mathematical expectation of random processes (mean),

$r\xi$ --autocorrelation function,

$r\xi\eta$ --cross-correlation function,

$D\xi(t)$ --structural function,

$S\xi(w)$ --spectral density, /18

$S\xi\eta(w)$ --reciprocal spectral density,

$S(Xi)$, Xi --eigenvalues and eigenfunctions of correlation matrix K,

P, p --one-dimensional and two-dimensional probabilities and distribution functions.

In processing of the results of experimental research in a Minsk-22 computer the statistical characteristics of the random process were determined by the discrete values of the latter forming a random sequence.

Algorithms for estimation of the characteristics of random sequences are given below.

a. Mathematical expectation (mean) is expressed by:

$$\overline{\xi(t)} = \frac{\sum_{i=1}^{N} \xi(t_i)}{N}, \tag{1.1}$$

where $\xi(ti)$ is the value of the random process at the ith readout, and N the number of consecutive readouts according to which the mean is taken.

b. Dispersion is found from the formula given in reference [1]:

$$\sigma^2 = \frac{1}{N} \sum_{i=1}^{N} [\xi(t_i) - \overline{\xi(t)}]^2. \tag{1.2}$$

c. The normalized cross-correlation and autocorrelation functions $r\xi$ and $r\xi\eta$ along the section of variation of the argument from 0 to $M\Delta t$ are obtained from the formulas given in reference [1]:

$$r_\xi(k\Delta t)=\frac{1}{\sigma_\xi^2(N-k)}\sum_{i=1}^{N-k}[\xi(t_i)-\overline{\xi(t)}][\xi(t_{i+k})-\overline{\xi(t)}], \tag{1.3}$$

$$r_{\xi\eta}(k\Delta t)=\frac{1}{\sigma_\xi\sigma_\eta(N-k)}\sum_{i=1}^{N-k}[\xi(t_i)-\overline{\xi(t)}][\eta(t_{i+k})-\overline{\eta(t)}], \tag{1.4}$$

where k = 0, 1, ... M and Δt is the interval between adjacent readouts.

d. The structural function is calculated from the formula given in reference /19 [2]:

$$D_\xi(k\Delta t)=\frac{1}{N-k}\sum_{i=1}^{N}\{[\xi(t_{i+k})-\xi(t_i)]-$$

$$-\frac{1}{N-k}\sum_{i=1}^{N-k}[\xi(t_{i+k})-\xi(t_i)]\}^2. \tag{1.5}$$

e. Before the spectral densities are calculated the correlation functions are filtered by the Bartlett method [1,3,4]:

$$r^*(k\Delta t)=\left(1-\frac{k}{M}\right)r(k\Delta t), \tag{1.6}$$

where k = 1, ... M.

The spectral densities and reciprocal densities based on the corresponding autocorrelation and cross-correlation functions are calculated from the formulas given in [1,5]:

$$S_\xi(m\Delta\omega)=\frac{\Delta t}{2\pi}[r_\xi(0)+2\sum_{q=1}^{M-1}r^*(q\Delta t)\cos mq\Delta t\Delta\omega+$$

$$+r^*(M\Delta t)\cos mM\Delta t\Delta\omega \tag{1.7}$$

and in

$$S_{\xi\eta}(m\Delta\omega)=A(m\Delta\omega)+jB(m\Delta\omega), \tag{1.8}$$

where

$$A(m\Delta\omega)=\frac{\Delta t}{2\pi}\left\{\frac{1}{2}[r^*_{\xi\eta}(0)+r^*_{\eta\xi}(0)]+\right.$$

$$+\sum_{q=1}^{M-1}[r^*_{\xi\eta}(q\Delta t)+r^*_{\eta\xi}(q\Delta t)\cos mq\Delta t\Delta\omega+ \tag{1.9}$$

$$\left.+\frac{1}{2}[r^*_{\xi\eta}(M\Delta t)+r^*_{\eta\xi}(M\Delta t)]\cos mM\Delta t\Delta\omega\right\}$$

and

$$B(m\Delta\omega)=\frac{\Delta t}{2\pi}\sum_{q=1}^{M-1}[r^*_{\eta\xi}(q\Delta t)-r^*_{\xi\eta}(q\Delta t)]\sin mq\Delta t\Delta\omega \tag{1.10}$$

are respectively the real and imaginary parts of the spectral density, and $\omega=m\Delta\omega$ is the circular frequency of the spectral density. In the present study

use is made of linear frequency f=ω/2π along with the circular frequency. The spectral densities for linear and circular frequencies are related by the equation /20

$$S(f)=S[\omega(f)]\frac{d\omega}{df}=2\pi S[\omega(f)]. \tag{1.11}$$

The following auxiliary functions are employed to provide for interpretation of the results of reciprocal spectral analysis:

(1) coherence

$$C(\omega)=\frac{A^2(\omega)+B^2(\omega)}{S_\xi(\omega)S_\eta(\omega)}, \tag{1.12}$$

the value of which can be found over the range $0\leq C(\omega)\leq 1$, and its behavior is analogous to the behavior of the square of the ordinary correlation coefficient.

(2) phase characteristic

$$t(\omega)=\frac{1}{\omega}\operatorname{arctg}[B(\omega)/A(\omega)], \tag{1.13}$$

which makes it possible to trace the phase shift between two processes as a function of frequency.

f. In order to determine the parameters of the statistical structure of sky brightness and cloud coverage of the direction of sighting as a function of the zenith angle of observation ϑ expansion has been made into a Fourier series on the base line system of orthogonal and normalized functions Xi(ϑ), which yield the optimum approximation of measurement of random function, $\xi(\vartheta)$ (see [6,7]). In this instance eigenvalues S(Xi) represent dispersion of the corresponding orthonormalized base line functions Xi(ϑ).

The eigenfunctions and eigenvalues are obtained by solving integral equation

$$S(X_i)X_i(\vartheta_m)=\int_0^{\pi/2}K(\vartheta_m,\vartheta_q)X_i(\vartheta_q)\,d\vartheta_q, \tag{1.14}$$

where K(ϑm,ϑq) are the elements of correlation matrix K, i.e., the correlation coefficients of the random function investigated in sighting directions ϑm and ϑq. Expansion based on the orthonormalized eigenfunctions assures minimum dispersion of the residual term in comparison with other possible orthonormalized functions. /21

The relative accuracy of expansion

$$\lambda_{im}=\frac{S(X_1)+S(X_2)+\ldots+S(X_i)}{S(X_1)+S(X_2)+\ldots+S(X_i)+\ldots+S(X_m)} \tag{1.15}$$

expresses the portion of total dispersion of the first i components in the total dispersion of all m components. Research completed up to the present time has shown that in the approximation of meteorological and radiation fields adequate accuracy is achieved by means of the first few eigenfunctions. This remarkable characteristic also explains their wide application in the solution of a great variety of problems [8-16].

g. One-dimensional and two-dimensional functions of probability distribution $P(\xi_1)$ and $P(\xi_1,\xi_2)$ characterize the probability of events $\xi(t)\leq\xi_1$ and $\xi(t)\leq\xi_1$, $\xi(t+\Delta t)\leq\xi_2$, i.e.,

$$P(\xi_1)=P[\xi(t)\leqslant\xi_1], \tag{1.16}$$

$$P(\xi_1,\xi_2,\Delta t)=P[\xi(t)\leqslant\xi_1;\ \xi(t+\Delta t)\leqslant\xi_2], \tag{1.17}$$

where Δt is the shift of readout moments $\xi(t)$. One-dimensional and two-dimensional probability distribution functions are obtained by differentiating distribution functions (1.16) and (1.17) respectively:

$$p(\xi_1)=\frac{dP(\xi_1)}{d\xi_1}=\frac{P[\xi_1\leqslant\xi(t)\leqslant\xi_1+\Delta\xi]}{\Delta\xi}, \tag{1.18}$$

$$p(\xi_1,\xi_2,\Delta t)=\frac{\partial P(\xi_1,\xi_2,\Delta t)}{\partial\xi_1\partial\xi_2}=$$
$$=\frac{P[\xi_1\leqslant\xi(t)\leqslant\xi_1+\Delta\xi;\ \xi_2\leqslant\xi(t+\Delta t)\leqslant\xi_2+\Delta\xi]}{(\Delta\xi)^2}, \tag{1.19}$$

where $\Delta\xi$ is the quantization level interval.

In analysis of the statistical structure the cumulus cloud cover is also characterized by the frequency of clouds or clear gaps, i.e., the average number of clouds or clear gaps $\varkappa$ per unit time in the case of ground measurements /22 or per unit length in the case of aircraft measurements:

$$\varkappa=\lim_{M\to\infty}\frac{K_M}{M}, \tag{1.20}$$

where K_m is the total number of clouds (or clear gaps) per measurement of duration M.

Section 3. Estimation of Dependability of Experimental Determination of Cloud and Radiation Characteristics in a Real Atmosphere

Cloud and Radiation fields are considered to be locally homogeneous and in certain instances also isotropic random fields (random processes). In this case determination of the empirical statistical characteristics is based on utilization of the well-known property of ergodicity.

Questions of statistical treatment of the results of measurement of cloud and radiation characteristics, with allowance made for the statistical reliability provided by measurements over a limited interval of time, will be considered in what follows.

As will be demonstrated later, errors in determination of the statistical characteristics of cloud and radiation fields depend on the duration of recording (measurement), the methods of processing the experimental data in a computer, and the distortions occasioned by the array of measuring instruments.

The maximum scale (duration of recording) is determined by the extent of cloud formations of different shapes; in our experimental studies it was approximately 50-500 km in aircraft measurements or 1-4 hours in ground measurements. The results of the experimental measurements were processed by computer on the basis of the algorithms given in the second section of this chapter. In this instance the quantization interval for ground measurement was Δt = 12 sec, and for aircraft measurements, depending on the nature of variation in the quantity studied, Δt = 0.5, 1, 2 sec. A spatial quantization interval $\Delta x \approx$ 35, 70, 140 m corresponds to the latter.

For the purpose of quantitative estimation of errors in the statistical characteristics obtained the dispersion and root mean square deviation and the variation coefficients of the latter were determined, and for mathematical expectation also the confidence intervals, effectiveness index, effective number of measurements, and optimum quantization interval [17]. /23

As is known [18,19], mean dispersion $\sigma^2_{\bar{\xi}}$ is determined by the expression

$$\sigma^2_{\bar{\xi}} = \frac{\sigma^2}{N^2}\left[N + 2\sum_{k=1}^{N-1}(N-k)\,r(k\Delta t)\right], \qquad (1.21)$$

where N is the number of consecutive readouts in calculation of mathematical expectation (See formula (1.1)). The normalized autocorrelation function in calculations based on formula (1.21) is approximated by a function of the form $r(k\Delta t) = e^{\alpha k \Delta t}$.

The dispersion range of root mean square deviations $\sigma\xi$ for mean radiation fluxes and the presence of clouds at the zenith is plotted in Figure 1 against averaging scale t or x for ground and aircraft measurements.

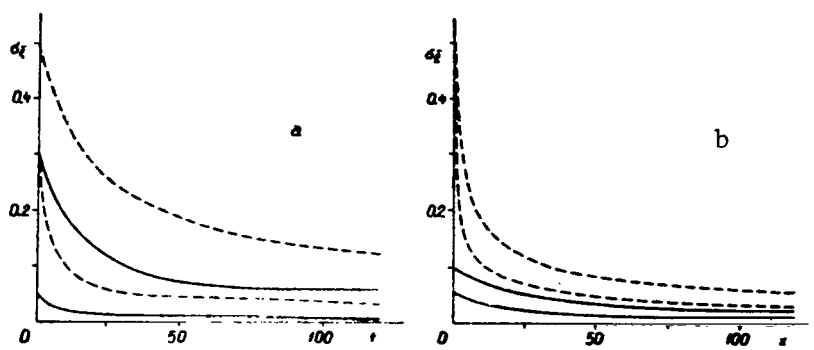

Figure 1. Root Mean Square Deviations of Mean Total Radiation Flux (--) and Mean Cloud Coverage of Zenith (-- -- --) Versus a, Time Averaging Scale (t min), b, Spatial Averaging Scale (x, km).

In the first approximation, if the distribution of deviations of mathematical expectation estimation from the true normal expectation is considered, the confidence intervals with probability P of mathematical expectation falling within /24

a given interval $[-\Delta\xi(P),+\Delta\xi(P)]$ are calculated by the formula

$$\Delta\overline{\xi}(P) = \sigma_{\overline{\xi}} \arg \operatorname{erf} P, \tag{1.22}$$

where arg erf is the value of the probability integral argument at which the probability equals P. A confidence interval of probability P = 0.68 corresponds to interval $\Delta_{\overline{\xi}}(0.68)=\sigma_{\overline{\xi}}$, and for probability 0.90, 0.95, and 0.99 arg erf P assumes the values respectively of 1.643, 1.960, and 2.576.

The mathematical expectation estimation is the more accurate, the smaller is its dispersion relative to the mean. We employ the coefficient of variation (relative root mean square error).

$$V_{\overline{\xi}} = \frac{\sigma_{\overline{\xi}}}{\overline{\xi}}. \tag{1.23}$$

as the measure of dispersion. The dispersion range of the coefficient of variation is plotted against the averaging scale in Figure 2.

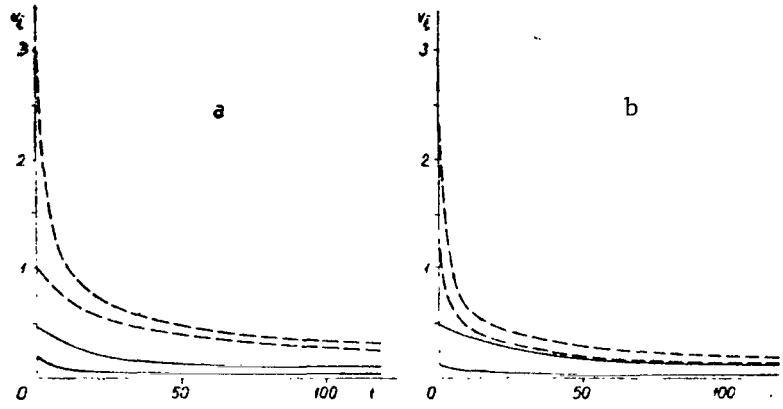

Figure 2. Coefficients of Variation of Total Radiation (--) and Cloud Coverage of Zenith (-- -- --) Versus a, Time Averaging Scale (p, min), Spatial Averaging Scale (x, km).

As may be seen from formula (1.23), the coefficient of variation depends on the level of fluctuation relative to the mean as well as on the averaging. Hence for the purpose of quantitative estimation of the influence of averaging on the accuracy of results use has been made of the effectiveness index /25

$$K_e = \frac{\sigma_{\overline{\xi}}}{\sigma^2_{\xi}}$$

which indicates the share represented by mean dispersion in the dispersion of a non-averaged random function. The reciprocal, $N_e=1/K_e$, is the effective number of measurements indicating how many individual independent measurements must be performed in order to achieve the same accuracy as when the mean arithmetic method of

treatment based on formula (1.1) is employed. The range of variation of effectiveness index K_e with a scale of effective number of measurements N_e is shown in Figure 3 plotted against the averaging scale.

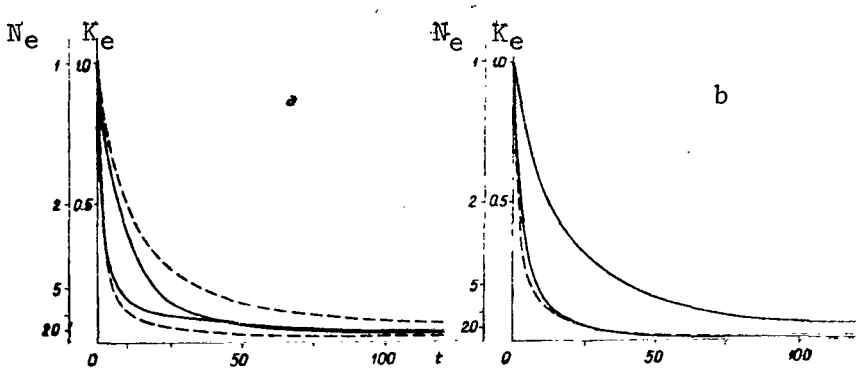

Figure 3. Effectiveness Index K_e With Scale of Effective Number of Measurements N_e of Mean Total Radiation Flux (--) and Mean Cloud Coverage of Zenith (-- -- --) Versus a, Time Averaging Scale (t, min) b, Spatial Averaging Scale, (x km).

As we know [18], with small averaging scales the effectiveness of mean estimation depends on interval Δ between discrete readings. Hence in conducting mass measurements it is advisable also to determine the optimum interval Δ_{opt} further decrease in which leads to no appreciable increase in mean accuracy. The optimum interval is determined in approximation from the equation [18] /26

$$\frac{4}{3}r\left(\frac{\Delta_{opt}}{2}\right)-\frac{5}{6}r(\Delta_{opt})=\frac{1}{2}.$$

In measurements of the mean total radiation flux the optimum interval between readings ranges from 0.5 to 20 min or 0.4-7 km, and in measurement of the mean values of intensity for cloud coverage of the direction of sighting from 1 to 3 min or from 0.5 to 1 km for ground and aircraft measurements respectively.

As is demonstrated by Figures 1-3, in measurements of radiation fluxes and intensities and with clouds present at the zenith, averaging over a range of no less than 40 minutes in ground measurements or no less than 80 km in aircraft measurements is required in order to achieve substantial increase in the accuracy of their mean value. The same accuracy can be achieved by 5-10 independent vertical atmosphere probes (see Figure 3), in which case independence is defined as absence of correlation of the characteristics investigated for individual probes

Spatial and temporal averaging or averaging by independent measurements makes it possible to reduce the mean dispersion by an order of magnitude (the root mean square deviation of the mean is reduced by a factor of 3-4) in comparison to the instantaneous values (1.3). Considerable enlargement of the averaging scale

is required for further substantial increase in the mean accuracy. This is virtually impossible on the basis of a single measurement, since cloud fields of an extent sufficient for these purposes are very rarely encountered under natural conditions. This indicates a need for revising the approach toward experimental measurements of the characteristics of clouds and radiation in the atmosphere, and also to revise the goals set in advance of the experiment. For example, the representative intensity and flux data employed in theoretical operations within the framework of the deterministic transfer theory can be obtained by way of experiment only in the form of mean values. In the majority of cases an accuracy which in effect can be achieved by averaging over a large number of measurements (fields) is required for adjustment of the transfer theory to experiments. As a result, the minute details of radiation fields ascertained from the transfer theory cannot be confirmed quantitatively by full-scale measurement. /27

Determination of the accuracy of estimation of dispersion (1.2) requires knowledge of the correlation function of the square of the random process [18], which function is fully defined by correlation function (1.3) only in the case of a normal (Gaussian) random process. In view of the foregoing, dispersion $\sigma^2_{\sigma^2}$ of estimated dispersion σ^2

$$\sigma^2_{\sigma^2}=\frac{2\sigma^4}{N}\left[1+2\sum_{k=1}^{N-1}\left(1-\frac{1}{N}\right)r^2(k\Delta t)\right], \tag{1.24}$$

its relative error (variation coefficient)

$$V_{\sigma^2}=\frac{\sigma_{\sigma^2}}{\sigma^2} \tag{1.25}$$

and the dispersion of the correlation function

$$\sigma^2_{r(k\Delta t)}=\frac{\sigma^2_{R(k\Delta t)}[1-r^2(k\Delta t)]^2}{2\sigma^4} \tag{1.26}$$

in which

$$\sigma^2_{R(k\Delta t)}=\frac{\sigma^4}{(N-k)^2}\sum_{i=-(N-k)}^{N-k}(N-k-|i|)\{r^2(i\Delta t)+$$
$$+r[(i+k)\Delta t]r[(i-k)\Delta t]\} \tag{1.27}$$

is the dispersion of the non-normalized correlation function, have been calculated on the basis of the assumption that the stationary random processes investigated are normal.

The range of variation of dispersions σ^2, their dispersions $\sigma^2_{\sigma^2}$, and the range of variation coefficient V_{σ^2} for the total radiation flux and coverage of the zenith with clouds or intensity for ground and aircraft measurements are presented in Tables 1 and 2. Figure 4 shows typical correlation functions $r(k\Delta t)$, their root mean square deviations σ_r, and variation coefficients $V_r=\sigma_r(k\Delta t)/r(k\Delta t)$. /28

As was to be expected, the dispersion and the correlation function as second factors are determined with much less accuracy than the mathematical expectation. In individual cases the dispersion error exceeds 100 percent, this clearly indicating that the measurement length is inadequate. With the normalized correlation functions determined at $r(k\Delta t)<0.1$, the error is more than 100 percent. /29

TABLE 1. VARIABILITY OF DISPERSION IN GROUND MEASUREMENTS.

	M (min)	σ^2	$\sigma^2_{\sigma^2}$	σ_{σ^2}	V_{σ^2}
Q^*	60	$3.14\ 10^{-3}$	$2.46\ 10^{-7}$	$4.96\ 10^{-4}$	0.16
	120	$3.07\ 10^{-3}$	$1.16\ 10^{-7}$	$3.41\ 10^{-4}$	0.11
	180	$3.05\ 10^{-3}$	$7.69\ 10^{-8}$	$2.77\ 10^{-4}$	0.09
	60	0.098	$8.45\ 10^{-3}$	$9.19\ 10^{-2}$	0.94
	120	0.093	$3.84\ 10^{-3}$	$6.20\ 10^{-2}$	0.67
	180	0.091	$2.45\ 10^{-3}$	$4.95\ 10^{-2}$	0.54
$n(0)$	60	0.092	$1.87\ 10^{-4}$	$1.37\ 10^{-2}$	0.15
	120	0.091	$9.06\ 10^{-5}$	$9.50\ 10^{-3}$	0.10
	180	0.090	$6.05\ 10^{-5}$	$7.80\ 10^{-3}$	0.09
	60	0.285	$1.05\ 10^{-2}$	$1.05\ 10^{-1}$	0.37
	120	0.267	$4.65\ 10^{-3}$	$6.82\ 10^{-2}$	0.26
	180	0.262	$3.02\ 10^{-3}$	$5.50\ 10^{-2}$	0.21

TABLE 2. VARIABILITY OF DISPERSION IN AIRCRAFT MEASUREMENTS.

	M (km)	σ^2	$\sigma^2_{\sigma^2}$	σ_{σ^2}	V_{σ^2}
Q	50	$7.87.\ 10^{-3}$	$6.26\ 10^{-3}$	$7.91\ 10^{-2}$	0.21
	100	$7.70\ 10^{-3}$	$3.04\ 10^{-3}$	$5.51\ 10^{-2}$	0.15
	150	$7.65\ 10^{-3}$	$1.99\ 10^{-3}$	$4.46\ 10^{-2}$	0.12
	200	$7.61\ 10^{-3}$	$1.49\ 10^{-3}$	$3.86\ 10^{-2}$	0.11
	50	$7.48\ 10^{-3}$	$1.99\ 10^{-3}$	$4.46\ 10^{-2}$	0.12
	100	$6.92\ 10^{-3}$	$8.74\ 10^{-4}$	$2.78\ 10^{-2}$	0.09
	150	$6.75\ 10^{-3}$	$5.54\ 10^{-4}$	$2.35\ 10^{-2}$	0.07
	200	$6.65\ 10^{-3}$	$4.06\ 10^{-4}$	$2.01\ 10^{-2}$	0.06
$n(0)$	50	0.247	$1.86\ 10^{-3}$	$4.30\ 10^{-2}$	0.174
	100	0.244	$9.10\ 10^{-4}$	$3.02\ 10^{-2}$	0.124
	150	0.242	$6.03\ 10^{-4}$	$2.46\ 10^{-2}$	0.102
	200	0.242	$4.50\ 10^{-4}$	$2.12\ 10^{-2}$	0.088
	50	0.142	$3.24\ 10^{-4}$	$1.80\ 10^{-2}$	0.127
	100	0.141	$1.60\ 10^{-4}$	$1.26\ 10^{-2}$	0.089
	150	0.141	$1.06\ 10^{-4}$	$1.03\ 10^{-2}$	0.073
	200	0.140	$7.90\ 10^{-5}$	$8.89\ 10^{-3}$	0.063

Structural functions, as well as sliding mean mathematical expectations and dispersions, were utilized to estimate the stationary nature of the random processes investigated. For stationary random processes $D\xi(\infty)=2\sigma^2$ the correlation function as well may be expressed by means of structural function /30

(1.28)

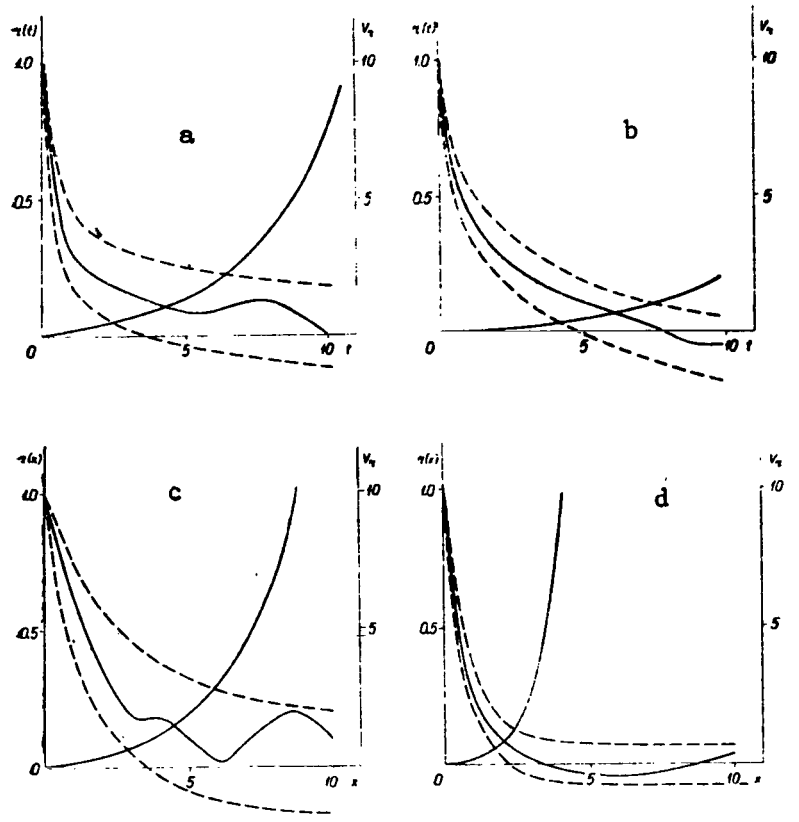

Figure 4. Correlation Functions r With Root Mean Square Deviations σ_r and Variation Coefficients V_r for Total Radiation Flux (a,c) and Cloud Coverage of Zenith (b,d); a,b, Ground Measurements; c,d, Aircraft Measurements.

Utilization of the structural function is always more dependable, inasmuch as the value of $D\xi(k\Delta t)$ is not affected by error in determination of mean value $\overline{\xi t}$, which was not taken into account in formulas (1.24-1.27) in estimation of the accuracy of dispersion and correlation functions. A constant structural function with large values of argument $k\Delta t$ is an indicator of a stationary state.

In order to increase the effectiveness of estimation of the spectral density, /31 the correlation function is filtered by the Bartlett method (see (1.6)) before the Fourier transformation is performed.

The accuracy of evaluation of spectral density is affected by the discrete nature of the random function, as well as by the duration of measurement. Since the time of measurement is finite, the spectral density is discrete. At the same time, the spectral density values are generally too low. Since fixation of the random process is discrete, the values obtained in estimation of spectral density

are too high as a result of redistribution of the spectral density of the higher frequencies over the estimated spectral densities of the lower frequencies.

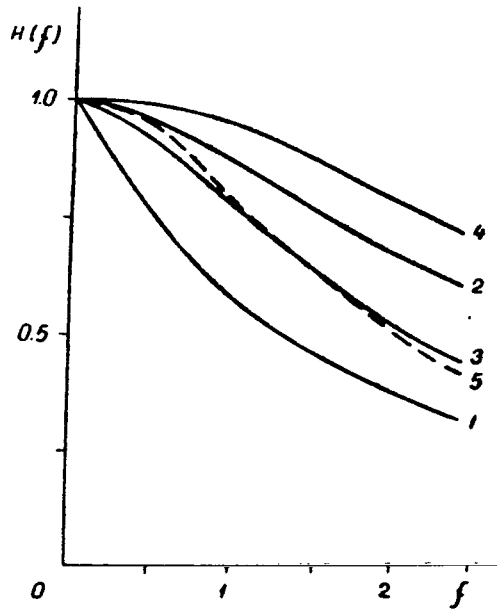

Figure 5. Spectral Characteristics H(f) of Filters: 1, According to Formula (1.29) (Δ=12 sec); 2, for Thermoelectric Actinometer in Set with KBT Electronic Potentiometer; 3, for Thermoelectric Pyranometer in Set with KBT Electronic Potentiometer; 4, for Narrow-angle Longwave Radiation Receiver in Set with F-18 Amplifier and EPP-09 Electronic Potentiometer; 5, for Thermoelectric Pyranometer in Set With POB-14 Oscillograph.

If the correlation function does not depend on displacement of the reading points in measurement within the limits of fixation frequency Δt (the interval between adjacent readouts is sufficiently small), the spectral density of the continuous function is obtained by multiplying spectral density (1.7) arrived at through discretization by filter function [20, 21]

$$H_{\Delta t}(f)=\frac{1-e^{-2\pi f\Delta t}}{2\pi f\Delta t}. \qquad (1.29)$$

As may be seen from Figure 5, discrete fixation of the process in the frequency sector to be determined greatly increases the value of the spectral density, the value being the greater, the higher is the frequency.

The minimum frequency for which it is reasonable to determine the spectrum equals $\omega_{min}=2\pi/M\Delta t$, where $M\Delta t$ is the time interval of determination of the correlation function, while the maximum frequency according to the Kotel'nikov theorem equals $\omega_{max}=\pi/\Delta t$ [18, 19]. Thus the duration of measurement and the reading frequency impose limits on the frequency range within which the spectral density evaluation is made. At the same time, the evaluation of the spectral

density of the higher frequencies is considerably overstated. On the basis of measurement data the spectral density is determined within the frequency range from $6\pi/M\Delta t$ to $\pi/2.5\Delta t$.

In numerical processing of the results of experimental studies one cannot dispense with quantization by levels as determined by the accuracy of reading of the ordinates of the random process. In accordance with reference [22] (the random process under consideration being assumed to be normal), the dispersion of quantization noise is defined as $\sigma_\delta^2=\delta^2/12$, where δ is the quantization interval by levels, or $\sigma_\delta^2=(\delta/\sigma)^2$, and σ is the root mean square deviation for the random function. In the processing of automatic recording instrument tapes there is virtually no correlation of quantization noise with a random process. As a result, the dispersion of the random process is overstated by the value of dispersion of the quantization noise. In the spectral density the quantization noise is distributed over the frequency and increases it. In view of the fact that precise recording of quantization noise is difficult because the processes being investigated may not always be assumed to be normal, and the distribution of the noise in the spectral density by frequencies is unknown, in experimental measurements it is necessary to make certain that their value is considerably smaller than the errors depending on the nature of the random processes. In our studies the quantization noise represented less than 0.5 percent of the dispersion of the random process. /32

The distortion occasioned by the array of measuring equipment is determined chiefly by the inertia of the radiation receivers and the recording system. The random process measurements are accordingly smoothed out, with the result that dispersion is reduced, correlation is improved, and the spectral density values are correspondingly reduced. Inertial measuring equipment may be considered to be a high-frequency filter [22,23]. Figure 5 illustrates the frequency characteristics of the equipment for spectral densities demonstrating how the spectral density is attenuated as a function of frequency owing to the inertia of the equipment.

Once the frequency characteristic of the filter is known, a correction may be made in the spectrum calculated on the basis of the experimental data and an evaluation may be made in the spectrum calculated on the basis of the experimental data and an evaluation may be made of the true spectrum, dispersion, and correlation function obtained as a result of analysis of the data of observations based on an ideal inertialess instrument.

It follows from the foregoing that determination of the statistical parameters of radiation and cloud fields by way of experiment entails considerable errors. In addition, increase in the accuracy of their determination within the limits of one concrete measurement is limited by the scales of the cloud formations. Hence further increase in the accuracy of evaluation of statistical parameters can be achieved only by averaging the individual measurements obtained under identical meteorological conditions. Hence statistical characteristics based on average measurements are virtually the only ones employed in theoretical analysis of the structure of cloud and radiation fields and their relationships. We now have available to us 441 measurements suitable for analysis, 314 of which /33

are based on cumulus clouds, and the remainder on clouds of various kinds, chiefly those of the lower tier. The results of 203 measurements (149 based on cumulus clouds) were fully processed and utilized in the present project.

Section 4. Linear Conversions of Statistical Characteristics of Cloud and Radiation Fields

In study of cloud and radiation structure use is often made of one or another type of linear filtration, both deliberately and directly in measurement or in the processing of experimental data (see preceding section), and consciously in interpretation of the data, i.e., in search for relationships between the statistics of random functions related by a linear operator.

Various parameters have been employed in atmospheric physics to describe both radiation properties and cloudiness conditions.

The basic radiation intensity, by which radiation fluxes, i.e., the spherical flux density and the flux through a unit of area, are determined. The amount of clouds over the sky and coverage in individual directions are utilized as cloudiness parameters. In study of the statistical structure of radiation and cloud fields establishment of the relationships among the various parameters both of the radiation fields and of cloudiness represents an independent problem. The statistical characteristics of parameters integrated on the basis of the hemisphere, ones such as the amount of clouds, the density of the radiation flux, etc. depend on the altitude of the clouds, or in the general case the distance to them, since the area of a cloud formation covered by the averaging field is determined by the altitude of the clouds. Hence in analysis of the structure of cloud and radiation fields it is absolutely necessary to make a division between the relationships determined by the structure itself of these fields and by their transformation. /34

In the solution of many problems it is necessary to know the statistical characteristics of cloud and radiation fields averaged over certain time intervals or over space, along with the statistical relationships among the various parameters.

The relationship between radiation and cloudiness parameters is a linear or nearly linear one. The radiation and cloud parameters associated with averaging over time or space are also linear.

Let us now consider the relationships among dispersions, correlation functions, and spectral densities in the case of linear transformation of random functions.

Two approaches, equally valid and closely related to each other, may be applied to solve the problems assigned.

First of all, the relationships among the dispersions and correlation functions of the parameters are calculated on the basis of the relationships between the parameters in which allowance is made for the distance to the cloud cover. The spectral density is found from the correlation function by means of the Fourier transform.

Secondly, the filter functions determining the relationships among the spectral densities are calculated on the basis of the relationships among the parameters, after which the relationships among the dispersions and correlation functions are found by means of the inverse Fourier transform of the filtered spectrum. In the solution of concrete problems the method is selected which makes it possible to obtain results by the simplest means.

Let us consider linear conversions in greater detail.

The linear operators employed by us may be represented in the form

$$\psi(t) = \int_{\Omega} u(t, t_1)\xi(t_1)dt_1, \tag{1.30}$$

where $\xi(t)$ is the random function to which the linear operator in question is applied, $u(t,t_1)$ is the assigned weighting function, the form of which determines the properties of the operators, and Ω is the integration region, i.e., the region within which weighting function $u(t,t_1)$ differs from zero, and $\psi(t)$ is the linearly transformed random function. /35

The probability characteristics of function $\psi(t)$ are obtained very simply within the framework of the correlation theory [19,23-25].

On the one hand, we obtain the mathematical expectation by applying the linear operator to the mathematical expectation of the initial function

$$\psi(t) = \overline{\int_{\Omega} u(t, t_1)\xi(t_1)dt_1} = \overline{\xi(t)}\int_{\Omega} u(t, t_1)dt_1. \tag{1.31}$$

The dispersion and the correlation function of the linearly transformed random process are obtained by applying the linear operator twice to the correlation function of the initial random process

$$r_{\psi}(t_1, t_2) = \iint_{\Omega} u(t_1, t')u(t_2, t'')r_{\xi}(t', t'')dt'dt'', \tag{1.32}$$

and the spectral density for random function $\psi(t)$ by Fourier transformation of correlation function r_{ψ}. On the other hand, by employing the contraction theorem [19,26] and the definition of spectral density one can calculate the characteristics of filters reflecting the relationships between the spectral densities of function $\xi(t)$ and $\psi(t)$

$$S_{\psi}(\omega) = H(\omega)S_{\xi}(\omega), \tag{1.33}$$

where

$$H(\omega) = \Phi(\omega)\Phi^{*}(\omega), \tag{1.34}$$

and $\Phi(\omega)$ is the Fourier transform of weighted function $u(t)$ normalized at $\omega = 0$ zero, i.e., $\Phi(0) = 1$. Function $H(\omega)$ is termed the filter frequency characteristic. Correlation function $r_{\psi}(t)$ is calculated by means of the inverse Fourier transform of spectral density $S_{\psi}(\omega)$.

It is to be noted that forced smoothing of a random process such as filtration due to the inertia of the detection and recording system (see end of preceding section) can be eliminated only by means of reverse filtration of the spectral density:

$$S_\xi(\omega)=\frac{S_\psi(\omega)}{H(\omega)}. \tag{1.35}$$

In this instance the maximum frequency of restored spectral density is determined by the noise level relative to spectrum $S_\psi(w)$. The true dispersions and correlation functions, as with direct filtration, are obtained by means of the inverse Fourier transform. /36

Formulas (1.30) - (1.35) given in the foregoing apply to one-dimensional random functions. In reality the radiation and cloud fields of the Earth's atmosphere are multidimensional random space-time functions (random fields).

The concept of random field is analogous to the concept of random function. As in formulas (1.30) -- (1.35) the statistical characteristics of the random field are also converted under the influence of the linear operator. For random fields the correlation function, the weighting function, the spectral density, and the integration region in formulas (1.30) -- (1.34) are replaced by the corresponding multidimensional characteristics [2]. To establish a relationship between the space and the time structure of the cloud cover and the radiation we employ the hypothesis of "freezing" advanced by J. Taylor for turbulence [2]; according to this hypothesis, the space picture of a random field moves at the average wind velocity and does not vary in time.

Since experimental studies of random fields have been conducted chiefly with cross-sections, in analyzing the relationships among statistical characteristics one must necessarily assume that the latter are isotropic. It is to be noted that cross-sectional measurements of a random field yield a random function with one variable, which is described by formulas (1.30) -- (1.34). If in the filtration of spectral densities (1.33) the weighting function and the filter are two-dimensional, filtered spectral density $S_{2\xi}(\omega)$ must accordingly be two-dimensional as well. The latter is obtained by means of the two-dimensional transform of the correlation function, which in the isotropic case amounts to the Hankel transform /37

$$S_{2\xi}(\omega)=\frac{1}{(2\pi)^2}\int_{-\infty}^{+\infty}\int r_\xi(l)\,e^{-j(\omega_x x+\omega_y y)}\,dx\,dy=$$

$$=\frac{1}{2\pi}\int_{0}^{+\infty} r_\xi(l)\,J_0(\omega l)\,l\,dl, \tag{1.36}$$

where $\omega=\sqrt{\omega_x^2+\omega_y^2}$, $l=\sqrt{x^2+y^2}$, and J_0 is the zeroth order Bessel function. The cross-sectional one-dimensional spectral density is obtained after linear transformation of the random field, by integration of the two-dimensional spectral density over one frequency component [2,27]:

$$S_{\psi}(\omega) = \int_{-\infty}^{+\infty} S_{2\xi}(\omega) H_2(\omega) d\omega_y. \tag{1.37}$$

Section 5. Nonlinear Relationships Between Random Cloud and Radiation Fields

As we know, radiation interacting with the real atmosphere, scattered radiation, and the properties of the atmosphere are related by an integral-differential radiative transfer equation. It is to be seen from the transfer equation or approximation formulas that the light conditions in a light-dispersing and absorbing medium is connected by a nonlinear relationship to the parameters of the medium currently employed, the scattering and absorption coefficient, the form of the indicatrices, and the optical thickness. Thus in analysis of the relationships between the statistical parameters of the atmosphere (the cloud cover in the first approximation) and radiation fields one cannot dispense with nonlinear transformations of random fields (functions). It must be noted that nonlinear transformations are much more complex than are the linear ones discussed in the preceding section. It is not enough for nonlinear transformations to have knowledge only of the first two factors of the random function. At the same time, calculation of the higher factors on the basis of experimental data involves great difficulties because of the insufficient accuracy of the experiment (see section 3). However, nonlinear transformations can be substantially simplified if the initial random process may be considered to be normal. The /38
possibilities of modeling cloud and radiation fields by means of normal random processes will be analyzed in the next section.

Of the nonlinear transformations of random processes use is made in the present study of the simplest one, i.e., a transformation in which output function $\psi(t)$ is at any given instant determined only by filtered function $\xi(t)$ at the same instant. Such transformations are usually termed inertialess transformations in statistical radio engineering [23].

Let us now proceed to more detailed examination of the inertialess nonlinear transformations employed.

Probability densities are transformed with the formula

$$p(\psi) = p(\xi) \left| \frac{d\xi}{d\psi} \right| \tag{1.38}$$

In transformation of two-dimensional or multidimensional probability densities, derivative $d\xi/d\psi$ in formula (1.38) is replaced the Jacobian transform. The mathematical expectation, dispersion, and correlation function have been calculated by various methods [28,29]. Firstly, use being made of the nonlinear relationships and probability densities the mathematical expectation, correlation function, and dispersion have been calculated with the formulas

$$\overline{\psi(t)} = \int_{-\infty}^{+\infty} \psi p(\psi) d\psi, \tag{1.39}$$

$$\sigma_{\psi}^2 = \int_{-\infty}^{+\infty} \psi^2 p(\psi) d\psi - [\overline{\psi(t)}]^2 \tag{1.40}$$

and

$$r_{\psi}(t)=\frac{1}{\sigma_{\psi}^{2}}\int_{-\infty}^{+\infty}\int_{-\infty}^{+\infty}\psi_1\psi_2 p(\psi_1,\psi_2,t)\,d\psi_1\,d\psi_2-[\overline{\psi(t)}]^2, \tag{1.41}$$

where t is the time shift of ordinates ψ_1 and ψ_2.

Secondly, if the nonlinear relationships between random functions $\psi=g(\xi)$ are analytical functions in the vicinity of $\xi=0$, the factor method may be employed. Expanding nonlinear relationship $\psi=g(\xi)$ into a Maclauren series and taking from the series the first term assuring the required accuracy, and then performing statistical averaging, we obtain mathematical expectation /39

$$\overline{\psi(t)}=\overline{g[\xi(t)]}=a_0+a_1\overline{\xi(t)}+a_2\overline{\xi^2(t)}+\ldots+a_k\overline{\xi^k(t)}, \tag{1.42}$$

where a_i are constant expansion coefficients.

The dispersion is obtained by squaring the expansion, averaging, and subtracting the square of the mathematical expectation,

$$\sigma_{\psi}^2=\overline{\psi^2}(t)-[\overline{\psi(t)}]^2=\overline{[\sum_{i=0}^{k}a_i\xi^i(t)]^2}-\overline{[\sum_{i=0}^{k}a_i\xi^i(t)]^2}. \tag{1.43}$$

The correlation function is obtained as is the dispersion, by taking the expansion for two moments in time

$$r_{\psi}(t_1,t_2)=\frac{1}{\sigma_{\psi}^2}\overline{\sum_{i=0}^{k}a_i\xi^i(t_1)\sum_{m=0}^{k}a_m\xi^m(t_2)}-\overline{[\sum_{i=0}^{k}a_i\xi^i(t)]^2}. \tag{1.44}$$

It is to be seen from formulas (1.42) - (1.44) that the factors of transformed process $\psi(t)$ include the higher factors of process $\xi(t)$ which is to be transformed. And it is this that represents the characteristic feature of nonlinear transformation. Only if $\xi(t)$ is a normal random process are the higher factors expressed by the factors of the first two orders [30]. In the general case the higher factors are unknown and we are forced to restrict the series by including the first two factors only. In concrete cases such a restriction may not correspond to the required accuracy. In addition, the approximation error cannot be estimated without the higher factors.

As with the linear transformations, in the nonlinear ones the method is selected which makes it possible to obtain results by the simplest means.

Section 6. Modelling Cloud and Radiation Fields by Means of Normal Random Processes

The methods which are linear in the first approximation and the nonlinear methods of investigating random cloud and radiation fields, such as those described in the preceding sections, are based on utilization of the first two factors of random fields and thus do not go beyond the framework of spectral correlation analysis. As will be demonstrated later (in Chapters III - V), an approach such as this is entirely acceptable for the solution of many problems. However, /40 there are a large number of problems for the solution of which the apparatus of

the correlation theory is found to be inadequate. Such problems include primarily: (a) determination of the one-dimensional, two-dimensional, and multidimensional probability densities of cloud coverage of directions of sighting, (b) determination of the probability density of distribution of cloud frequency, i.e., the number of clouds per unit interval, (c) more nearly correct solution of nonlinear problems, etc. Solution of these and similar problems occasions great difficulties for random processes. But even in this case, as will be demonstrated later, success can be achieved by relatively simple means, by restricting consideration to random processes possessing certain special properties.

In reference [31] the hypothesis was advanced that cumulus clouds may be described by means of a stationery Gaussian process. Stratiform clouds were later described in [32,33] by means of a Gaussian process. Subsequent experimental and theoretical research demonstrated that the hypothesis advanced can be successfully applied to varied description of the structure of cloud and radiation fields, despite the fact that there are no grounds for assuming a cloud cover to be strictly Gaussian [34]. As a result there has been constructed and experimentally verified a theoretical model which in our opinion is sufficiently complete for description of the structure of the cloud and radiation fields of the real atmosphere. At the same time, the degree of detail of the theoretical model we have constructed is fully in keeping with the information on cloud structure available to us in the current stage of development of experimental research.

Let us now proceed to a description of the model. We employ as the model a random Gaussian surface bounded underneath at a certain level (Figure 6). Diagram a in Figure 6 applies to variable cloudiness, in which the limitation level excludes a considerable portion of the normal random surface from consideration, while diagram b illustrates the case of an unbroken cloud cover, in which there is a negligibly small probability that the cutoff level intersects the random surface. At the same time, it is assumed that the portion of the random suface situated above the cutoff level is a theoretical fiction. With elevation of the limitation level the amount of clouds decreases, a cloudless sky being obtained at the limits, while the amount of clouds increases with lowering of the level, there being obtained at the limit an unbroken cloud cover the thickness of which depends on the depth of the limitation levels. Consequently one model covers all possible cloud conditions of the Earth's atmosphere (from a clear sky to an unbroken cloud cover). /41

Information on the dimensions of the bases of the clouds alone is required for the solution of a large number of problems of great interest. In this case the clouds can be conveniently approximated as rectangles (Figure 6 a). The restricted normal process is consequently transformed into a relay signal (rect-signal). There remains to be resolved the matter of the cloudiness parameter whose variability it is advisable to describe by means of the normal random surface. As we know, the variability of the optical thickness of the cloud cover is determined by the random variability of the altitude of the upper and lower boundaries, moisture content, and both the vertical and the horizontal microstructure, etc. In addition, we know from statistics that the probability density of the sums of the terms, independent or only slightly dependent, which play approximately the same role, approach the normal distribution law when their /42

number is increased, regardless of the distribution laws obeyed by the terms (A. M. Lyapunov's central limit theorem). In view of this fact, in our model we assume that the optical thickness of the cloud cover, and in some cases of cumulus clouds its vertical extent as well, represent a normal random process. It has additionally been assumed that there is a linear relationship between the optical thickness and the dimensions of the clouds.

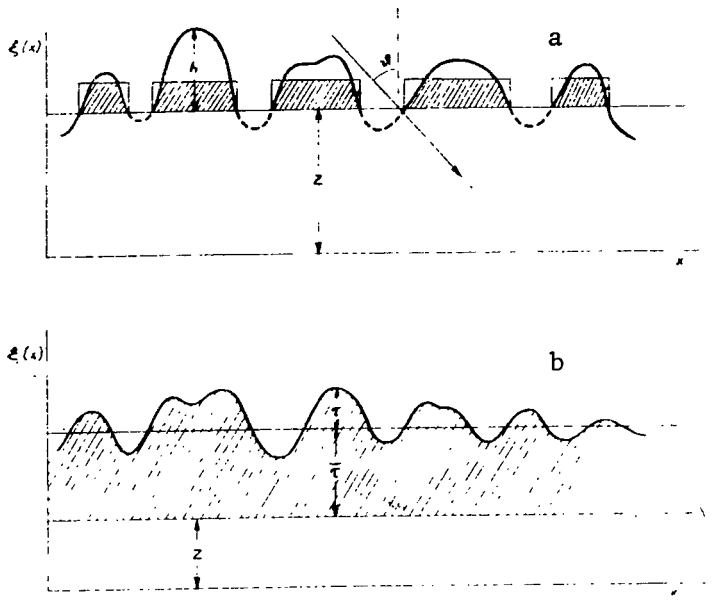

Figure 6. Diagram of Normal Random Surface.

Because of mathematical considerations, in analyzing the structure of cumulus clouds we are forced in individual cases to restrict ourselves to examination of normal random processes the correlation function of which is of the form of a damping exponent, i.e., the normal random process is at the same time a Markovian one.

It is to be noted that limitation of the cloud cover by the plane underneath is justified from the physical standpoint. The lower boundary of the cloud cover, which is determined by the condensation level, undergoes but little change in space. The bases of cumulus clouds are accordingly situated approximately on one level, and the lower boundary of stratified clouds is much less variable with altitude than is the upper one.

The chief advantages of the model constructed include the following possibilities:

(1) Utilization of the results of the theory of dispersion of normal random processes, which permits description of the structure of the cloud field from various standpoints, in many instances by means of relatively simple analytical expressions;

(2) Establishment of relationships between the statistical characteristics /43
of radiation cloud fields;

(3) Experimental determination of the few initial parameters required which are applied in the theory, such as the cutoff level, the dispersions of the normal random surface and its derivative, and the correlation radius.

The justifiability of utilization of this model has been confirmed by the quite good agreement between calculations based on the model and experimental data, as well as by the slight variation in the parameters of the model from measurement to measurement. The main results of calculations based on the model and comparison of the latter with experimental data are presented in Chapters III and IV of the present study.

It is to be noted that the model constructed is not the only one possible. It is virtually always possible to advance a number of other hypotheses which agree to one extent or another with the experimental data.

For example, a model of cumulus clouds has been constructed by means of the Poisson flux in [35,37], while in [38,39] various probability distribution functions have been employed to describe the distribution of the optical thickness of stratified clouds.

Modeling of cumulus clouds by means of the Poisson flux makes it possible to solve a number of particular problems (such as decrease in cloudiness toward the horizon), although such modeling is incorrect from the physical standpoint, since in this case the individual cloud formations are assumed not to be correlated with each other.

By means of probability densities differing from the normal it is possible to ascertain the influence of variability of the optical thickness on the mean radiation characteristics [38,39] and on the dispersion of the latter. At the same time, the possibility is excluded of studying the relationships between the spatial structures of cloud and radiation fields, since, aside from those for normal processes, there are at the present time no prescribed and rigorous methods making it possible to ascertain the relationships between two-dimensional and multidimentional probability densities and the correlation function of the random process.

The brief survey given in the foregoing of a model based on utilization of normal random processes demonstrates that, while the cloud cover can be approximated by a normal random process, in particular cases by a Markovian process, the range of problems to be resolved is considerably broadened. At the same time, a number of problems are relatively simple to solve.

Although quite good agreement is observed between the model and experimental data, further experimental study of the cloud and radiation fields over the widest possible range of variation of the cloud and radiation flux parameters is nevertheless required, since extrapolation beyond the limits of the region investigated by experiments may lead to major errors. It is to be noted that the need for refinement of the theoretical model constructed may arise only with subsequent

elevation of the level of information on the structure of the cloud cover and radiation parameters. The most promising approach in this instance appears to be description of the optical thickness (cloud cover thickness) or any suitable parameters of cloudiness or radiation by a random function which is unambiguously related by linear or nonlinear operators to normal functions or which may be represented by multidimensional normal or Markovian processes.

CHAPTER II. EQUIPMENT FOR STUDY OF VARIABILITY OF RADIATION AND CLOUD FIELDS IN THE ATMOSPHERE IN TIME AND SPACE /45

Section 1. Introduction

Experimental studies of the variability of radiation and cloud fields in time and space are impossible by means of the existing equipment usually employed in physics of the atmosphere and generally designed for study of averaged energy parameters. Transition from rigidly defined examination of the problem of radiative transfer in a real atmosphere to statistical description of radiation and cloud fields and their relationships sets specific requirements of its own on experiments as well. Above all this applies to the frequency characteristics of the entire measurement system, from the sensor to the recording apparatus. The passband of the array of measuring instruments must correspond to the frequency interval being investigated, and this sometimes creates certain difficulties in the region of the high frequencies.

In studies of the variability of fields in space it is also necessary to guarantee that the equipment will possess sufficient spatial resolving power, that is, the optical systems must have a small field of view. This requirement usually causes no fundamental difficulties, but renders the equipment cumbersome and complex, and this in turn in some instances limits the possibilities of employing individual instruments under field conditions, especially on moving vehicles (aircraft and so forth). A general requirement in any measurements followed by processing of the results by statistical methods is recording of the data either in the form of a continuous recording, or in discrete form of a /46 frequency sufficient for the process being studied. The large amount of initial material necessary for dependable determination of statistical characteristics accompanied by maximum reduction of manual processing inevitably necessitates the production of suitable equipment.

The statistical approach also makes certain concessions in the absolute accuracy of measurements, instrument graduation, long-term stability of instrument parameters, etc. This often makes it possible to conduct measurements with the aid of relatively simple and readily accessible equipment.

In creating the array of equipment for the experimental aspect of the research under consideration here we set the following as our chief aim: to guarantee measurement of all the parameters required as initial ones for the theoretical models, and for verification of one or another theoretical conclusion, with instruments of the utmost simplicity and accessibility. This array was created gradually in the course of work and was constantly improved as new theoretical requirements and experimental possibilities made their appearance. It has by now become obvious that certain instruments hold out no promise whatever and must be replaced by more modern ones, but for the sake of completeness a description of them has nevertheless been included in the survey of equipment. No discussion is devoted here to instruments which are in the development or testing stage, or to instruments the data on which were not used by us in the present study.

Section 2. Equipment for Determination of Cloudiness Conditions

In order to establish the relationship between radiation field and cloudiness parameters it is necessary to use equipment to determine these parameters. The amount and shape of clouds as determined visually are unsuitable for this purpose due to the insufficient information content and the large proportion of subjectivity. Hence in our studies we have made use of the method of photographing the entire sky. This has been accomplished basically by means of a convex spherical mirror [40]. Various equipment modifications and different photographing methods have been utilized, as a function of the concrete problem and the nature of the cloud cover. If the problem has been solely that of obtaining an objective representation of cloud conditions, the image has been photographed from the spherical mirror on 35-millimeter film of the KM-2 type, usually through a color filter of OS-12 glass. Enlarged prints with a coordinate grid applied during the positive process served as material for subsequent processing. The grid was determined experimentally for all the optical systems employed, which consist of a spherical mirror and a camera lens. The interval chosen between individual photographs was 5 to 30 minutes. Processing of the photographs obtained in this manner provided the possibility of determining the total number of clouds, the zonal distribution of cloud coverage of the sky, and the variation in cloudiness, as well as evaluation of the shapes of clouds. Of late an afocal adaptor of the "fish eye" type has been used for these purposes, so that the entire unit is small in size and low in weight. /47

More detailed information on the variation and displacement of the cloud field has been found to be necessary in some projects. In such cases use has been made of time-lapse moving picture filming with 16-millimeter black-and-white OCh-45 film, gernerally with an interval of six seconds. Selected frames have been projected onto a screen having a coordinate grid for the purpose of processing of the frames.

In ground measurements the variability of the radiation field is determined both by the nature of the cloud cover and by the rate of its displacement above the point of observation. In all experiments determination has been made of the angular velocity of displacement of clouds in the area around the zenith. For this purpose we have used a simple device consisting of a lens having a focal distance of 210 mm the optical axis of which was oriented toward the zenith, from a plane mirror at an angle of 45° to the optical axis, and matte glass situated vertically in the focal plane and having a coordinate grid applied to it. By observing the displacement of the image of any point of a cloud through the zenith and by fixing the time it requires to pass through a certain angular distance one can determine the rate of cloud movement easily and with sufficient accuracy. /48

It is to be noted that for more detailed study of cloudiness characteristics use has been made of narrow-angle radiation detectors produced especially for this purpose. A description of these detectors is given in the following sections.

Section 3. Equipment for Sky Brightness Measurement

The array of narrow-angle radiation detectors is used for studies of two kinds:

(1) determination of the relationships between sky brightness in a particular direction and the radiation flux;

(2) determination of cloudiness conditions in the direction of sighting.

The following instruments were employed, depending on the specific problem:

a. A narrow-angle detector of integral shortwave radiation based on the sensing element (thermopile) of the Linke-Feussner actinometer with the addition of a glass lens optical system. The optical system provides a viewing angle of the order of 1° for the instrument. The spectral sensitivity range of the instrument is determined by the transmission of the glass; the possibility has been provided of using glass or interference light filters. The output signal of the instrument is amplified by an F-18 amplifier and recorded by an EPP-09 electron potentiometer.

b. Narrow-angle spectral detectors of shortwave radiation of various types. A diagram of the latest modification of a general-purpose ground instrument permitting the conduct of measurements in accordance with various programs is presented in Figure 7. The instrument consists of a lens with the cathode of an FEU-22 photomultiplier placed in its focal plane. Diaphram 2 determines the viewing angle of the instrument, which in our measurements was 30'. Disc 3 with interference light filters can be rotated by electric motor M1. Use was made of interference light filters with passband centers of 420, 707, and 723 mm. The /49
instrument has an attachment for sky scanning which consists of a plane scanning mirror 5, which is rotated by electric motor M2 at a rate of 180° in two minutes. The output signal amplified by a direct-current amplifier and recorded by an EPP-09 or directly by an EPPV-60. The instrument permits the conduct of observation in three modes:

(1) Measurement of brightness in one specific direction and spectral interval; in this case the disc with filters and scanning mirror are stationary;

(2) Measurement of spectral brightness in one direction but consecutively in three spectral intervals; in this case the disc with filters rotates and mirror 5 is stationary;

(3) Sky scanning within the limits of 180°; mirror 5 rotates, while the disc with filters is stationary.

A simplified narrow-angle spectral detector the diagram of which is presented in Figure 8 has been produced for aircraft measurements. The instrument consists of a lens 3 with a focal distance of 52 mm which projects an image through diagram 4 onto one of sensing elements 5. There are additionally in the path of the rays a glass light filter 2 and light filter 1 to reduce the effect of the

radiation scattered within the instrument. Either germanium photodiodes of the FD-3 type or FD-K silicon photodiodes operating in the photogalvanic mode were used as the sensing elements. In order to reduce the dependence of the dark flow of the photodiodes on temperature use was made of a differential measurement circuit, for which purpose two photodiodes identical in parameters and connected in opposition to each other were placed side by side in good thermal contact, one of them being shielded against radiation. The glass light filter serves to improve the spectral characteristics of the photodioe somewhat, so that a contrast of 2 to 10 is achieved between clear sky brightness and clouds, depending on the shape and thickness of the clouds. Curves of the spectral sensitivity of the photodiodes of the FD-3 and FD-K types with and without the OS-12 glass light filter are presented in Figures 9 and 10.

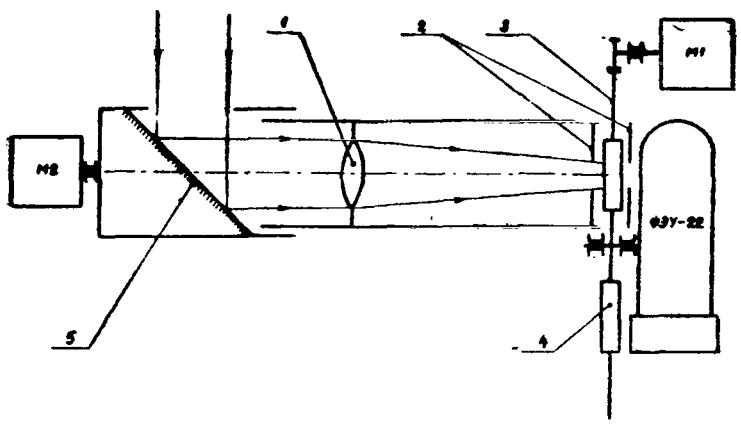

Figure 7. Diagram of Narrow-angle Spectral Radiation Detector: 1, Lens; 2, Diaphragm; 3, Rotating Disc; 4, Interference Light Filter; 5, Scanning Mirror.

The signal from the detector comes to the input of a transistorized direct- /50
-current differential amplifier constructed on the basis of the example of the tensometric amplifier described in [41]. The amplifier receives its power from the aircraft power supply system through a transistorized voltage stabilizer. The output voltage is recorded by a K-4-21 or POB-14 loop oscillograph at a tape advance rate of 0.5 to 2 mm/sec. A block diagram of the narrow-angle aircraft measuring system with two detectors oriented upward and downward is given in Figure 11.

In addition to the narrow-angle instrument systems operating in the visible /52
or near infrared region of the spectrum, use is also made of instruments for determination of brightness in the region of longwave (thermal) radiation. All these instruments are identical in optical system and design, differing only in the thermopiles and filters employed. A mirror optical system (Fig. 12) and sensing element 1 are mounted in a solid housing of a material possessing good thermal conductivity and thermal insulation. The mirror and housing are heated slightly by heater 3 to prevent the formation of dew in nighttime measurements. The output signal is amplified by an F-18 amplifier and recorded by an EPP-09 electron potentiometer. The viewing angle of the longwave instrument is of the order of 1°.

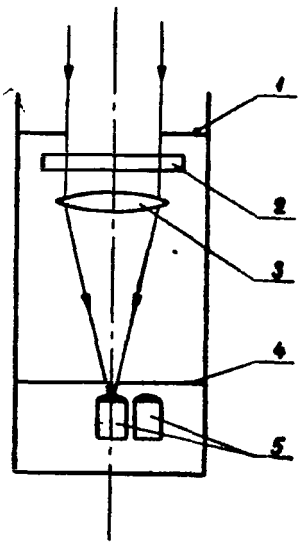

Figure 8. Diagram of Narrow-Angle Aircraft Radiation Detector: 1, Inlet Diaphragm; 2, Light Filter; 3, Lens; 4, Diaphragm; 5, Photodiodes.

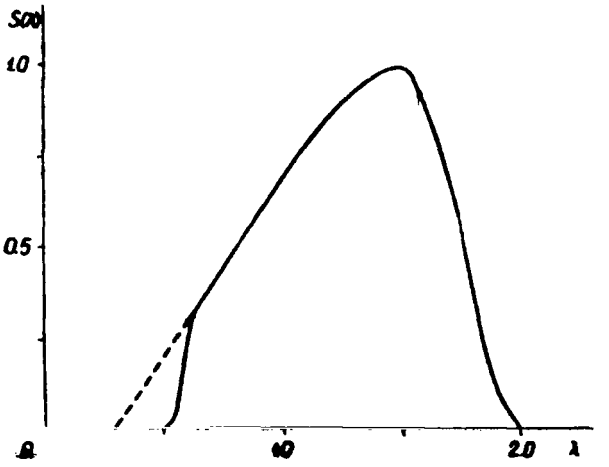

Figure 9. Relative Spectral Sensitivity of Narrow-Angle Aircraft Radiation Detector With FD-3 Photodiode Equipped With OS-12 Light Filter (Solid Curve) and Without the Light Filter (Broken-Line Curve).

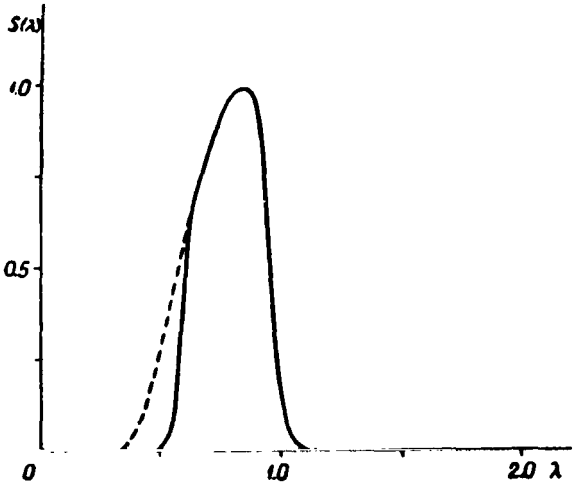

Figure 10. Relative Spectral Sensitivity of Narrow-Angle Aircraft Radiation Detector With FD-K Photodiode Equipped With OS-12 Light Filter (Solid Curve) and Without the Filter (Broken-Line Curve).

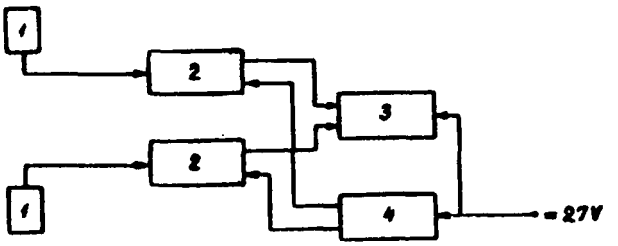

Figure 11. Diagram of Aircraft Brightness Measurement System: 1, Radiation Detector; 2, Differential Direct-Current Amplifier; 3, Loop Oscillograph; 4, Voltage Stabilizer.

Thermopiles developed specifically for the purpose are used as the radiation detectors in the longwave instrument. The diagram of a thermopile for integral thermal radiation is presented in Figure 13. The thermopile consists of a thermopile housing 6 and 7 of latten brass incorporating frame 5 in good thermal contact. 50-60 turns of insulated constantan wire 4 0.06 mm in diameter are wound on the latter. To form the thermopile, sections 2 or the constantan wire are stripped of insulation and have a layer of copper applied to them by electrolytic means. The detector has two inlet apertures located side by side above the thermopile juncture. Both apertures are covered by a germanium filter 3. To cut off the end of the spectrum of shortwave radiation passed by the germanium, one of the apertures is additionally provided with a glass filter 1. The spectral characteristics of the detectors described with and without the compensating glass filter are shown in Figure 14.

Passband interference filters were employed for measurements in narrow spectral thermal radiation intervals, generally in the water vapor "window" of 8-12 μ. In this case the thermopile is somewhat different in design (Figure 15). It has (1) only one inlet aperture, behind which is light filter 1, (2) a compensating plate 6 of the same thermal inertia as the filter used to reduce the zero drift on change in the detector temperature, and (3) the thermocouple junctions in a different arrangement. /54

In both instances the thermocouples are coated with black matte optical varnish manufactured by Parsons. The external surfaces of the housing are polished and nickleplated to reduce radiative heat exchange between the instrument and the surrounding atmosphere. In the course of the work both detector modifications, and especially the first one, exhibited very good zero stability and proved themselves to be useful. The time constant varied somewhat from set to set, but did not exceed tenths of a second; this fully meets the requirements for ground measurements.

Section 4. High-Speed Radiometer and Results of Testing of Mercury-Alloyed Germanium Radiation Detector.[1] /55

High-speed equipment of high spatial resolving power and high sensitivity is required for solution of various kinds of problems associated with investigation of the radiation structure of various cloud transformations. In the building of such equipment more rigid requirements are also generally set for measurement accuracy, and this necessitates knowledge of the additional parameters of various elements of the equipment.

In what follows a description is given of a high-speed radiometer-pyrometer for measurement of small fluctuations in the radiation temperature or brightness of various natural formations, including clouds. /56

The results of testing of a Ge:Hg (mercury-alloyed germanium) radiation detector cooled by solid nitrogen (51°K) are cited for the purpose of evaluation of instrument accuracy.

[1]The authors wish to express their thanks to B. M. Rogov for assistance rendered in the work.

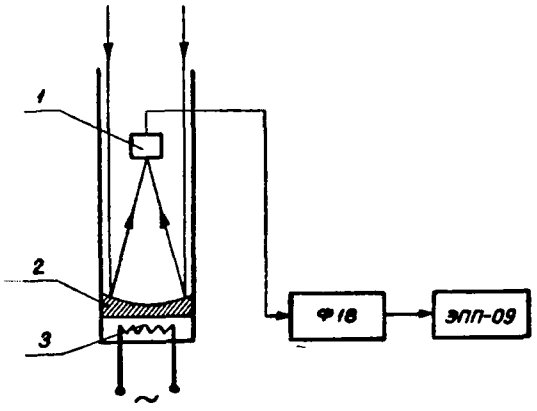

Figure 12. Diagram of Thermal Radiation Brightness Measurement: 1, Radiation Detector; 2, Lens; 3, Heater.

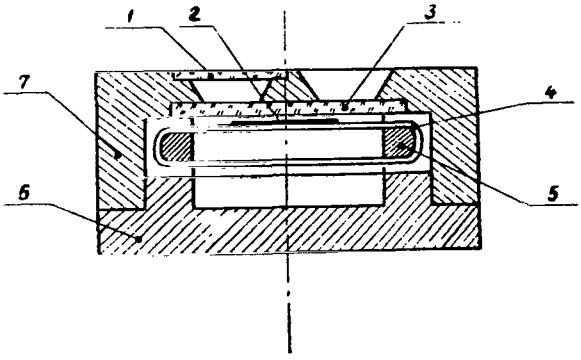

Figure 13. Thermopile for Measurement of Integral Thermal Radiation: 1, Glass Compensating Filter; 2, Portion of Thermopile Coated With Copper; 3, Germanium Light Filter; 4, Constantan Wire; 5, Frame; 6, 7, Housing.

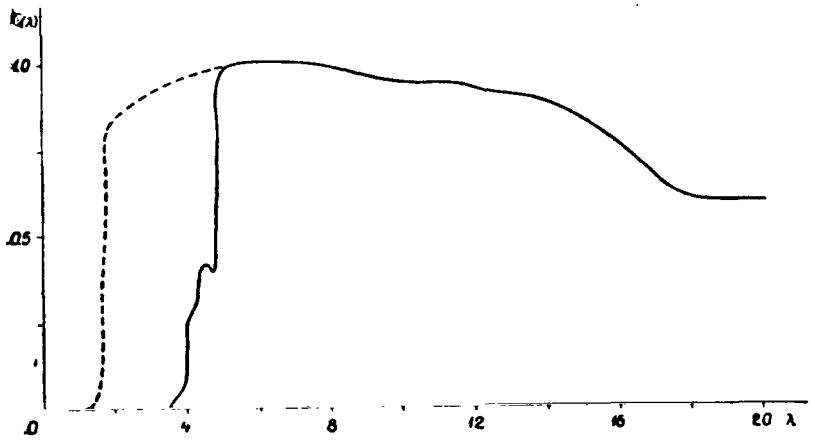

Figure 14. Relative Spectral Sensitivity of Integral Thermal Radiation Detector With Compensating Filter (Solid Curve) and Without it (Broken-Line Curve).

Although the rating is usually taken as a basis in selection of the radiation detector, in a number of cases more detailed additional information is needed on its parameters, ones such as the variation in the threshold and volt sensitivity and resistance of the detector as a function of the value of unmodulated radiation created by the internal elements of the instrument, the linearity of the voltage characteristic, the behavior of the signal-noise ratio as a function of the frequency of modulated radiation, the variation in sensitivity with the degree of cooling of the sensing element, and the capacity for

detection of bodies of various temperatures. Let us consider some of these parameters.

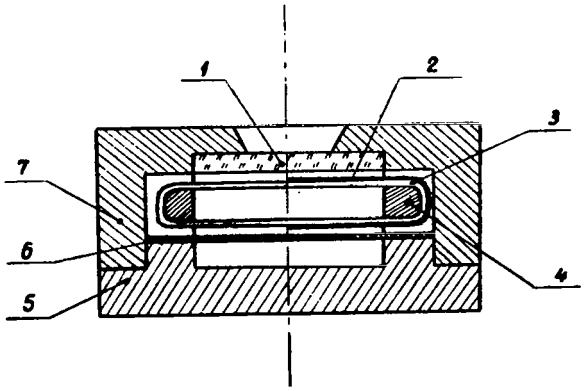

Figure 15. Thermopile for Spectral Measurements of Longwave Radiation: 1, Interference Light Filter; 2, Portion of Thermopile Coated With Copper; 3, Constantan Wire; 4, Frame; 5 and 7, Housing; 6, Compensating Plate.

A. Influence of Unmodulated Radiation on Detector Parameters

The detector is always subjected to the influence of radiation fields, which vary widely from case to case. Reports have been published in the literature [42-45] on study of the exposure characteristics of receivers of PbTe, InSb, PbSe, and PbS. The results of similar study of a Ge:Hg detector cooled by solid nitrogen to 51°K are presented in what follows.

The influence of unmodulated radiation, exposure, on the parameters of the detectors was determined by the procedure described in [42,43,45]. This procedure consists in using an absolute black body or tape lamp with radiation of known spectral distribution (in our case a black body at a temperature of 700°K) for imitation of the exposure. The unmodulated radiation value was established by reducing the flux from the radiator and by varying the distance between the source and the radiation detector. /57

Another black body the flux from which did not vary in magnitude during the experiment was used as the source of modulated radiation. The effect of exposure on the parameters of a Ge:Hg radiation detector cooled by solid nitrogen to 51 ± 1°K is noted in [46], in which study was made of 3 models the threshold sensitivity of which does not differ by more than 40%. Diaphragms cooled by solid and liquid nitrogen were used in the detectors to reduce the influence of the initial background exposure. It is noted in this paper that on change in the effective exposure $E_{0,\text{eff}}$ from $1.1 \cdot 10^{-4}$ to $8.8 \cdot 10^{-4}$ w the voltage sensitivity of the various detectors was reduced by a factor of 1.54, and the threshold sensitivity deteriorated by a factor of 1.5 to 3. Additional results have been produced with viewing angles of 0.012 steradian formed by diaphragms cooled by solid and liquid nitrogen. The equipment and the procedure of the experiment are described in [46]. The value of the effective initial background exposure active at an angle of 0.012 steradian, as converted to terms of radiation of an absolute black body of a temperature of 298°K (the background temperature at which the experiment was conducted), was calculated from the formula

$$E_{0,\text{eff}} = \sin^2\frac{\theta}{2}\int_0^\infty r_\lambda(298°)S(\lambda)\,d\lambda, \qquad (2.1)$$

and the value of exposure from a 700°K source was calculated from the formulas

$$E_{\text{eff}\,(2-14)}=\frac{g_{\text{bb}}}{\pi L^2}\int_0^\infty r_\lambda(700^\circ)S(\lambda)\,d\lambda, \tag{2.2}$$

$$E_{\text{eff}\,(8-14)}=\frac{g_{\text{bb}}}{\pi L^2}\int_0^\infty r_\lambda(700^\circ)S(\lambda)W_\Phi(\lambda)\,d\lambda, \tag{2.3}$$

where $E_{0,\text{eff}}$, $E_{\text{eff}(2\text{-}14)}$, $E_{\text{eff}(8\text{-}14)}$ are the effective initial and additional exposures in w/cm active in the spectral angles of 2-14 and 8-14 μ; θ is the viewing angle of the radiation detector: r_λ (298°) and r_λ (700°) are the spectral densities of radiation of a black body having temperatures of 298 and 700°K; S(λ) is the relative spectral sensitivity of a radiation detector having a window of coated germanium; $W_f(\lambda)$ is the spectral function of the filter transmission coefficient; g_{bb} is the area of the black body diaphragm; and L is the distance between the black body diaphragm and the sensing area of the detector. /58

The radiation of the cooled diaphragms and the deviation from the inverse square law due to atmospheric absorption were not taken into account in (2.2) and (2.5).

Verification of the stability of the black body temperature by means of thermocouples cannot be accomplished with high accuracy, so that the extent of cooling of the sensing elements was determined on the basis of its resistance, which at $E_{0,\text{eff}}$ remained constant during the experiment. The graphs in Figures 16 and 17 show the behavior of the relative voltage S/S_0 and threshold $\varepsilon/\varepsilon_0$ sensitivities as a function of the exposure value. In Figure 16 the voltage sensitivity is also plotted against the temperature of the background active in the aperture angle of the detector for spectrum ranges of 10-11.15 (curve 1) and 8-13 μ (curve 2).

We know that for extrinsic semiconductors under conditions of background exposure the relative voltage and threshold sensitivities for a backgound--limited detector are defined as

$$S/S_0=E_{0,\text{eff}}/E_{\text{eff}},\quad \varepsilon/\varepsilon_0=(E_{\text{eff}}/E_{0,\text{eff}})^{1/2}, \tag{2.4}$$

where S_0, ε_0 are the voltage and threshold sensitivities for initial exposure $E_{0,\text{eff}}$; and S, ε are the voltage and threshold sensitivities for various values E_{eff}.

In the graphs in question the S/S_0 and $\varepsilon/\varepsilon_0$ differ somewhat from the relationship described in the foregoing. This difference is apparently due to the fact that the optimum cooling temperature for a Ge:Hg detector is not 51°K but is within the range of 30 to 35°K (see [47,48]). It should be observed that the

behavior of the relative threshold sensitivity of radiation detectors (curve 1 in Figure 17) differs but little from that calculated on the basis of equation /60

$$\varepsilon = \frac{2E_0\left[(N_a - N_\alpha)\frac{1}{N_\alpha}N_v V \exp\left(-\frac{\Delta E}{kT}\right) + g_{de}\eta(\nu) j_\phi t \sin^2\frac{\theta}{2}\right]^{1/2}}{l^2\eta(\nu) j_c \sqrt{t}}, \quad (2.5)$$

where E_0 is the integral flux from the black body in w; N_a N_α is the concentration of acceptors and donors in the sample, $N_a - N_\alpha = (4\text{-}5)\ 10^{14}$ cm^{-3}; N_v is the effective density of the states in the valence zone, $N_v \approx 1.17 \cdot 10^{15}\ (T)^{3/2}$ cm^{-3}; l is the distance between the black body diaphragm and the radiation detectors; ΔE is the level of ionization energy, $\Delta E = 0.087$ ev; V is the volume of the sample; k is the Boltzmann constant; T is the temperature of the sensing element; N_v is the quantum efficiency; T is the lifetime of the carrier; $j_b j_m$ is the current density of the quanta from the background and the modulated radiation source.

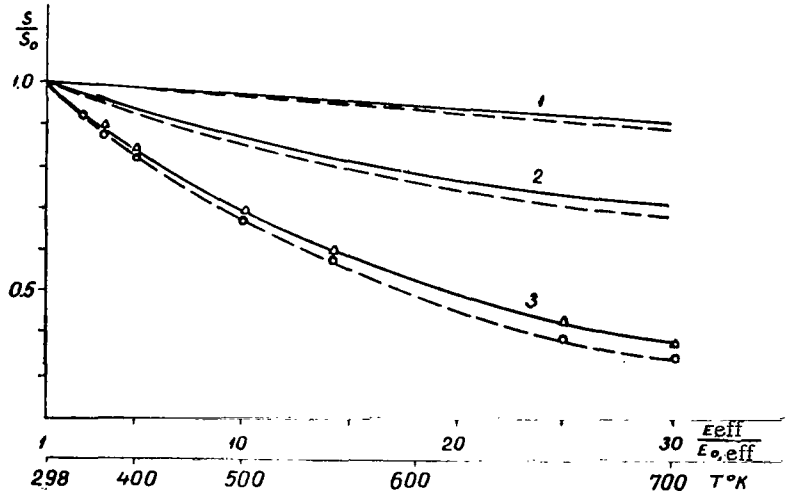

Figure 16. Voltage Sensitivity S/S_0 Versus Exposure (Background Temperature) at $E_{0,eff} = 1.67 \times 10^{-4}$ w · cm. First detector, broken-line curve; second detector, solid curve; 1, $\Delta\lambda$ = 10-11.5 μ; 2, $\Delta\lambda$ = 8-14 μ; 3, $\Delta\lambda$ = 2-14 μ.

Calculations based on equation (2.5) with the model parameters and experimental conditions illustrated demonstrate that the threshold sensitivity due to the effect of exposure varies with variation in the limited background of the detector. The behavior of S/S_0 and $\varepsilon/\varepsilon_0$ as a function of $E_{eff(8\text{-}14)}$ permits the conclusion that when use is made of a detector having a viewing angle of 26-28° (to the lens of the radiometer) the influence of the unmodulated radiation of

the instrument elements on the parameters of the Ge:Hg detector over the operating temperature range of the radiometer-pyrometer from -30 to +50°C may be virtually eliminated. In operation with a radiometer using a filter with a pass-band of 10-11.5 μ the detector parameters were found to remain unchanged over a wider range of operating temperatures. The results obtained prove one of the advantages of quantum radiation detectors over the thermal ones, which are sensitive both to modulated and to unmodulated radiation.

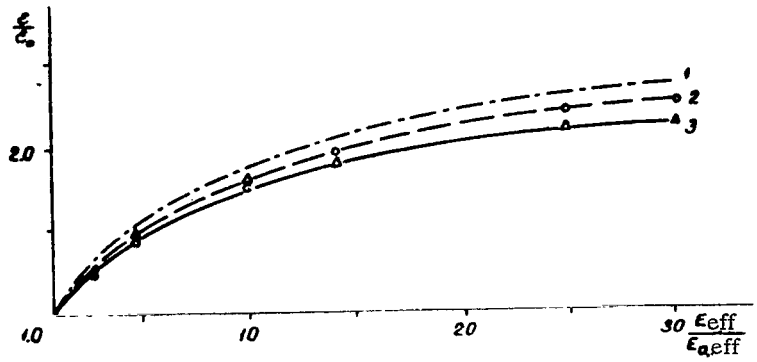

Figure 17. Threshold Sensitivity $\varepsilon/\varepsilon_0$ Versus Exposure; 1, Theoretical Curve; 2, First Detector; 3, Second Detector

B. Study of Linearity of Watt-Voltage Detector Characteristic

The watt-voltage characteristic is directly related to the amount of free current carriers of the sensing element. The influence of unmodulated radiation /61 on the parameters of the Ge:Hg detector to some extent also explains the linearity of the watt-voltage characteristic.

In what follows we shall restrict ourselves to the results of experiments confirming the considerable dynamic range of the detector, since determination of the relationship of the latter to the exposure characteristics (see equation 2.5) goes beyond the framework of the present study.

A black body of adjustable temperature was used to imitate the modulated radiation. The flux value ranged from 10^{-9} watts, this exceeding the power equivalent to the detector noise, to 10^{-5} watts; the unmodulated radiation remained constant.

In Figure 18 the voltage at the detector output is plotted against the modulated flux value E calculated from the formula

$$E=\frac{g_{de}g_{bb}}{\pi L^2}\left(\int_0^\infty r_\lambda(T_n)S(\lambda)\,d\lambda-\int_0^\infty r_\lambda(298^\circ)S(\lambda)\,d\lambda\right), \qquad (2.6)$$

where $r_\lambda(T_n)$ is the spectral density of black body radiation at various temperatures T_n; r_λ (298°) is the spectral density of modulator radiation at a temperature of 298°K; G_{de} is the area of the sensing element of the radiation detector. /62

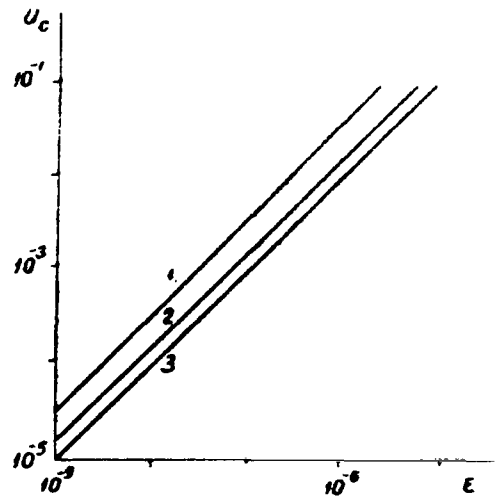

Figure 18. Watt-Voltage Characteristics of Ge:Hg Detectors.

It is to be seen from Figure 18 that the detectors in question possess sufficiently high linearity over the radiation flux range indicated.

C. Determination of Ge:Hg Detector Sensitivity as a Function of Degree of Cooling

The basic error in measurement of cloud radiation results from the temperature instability of the detector sensing element. In order to reduce measurement errors in the processing of results it is necessary to introduce a correction for variation in the detector sensitivity. As was observed earlier, monitoring of the crystal temperature by means of thermocouples or thermistors does not yield a high accuracy. For this reason the instability of the detector sensitivity was monitored on the basis of the resistance of its sensing elements, by means of an M-95 instrument.

The resistance of the detector sensing element was varied by evacuation of nitrogen vapor from a Dewar flask with a VN-461 pump. At the end of the cycle of operation of the radiation detector, when its resistance was slowly decreasing, measurement was made of the sensitivity at various resistance values of the element. The load resistance remained constant in this case for each detector. This method was employed to determine the sensitivity as a function of element resistance in three radiation detectors of special design. These detectors were used in the radiometer.

In Figure 19 the relative threshold sensitivity $\varepsilon/\varepsilon_0$ is plotted against the relative variation in resistance R/R_0, with $E_{0,eff}$ = const. A variation in

element resistance no greater than 15% was permitted in cloud formation measurements, a correction factor being introduced in processing of the results for every 3% of variation in resistance.

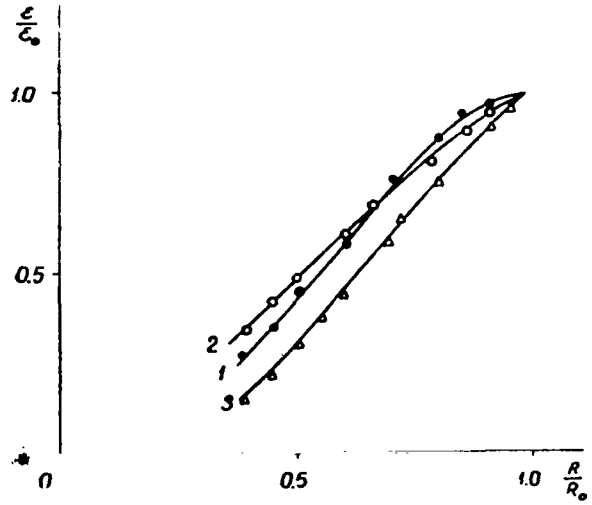

Figure 19. Watt-Voltage Sensitivity of Detectors Versus Variation in Detector Resistance

D. Determination of Detection Power of Ge:Hg Detector /63

The photon noise generated by any radiating body is known to impose limits on the detection power of a radiation detector [47,48]. Cooling of the internal parts of the detector is sometimes employed to reduce this noise; cooled filters and diaphragms are inserted which limit the aperture angle, since the detection power of a detector limited by noise is defined by the formula

$$D^*_{(\Theta)} = \frac{1}{\sin^2 \frac{\Theta}{2}} D^*(\pi), \qquad (2.7)$$

where $D^*(\pi)$ is the detection power of a detector having an aperture angle π.

When infrared detectors are used allowance must be made for the difference /64 between thermal and photon detectors, since the former react to the intensity of radiation but the latter to the rate of photon absorption. Thermal detectors have a spectral detection power D* equaling detection power D* for total black body radiation of any temperature, that is, $D_\lambda^* = D^*(T,f,\Delta f)$. This realtionship may not be satisfied for photon infrared radiation detectors. Hence knowledge of the detection power especially for low-temperature bodies is required for selective infrared detectors, ones such as detectors of Ge:Zn, Ge:Cu, Ge:Cd, Ge:Hg, and others.

The relationship of detection power D* for the total flux from a black body to the detection power based on the wavelength spectrum D* is according to [47] defined for a detector limited by photon noise by the formula

$$D^* = D_\lambda^* G, \tag{2.8}$$

with

$$G \approx \frac{2\pi\nu_0^3 k}{\sigma T_1^3 c_0^2} \exp\left(-\frac{h\nu_0}{kT_1}\right)\left[1+\frac{2kT_1}{h\nu_0}+2\left(\frac{kT_1}{h\nu_0}\right)^2\right],$$

$$D_\lambda^* = \frac{c_0[\eta(\nu_0)]^{1/2}\exp\left(\frac{h\nu_0}{2kT_2}\right)}{2\pi^{1/2}h^{1/2}\nu_0^2(kT_2)^{1/2}\left[1+\frac{2kT_2}{h\nu_0}+2\left(\frac{kT_2}{h\nu_0}\right)^2\right]^{1/2}},$$

where ν_0 is the photon equation, defining the longwave boundary of the infrared detector; c_0 is the velocity of light; k is the Boltzmann constant; h is the Planck constant; σ is the Stefan-Boltzmann constant; T_1, T_2 are the temperatures of an absolute black body and the background; and $\eta(\nu_0)$ is the quantum efficiency (assumed in the calculation to equal unity).

With the background and black body temperature and the longwave detector known, one can determine with sufficient accuracy D* (T_n,f,Δf) for black bodies of varying temperatures T_n provided that $h_{\nu 0} > kT_1$ and $h_{\gamma 0} \gg kT_2$.

Inasmuch as the detectors in question have an aperture angle of 26-28° and a cooling temperature of 51 ± 1°K, this being somewhat higher than the optimum [47,48], and $\eta(\nu_0)$ depends on the wavelength and is always smaller than unity, the equation given above may cause considerable errors in determination of D*. Hence additional study of D* for low-temperature bodies for determination of measurement error is of practical importance because of the fact that the radiation of a cloudless sky, say in the "water vapor window" of 8-12 μ, may have a radiation temperature of the order of 180°K [49]. /65

Various standards, black body models, are generally employed for comparison and determination of D*. Utilization factor q is introduced in determination of detection power D*. No work has been done on the basis of our information for determination of D* (T_n,f,Δf) of longwave radiation detectors for bodies having temperatures 200-300°K. We present the results of an experiment for determination of D* for black bodies of a temperature of 200-500°K with a Ge:Hg infrared detector cooled by solid nitrogen. The test unit with which the experiment was conducted is illustrated in Figure 20. The black body model 1 was represented by a disc blackened with carbon black and placed in a case with a heat-insulating jacket. The inner surfaces of the case and the surfaces of the disc were of a degree of blackness $b(\lambda) > 0.99$ in the range up to 15 μ as calculated on the basis of [50-51]. Vapors of liquid nitrogen were introduced into the interior of the case under low pressure. The rate of vapor flow was varied in order to /66

vary the temperature of the black body over the range of 200-298°K. Even cooling of the radiating disc was achieved by rotating the latter at a rate of 6000 rpm. The flow from the cooled black body was interrupted by modulator II of a frequency of 900 Hz similar in construction to black body I. The modulator was at a constant temperature of 180°K. The temperature of the black body and the modulator were checked by means of T1-15 petroleum ether thermometers graduated in the same medium.

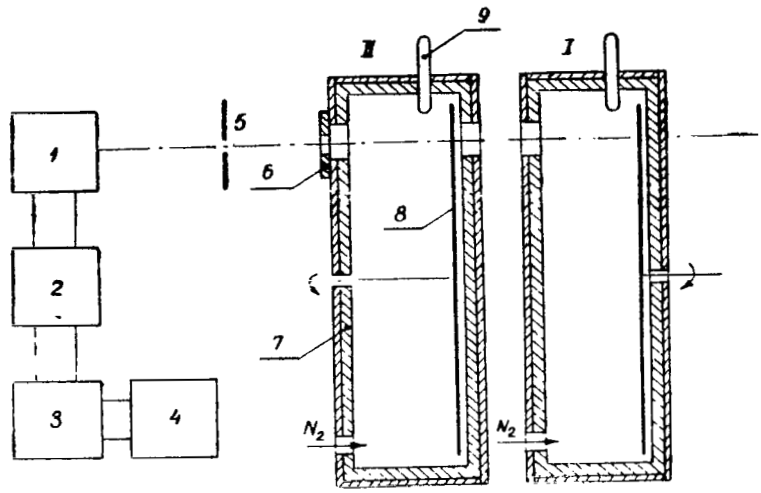

Figure 20. Block Diagram of Test Unit: I, Model of Absolute Black Body; II, Model of Absolute Black Modulator; 1, Radiation Detector; 2, Preamplifier; 3, V6-2 Selective Millivoltmeter; 4, ENO-1 Oscillograph; 5, Screen; 6, Diaphragm; 7, Heat-Insulating Jacket; 8, Rotating Disc with Blades; 9, Thermometer.

The low-temperature black body was replaced by a high-temperature heated one for determination of the detection power of Ge:Hg detectors or black bodies of a temperature of 298 to 500°K. The temperature of the black bodies was kept accurate to within 0.5°. The detector, modulator, black body, and diaphragm were arranged in such a way that the flux from the black body only was modulated. In order to make certain that the unmodulated background radiation would be constant, there was placed between the detector and the modulator a screen having an opening through which only modulated radiation passed. During the experiment the screen was at an ambient temperature of 298°. The signal from the detector was amplified by a preamplifier having an input resistance of R_{in} = 5.7 millohm and was fed to a V6-2 selective millivolt-meter with a band of Δf = 180 Hz. An ENO-1 oscillograph was employed for visual observation of the signal and noise. The study was conducted with two detectors, the cooling temperature of which was checked on the basis of their resistance. The detection power for bodies of different temperatures was calculated from the formulas

$$D^*(T_n, 900, 1) = \frac{AU_0}{\int_0^\infty r_\lambda(T_n)\,d\lambda - \int_0^\infty r_\lambda(180°)\,d\lambda}, \tag{2.9}$$

$$D^*_{(2-14)}(T_n, 900, 1) = \frac{AU_{c(2-14)}}{\int_0^\infty r_\lambda(T_n)S(\lambda)\,d\lambda - \int_0^\infty r_\lambda(180°)S(\lambda)\,d\lambda}, \tag{2.10}$$

/67

$$D^*_{(8-14)}(T_n, 900, 1) =$$

$$= \frac{AU_{c(8-14)}}{\int_0^\infty r_\lambda(T_n)S(\lambda)W_\Phi(\lambda)\,d\lambda - \int_0^\infty r_\lambda(180°)S(\lambda)W_\Phi(\lambda)\,d\lambda}, \tag{2.11}$$

$$A = \frac{\pi L^2}{g_{rr}}\sqrt{\frac{\Delta f}{g_{de}}}\frac{1}{U_n},$$

where D* (T_n, 900, 1) is the detection power of the detector for the total flux from a black body of temperature T_n; $D^*_{(2-14)}(T_n, 900, 1)$, $D^*_{(8-14)}(T_n, 900, 1)$ is the detection power for the effective flux from a black body of a temperature T_n over spectral ranges 2-14 and 8-14 μ respectively; T_n is the black body temperature, which ranges from 200 to 500°K; r_λ (180°), r_λ (T_n) is the spectral density of radiation of a black body of a temperature of 180°K and T_n^0; U_s, $U_{s(8-14)}$, and U_n are the signal voltages caused by the total and spectral fluxes, and the noise voltage, respectively, at the output of the V6-2 amplifier.

In the caluculations of D*, $D^*_{(2-14)}$, and $D^*_{(8-14)}$ the integrals were replaced with sums with a summation interval of 0.1 μ; the radiative flux losses in the absorption bands of the atmosphere were disregarded. Calculations of $r_\lambda(T_n)$, $r_\lambda(180°)$ over the temperature range from 180 to 300°k at intervals of ΔT=5°K were performed by means of a BESM-4 computer and reference tables [52]. The averaged results of the study are presented in Figure 21. A certain increase in the relative detection power for low-temperature radiation is to be observed in the graph. This unexpected aspect was verified in twelve experiments, the nature of the behavior of $D^*_{(2-14)}$ and $D^*_{(8-14)}$ being repeated in each of them. The slight increase in $D^*_{(2-14)}$ and $D^*_{(8-14)}$ may be ascribed to the difference in the radiation factor of the black body or modulator from unity. Thus with a radiation factor b(λ) = 0.99 the radiation from the surrounding background not absorbed by the black body (298°K) may lead to an error of 6.4% in determination of $D^*_{(8-14)}$ (213°, 900, 1). The temperature instability of the modulator and /68 black body, which equals 0.5°, may also lead to an error of 4-5% in determination of the detection power for black body radiation at a temperature of 213°K. Thus the anticipated total error may be ascribed both to the former and to the latter assumption; the latter is less probable, inasmuch as $D^*_{(2-14)}$ and $D^*_{(8-14)}$ might

decrease as well as increase. A third assumption regarding increase in the detection power for low-temperature radiation, that advanced in [47] and consisting in allowance for the relative number of photons per watt of power from radiation sources of different temperatures, cannot be accepted, since the cooling temperature of a Ge:Hg detector is 51°K rather than 30-35°K, and the longwave threshold of the detector equals 14 μ rather than 18 μ (a detector with a longwave limit of 18 μ can perform identical detection of radiation sources of a temperature both of 500°K and of 290°K in noise from a background of 290°K [47]). In determination of $D^*_{(2-14)}$ and $D^*_{(8-14)}$ allowance was made for the effective rather than the total flux. Hence only the first two assumptions can account for the increase in detecting power. /69

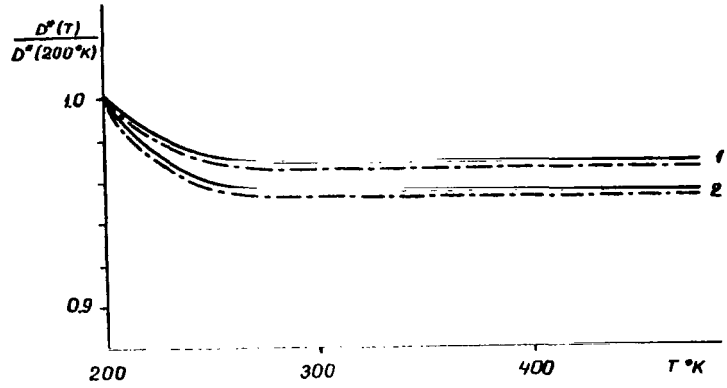

Figure 21. Detector Detection Power Versus Radiation Source Temperature. First detector: dot-and-dash curve; second detector: solid-line curve; 1, for Δλ=8-14 μ; 2, for Δλ=2-14 μ.

The variation in the utilization factor calculated for spectral regions of 2-14 μ and 8-14 μ and temperatures from 200 to 900°K is illustrated in Figure 22. To determine the relationship of D*, $D^*_{(2-14)}$, and $D^*_{(8-14)}$ the utilization factor was calculated with the formulas

$$q_{(2-14)} = \frac{\int_0^\infty r_\lambda(T_n)S(\lambda)d\lambda - \int_0^\infty r_\lambda(180°)S(\lambda)d\lambda}{\int_0^\infty r_\lambda(T_n)d\lambda - \int_0^\infty r_\lambda(180°)d\lambda}, \quad (2.12)$$

$$q_{(8-14)} = \frac{\int_0^\infty r_\lambda(T_n)S(\lambda)tW_\Phi(\lambda)d\lambda - \int_0^\infty r_\lambda(180°)S(\lambda)W_\Phi(\lambda)d\lambda}{\int_0^\infty r_\lambda(T_n)d\lambda - \int_0^\infty r_\lambda(180°)d\lambda}. \quad (2.13)$$

For the sake of comparison the behavior of q for a PbTe infrared detector cooled by liquid nitrogen [44] is illustrated in Figure 22. The comparison presented is that for a detector having an averaged spectral sensitivity characteristic. The behavior of factors q for Ge:Hg and PbTe detectors may be /70

utilized to solve practical problems relating to optimum indication of bodies of various temperatures. The maximum utilization factor, q = 0.39-0.40, corresponds for Ge:Hg detectors to temperatures of 430-480°K. In the case of detection of a flux distributed over the entire spectral band of the detector in accordance with the law of black body radiation distribution it may be inferred that for the indication of bodies having a temperature of 450°K and below it is advisable to use infrared detectors operating in the water-vapor window of 8-13 μ, and Ge:Hg and Ge:Zn detectors in particular.

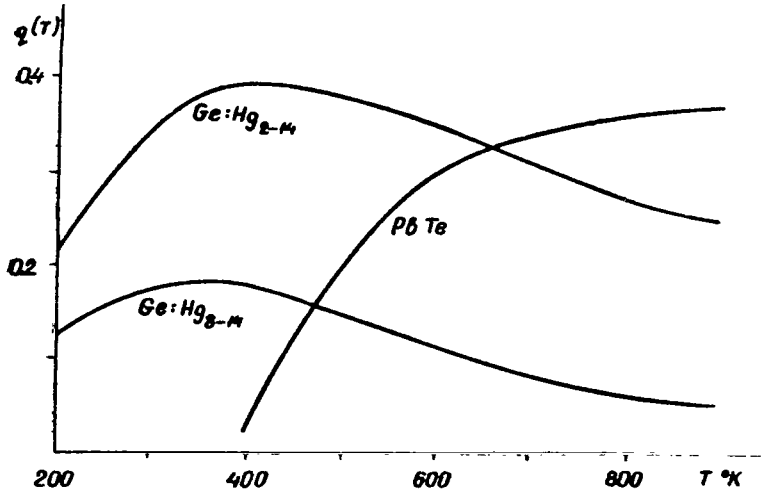

Figure 22. Utilization Factor q(T) of Various Detectors Versus Radiation Source Temperature.

E. Selection of Modulation Frequency

The noise power spectrum and frequency characteristic of the detectors were plotted for the purpose of determination of their maximum sensitivity. The noise power spectrum was recorded by means of an S5-3 harmonic analyzer. The /71 ratio of signal power to noise power is plotted against frequency in Figure 23, which illustrates a typical curve for three radiation detectors.

F. High-Speed Radiometer for Measurement of Spatial Inhomogeneities of Clouds

The results of the studies made of the parameters of the Ge:Hg radiation detector and comparison of the latter with other detectors in the water vapor window of 8-13 μ permitted the conclusion that it satisfies the requirements set (high speed, sensitivity, dynamic range, dependability, etc.) better than do detectors of Ge:Zn, Ge:Cd, Ge:Cu, Ge:Te and bolometers of various types. For example, at the same cooling temperature (51°K) Ge:Zn detectors are inferior in sensitivity to detectors based on Ge:Hg. Detectors of Ge:Cd require deeper cooling, and this complicates their use in radiometric equipment. It should be

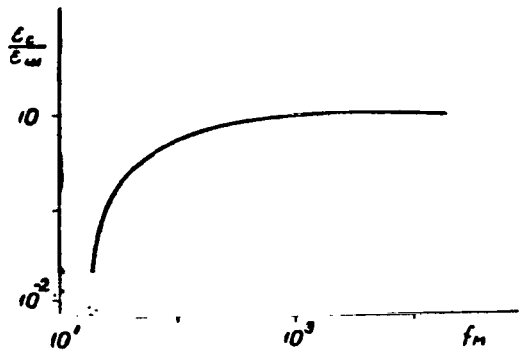

Figure 23. Relative Threshold Sensitivity of Detectors $\varepsilon_c/\varepsilon_m$ Versus Modulation Frequency f_m.

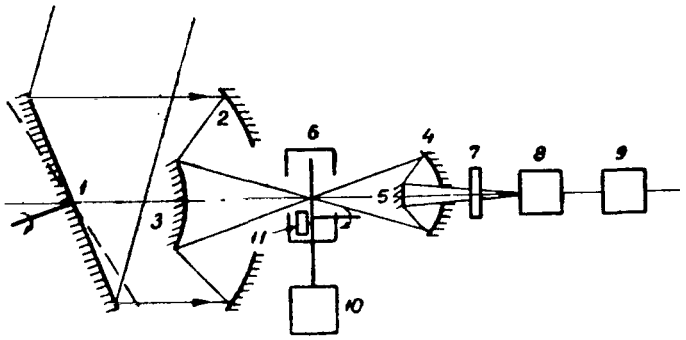

Figure 24. Block Diagram of Radiometer: 1-5, Optical System; 6, Modulator; 7, Filter; 8, Detector; 9, Recording System; 10, Temperature Regulation Device; 11, Temperature Sensing Element.

noted that the cooling requirements for a Ge:Hg detector also lead to inconvenience in operation, it being manifested chiefly in pouring of the nitrogen, exhausting the nitrogen vapors, and checking the sensitivity of the detector. However, the great number of its advantages over bolometers and other radiation detectors, as noted in the foregoing, indicate that it is advisable to use this detector in the radiometer. A block diagram of the radiometer is presented in Figure 24. The object being investigated and the comparison reference source, modulator 6, are placed on the axis of the optical system (mirrors 1-5), which focusses the radiation passing through filter 7 to detector 8 connected electrically to recording system 9. Reference source 6 is connected to device 10 for regulation of its temperature and is provided with temperature sensing element 11.

The independent control of the scanning mirror and the modulator reference source, and the displacement of the instantaneous viewing field of the instrument /72 in space in mutually perpendicular planes at different radiometer speeds, permit absolute and contrast measurements of the radiation of objects. The passband of the radioelectronic channel may vary over the frequency range $\Delta f=1\text{-}3 \cdot 10^4$ Hz as a function of the operating conditions of the radiometer, the rate of displacement of its instantaneous field of view in space, and the type of scanning [53].

The use of a modulator reference source of adjustable temperature makes it possible to set the brightness of the objects being investigated to equal that of the reference source. The method of equalizing the brightnesses of the reference source and the object under study by means of filters is described in [54]. This is accomplished by inserting between the infrared radiation detector and the reference source one of a group of neutral light filters until the signal degenerates into noise, this indicating equality of radiation of the reference source and the object under study. In this instance the temperature of the object is calculated on the basis of the known temperature values and the radiating power of the reference source, and on the basis of the transmission coefficient of the light filter inserted. This method is undoubtedly of merit, but applying it in low-temperature pyrometry occasions a number of difficulties, such as the need for using a large set of neutral light filters. Along with the indefinite /73 nature of their transmission coefficients, the accuracy of measurement of the temperature of slightly heated or cooled objects will also be affected by other factors: the natural radiation of the light filter inserted, the modulator, and other elements of the optical channels. The speed of operation of a device such as this is, of course, determined by the time required for equalization of the radiation of the reference source and the object under study, which cannot be great and depends on the skill of the person conducting the experiment. In the instrument described allowance must be made for the natural radiation of the lens, but the adequate speed of operation, sensitivity, spatial resolution, and independent scanning and reference source control represent unquestionable advantages permitting increase in the potential application of the instrument.

Comparison of the radiation of the object being studied with the modulator reference source is accomplished in a simpler manner than in [54]. For this purpose the modulator reference source is made in the form of a bladed disk blackened with carbon black. Because of the excess pressure inside the cavity it was possible to avoid freezing of the water vapor on the disk and in the cavity itself. A stream of the working gas, nitrogen, of variable speed and temperature was used to vary the temperature of the reference source. The

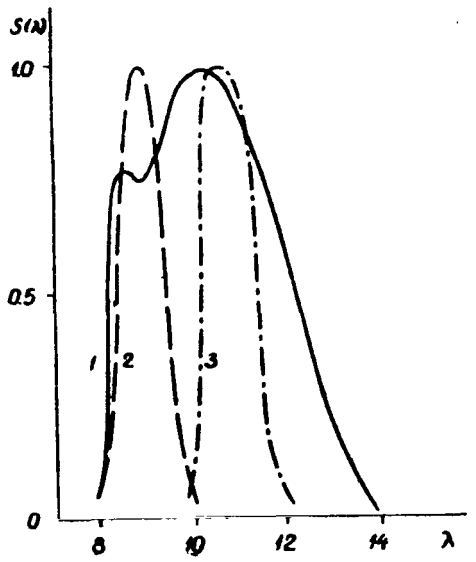

Figure 25. Relative Spectral Sensitivity of Radiometer with Different Interference Spectrometers.

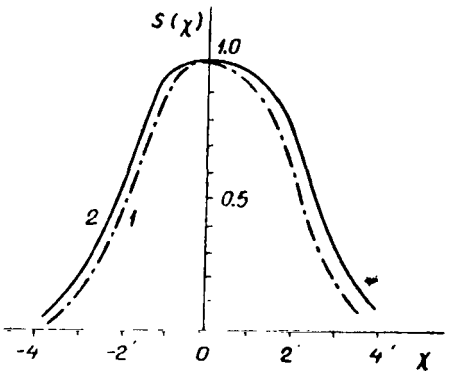

Figure 26. Distribution of Sensitivity over Instantaneous Field of View of Radiometer: 1, Horizontally; 2, Vertically. X, angle from optical axis of radiometer.

emerging stream of gas is not modulated and for this reason introduces no errors into the results of measurement. Equalization of the brightness or temperature of the object under study to that of the reference source is effected as it is in [54], to the point of degeneration of the signal into noise, the temperature reading of the reference source being taken from the temperature sensing element. The brightness equalization accuracy is determined by the sensitivity threshold of the radiation detector, while the accuracy of the absolute measurements depends chiefly on the accuracy of graduation of the heat sensing element (0.1°) and the graduation of the instrument (0.3°). Contrast measurement can be accomplished with the modulator either switched on or off, circular scanning with an angle of turn of 10° of the field of view in space being employed.

As was stated earlier, the position of the field of view may also be displaced through the azimuth and zenith angle at varying speeds by means of reducing gears. /74 For the purpose of visual observation of objects being measured the radiometer is provided with an optical system combined with the instantaneous field of view of the instrument. The instrument has the following parameters:

(1) threshold sensitivity to energy brightness in the spectral range of 8-14 μ, $\varepsilon_m(i) = 10^{-6} w \cdot cm^{-2} \cdot ster^{-1}$;

(2) the spectral range (Figure 25) is selected by interference light filters and can be widened considerably into the shortwave region of the spectrum;

(3) instantaneous field of view of the instrument, $1.4 \cdot 10^{-3} \times 1.4 \cdot 10^{-3}$ rad;

(4) the error of absolute measurement in the 180-320°K temperature range is 0.5°; this has been assured as a result of study of the radiation detector parameters;

(5) scanning: (a) circular: scanning frequency 7 Hz; (b) linear: angular /75 azimuth displacement from 4'/sec to 30°/sec; angular zenith angle displacement from 4'/sec to 9°/sec.

(6) modulation frequency 15 kHz.

These parameters were obtained by use of Ge:Hg radiation detectors with an angle of view of 26-28° made to conform to the radiometer lens, so that it was possible virtually to eliminate internal instrument radiation exposure. The design of the detector and of the modulator radiation reference source makes it possible to vary the phase of the radiation relative to the pulse polarity. The radiometer was graduated by the well known methods [55-57]. Hot and cooled black body models were used as radiators. To allow for the natural radiation of the lens the radiometer was installed in a BKK-8000 heat and pressure chamber the temperature of which varied from -10 to +30°C. The radiometer was graduated on the basis of sources situated at distances of 0.5 and 80 m from the instrument. The graduation curves based on the temperature are presented in Figure 27, which shows series of curves for the spectral regions of 10-11.5 and 8-12 μ characterizing variation in the signal as a function of the black body temperature, with the comparison source at constant temperature. The signal degenerates into noise

when the temperatures of the comparison source and the black body are equal. It should be noted that the behavior of the curves for radiation source temperatures below 220°K has been determined by theeretical calculations. The amplitude of the /76 modulated energy brightness was determined from the formula

$$I_m = \int_0^\infty \{[I(\lambda, T) W_{\text{атм}}(\lambda) + I(\lambda, T_{\text{атм}})] W_0(\lambda) + \\ + I(\lambda, T_{\text{атм}}) W'_{\text{атм}}(\lambda) - I(\lambda, T_2) W''_{\text{атм}}(\lambda)\} S(\lambda_n) d\lambda, \quad (2.14)$$

in which $I(\lambda, T_1)$ and $I(\lambda, T_2)$ are the spectral energy brightness of the source and modulator at temperatures T_1 and T_2; $I(\lambda, T_{atm})$ and $I_0(\lambda, T_{atm})$ are the spec- /77 tral energy density of the air column and the lens at temperature T_{atm}; $S(\lambda_n)$ is the relative spectral sensitivity of the instrument as determined by the spectral characteristic of the radiation detector and the interference filter *n = 1, 2, 3 is the filter number); $W_{atm}(\lambda)$ is the transmission of the air column between the black body and the radiation detector; $W'_{atm}(\lambda)$ is the transmission of the air column between the lens (mirrors 1-3) and the infrared detector; $W''_{atm}(\lambda)$ is the transmission of the air column between the modulator and the infrared detector; and $W_0(\lambda)$ is the transmission of the lens.

Generally speaking $I_0(\lambda, T_{atm})$ depends both on the relative aperture of the optical system and on the transmission of each of the lens mirrors. It may be disregarded in measurements of radiation sources of 180°K and above, since the integral lens radiation value over the range $\Delta\lambda$=8-13 μ is equivalent to the black body temperature, approximately 170°K (at a mirror temperature of 298°K), owing to the small radiation coefficients of the mirror layers. Over the spectral range of 8-13 μ the air column trasmission is near unity under graduation conditions, while its radiation virtually equals zero, so that formula (2.14) is simplified to

$$I_m = \int_0^\infty [I(\lambda, T_1) W_0(\lambda) - I(\lambda, T_2)] S(\lambda_n) d\lambda. \quad (2.15)$$

The sensitivity to monochromatic radiation was determined from the formula

$$I(\lambda_n) = \frac{S(\lambda_n) \Delta U_c}{\int_0^\infty S(\lambda_n) \Delta I(\lambda, T_1, T_2) d\lambda}, \quad (2.16)$$

in which $\Delta I(\lambda, T_1, T_2)$ is the recorded contrast brightness, and ΔU_s is the signal at the radiometer output caused by modulated radiation I_m.

The brightness and temperature threshold sensitivity was determined from the formulas

$$\varepsilon_m(I) = \frac{U_n}{\Delta U_c} I_m; \quad \varepsilon_m(T) = \frac{U_n}{\Delta U_c} \Delta T, \quad (2.17)$$

in which U_n is the noise voltage of the recording system.

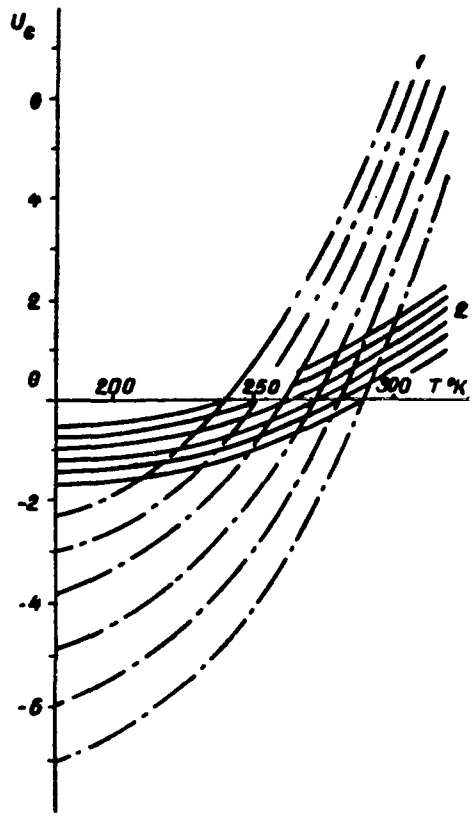

Figure 27. Graduation Characteristics of Radiometer:
1,$\Delta\lambda$ = 8-13 μ; 2,$\Delta\lambda$ = 10-11.5 μ.

By means of the circular scanning of the instrument mirror one can measure /78
the value of the spatial inhomogeneities of the object under study by expanding the periodic signal from the optical system into a Fourier series [58] by means of a computer or spectral analyzer (in our case the S5-3 harmonic analyzer, the Minsk computer, and the BESM-4).

Linear or circular scanning, or simultaneous linear and circular scanning, makes it possible to derive a stationary and ergodic process from cloud formations; this is of importance in obtaining the statistical brightness characteristics of various forms of clouds and in investigating the isotropicity of cloud radiation fields. Fluctuations in the radiation of various clouds over the spectral range of 8014 μ were measured by means of the instrument described [59].

Section 5. Ground and Aircraft Systems and Measurement Methods

A. Ground Measurements

The ground measurements were generally conducted at a stationary point at the Tyravere Observatory. Certain episodic measurements based on an incomplete

program were conducted at Dnepropetrovsk and later by means of a mobile laboratory at various points in Estonia.

The full array of ground research currently includes the following measurements:

1. Recording of the fluxes of total (or scattered) and direct radiation by means of an M-80 pyranometer and AT-50 actinometer mounted on a heliostat.

2. Recording of brightness in the shortwave region of the spectrum in the direction of the zenith by means of the equipment described in Section 2.

3. Recording of brightness in the longwave region of the spectrum in the direction of the zenith by means of the equipment described in Section 2.

4. Measurement of distribution of brightness over the sky by scanning within the limits of 180° through the zenith with a narrow-angle scanning instrument (See Chapter II, Section 2).

5. Determination of the angular velocity of displacement of clouds in the zone around the zenith.

6. Photographing (or filming) of the cloud cover. /79

7. Visual observations of cloud conditions.

Electron potentiometers of the EPP-09 or EPPV-60 type were used as recording instruments for all the recorders. The tape advance rate is 1200mm/hr, with the exception of the scanning detector recording instrument, which has a rate of 9600 mm/hr. A system was employed of synchronous recording of time signals on the recording instrument tapes either manually or automatically by a contact clock. The possibility was additionally provided of parallel recording of the results on punched tape (See the following section). The entire system was operated by one or two observer operators.

The ground observations were conducted irregularly; cases of "pure" cloudiness were selected insofar as possible, and generally during the hours around noon. The duration of observation, which was determined by the steadiness of the cloud cover, ranged from 1 to 4 hours.

Measurements using the equipment described in Section 3 of this chapter were conducted from ground observation points in accordance with a special program and independently of the other studies.

B. Aircraft Measurements

The aircraft measurements in 1967-1969 were conducted in airplanes of the Il-14 type of the Ukrainian Hydrometeorological Scientific Research Institute over the territory of the Ukraine, in conjunction with other research on the physics of clouds and radiative heat exchange. Starting in 1970 an An-2 airplane was used and flights were made over the territory of the Baltic republics and

Leningrad Oblast along various routes as determined by the synoptic situation. The following measurements were performed:

1. Recording of the fluxes of total and reflected radiation by means of M-80 pyranometers situated at the top and the bottom of the aircraft fuselage.

2. Recording of brightness in the shortwave region of the spectrum in the direction of the zenith and the nadir by means of the equipment described in Section 2 of this Chapter (See Figure 11). /80

3. Recording of the shortwave albedo.

4. Visual observations of the cloud cover.

5. Recording of the speed, flight altitude, and heading of the aircraft, and of the temperature on the basis of the aircraft instruments, as well as the ground meteorological data at the request of the State Air Weather Service along the route at the time of overflight.

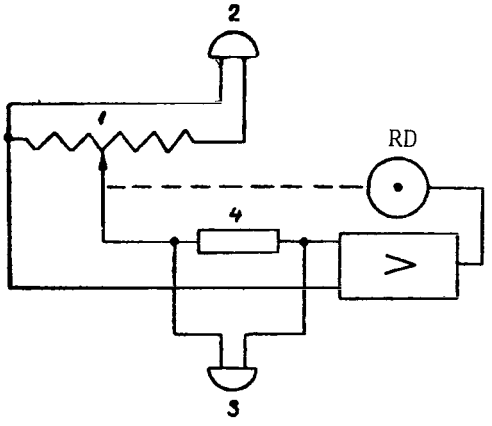

Figure 28. Block Diagram of Aircraft System for Measurement of Shortwave Albedo: 1, Slide Wire of Electron Potentiometer; 2 and 3, Pyranometers Directed Upward and Downward; 4, Shunt for Lower Pyranometer; RD, Reversible Motor.

Electron potentiometers of the KBT type (manufactured in the GDR) with a tape advance rate of 1200 mm/hr were used as the recording instruments for the fluxes of total and reflected radiation. A third potentiometer and two additional pyranometers directed upward and downward were employed for direct recording of the shortwave albedo (Figure 28). For this purpose the measuring bridge was disconnected from slide wire 1 of the potentiometer and the supply to the slide wire was taken from upper pyranometer 2. The signal from the lower pyranometer, shunted by resistance 4 for sensitivity matching of the pyranometers, was delivered to the potentiometer input. As a result, the potentiometer reading was proportional to the ratio R_k/Q, or in other words, to the instantaneous value /81

of shortwave albedo A_k. Graduation of the system is very simple: in the absence of a signal from the lower pyranometer a reading is obtained which corresponds to $A_k = 0$, and the reading $A_k = 1$ when the exposure of the two pyranometers is the same, so that all intermediate values of A_k will fall between these extreme points over an evenly divided scale.

All three electron potentiometers are supplied by the aircraft power supply network by means of a converter of direct current (27 v) to alternating current (220 v) of a frequency of 50 Hz and power of 200 w. The converter was transistorized on the basis of a circuit kindly made available to us by Yu. Reemann. In addition, provision was made for recording synchronous time marks on the electron potentiometer tapes.

The aircraft measurement system was operated by two observers. The aircraft measurements were conducted in horizontal flight, generally under clouds, but sometimes also above the cloud stratum or between strata, over specific routes within the limits of a particular cloud system. The observation stretch ranged from 50 to 500 km, depending on the concrete situation.

Section 6. Automation of Primary Data Processing

As was stated earlier, all the measurement results were recorded on the tapes of electron potentiometers or loop oscillographs, and final processing of the data was effected in a digital computer. Preparation of the initial material for the computer involves considerable expenditure of time and labor, since it is necessary to take the ordinates from the recording instrument tapes with a small discretization interval and record the results on punched tape. Hence a simple angle-to-code converter was developed for the EPP-09 and KBT electron potentiometers, one which provided the measurement results in digital code simultaneously with the recording on the tape. The converter is a cylinder with the /82 code mask of the eight-digit Gray code applied to it. All the code tracks are electrically isolated from each other and have individual leads. In addition to the code tracks, there are two contact tracks on the cylinder for the electric power supply of the system. The cylinder is fixed in position on the slide wire of the electron potentiometer. A contact group consisting of a series of contacts sliding over the surface of the code cylinder, which are arranged in one row parallel to the axis of the cylinder and connected electrically to each other, is connected mechanically to the sliding contact of the slide wire (slide wire shaft). Depending on the arrangement of the sliding contacts (turning angle of the slide wire axis), the voltage from the power supply tracks is fed through the sliding contacts to the leads of the digits whose uninsulated sections are under the contacts. A diagram of the converter is presented in Figure 29. For the sake of simplicity a four-digit code mask is illustrated. The converters for the EPP-09 and KBT are identical in principle, differing only in structural design. The eight-digit binary code (Gray code) was selected on the basis of the accuracy classification of electron potentiometers, in order to ensure that the conversion error would be no greater than the potentiometer error.

The parallel eight-digit code obtained at the output of the converter may be fed directly to the input of an eight-channel tape puncher, but since the majority

of digital computers (in our case chiefly a computer of the "Minsk" type) have a /83
five-channel input, it is necessary to reshape the code output by the converter. For this purpose a special matching and control desk was developed, by means of which the eight-digit code from the converter output is converted to two consecutive four-digit characters which are output to the puncher. First the more recent four digits are punched, and then the older ones. After each character (two four-digit signals) the desk shapes a dividing signal, which is also punched in the tape to avoid errors associated with possible intermissions in the system. In addition, the matching and control desk has a control signal generator permitting interrogation of the converter and punching at time intervals of 1, 2, 3, 6, or 10 sec, as well as on the basis of external timing signals. With each punching cycle a pulse is emitted which may be used to synchronize the operation of other instruments, such as time-lapse motion picture equipment. There is a keyboard for manual insertion of additional characters and data into the tape. In a number of cases it is necessary to know the amount of numbers in the array, for which purpose an electromechanical pulse counter is incorporated in the system. A /84
block diagram of the punching system is presented in Figure 30.

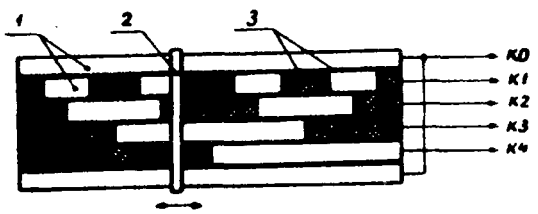

Figure 29. Diagram of Angle-to-Code Converter Code Mask: 1, Current-Conducting Sections; 2, Sliding Contacts; 3, Insulating Sections; K0, Converter Power Supply Tracks; K1-K4, Leads of Individual Digits.

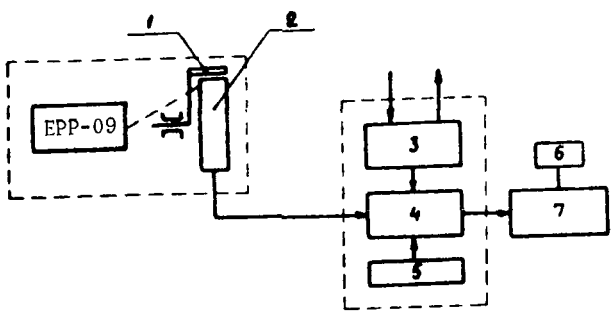

Figure 30. Block Diagram of System for Recording of Data on Punched Tape: 1, Sliding Contacts of Angle-to-Code Converter; 3, Converter Code Mask; 3, Control Signal Generator; 4, Code Converter; 5, Keyboard; 6, Counter; 7, Tape Puncher.

Owing to a shortage of punchers and transitional units, in our experiments not all of the results were recorded on punched tape directly in the measurement process. Hence a part of the tapes containing the results of ground measurements and all the aircraft data had to be processed after the measurements had been performed. In accordance with the example presented in [60] a system of semi-automatic tape reading was devised. The basic portion of the system is represented by a stabilized adjustable voltage source with the shaft of the master potentiometer of the latter connected to an angle-to-code converter analogous to that described in the foregoing. The output voltage, which can be adjusted manually by means of a knob, is fed to the input of the electron potentiometer on which the tape to be processed is displaced and the pen of which is replaced by a pointer. Constant following of the curve recorded on the tape is accomplished by rotating the knob of the master potentiometer (electron potentiometer slide wire). The output signal from the converter is recorded in the punched tape in a manner analogous to that described in the foregoing. Experience acquired in use of the system indicates that in the processing of tapes the rate of tape advance may be three times faster than in the measurement process, but if the operator is sufficiently experienced the errors are negligible.

CHAPTER III. THE STOCHASTIC STRUCTURE OF CLOUD FIELDS /85

Section 1. Average Characteristics of Cumulus Clouds

In meteorological practice the cloud cover is usually characterized by the quantity and shape of clouds. For the majority of cases, however, these characteristics provide too little information for study of the structure of cloud fields and their interrelations with the structure of radiation fields. In the present work the cloud cover is additionally characterized by the coverage of individual zones and narrow directions of sighting, as well as by the quantity and shape of clouds (See Chapter I).

The quantity of clouds in the atmosphere is most often determined at the present time on the basis of ground or satellite observations. In the case of ground observations the quantity of clouds is expressed as the percentage of cloud coverage of an imaginary hemisphere having the observation point as its center, this quantity being termed "relative cloudiness." By projection of the clouds onto an imaginary sphere having its center at the center of the Earth or, in the plane-parallel model of the atmosphere, onto a horizontal surface, the mean quantity of clouds, called "absolute cloudiness," is obtained. Note that absolute cloudiness coincides with the mean cloud coverage of the zenith averaged over space. A value near that of absolute cloudiness may be obtained on the basis of satellite photographs taken at small angles to the zenith. In view of the considerable vertical dimensions (thickness) of cumulus clouds, the probability of coverage of the direction of sighting increases with increase in the zenith angle of observation. The absolute cloudiness value is consequently always smaller than the relative value. /86

We now proceed to discussion of the laws governing increase in coverage of the direction of sighting toward the horizon. We employ the ejection theory for purposes of theoretical analysis.

Consider a vertical cross-section of a normal random surface $\xi(x)$ bounded at altitude Z (Figure 6a). Taking [61, 62] into account, we find that the average multiplicity of intersection of the direction of sighting with function $\xi(x)$ at the entrances will be

$$N(\vartheta)=\frac{1}{2}+\frac{1}{2}\operatorname{erf}\frac{\cot\vartheta}{\sqrt{2}\,\sigma_{z'}}+\frac{\sigma_{z'}}{\sqrt{2\pi}\cot\vartheta}e^{-\frac{\cot^2\vartheta}{2\sigma^2_{z'}}} \tag{3.1}$$

in which $\sigma^2_{z'}$ is the dispersion of the slopes of the normal random surface in direction x, and erf is the probability interval.

The mean multiplicity of intersections at the exits is expressed by

$$M(\vartheta)=N(\vartheta)-1, \tag{3.2}$$

and the mean multiplicity of exits from surface $\xi(x)$ to level Z will be

$$M_Z(\vartheta) = n(0)M(\vartheta) = n(0)[N(\vartheta) - 1], \tag{3.3}$$

in which $n(0) = N_Z(0)$ is the mean multiplicity of entrances into the surface to level Z at $\vartheta = 0$, that is, the mean cloud coverage of the zenith.

Assuming the exits from the surface to be statistically independent, on the basis of the Poisson distribution we obtain the probability that the direction of sighting entering a cloud will exit through its base:

$$P_0 = e^{-n(0)[N(\vartheta)-1]}, \tag{3.4}$$

and the direction of sighting will exit from the sides of clouds from 1 to an infinite number of times with probability $1 - P_0$.

The probability of finding a cloud in the direction of sighting consists of the sum of the probability of exits of the direction of sighting from the base and sides of clouds, that is,

$$n(\vartheta) = n(0)e^{-n(0)[N(\vartheta)-1]} - e^{-n(0)[N(\vartheta)-1]} + 1. \tag{3.5}$$

As is to be seen from formula (3.5), up to zenith sighting distances /87
$\vartheta \leq \pi/2 - \vartheta_{n,max}$, in which $\theta_{n,max}$ is the maximum slope of the sides of the clouds, the probability of coverage of the direction of sighting is constant, and at large sighting angles probability $n(\vartheta)$ increases monotonically, approaching unity when $\theta \to \pi/2$.

When the Poisson distribution is used for the mean number of intersections there is no need for determining the combined probabilities of finding a random surface along different sections of the line of sight [30, 63]; this greatly simplifies solution of the problem assigned. We must note that there are as yet no empirical data for determination of the conbined probabilities. In the region of variation of zenith angles, in which $M_Z(\vartheta)$ is small, the exits from the surface are correlated and formula (3.5) yields slightly understated values for $n(\theta)$.

If the field is isotropic, the relative cloudiness is determined from the formula

$$n = \int_0^{\pi/2} n(\vartheta)\sin\vartheta\, d\vartheta. \tag{3.6}$$

The relationship of the coverage of the direction of sighting with clouds, $n(\theta)$, to the zenith angle of observation can be determined by employing the cloud frequency $\varkappa$ (average number of clouds or gaps per unit length), the probability density of distribution of gaps between clouds, p(s), and the probability density of the vertical thickness of individual clouds p(h) [64]:

$$n(\vartheta) = 1 - \varkappa \int_0^\infty p(h)\,dh \int_{h\,\mathrm{tg}\,\vartheta}^\infty (s - h\,\mathrm{tg}\,\vartheta)\,p(s)\,ds. \tag{3.7}$$

In derivation of formula (3.7) the clouds were approximated by straight cylinders having bases of arbitrary configuration, while the distribution function of the probabilities of the horizontal and vertical dimensions of the cloud cover were assumed to be statistically independent. Cloud frequency κ and probability density p(s) were determined empirically on the basis of ground and aircraft measurements (See Section 3 of this chapter). Empirical determination of p(h) entails great difficulties; hence it was necessary to restirct ourselves to the mean effective thickness, making use of formula (3.7). Only slight errors result if this thickness is skillfully selected [64]. /88

In [35-37] cumulus clouds are approximated as cylinders forming a Poisson flux. Poisson flux approximation yields exaggerated values for $n(\vartheta)$ when $n(0) > 0.6$. The reason for this is that cumulus clouds are not distributed independently of each other in space; rather extensive correlation of the clouds present is observed (See the following sections). With maximum decrease in the quantity of clouds at the zenith, that is, when $n(0) \to 0$, the cloud elements obtained in theory by limitation of the random Gaussian surface at the bottom also form a Poisson flux. The clouds present may be assumed [29] to be uncorrelated if $n(0) < 0.03$. This last-named circumstance also explains the close agreement of all models at small values of n(0).

The increase in cloudiness toward the horizon was determined empirically on the basis of photographs). The sky coverages at intervals of 10°, with zenith distances ranging from 5 to 85°, have been determined by processing the phtographs.

Figure 31 illustrates typical coverages of the direction of sighting as a function of the zenith angle as determined on the basis of individual photographs at a relative cloudiness of 0.5. Averaging over the azimuth up to zenith distances of 75-80° is obviously inadequate for obtaining stable mean values. In individual instances a monotonic behavior of $n(\vartheta)$ is established even at $\vartheta \approx 70°$. The dispersions of coverages of the direction of sighting averaged over the azimuth as a function of zenith angle ϑ are presented in Section 6 of this chapter.

Sky coverages averaged over photographs at a relative cloudiness of 0.1 to 0.9, as a function of the zenith direction of sighting, are shown in Figure 32. A monotonic trace of the curve up to small zenith distances is established with a number of photographs no smaller than 25.

The mean values of parameters $\sigma_{z'}$ and n(0) are obtained by use of the results shown in Figure 32 for calculations based on formula (3.7). It is found that $\sigma_{z'}$ /90 increases somewhat with increase in the amount of relative cloudiness. Unfortunately, the small number of experiments and their low accuracy prevented positive establishment of the lastnamed relationship. On the average the root mean square deviation of the derivative for a normal random surface equals $\sigma_{z'} = 1.2$.

The mean coverages of the direction of sighting calculated with formula (3.7) are plotted in Figure 33 against the zenith angle of the direction of sighting. Comparison of Figure 32 and Figure 33 indicates satisfactory agreement between the empirical and theoretical results (formula (3.7)). In the case

of cumulus clouds the coverage of the direction of sighting begins to increase substantially starting at the zenith distance of around 50°. The latter, for example, reduces the duration of sunshine with decrease in the altitude of the Sun with the cloudiness condition remaining unchanged. /91

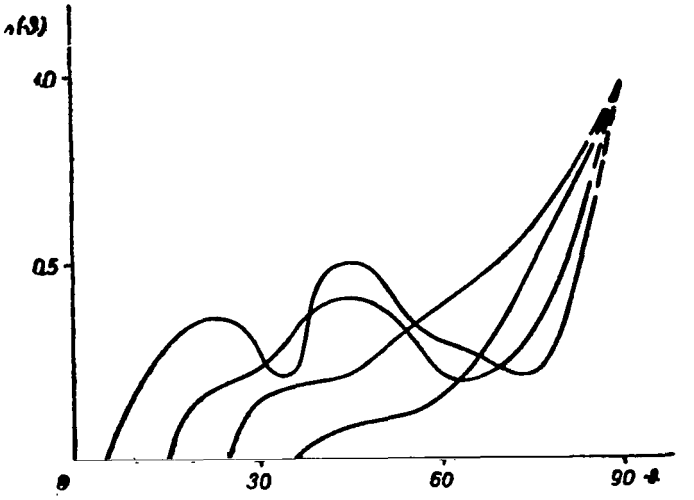

Figure 31. Coverage of Direction of Sighting n (ϑ) Versus Zenith Angle ϑ, Obtained on the Basis of Individual Photographs at a Relative Cloudiness of 0.5. /89

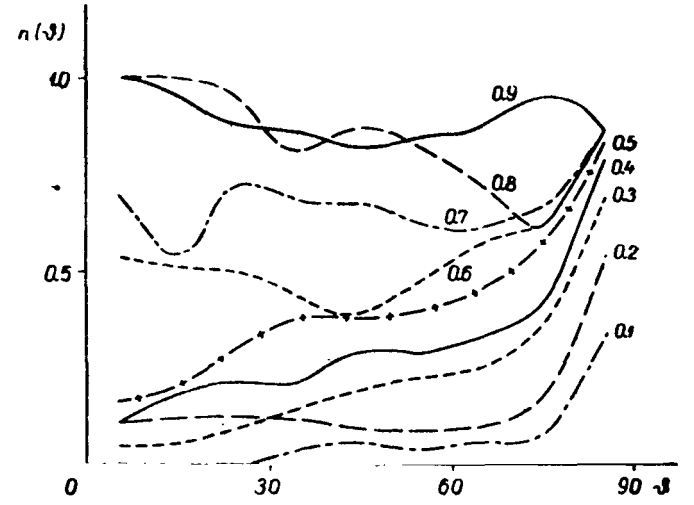

Figure 32. Coverages of Direction of Sighting n (ϑ) Averaged over Photographs Versus Zenith Angle ϑ at a Relative Cloudiness of 0.1 to 0.9.

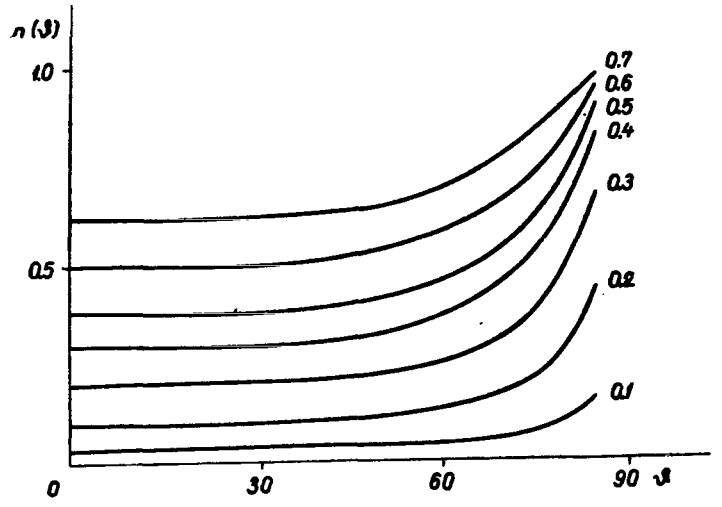

Figure 33. Mean Coverages of the Direction of Sighting $n(\vartheta)$ Calculated on the Basis of Formula (3.7) Versus Zenith Angle ϑ with a Relative Cloudiness Ranging from 0.1 to 0.7.

The amount of relative cloudiness always exceeds the mean coverage at the zenith. The differences are at the maximum when n(0) = 0.5, being 0.13 on the average. The relationship between the relative and the absolute cloudiness may be described by the following empirical formula:

$$n = n(0) + 0.5[1 - n(0)]n(0). \tag{3.8}$$

Relation (3.8) is illustrated in Figure 34. With zenith coverages ranging from 0.1 to 0.2 formula (3.8) yields values for the relative cloudiness which are somewhat understated in comparison to the empirical data. With low cloudiness values the relationship between the relative and the absolute cloudiness is described more accurately by approximation formula (5.8), which is given in Chapter V, Section 1. However, the latter yields exaggerated values for relative cloudiness when $0.3 < n(0) < 0.8$ and is less convenient to use in theoretical calculations and numerical operations.

Section 2. The Statistic Structure of Cumulus Cloud Fields /92

To study the structure and distribution of cumulus clouds within cloud masses recording on the ground of coverage of the sky with clouds in the direction of the zenith and the Sun was conducted along with photographing of the sky, and aircraft measurements were also made of the presence of clouds in the direction of the zenith (nadir) along the route of flight. Study of cloudiness from aircraft was conducted above the Ukraine in 1967-1969 in collaboration with the Ukrainian Hydrometeorological Research Institute, and starting in 1970 above the Baltic Republics and Leningrad Oblast. Correlation and spectral analysis of the time and space cross-sections of the cloud fields was performed. The cloud cover

was simulated by a sequence of rectangular pulses (see Chapter I, Section 6). Analysis was made of the results of 102 observations of the presence of cumulus clouds. Of this number, 55 observations were completely processed. It is to be noted that information on the statistical structure of the cloud cover may also be obtained by processing photographs of the sky. However, automated processing of photographs entails considerable difficulty, since there are no satisfactory methods of distinguishing clouds from the clear sky against a variable background.

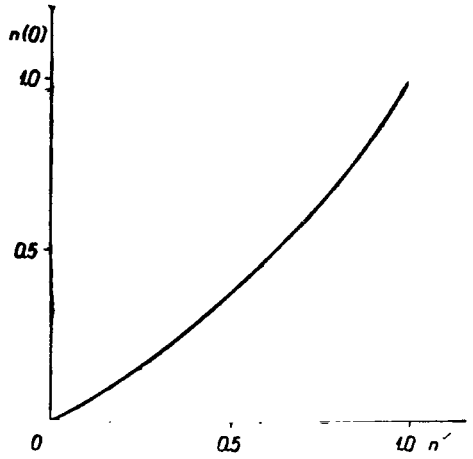

Figure 34. Relative Cloudiness Versus Absolute Cloudiness Value Calculated with Formula (3.8).

The results of the experimental studies have been grouped on the basis of the mean cloud coverages of the direction of the zenith or Sun. The studies of cloud coverage of the Sun were in the vast majority of cases conducted at zenith distances $\vartheta < 50°$. As may be seen from the results presented in the preceding section, virtually no increase in cloudiness toward the horizon is observed at zenith distances of $\vartheta < 50°$. This circumstance also explains the fact established empirically by us that the statistical structure of cloud coverage of narrow directions of sighting is in effect independent of the angle of observation at zenith angle $\vartheta < 50°$. On the basis of the foregoing, we do not examine coverages in the direction of the Sun and zenith separately in performing our analysis.

If the cloud cover is simulated by a sequence of rectangular pulses, the dispersion of the presence of clouds is expressed by the simple relation

$$\sigma^2_{n(0)} = n(0) - n^2(0). \tag{3.9}$$

As may be seen from formula (3.9) the dispersion is at the maximum with n(0) = /94
= 0.5 and decreases with decrease or increase in the mean coverage at the zenith.

Typical autocorrelation functions of the presence of clouds at $0.45 \leqslant n(0) \leqslant 0.55$ for ground measurements and at $0.35 \leqslant n(0) \leqslant 0.45$ for aircraft measurements are presented in Figure 35, a and b. As this drawing shows, the empirically determined correlation functions are characterized by considerable dispersion, which increases with increase in displacement in time or space. The chief reasons for this are the limited number of observations, the variability of the meteorological situation from observation to observation (see Chapter I, Sections 1, 3), and in the case of ground measurements also the variation in the rate of cloud displacement. Hence in theoretical analysis we employ correlation functions averaged over the aggregate number of observations (Figure 36). A dependence of the correlation function on the mean coverage of the zenith, n(0), was detected /95

only for the ground measurements, since the aircraft measurements relate chiefly to zenith coverage cases n(0) = 0.3-0.4. As may be seen from Figure 36, the correlation is at the maximum with n(0) = 0.5, and the correlation scale contracts with increase or decrease in n(0).

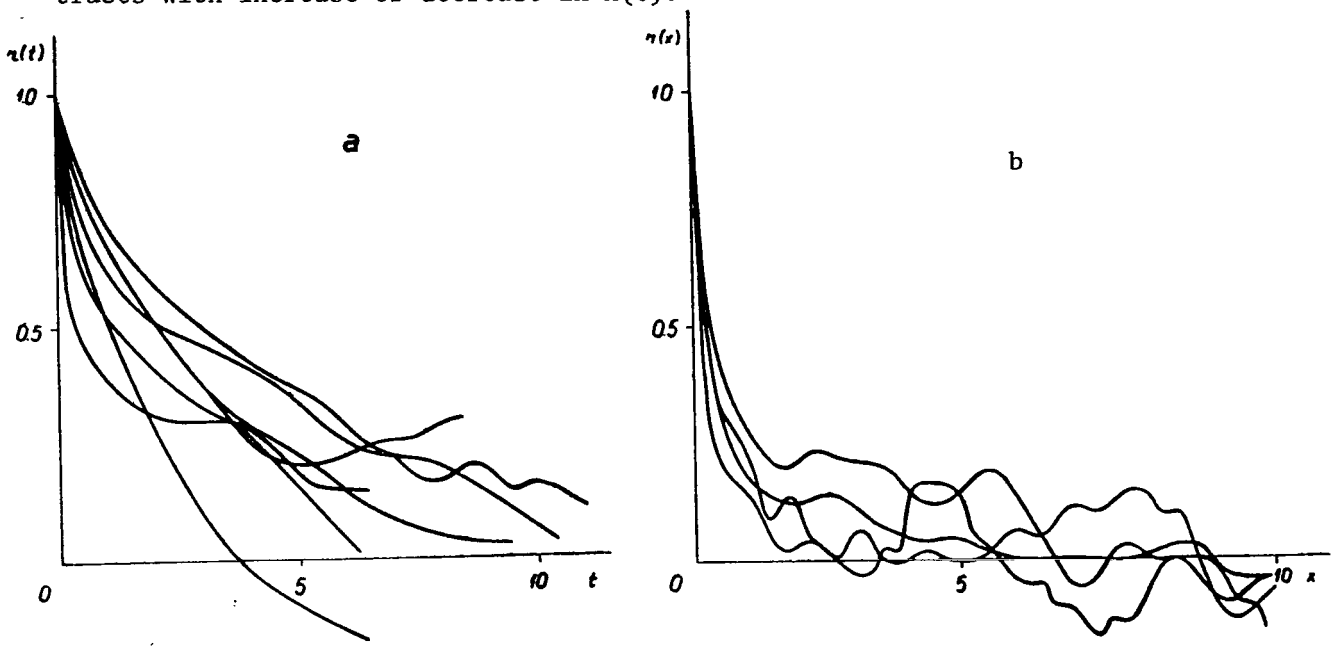

Figure 35. Examples of Autocorrelation Functions of Coverage of Zenith by Cumulus Clouds: a, Ground Measurements at n(0) = = 0.5 (t = Time, min); b, Aircraft Measurements at n(0) = = 0.4 (x = Space Coordinate, km).

In simulation of the cloud cover by a normal random process (see Chapter I, Section 6) the theoretical autocorrelation function of the process of occurrence of clouds over the cloud field cross-section is of the form [28, 29]

$$r_{n(0)}(t) = \frac{1}{n(0) - n^2(0)} \sum_{k=1}^{\infty} \left[\Phi^{(k)}\left(\frac{w}{\sigma}\right) \right]^2 \frac{r^k_{\xi}(t)}{k!}, \qquad (3.10)$$

in which $\Phi^{(k)}$ is the derivative of order k of the probability integral, w/σ is the relative cutoff level, and $r_{\xi}(t)$ is the correlation function of a normal random process.

If n(0) = 0.5, that is, $w/\sigma = 0$, the expression for correlation function (3.10) is simplified and assumes the form

$$r_{0.5}(t) = \frac{2}{\pi} \arcsin r_{\xi}(t). \qquad (3.11)$$

The empirically determined mean correlation functions of the presence of clouds over the cloud field cross-section for n(0) from 0.1 to 0.9 are closely approximated by the formula taken from [34]

$$r_{n(0)}(t) = \frac{2}{\pi} \arcsin e^{-\alpha[n(0)]\cdot|t|} \qquad (3.12)$$

and parameter α as a function of n(0) may be expressed by the formula

$$\alpha[n(0)] = 0.27 + 0.8[n(0) - 0.5]^2. \qquad (3.13)$$

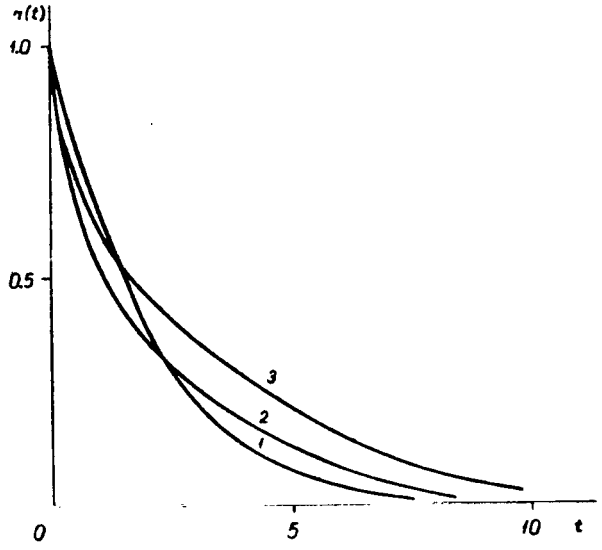

Figure 36. Autocorrelation Functions, Averaged over Aggregate Number of Observations, of Coverage of Zenith by Cumulus Clouds Based on Ground Measurements (t = Time, min): 1, n(0) = 0.8; 2, n(0) = 0.2; 3, n(0) = 0.5.

The space function of the correlation is obtained by multiplying parameter $\alpha[n(0)]$ in expression (3.12) by 3.0 and replacing time t in minutes by space coordinate x in km. Parameter α is plotted against n(0) on the basis of formula (3.13) for ground and aircraft measurements in Figure 37, in which dots and crosses designate the empircally determined values. As may be seen from Figure 37, in the first approximation the empirical data confirmed the theoretically derived trace of $\alpha[n(0)]$. The small number of empirical ground studies at $n(0) > 0.5$ and the absence of aircraft studies under the same conditions prevent study of the possible asymmetry relative to $\alpha[n(0)] = 0.5$ /96

When n(0) = 0.4 the empirically determined values of the parameters are considerably larger than the theoretical ones determined on the basis of formula (3.13). Since when n(0) = 0.3, 0.4, and 0.5 sufficient empirical material is available for the drawing of statistical conclusions, a divergence such as this indicates the existence of substantial departures of the process under study from the normal random model if $n(0) \approx 0.4$. According to the theoretical model the amount of clouds increases from 0.3 to 0.4 chiefly as the result of increase in the dimensions of the individual clouds, but under natural conditions increase in cloudiness as a result of increase of the number of clouds predominates over this range. It is this which explains the increase in parameter α at $n(0) \approx 0.4$, that is, the "contraction" of the correlation function.

Figures 38-40 illustrate the spectral densities of the presence of clouds and gaps as calculated on the basis of the autocorrelation function. The spectral densities at n(0) = 0.5 for individual observations are given in Figure 38, while Figure 39 presents the spectral densities grouped according to n(0) and averaged over the observations. Comparison of Figures 36 and 38 reveals that /99

widening of the energy spectrum corresponds to contraction of the correlation time. This conclusion is a very general one.

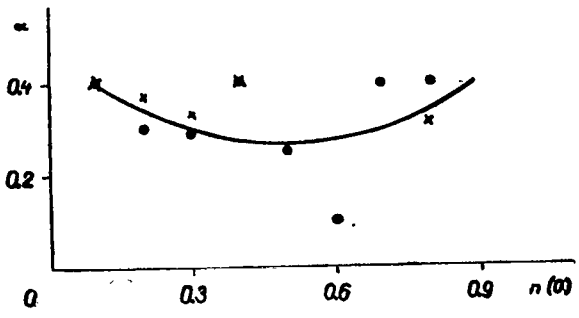

Figure 37. Parameter α, min^{-1}, Versus n(0): the Curve was Obtained by Use of Formula (3.13); the Dots Denote Values Based on Ground Measurements and the Crosses Values Based on Aircraft Measurements.

The spectral densities in the range of linear frequencies f from 0.12 to 2.4 min^{-1} are closely approximated by the formula $S(f) \sim f^{-k}$, in which exponent k ranges from 5/3 to 4/3 (Figure 40). Exponent k is the smallest when n(0) = 0.5 and increases with increase or decrease in the mean coverage at the zenith.

Section 3. Distribution Functions of Cloudiness Parameters

The cloud cover is characterized by the probability densities of the various elements of cloud formations as well as by the results of spectral correlation analysis.

In order to determine the parameters of distribution of the duration of cloud coverage of the zenith we employ the density of probability relative to the number of gaps or clouds p(s), which determine their share in the form of time t or length s of the time or space cross-section.

With n(0) = 0.5 and a correlation function of the presence of cloudiness of the form of (3.12), the theoretical formula for the probability density of the number of gaps or clouds is of the form

$$p(s)=\frac{\alpha(0.5)}{\pi}\frac{e^{-\alpha(0.5)s}}{[1-e^{-2\alpha(0.5)s}]^{1/2}}, \qquad (3.14)$$

in which parameter $\alpha(0.5)$ is determined from formula (3.13).

Formula (3.14) was derived on the assumption that the normal random process is at the same time also a Markovian one [65, 66]. According to the properties of continuous Markovian processes, formula (3.14) is not applicable when $s \to 0$.

The empirically obtained probability densities averaged over the observations and grouped according to n(0) in the interval from 0.1 to 0.9 are closely approximated by the formula taken from [34]

$$p[s, n(0)]=\frac{\alpha_s[n(0)]}{\pi}\frac{e^{-\alpha_s[n(0)]s}}{\{1-e^{-2\alpha_s[n(0)]s}\}^{1/2}}, \qquad (3.15)$$

in which parameter α_s as a function of n(0) is described by the empirical expression /100

$$a_s[n(0)]=0.27\pm0.8[n(0)-0.5]^2. \quad (3.16)$$

which is analogous to formula (3.13).

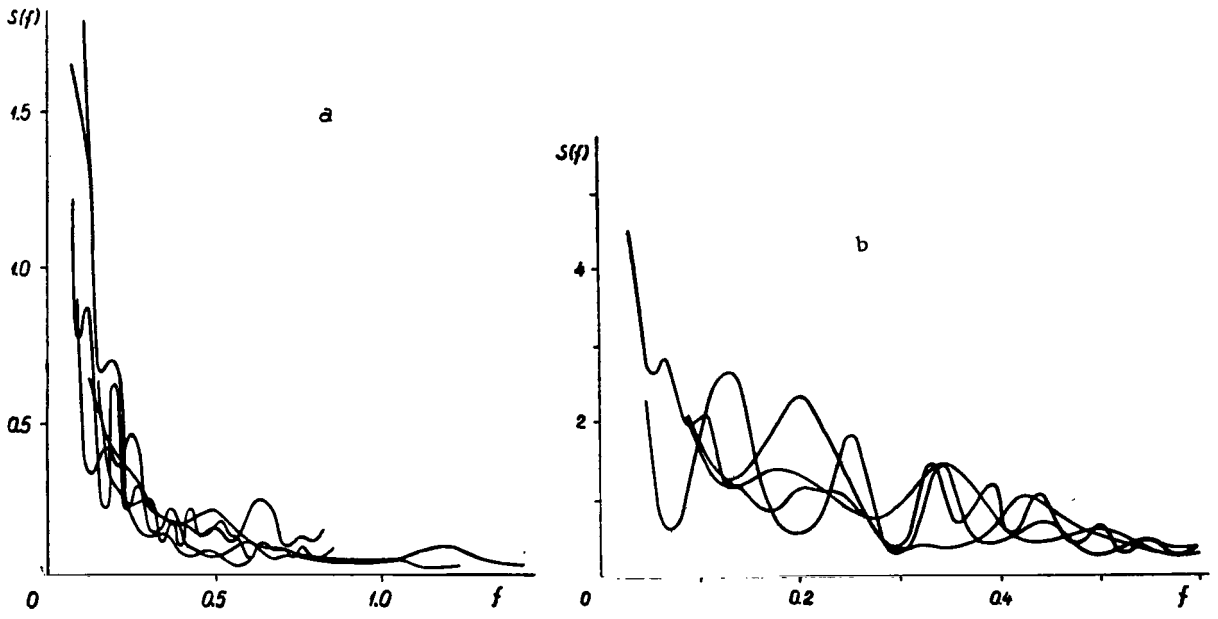

Figure 38. Examples of Spectral Densities of Zenith Coverage by Cumulus Clouds (in Relative Units): Ground Measurements at n(0) = 0.5 (f in min^{-1}); b, Aircraft Measurements at n(0) = 0.4 (f in km^{-1}). /97

In the calculations of the probability density of the number of clouds as a function of their duration, in formula (3.16) the "+" corresponds to $n(0) - 0.5 < 0$, and the "–" to $n(0) - 0.5 > 0$.

The probability density for gaps is obtained by replacing n(0) in formulas (3.15) and (3.16) with the mean probability of a free line of sight c(0) = 1 – – n(0).

The empirically determined probability densities of the numbers of clouds /101 are plotted against their duration in Figure 41. It is to be seen that short gaps and small clouds are the ones the most often encountered over the cloud field cross-section. Formula (3.15) and the curves in Figure 41 characterize the cloud cover at zenith angles of the direction of sighting $\vartheta < 50°$. At large zenith distances an essential role is played by the lateral portions of the clouds (see Chapter III, Section 1), which reduce the apparent dimensions

of the gaps. It is to be observed that the probability densities determined over the cloud field cross-section on the bases of (3.15) do not coincide with the probability densities of distribution of the basis of the clouds based on the dimensions (area).

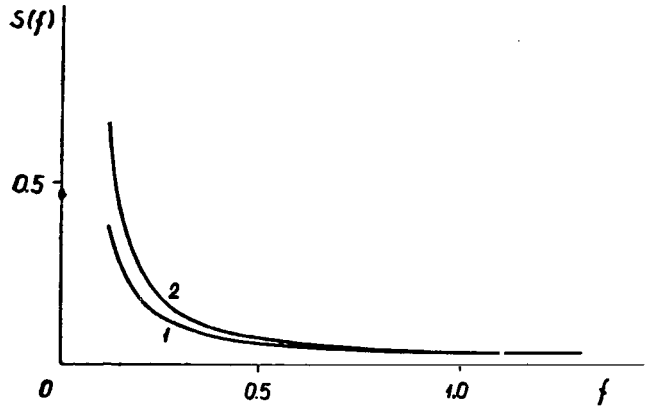

Figure 39. Spectral Densities of Presence of Clouds and Gaps at the Zenith Based on Ground Measurements, Grouped According to n(0) and Averaged Over Observations: 1, n(0) = = 0.5; 2, n(0) = 0.2 or 0.8 (f in min^{-1}).

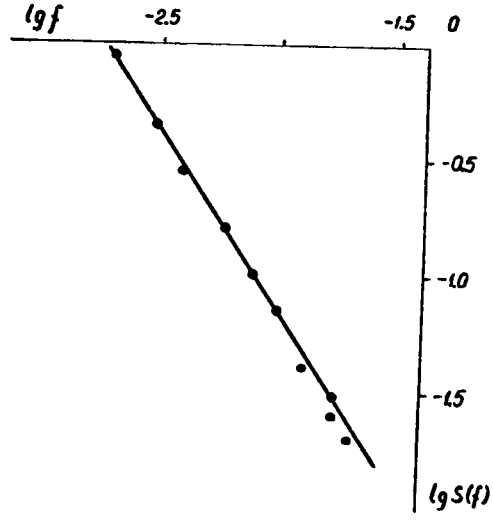

/98

Figure 40. Spectral Density, Averaged over Observations, of Zenith Coverage by Cumulus Clouds Based on Ground Measurements on Logarithmic Scale with n(0) = 0.5.

By approximation of the basis of clouds as circles of diameter D, and on the assumption that the cloud field is isotropic, in [36] the probability density is derived for the distribution of clouds over the diameters on the cloud field cross-section:

$$p(D)=-\frac{2}{\pi}D^2\frac{d}{dD}\left[D\int_D^\infty\frac{p(s)ds}{s^2(s^2-D^2)^{1/2}}\right] \tag{3.17}$$

The distribution function of clouds on the basis of area can easily be derived from the latter:

$$p_S(D)=\frac{p(D)}{D\int_D^\infty p(D_1)\frac{dD_1}{D_1}}. \tag{3.18}$$

We see by comparing formulas (3.17) and (3.18) with formula (3.15) that the weight of the short cloud cross-sections considerably exceeds that of the small clouds. In this case $p(D = 0) = p_S(0) = 0$. However, as has already been observed in [36], the calculations based on the formulas entail substantial errors. Empirical studies of the distribution of the bases of clouds by areas are thus needed to solve this problem.

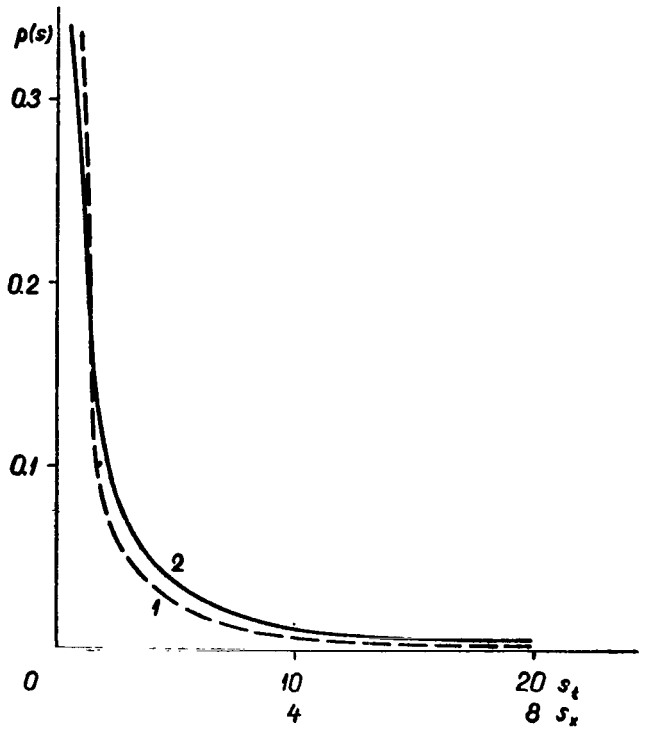

/100

Figure 41. Probability Densities, Averaged over Observations, of Dimensions of Cumulus Clouds Based on Ground (s_t in min) and Aircraft (s_x in km) Measurements: 1, n(0) = 0.1; 2, n(0) = 0.9.

As may be seen from the foregoing, the probability densities of distribution of the number of gaps or clouds are virtually independent of the mean coverage of the zenith. The cloud frequency, that is, the number of them per unit time in ground measurements or per unit length in aircraft measurements, is more sensitive to variation in n(0).

For a normal random model the frequency of clouds and gaps is expressed by the formula /102

$$\varkappa[n(0)]=\frac{1}{2\pi}\frac{\sigma_{z'}}{\sigma_z}\exp\{-[\arg\operatorname{erf}|1-2n(0)|]^2\}, \tag{3.19}$$

in which σ_z and $\sigma_{z'}$ are the root mean square deviations of the normal random surface and its derivative from the mean.

The relationship of the frequencies of clouds and gaps is illustrated in Figure 42, in which the solid-line curve corresponds to calculations based on formula (3.19) and the dots and crosses represent the results of empirical ground and aircraft studies averaged over the observations and grouped according to n(0). The cloud frequency is at the maximum when n(0) = 0.5 and

undergoes nearly twofold variation with variation in zenith coverage n(0) from 0.1 to 0.9. Owing to the small number of experimental studies the cloud frequency at n(0) = 0.7 is characterized by the greatest error. It is to be noted /103 that the experimental studies are also insufficient for investigation of possible asymmetry of the curve of cloud frequency relative to the frequency at n(0) = = 0.5.

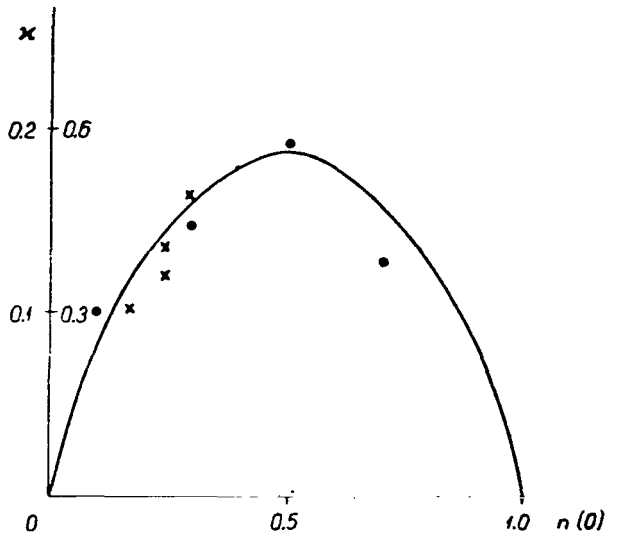

Figure 42. Frequency (in min^{-1}) of Cumulus Clouds at the Zenith: Curve, Values Based on Formula (3.17); •, Values Based on Ground Measurements, ×, Values Based on Aircraft Measurements.

By approximating the cloud frequency with formula (3.19) we find that $\frac{1}{2\pi}\frac{\sigma_{z'}}{\sigma_z} = 0.18$ min^{-1} or 0.45 km^{-1}. But it is found from the observations of increase in cloudiness towards the horizon (Chapter III, Section 1) that $\sigma_{z'} = 1.2$. Hence evaluation of the root mean square deviation of the normal random surface yields $\sigma_z = 0.4$ km^{-1}. The latter determines the distribution function of the probabilities of a normal random process

$$p[h, n(0)] = \frac{1}{0.4\sqrt{2\pi}\, n(0)} e^{-\frac{(h+w)^2}{2\cdot 0.4^2}}, \qquad (3.20)$$

which, in keeping with the model, describes the distribution of the surfaces of cumulus clouds with increase in altitude. In this instance h ranges from 0 to ∞, while w = arg erf [1 - 2n(0)], if $n(0) \geqslant 0.5$, or w = -arg erf [2n(0) - 1], if $n(0) \leqslant 0.5$.

On the basis of the results obtained in studies of the structure of cumulus clouds and in keeping with [29] it may be inferred that the altitudes of the summits of individual clouds are also distributed normally. Empirical

determination of the distribution of the summits in altitude remains a task for subsequent research.

We employ two-dimensional distribution functions to describe the distribution of coverage of the direction of sighting in a cross-section of cloud fields in time or space. The probabilities that the directions of sighting at moments separated by interval t in time (or interval x in space) will be covered with clouds or free of clouds are expressed respectively by the formulas

$$P[n(0), n(0), t] = r_{n(0)}(t)[n(0) - n^2(0)] + n^2(0) \tag{3.21}$$

and

$$P[c(0), c(0), t] = P[1 - n(0), 1 - n(0), t] = \\ = r_{n(0)}(t)[n(0) - n^2(0)] + [n(0) - 1]^2. \tag{3.22}$$

For the combined probability of observation of clouds at a particular moment and their absence after time interval t we obtain /104

$$P[n(0), c(0), t] = P[c(0), n(0), t] = n(0) - P[n(0), n(0), t] = \\ = [1 - r_{n(0)}(t)][n(0) - n^2(0)]. \tag{3.23}$$

/105

Formulas (3.21)-(3.23) have been normalized by the condition

$$P[n(0), n(0), t] + P[c(0), c(0), t] + 2P[n(0), c(0), t] = 1. \tag{3.24}$$

Figure 43 presents the entire body of two-dimensional functions P[n(0), n(0), t] obtained by way of experiment. The results of the empirical studies are grouped according to intervals $\Delta n(0) = 0.1$. The broken lines in Figure 43 reflect the probabilities at the ends of intervals n(0) calculated on the basis of formula (3.21) by use of correlation function (3.12). /106

The two-dimensional probabilities of the presence or absence of clouds for coverage interval $n(0) = 0.1$ to 0.9, as calculated on the basis of formulas (3.21)-(3.23) and (3.12), are illustrated in Figures 44 and 45.

As may be seen from Figures 43-45, the two-dimensional probabilities of the presence or absence of clouds do not depend on the interval if $t > 10$ min in the case of ground measurements and respectively $x > 4$ km in the case of aircraft.

Section 4. Representation of Cloud Distribution over the Sky by Means of Eigenfunctions

The statistical structure of the cloud cover in a time or space cross-section of the cloud field has been considered in the previous sections. However, owing chiefly to the increase in cloudiness towards the horizon, the vertical cross-section structure does not coincide with the zenith angle structure. The greatest differences are observed at $\vartheta > 50°$, at which the effect of shading is noticeable. To determine the parameters of the cloud structure in the sky we apply expansion of the presence of clouds on the basis of the optimum eigenvalues and eigenfunctions of the correlation matrix [6, 7]. The correlation matrix elements are represented by the coefficients of correlation /107

of the presence or absence of clouds at different zenith distances. It is to be noted that the expansion may be performed not merely on the basis of the eigenvalues and eigenfunctions of the correlation matrix but on that of any orthogonalized basis functions as well. It is clear, however, that expansion on the basis of arbitrary orthonormalized functions has neither physical nor statistical significance. From the statistical viewpoint expansion on the basis of the eigenfunctions of the correlation matrix corresponds to expansion to the basis /108
of the most frequently encountered combinations. The most frequently encountered eigenfunctions are those to which the largest eigenvalues correspond.

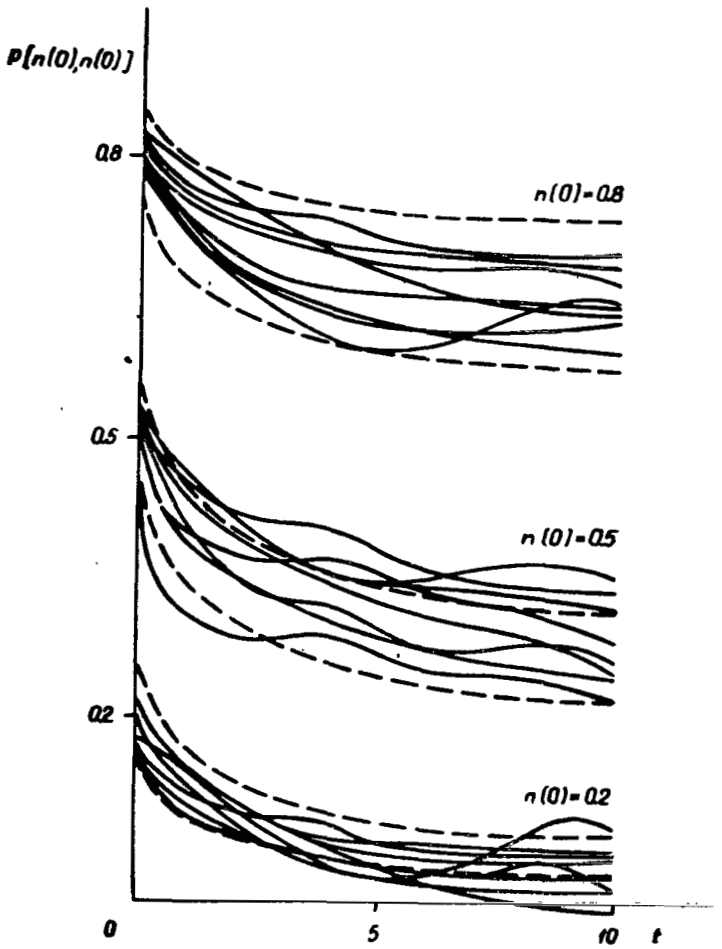

/104

Figure 43. Examples of Two-Dimensional Distribution Functions of Clouds or Gaps Calculated on the Basis of Formulas (3.21) and (3.22).

Making use of the results of the empirical results obtained by photographing the sky we have calculated, as a function of zenith angle ϑ, the eigenfunctions and eigenvalues for cloud coverage of the sky averaged over the azimuth and for the amount of relative zonal cloudiness. The normalized coefficients of /109

correlation at ϑ = 5, 35, or 65° with the coverages in directions ϑ = 5-85° for coverages of the direction of sighting averaged over the azimuth or for relative zonal cloudiness $K_{5\vartheta}$, $K_{35\vartheta}$ and $K_{65\vartheta}$ are presented in Figures 46-48. We see that the correlation coefficients are similar for different observations, and that the correlation radius decreases with increase in zenith angle ϑ. The latter circumstance is due to the averaging over the azimuth and to the fact that the distance in space increases with increase in the zenith angle at the same zenith angle distance. It is to be noted that the small number of experimental studies does not permit study of the relationship of the correlation matrices, as well as of the eigenvalues and eigenfunctions, to mean zenith coverage n(0). /110

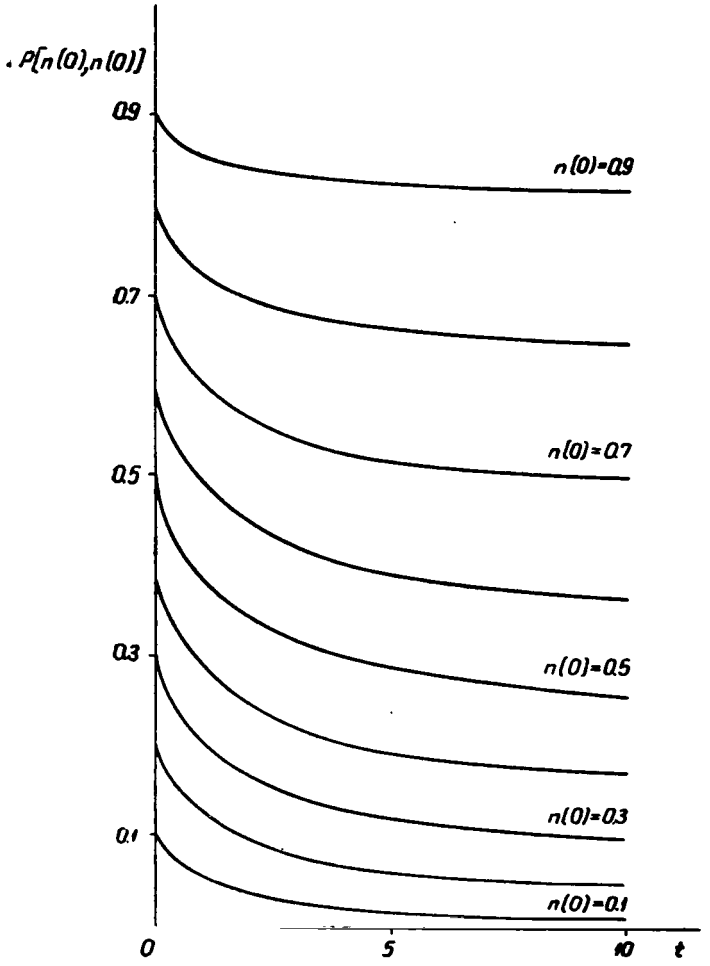

Figure 44. Two-Dimensional Distribution Functions of Clouds or Gaps Calculated on the Basis of Formulas (3.21) and (3.22).

/105

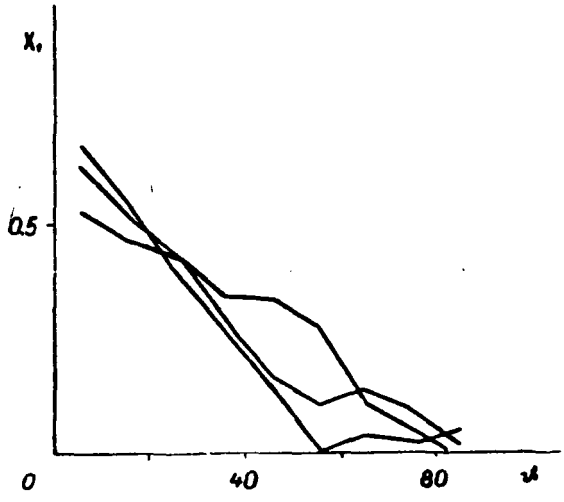

/106

Figure 45. Two-Dimensional Distribution Functions of Clouds of Gaps Calculated on the Basis of Formula (3.23).

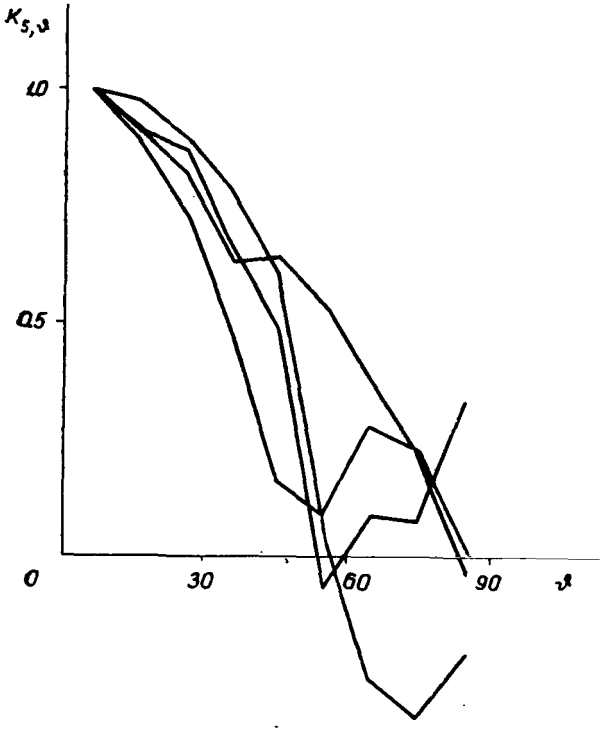

/107

Figure 46. Normalized Coefficients of Correlation of Sky Coverage with Cumulus Clouds Averaged over the Azimuth at ϑ = = 5° with Coverages at ϑ = 5-85°.

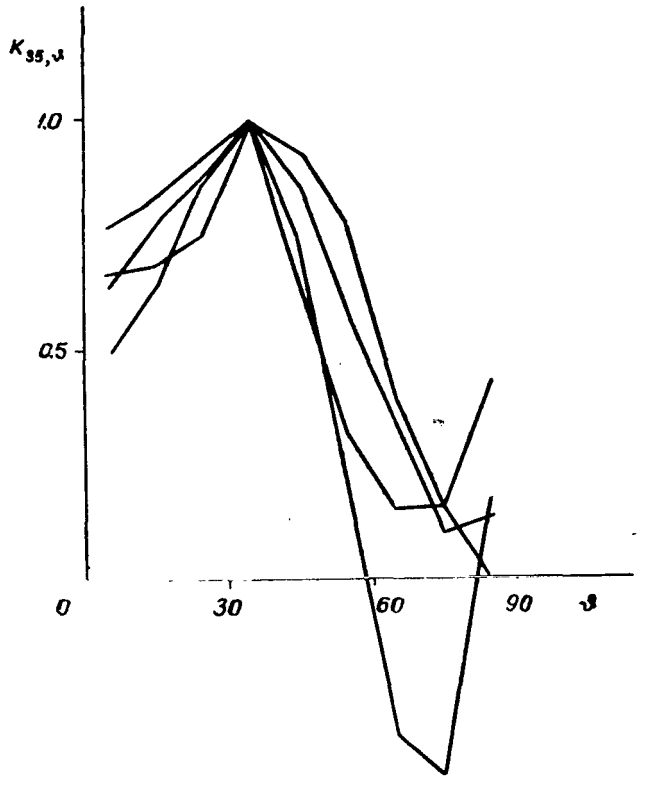

/108

Figure 47. Normalized Coefficients of Correlation of Sky Coverage with Cumulus Clouds Averaged over the Azimuth at ϑ = 35° with Coverages at ϑ = 5-85°.

Like the correlation coefficient (Figures 46-48), the eigenvalues of correlation matrix A as well do not vary appreciably from observation to observation. The eigenvalues and the relative accuracy of expansion when use is made of the first ith components for the coverage of the direction of sighting averaged over the azimuth are presented in Table 3. It is to be seen that the first eigenfunctions cover 65-79° of the dispersion, and the first 3 eigenfunctions 92-93%.

The first eigenfunctions $X_1(\vartheta)$ are shown in Figure 49. It is to be seen that they are close to each other from case to case. Attention is attracted by the circumstance that the first eigenfunctions have maximum values at the zenith and decrease monotonically with increase in the zenith angle of observation, coming to equal zero in the vicinity of the horizon. From the physical standpoint such a course of $X_1(\vartheta)$ signifies that the region around the zenith is the most frequently either completely covered with clouds or clouds are absent from it, but the horizon is constantly covered with clouds. The variability of the amount of clouds decreases in this case with increase in the zenith angles. The second eigenfunction (50) presents in some sense a distorted

/111

picture of the course of the first eigenfunction, in that the increase or decrease in the amount of clouds at the zenith is accompanied by corresponding decrease or increase in the amount of clouds at the mean zenith distances (40-60°). The third eigenfunction describes a finer structure of cloud cover variability based on zenith angles (Figure 51). Increase in cloudiness at the zenith is accompanied by simultaneous increase in it near the horizon (70°) and decrease in the area $\vartheta \approx 35°$, and vice versa.

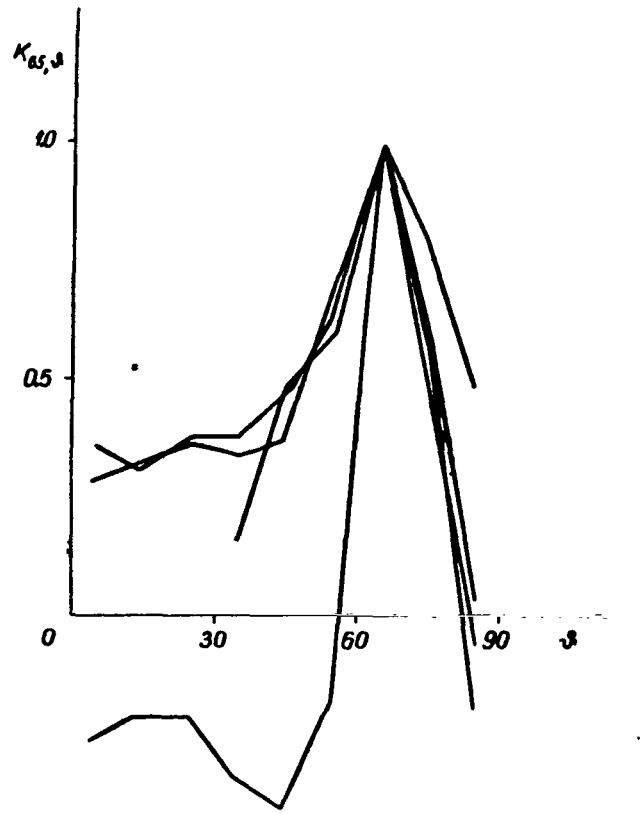

/109

Figure 48. Normalized Coefficients of Correlation of Coverage of the Sky with Cumulus Clouds Averaged over the Azimuth at $\vartheta = 65°$ with Coverages at $\vartheta =$ $= 5\text{-}85°$.

The similarity of the eigenfunctions from case to case decreases, as may be seen from Figures 49-51, as their index number becomes larger. This last-named /113 circumstance is quite natural, since they allow for a finer variability structure which does not recur from case to case.

The eigenfunctions vary widely starting with the fourth and for this reason do not lend themselves well to physical interpretation. Inasmuch as they are of but small weight in the total dispersion, we will not concern ourselves with them.

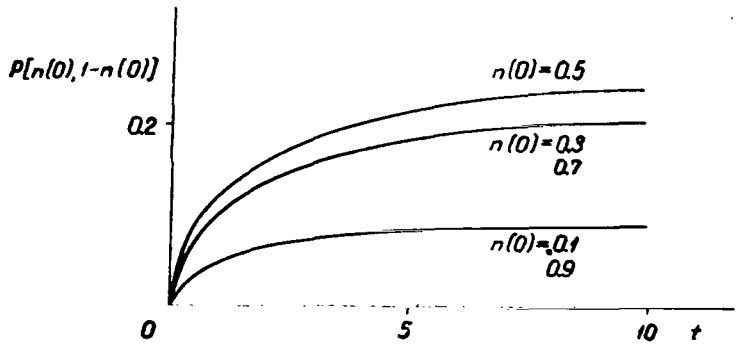

Figure 49. First Eigenfunctions of Sky Coverage by Cumulus Clouds Averaged over Azimuth Versus Zenith Angle ϑ.

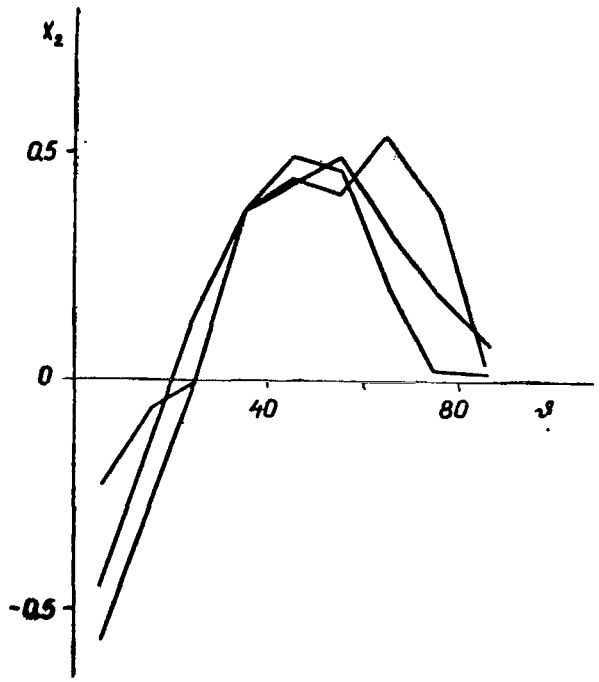

Figure 50. Second Eigenfunctions of Coverage of Sky by Cumulus Clouds Averaged over Azimuth Versus Zenith Angle ϑ.

The eigenvalues and eigenfunctions of the amount of relative zonal cloudiness were calculated for the same observations. The eigenvalues and the relative accuracy of expansion are presented in Table 4, the first kth components being used for the amount of relative zonal cloudiness. It is to be seen that the weight of the first eigenfunction is understated and that of the second exaggerated in comparison to the eigenvalues of the coverage of the direction of sighting averaged over the azimuth (Table 3). The first three eigenfunctions assure almost the same expansion accuracy in this case. They are presented respectively in Figures 52-54.

The first eigenfunction has its maximum at a zenith angle $\vartheta = 45°$, decreasing to zero at the zenith and on the horizon. The maximum is due to the greatest weight in relative cloudiness of the 45° zone, that is, the variability of the relative cloudiness is determined chiefly by the variability of the amount of clouds in the middle zone ($\vartheta = 30\text{-}60°$). The second and third eigenfunctions, like the coverage of the direction of sighting, describe a finer structure of cloud cover variability by zones. Comparison of Figures 49-51 with 52-54 reveals that the eigenfunctions differ more greatly among the individual cases in the latter figures. /115

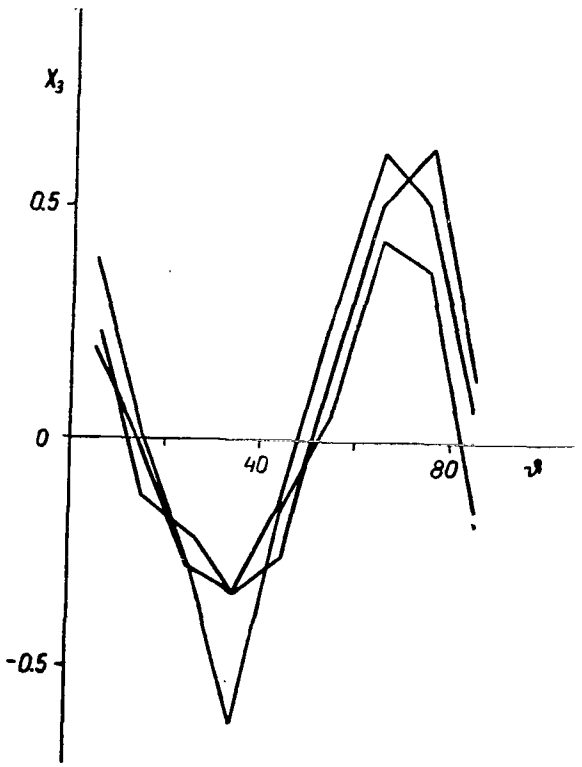

Figure 51. Third Eigenfunctions of Coverage of Sky by Cumulus Clouds Averaged over Azimuth Versus Zenith Angle ϑ.

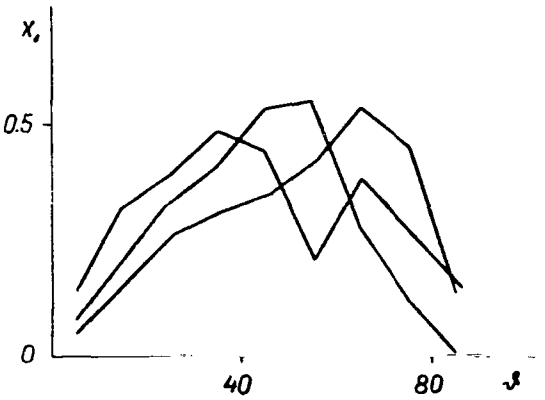

Figure 52. First Eigenfunctions of Amount of Relative Zonal Cloudiness Versus Zenith Distance of Zone.

Section 5. Relationships Among Statistical Characteristics of Various Cloudiness Parameters

Chiefly the results of investigation of the fine structure of cumulus cloud fields have been presented in the foregoing. Study has been made of the structure of the cloud coverage of narrow directions of sighting and the laws of distribution of the cloud cover over the sky as a function of the zenith angle of observation. At the same /116 time, on the one hand it is sufficient in meteorology for the solution of a large number of problems to characterize the cloud cover by various parameters averaged over space, such as the distribution of clouds over individual zones, the amount of the clouds over the entire sky, the amount of clouds over a certain territory, and so forth. On the other hand, the entire array of parameters required for complete discription of cloud fields is not always determined by way of experiment. For example, at weather stations study is usually confined to determination of the amount and shapes of clouds in the sky. In our aircraft studies instrument measurement was made only of the presence or absence of clouds at the zenith (nadir) along the flight route, while the amount of clouds in the sky was determined very roughly from the aircraft by visual estimate, the results in this case depending largely on the distance between the aircraft and the cloud layer and so forth. Hence for the purpose of comprehensive description of cloud structure it is highly essential to ascertain the relationships among the statistical characteristics of the various cloudiness parameters.

TABLE 3. EIGENVALUES OF COVERAGE OF DIRECTION OF SIGHTING AVERAGED OVER AZIMUTH

	$n(0) = 0.2$ $n = 0.5$ $N = 34$		$n(0) = 0.3$ $n = 0.4$ $N = 15$		$n(0) = 0.3$ $n = 0.5$ $N = 21$		$n(0) = 0.5$ $n = 0.7$ $N = 28$	
i	$S(X_i)$	λ_{i9}	$S(X_i)$	λ_{i9}	$S(X_i)$	λ_{i9}	$S(X_i)$	λ_{i9}
1	0.3528	65.0	0.4652	78.9	0.2849	77.5	0.4946	76.3
2	0.0966	82.7	0.0553	88.3	0.0341	86.7	0.0728	87.5
3	0.0595	93.5	0.0254	92.6	0.0180	91.6	0.0362	93.1
4	0.0124	95.6	0.0219	96.3	0.0117	94.8	0.0200	96.2
5	0.0075	97.2	0.0082	97.7	0.0081	97.0	0.0090	97.6
6	0.0057	98.2	0.0078	99.0	0.0067	98.8	0.0078	98.8
7	0.0039	99.2	0.0044	99.7	0.0030	99.6	0.0048	99.5
8	0.0033	99.8	0.0018	99.9	0.0011	99.9	0.0022	99.8
9	0.0014	100.0	0.0005	100.0	0.0009	100.0	0.0016	100.0

/110

TABLE 4. EIGENVALUES OF RELATIVE ZONAL CLOUDINESS

	$n(0) = 0.2$ $n = 0.5$ $N = 34$		$n(0) = 0.3$ $n = 0.4$ $N = 15$		$n(0) = 0.3$ $n = 0.5$ $N = 21$		$n(0) = 0.5$ $n = 0.7$ $N = 28$	
i	$S(X_i) \cdot 10^{-2}$	λ_{i9}	$S(X_i) \cdot 10^{-2}$	λ_{i9}	$S(X_i) \cdot 10^{-2}$	λ_{i9}	$S(X_i) \cdot 10^{-2}$	λ_{i9}
1	0.2465	55.0	0.2373	54.9	0.0974	48.6	0.3629	67.4
2	0.1145	80.8	0.0720	71.6	0.0604	78.4	0.0821	82.5
3	0.0440	90.7	0.0541	84.0	0.0170	82.3	0.0447	90.9
4	0.0170	94.5	0.0339	92.0	0.0155	70.0	0.0233	95.3
5	0.0129	97.2	0.0205	96.5	0.0116	95.4	0.0116	97.4
6	0.0076	99.0	0.0076	98.6	0.0050	98.0	0.0093	99.0
7	0.0030	99.7	0.0055	99.9	0.0024	99.4	0.0037	99.7
8	0.0013	99.9	0.0004	99.9	0.0009	99.9	0.0012	99.9
9	0.0004	100.0	0.0005	100.0	0.0002	100.0	0.0003	100.0

/113

Solution of this problem amounts to linear conversions of the random fields by averaging with a weighting function (see Chapter 1, Section 4).

In what follows we will consider the relationships among the dispersions, autocorrelation functions, and spectral densities of the amount of clouds at the zenith with the corresponding statistical characteristics of the cloudiness parameters averaged over space or over the sky. Account has been taken in this case of the relationship of the statistical characteristics of parameters such as the amount of relative cloudiness by zones or over the sky to the distance between the observer's station and the lower boundary of the clouds.

In deriving the formulas relating the statistical characteristics of cloud coverage of the zenith to the statistical characteristics of the cloudiness parameters averaged over space, we shall assume the cloud field to be isotropic. This restriction, which is in keeping with the current level of our information

on cloud field structure (see Chapter 1, Section 4), substantially simplifies the design equations obtained in the following. /117

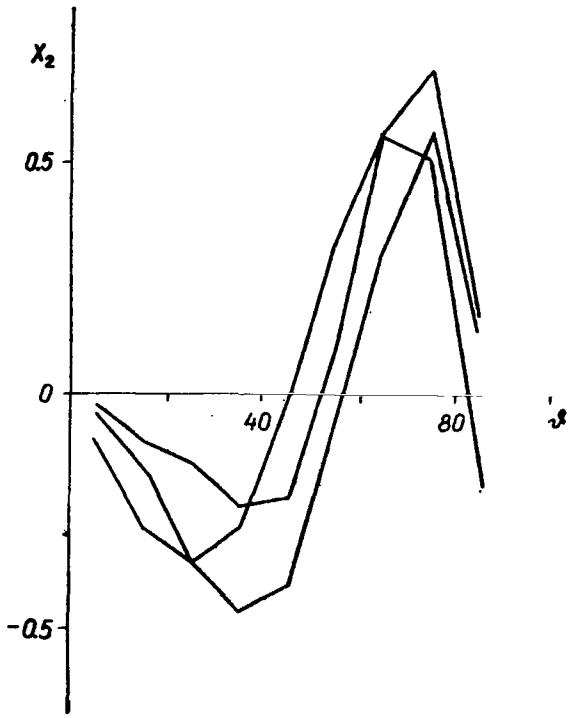

Figure 53. Second Eigenfunctions of Amount of Relative Zonal Cloudiness Versus Zenith Distance of Zone.

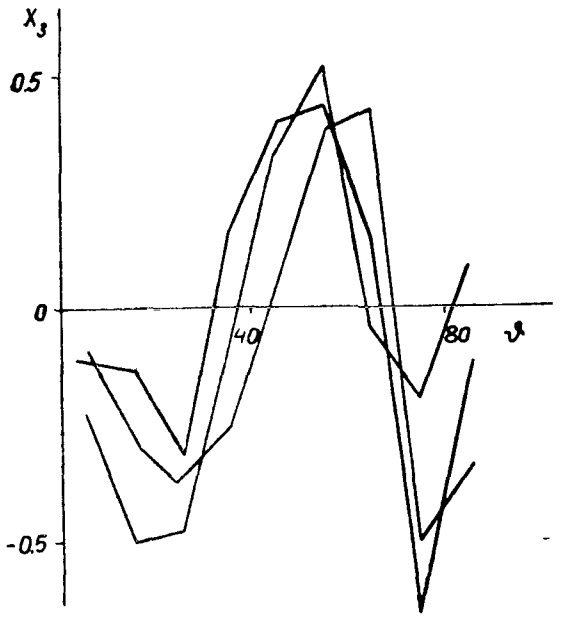

Figure 54. Third Eigenfunctions of Amount of Relative Zonal Cloudiness Versus Zenith Distance of Zone.

We apply two equally valid approaches to solve these problems: firstly, averaging of the statistical characteristics of the presence of clouds at the zenith with weighting functions and, secondly, filtration of the spectral densities (see Chapter 1, Section 4).

1. Averaging of the Statistical Characteristics of the Presence of Clouds with Weighting Functions

a. Averaging over Circumferences

In the case of averaging over circumferences the mean amounts of clouds on circumference R and at the zenith coincide:

$$n_R=\frac{1}{2\pi R}\int_0^{2\pi R} n(0)\,ds=n(0), \qquad (3.25)$$

in which ds is an element of the circumference.

If the cloud field is isotropic, correlation of the presence of clouds at /118
points M' and M'' of the circumference R depends only on distance $L = \sqrt{(x_1 - x_2)^2 + (y_1 - y_2)^2}$ between them or on angular distance φ (Figure 55). This makes it possible to derive from (1.32) a simple formula for the dispersion of the amount of clouds on the circumference:

$$\sigma^2_{n_R} = \frac{\sigma^2_{n(0)}}{2\pi^2} \int_0^{2\pi} (2\pi - \varphi) r_{n(0)}(\varphi)\, d\varphi, \tag{3.26}$$

in which $\sigma_{n(0)}$, $r_{n(0)}(\varphi)$ are the dispersion and correlation function of the presence of clouds at the zenith.

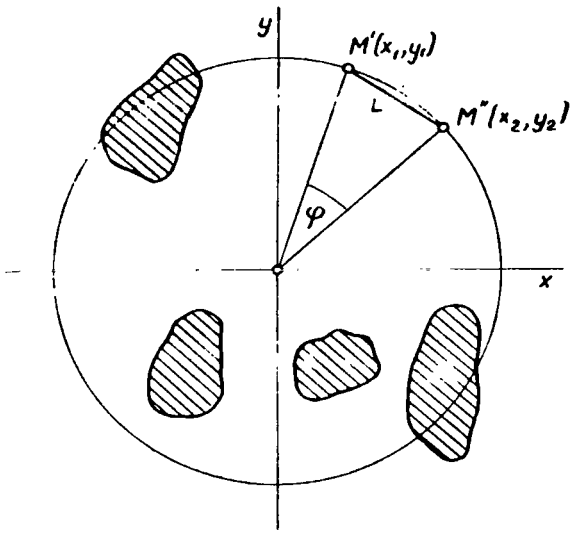

Figure 55. Diagram of Averaging of Random Function over a Circumference.

Calculation of the correlation function of the amount of clouds on circumferences is a more laborious problem. Let us consider the general case, in which the averaging is performed over circumferences of different radiuses R_1 and R_2. The reciprocal correlation function of the amount of clouds on the circumferences is expressed by the following formula:

$$r_{n_{R_1} n_{R_2}}(l) = \frac{\sigma^2_{n(0)}}{4\pi^2 \sigma_{n_{R_1}} \sigma_{n_{R_2}}} \int_0^{2\pi}\int_0^{2\pi} r_{n(0)}(L)\, d\varphi_1\, d\varphi_2, \tag{3.27}$$

in which

$$L = [R_1^2 + R_2^2 + l^2 - 2R_1R_2\cos(\varphi_1 - \varphi_2) - 2R_1 l\cos\varphi_1 + 2R_2 l\cos\varphi_2]^{1/2}, \tag{3.28}$$

and $\sigma_{n_{r1}}$ and $\sigma_{n_{r2}}$ are the root mean square deviations of the amount of clouds on circumferences of radiuses R_1 and R_2.

In the general case formula (3.27) is susceptible only of numerical integration. However, if, for example, the correlation function of the presence of clouds at the zenith $r_{n(0)}(L)$ may be approximated by the even power series

$$r_{n(0)}(L) = 1 + a_1 L^2 + \ldots + a_m L^{2m}, \tag{3.29}$$

then formula (3.27) may be integrated analytically and we finally obtain

$$r_{n_{R_1}n_{R_2}}(l)=\frac{\sigma^2_{n(0)}}{\sigma_{n_{R_1}}\sigma_{n_{R_2}}}\Big\{1+a_1[R_1^2+R_2^2+l^2]+$$
$$+a_2[R_1^4+R_2^4+l^4+4R_1^2R_2^2+4R_1^2l^2+4R_2^2l^2]+\ldots+ \tag{3.30}$$
$$+a_m\Big[\sum_{k=0}^{m}\sum_{i=0}^{m}(C_m^kC_{m-k}^i)^2R_1^{2(m-k-i)}R_2^{2k}l^{2i}\Big]\Big\},$$

in which C_m^k and C_{m-k}^i are combinations of m and m-k elements relative to k and i. /119

When $R_1 = R_2 = R$ formula (3.30) is simplified and the autocorrelation function of the amount of clouds on the circumference assumes the form

$$r_{n_R}(l)=\frac{\sigma^2_{n(0)}}{\sigma^2_{n_R}}\Big\{1+a_1[2R^2+l^2]+a_2[6R^4+l^4+8R^2l^2]+\ldots+ \tag{3.31}$$
$$+a_m\Big[\sum_{k=0}^{m}\sum_{i=0}^{m}(C_m^kC_{m-k})^2R^{2(m-i)}l^{2i}\Big\}.$$

In the particular case, if $R_2 = 0$ and $l = 0$, we obtain from formula (3.27) the following formula for the correlation coefficient between the amount of clouds averaged over the circumference and the amount of clouds at the center of the circumference:

$$r_{n(0)n_R}(0)=\frac{\sigma_{n(0)}}{\sigma_{n_R}}r_{n(0)}(R) \tag{3.32}$$

b. Averaging over a Circle

Since the averaging is in this instance performed by areas, in the calculations the multiplicity of integration is doubled in comparison to the averaging by circumferences of (3.25)-(3.27).

In averaging by circles the mean amount of clouds on a circle, $n_s(0)$, coincides, as it does in the previous case, with the amount of clouds at the zenith:

$$n_S(0)=\frac{1}{\pi R^2}\iint_S n(0)\,dx\,dy=n(0). \tag{3.33}$$

In this instance $S = \pi R^2$ is the area of the circle.

The dispersion of the amount of clouds over a circle is expressed by the quadruple integral

$$\sigma^2_{n_S}=\frac{\sigma^2_{n(0)}}{(\pi R^2)^2}\iint_S\iint_S r(\overline{M',M''})\,dx'\,dy'\,dx''\,dy'', \tag{3.34}$$

which we reduce by means of the conversions proposed in [2] to the single integral

$$\sigma^2_{n_S}=\frac{4\sigma^2_{n(0)}}{\pi R^2}\int_0^{2R}r_{n(0)}(L)\left[\arccos\frac{L}{2R}-\frac{L}{2R}\sqrt{1-\frac{L^2}{4R^2}}\right]l\,dL. \tag{3.35}$$ /120

The reciprocal correlation function of the amount of clouds over circles of areas S_1 and S_2 is also expressed by a quadruple integral similar in form to that of formula (3.34):

$$r_{n_{S_1} n_{S_2}}(l) = \frac{\sigma^2_{n(0)}}{\pi^2 R_1^2 R_2^2 \sigma_{n_{S_1}} \sigma_{n_{S_2}}} \iint_{S_1} \iint_{S_2} r_{n(0)}(\overline{M_1, M_2})\, dx_1\, dy_1\, dx_2\, dy_2, \tag{3.36}$$

in which M_1 and M_2 pertain respectively to circles of areas S_1 and S_2 the distance between the centers of which equals l.

With $S_1 = S_2$ we reduce the quadruple interval to a double one by the method developed in [2], and formula (3.36) for the autocorrelation function for the amount of clouds over a circle then assumes the form

$$r_{n_S}(l) = \frac{2}{\pi^2 R^2} \frac{\sigma^2_{n(0)}}{\sigma^2_{n_S}} \left[\int_0^{2R-l} r_{n(0)}(L)\, L\, dL \int_0^{2\pi} G(l, L, \varphi)\, d\varphi + \right. \tag{3.37}$$

$$\left. + \int_{2R-l}^{2R+l} r_{n(0)}(L)\, L\, dL \int_{\psi}^{2\pi-\psi} G(l, L, \varphi)\, d\varphi \right] \quad \text{when } l<2R,$$

and

$$r_{n_S}(l) = \frac{2}{\pi^2 R^2} \frac{\sigma^2_{n(0)}}{\sigma^2_{n_S}} \int_{l-2R}^{l+2R} r_{n(0)}(L)\, L\, dL \int_{\psi}^{2\pi-\psi} G(l, L, \varphi)\, d\varphi$$

$$\text{when } l>2R,$$

in which

$$\psi = \arccos \frac{4R^2 - l^2 - L^2}{2Ll}, \tag{3.38}$$

and

$$G(l, L, \varphi) = \arccos \frac{\sqrt{l^2+2Ll\cos\varphi+L^2}}{2R} - \tag{3.39}$$

$$- \frac{\sqrt{l^2+2Ll\cos\varphi+L^2}}{2R} \sqrt{1 - \frac{l^2+2Ll\cos\varphi+L^2}{4R^2}}.$$

The practical calculations based on formulas (3.34)-(3.39) are numerical ones only.

c. Averaging over the Sky /121

Within the framework of linear conversions the statistical characteristics of relative cloudiness can be obtained only in approximation. No allowance is made in this case for the increase in the amount of clouds toward the horizon. A simplification such as this yields considerably understated values for the amount of relative cloudiness (see Section 1 of this chapter). At the same time, the dispersion of relative cloudiness obtained is only slightly understated and the correlation is exaggerated. This is due to the low weight of the contribution

made by the zone around the horizon in relative cloudiness fluctuations. Sinc the design formulas for the dispersion and correlation functions of the amount of relative cloudiness do not lend themselves to simplifications, it is advisable to calculate them by the spectral density filtration method.

The spectral densities for the averaged cloudiness characteristics are obtained only in numerical form, by subjecting the corresponding correlation functions, (3.27), (3.30)-(3.32), (3.36), and (3.37), to the Fourier transform.

2. Spectral Density Filtration

a. Averaging over Circumferences

In averaging over circumferences the weighting function for transition from zenith coverage to the amount of clouds over a circumference is of the form

$$u(r,\varphi)=u(r)=\begin{cases}\dfrac{1}{2\pi R} & \text{when } r=R,\\ 0 & \text{when } r\neq R.\end{cases} \tag{3.40}$$

The two-dimensional frequency characteristic of the filter is obtained from the weighting function by means of the Hankel transform:

$$\Phi_2(\omega)=2\pi\int_0^\infty u(r)J_0(\omega r)r\,dr=J_0(\omega R), \tag{3.41}$$

in which $J_0(\omega R)$ is the zeroth order Bessel function and ω is the circular frequency.

The two-dimensional spectral density of the presence of clouds at the zenith $S_{2,n(0)}$ is transformed by multiplication by the square of the filter frequency characteristic for random functions $H_2(\omega) = H_2(\omega) = \Phi_2^2(\omega)$ /122

$$S_{2,n_R}(\omega)=J_0^2(\omega R)S_{2,n(0)}. \tag{3.42}$$

The dispersion and correlation function of the amount of clouds over the circumference are determined by means of the inverse Hankel transform from the formulas

$$\sigma_{n_R}^2=2\pi\int_0^\infty S_{2,n_R}(\omega)J_0^2(\omega R)\omega\,d\omega \tag{3.43}$$

and

$$r_{n_R}(l)=\frac{2\pi}{\sigma_{n_R}^2}\int_0^\infty S_{2,n_R}J_0^2(\omega R)J_0(\omega l)\omega\,d\omega. \tag{3.44}$$

The one-dimensional spectral density in the cloud field cross-section is obtained by integrating S_{2,n_R} relative to one frequency component:

$$S_{n_R}(\omega_x)=\int_{-\infty}^\infty J^2{}_0(\omega R)S_{2,n_R}(\omega)\,d\omega_y, \tag{3.45}$$

in which $\omega=\sqrt{\omega_x^2+\omega_y^2}$.

By averaging over the circumferences of radiuses R_1 and R_2 we obtain the formula for the filter of two-dimensional reciprocal spectral density of the amount of clouds over the circumferences in the form

$$H_2(\omega, R_1, R_2)=J_0(\omega R_1)J_0(\omega R_2). \tag{3.46}$$

In this case, as with formulas (3.42) and (3.44), the two-dimensional reciprocal density and the reciprical correlation function of the amount of clouds over the circumferences are expressed by

$$S_{2,n_{R_1},n_{R_2}}(\omega)=J_0(\omega R_1)J_0(\omega R_2)S_{2,n(0)}(\omega), \tag{3.47}$$

$$r_{n_{R_1}n_{R_2}}(l)=\frac{2\pi}{\sigma_{n_{R_1}}\sigma_{n_{R_2}}}\int_0^\infty S_{2,n_{R_1},n_{R_2}}(\omega)J_0(\omega R_1)J_0(\omega R_2)J_0(\omega l)\,\omega\,d\omega. \tag{3.48}$$

b. Averaging over Circles /123

The weighting function for transition from zenith coverage to the amount of clouds over a circle in polar coordinates r, φ is expressed by

$$u(r,\varphi)=u(r)=\begin{cases}\frac{1}{\pi R^2} & \text{when } r\leqslant R,\\ 0 & \text{when } r>R,\end{cases} \tag{3.49}$$

and the spectral density filter in this case has the frequency characteristic

$$H_2(\omega, R)=\frac{4J_1^2(\omega R)}{(\omega R)^2} \tag{3.50}$$

in averaging over circles of radius R, and

$$H_2(\omega, R_1, R_2)=\frac{4J_1(\omega R_1)J_1(\omega R_2)}{\omega^2 R_1 R_2}, \tag{3.51}$$

when we average over circles of radiuses R_1 and R_2.

The filtered two-dimensional spectral densities, dispersions, correlation functions, and one-dimensional filtered spectral densities for the amount of clouds over a circle are obtained as with formulas (3.42)-(3.48).

c. Averaging over the Sky

If the screening effect is disregarded, the weighting function for transition from zenith coverage to the amount of relative cloudiness in polar coordinates assumes the form

$$u(r,\varphi)=u(r)=\frac{1}{2\pi}\frac{Z}{(Z^2+r^2)^{3/2}}. \tag{3.52}$$

We see that the weighting function for the amount of relative cloudiness also depends on altitude Z of the lower boundary of the cloud cover. In the general case Z is the distance between the observer and the clouds.

The frequency characteristic of the filter for the weighting function of (3.52) may be represented in the form /124

$$H_2(\omega)=e^{-zz\omega}. \tag{3.53}$$

the one and two-dimensional spectral densities, dispersion, and correlation function for relative cloudiness are obtained as they are with formulas (3.42)--(3.48).

As may be seen from the foregoing, all the frequency characteristics of the filters are expressed in analytical terms. At the same time, the dispersions, correlation functions, and one-dimensional spectral densities from the two--dimensional spectral densities are obtained only in numerical form.

It is to be noted that no general recommendation may be made as regards use of the direct averaging method or the linear filtration method. The choice of method depends on the specific form of correlation function. In both instances it is advisable to approximate the correlation function in order that as many analytical calculations as possible may be performed. This makes it possible to reduce the error (noise) which inevitably occurs in the case of numerical calculations.

In approximating the correlation function we must bear in mind that not all of the correlation functions of the presence of cloudiness obtained by way of experiment may be the correlation function of a two-dimensional isotropic random field. This is due to the fact that the total number of functions which may be used as correlation functions of isotropic random fields is always much smaller than the total number of functions which may be used as correlation functions for one-dimensional processes [27].

Expanding the correlation function of the presence of cloudiness at the zenith into the series

$$r_{n(0)}(t)=\frac{2}{\pi}\arcsin e^{-\alpha|t|}=4\sum_{i=1}^{\infty}[\Phi^{(i)}(0)]^2\frac{e^{-\alpha i|t|}}{i!}, \tag{3.54}$$

in which $\Phi^{i}(0)$ is the ith derivative of the probability integral, for one--dimensional and two-dimensional spectral densities we have respectively

$$S_{n(0)}=\frac{4}{\pi}\sum_{i=1}^{\infty}\frac{[\Phi^{(i)}(0)]^2}{i!}\frac{\alpha i}{\alpha^2 i^2+\omega^2}, \tag{3.55}$$

$$S_{2,n(0)}=\frac{2}{\pi}\sum_{i=1}^{\infty}\frac{[\Phi^{(i)}(0)]^2}{i!}\frac{\alpha i}{(\alpha^2 i^2+\omega^2)^{3/2}} \tag{3.56}$$ /125

Formulas (3.53), (3.55), and (3.56) have been used in calculation of the statistical characteristics of relative cloudiness.

Transition from statistical characteristics of cloudiness at the zenith to averaged ones has been considered in the foregoing.

With increase in the degree of complexity of conversion the spectral filtration method is in the majority of cases known to be preferable to the method of direct averaging of statistical characteristics. The inverse transitions from the statistical characteristics of averaged cloudiness parameters to statistical characteristics of cloud coverage of the zenith or transition to statistical characteristics of other averaged parameters of cloudiness can be accomplished only by the spectral density filtration method. The inverse transformations always involve greater errors than does averaging.

Formulas (3.25)-(3.56) derived in the foregoing fully resolve the problems set in this section. All the integrals entering into these formulas can be calculated, but derivation of the final design formulas in analytical form involves tiring operations which in the majority of cases it is impossible to avoid without numerical integration. The results of calculations based on formulas (3.25)-(3.56) and comparison of these results with empirical data will be discussed in the following section.

Section 6. Statistical Characteristics of Averaged Cloudiness Parameters

It is to be seen from the formulas derived in the preceding section that in the case of averaging over circumferences or circles the statistical characteristics depend on radius R, while the statistical characteristics of the amount of relative cloudiness depend on the distance between the observer and the cloud layer. It is to be noted that the coverages of the directions of sighting averaged over the azimuth which were obtained in the processing of photographs of the sky (see Chapter III, Section 1) correspond to averaging /126
over circumferences of a radius of

$$R = Z \operatorname{tam} \vartheta, \tag{3.57}$$

in which Z is the distance to the cloud layer. In subsequent calculations the mean rate of advance of a cumulus cloud field has been assumed to be v = 24 km/hr, that is, a distance on the cloud field of 4 km or $Z = 0.4\ t_Z$ corresponds to a time interval of 10 minutes. In this case t_Z is the distance in minutes between the lower boundary of the cloud cover and the surface of the Earth obtained by means of the congelation hypothesis. We additionally assume that the bases of cumulus clouds are situated at an altitude of Z = 1 km from the Earth's surface, this corresponding in approximation to their mean real altitude. The relationships of the dispersion of the amount of clouds on a circumference to zenith angle ϑ (radius R), as calculated with formula (3.26), are shown in /127
Figure 56 for zenith cloud coverages n(0) = 0.5 and 0.1 (0.9). The experimental results obtained from sky photographs are entered as dots. Since the dispersions of the presence of cloudiness averaged over a circumference have been normalized by the dispersion of the presence of clouds at the zenith, the relative dispersions given are at the same time the coefficients of efficiency of averaging over circumferences (see formula (1.22)). As is shown by Figure 56, in the case of averaging over circumferences the normalized dispersions depend only slightly on the mean coverage of the zenith. Close agreement with the empirical data is observed in this instance.

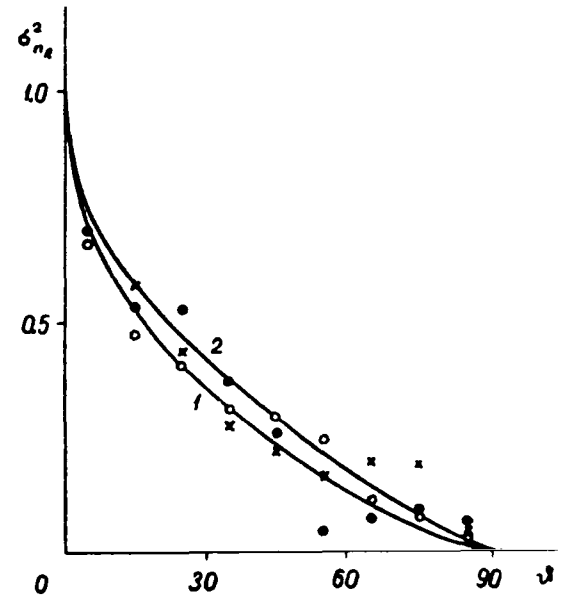

Figure 56. Dispersion of Presence of Clouds Averaged over Almucantar Versus Zenith Angle ϑ. Curves plotted on the basis of formula (3.26): 1, n(0) = 0.5; 2, n(0) = 0.4 and 0.6. Empirical data: ×, n(0) = 0.2; ·, n(0) = 0.3; ○, n(0) = 0.5.

The dispersion of the amount of clouds over a circle, as calculated from formula (3.34), is shown in Figure 57. It is to be seen that the relative dispersion of the amount of clouds over a circle (coefficient of averaging effectiveness) decreases somewhat more slowly with decrease in the radius (zenith angle) than does the dispersion of the amount of clouds over a circumference. As with the dispersion with the amount of clouds over a circumference, close agreement is observed in this instance between the theoretically calculated values of the dispersion of the amount of clouds over a circle and the empirical data (the dots in the graph), as well as slight dependence on the mean coverage of the zenith. It is to be noted that the empirical data on the dispersion of the amount of clouds over a circumference and over a circle have been obtained on the basis of photographs of the sky. Hence at zenith angles $\vartheta > 50°$, when the shading is appreciable, understated values are obtained from the sky photograph for the dispersion of the amount of clouds over a circumference and over a circle in comparison to those calculated from formulas (3.26) and (3.34). /128

The normalized dispersion (coefficient of efficiency) of the amount of relative cloudiness depends only on the altitude of the lower boundary of the cloud cover and on the mean coverage of the zenith.

Making use of frequency characteristic (3.53), approximation (3.54), and inverse Hankel transform (3.54), we obtain for the dispersion of the amount of relative cloudiness

$$\sigma^2 = \sum_{i=1,3,5\ldots} \left\{ \frac{2\pi}{i} C_i - 2\pi^2 C_i a Z [S_0(2iaZ) - N_0(2iaZ)] \right\}. \qquad (3.58)$$

In this formula S_0 is the Struve function, N_0 the Neumann function, and

$$C_i = \frac{2}{\pi} \frac{[\Phi^{(i)}(0)]^2}{(i-1)!}. \qquad (3.59)$$

Figure 58 illustrates the course of dispersion of the amount of relative cloudiness at mean zenith coverages n(0) = 0.5 and 0.1 (0.9) calculated by the spectral density filtration method. It is to be seen that the normalized dispersion of the amount of relative cloudiness also depends only slightly on the

mean coverage of the zenith. At Z = 0 the dispersion of the amount of relative cloudiness approximates the dispersion of the amount of clouds at the zenith. They coincide if the cloud thickness is slight, that is, $h \to 0$. According to the calculations (Figure 58), to an observer on the ground (Z = 1 km) the dispersion of the amount of relative cloudiness is 8-10% of the dispersion of the presence of clouds at the zenith. At the same time, it has been found by experimental studies with a spherical mirror that the dispersion of the relative cloudiness is for individual observations 3-13% of the dispersion of the presence of clouds at the zenith. As may be seen, there is entirely satisfactory agreement between the measured and the calculated relative cloudiness dispersions. If in calculations based on formula (3.58) the correlation functions of the individual observations are used in place of the correlation function averaged over the observations, the agreement between the measured and the calculated relative cloudiness dispersions is greatly improved in comparison to the data given in the foregoing. /130

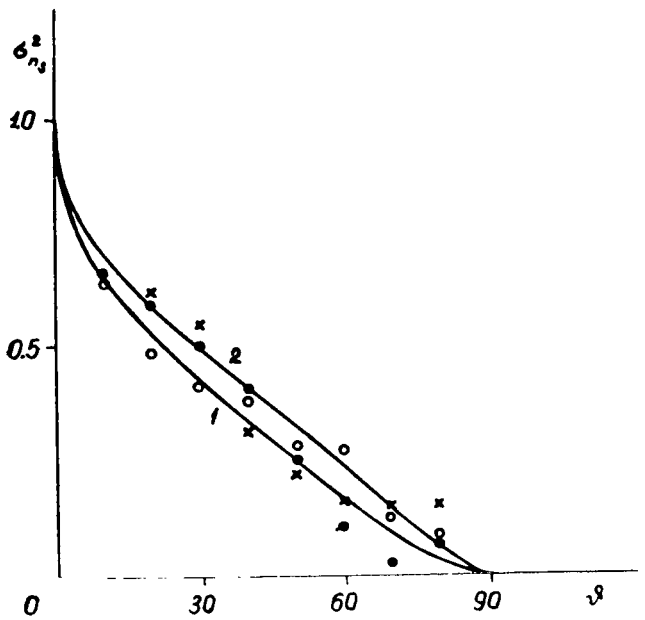

/127

Figure 57. Dispersion of Amount of Absolute Cloudiness Averaged over Circles Versus Angular Radius ϑ at Z = 1 km. Curves plotted on the basis of formula (3.34): 1, n(0) = 0.1; 2, n(0) = 0.4 and 0.6. Empirical data: ×, n(0) = 0.2; •, n(0) = 0.3; ○, n(0) = 0.5.

The correlation functions for the amount of clouds over a circumference and for the amount of relative cloudiness have been calculated by the spectral density filtration method. To ascertain the level of noise in calculation the correlation functions of the amount of clouds over a circle have been calculated both by the spectral density filtration method and by averaging the correlation function of the presence of clouds at the zenith. Both methods yielded identical results, with a divergence of less than 0.5%. Figures 59-61 /131

show respectively the correlation functions for the amount of clouds over a circumference, a circle, and the sky. It is to be seen that in averaging over circumferences the correlation is greater than in averaging over circles having the same radiuses, while the correlation function of the amount of relative cloudiness approximates the correlation function obtained in averaging over a circle of a radius of R = Z tan 60° (see Figures 60 and 61).

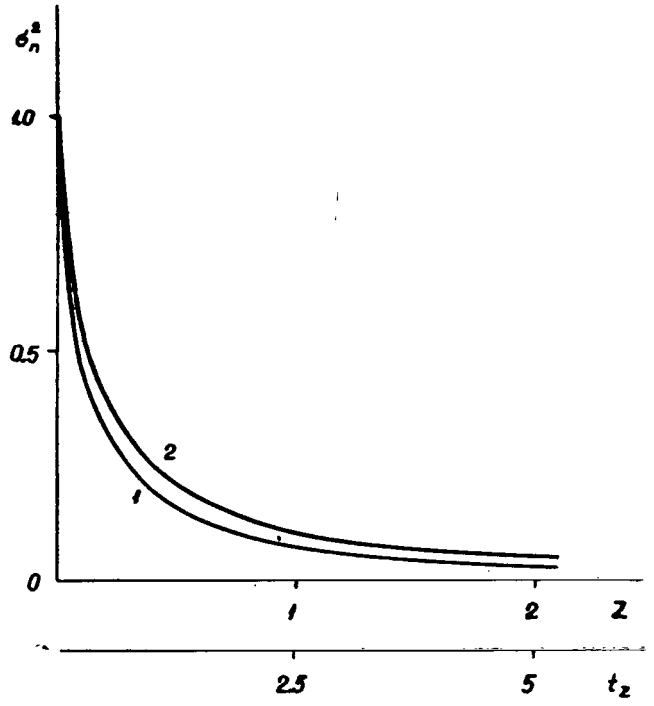

Figure 58. Dispersion of Amount of Relative Cloudiness Versus Height of Lower Boundary of Clouds (Z in km or t_Z in Min): 1, n(0) = 0.1; 2, n(0) = = 0.4-0.6.

The weight of the higher frequencies is reduced by averaging in spectral densities. The effect of averaging on the spectral density is clearly illustrated by Figure 62, /132 which shows the two-dimensional spectral characteristics of the filters calculated with formulas (3.46), (3.50) and (3.53). The frequency characteristics of all the filters decreases smoothly with increase in the frequency. The most abrupt drop is exhibited in this case by the characteristics of the filter for transition from relative cloudiness, and the gentlest slope by the characteristics of the filter corresponding to averaging over circles. More rapid decline of the frequency characteristic of the filter with increase in frequency denotes greater smoothing of the higher frequencies, that is, a filter such as this averages better.

The one-dimensional spectral densities of the presence of clouds at the zenith were given in Figures 38 and 39, but the frequency characteristics of the filter calculated from formulas (3.46), (3.50), and (3.53) may be applied only to two-dimensional spectra; hence for the sake of clarity we present in /133 Figure 63 the one-dimensional and two-dimensional spectral densities of the presence of clouds at the zenith calculated on the basis of approximation formulas (3.55) and (3.56).

The one-dimensional spectral densities of the presence of clouds at the zenith and the amount of relative cloudiness obtained by the filtration method are shown in Figure 64. We see that frequencies above $\omega \geqslant 0.4$ min^{-1} are absent from the spectral densities of relative cloudiness, that is, a substantial contribution is made by frequencies $\omega < 0.4$ min^{-1} for periods of a duration of more than 16 minutes. It is to be noted that we have not thus far determined the

correlation functions and spectral densities of the amount of relative cloudiness by experiment. It follows from the foregoing that when it is necessary to determine the correlation function and spectral densities of the amount of relative cloudiness by way of experiment the optimum time interval between readings is longer than 2 minutes. /134

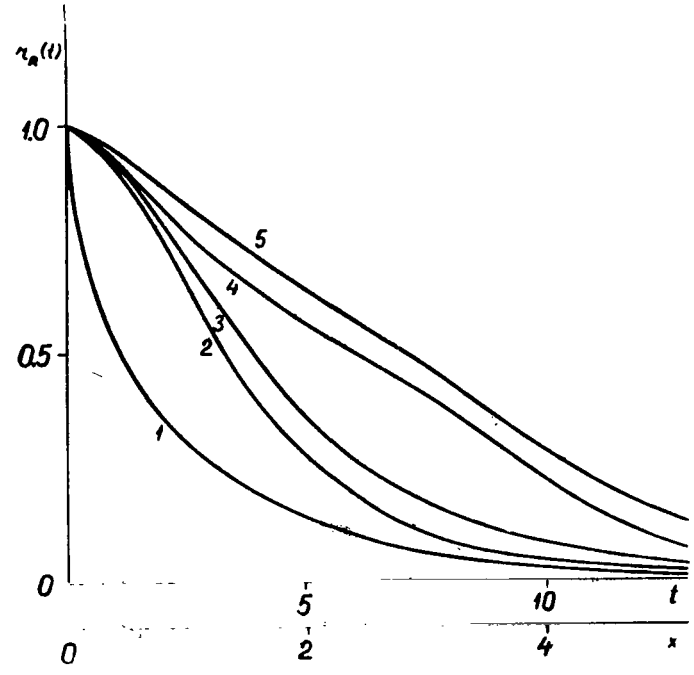

/130

Figure 59. Autocorrelation Functions of Amount of Absolute Cloudiness Averaged over Almucantar Versus t in min or x in km: 1, Correlation Function of Presence of Clouds at the Zenith at n(0) = 0.4-0.6; 2, ϑ = 30°, n(0) = 0.1; 3, ϑ = 30°, n(0) = 0.4-0.6; 4, ϑ = 60°, n(0) = 0.1; 5, ϑ = 60°, n(0) = 0.4-0.6.

Comparison of the dispersions, correlation functions, and spectral densities in averaging over circumferences and circles reveals that averaging over circumferences is the more effective. The method of processing photographs of the sky is based on the last-named circumstance (see Section 1 of this chapter). /135

Section 7. Relationships Between Statistical Cloud Characteristics and Turbulence Structure at the Level of Clouds

Since the genesis, development, and disintegration of cumulus clouds is closely associated with the vertical flows of air at the level of the clouds and in the vicinity of this level, the statistical characteristics of cloud coverage of the zenith may be utilized for indirect assessment of the statistical structure of the vertical components of turbulent flows at the level of the lower boundary of the cloud cover. /136

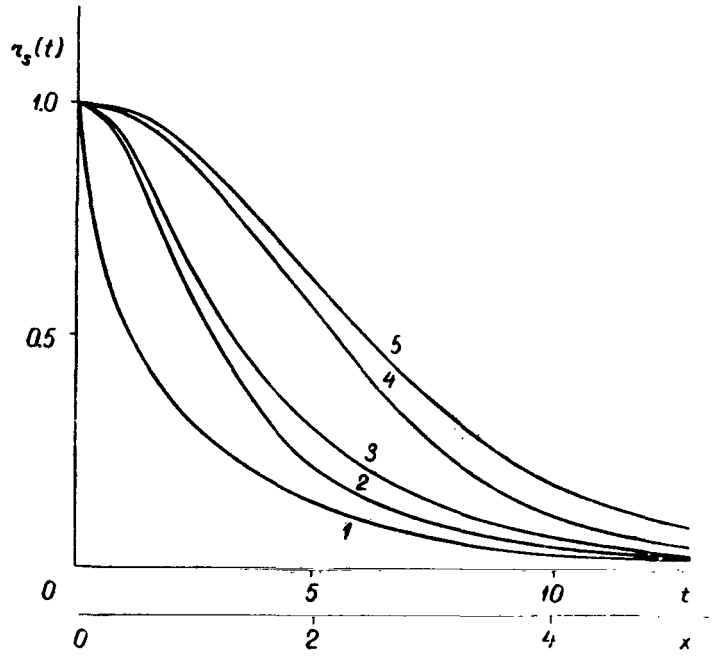

/131

Figure 60. Autocorrelation Functions of Amount of Absolute Cloudiness Averaged over Circles Versus t in min or x in km: 1, Correlation Function of Presence of Clouds at the Zenith at n(0) = 0.4-0.6; 2, $\vartheta = 30°$, n(0) = 0.1; 3, $\vartheta = 30°$, n(0) = 0.4-0.6; 4, $\vartheta = 60°$, n(0) = 0.1; 5, $\vartheta = 60°$, n(0) = 0.4-0.6.

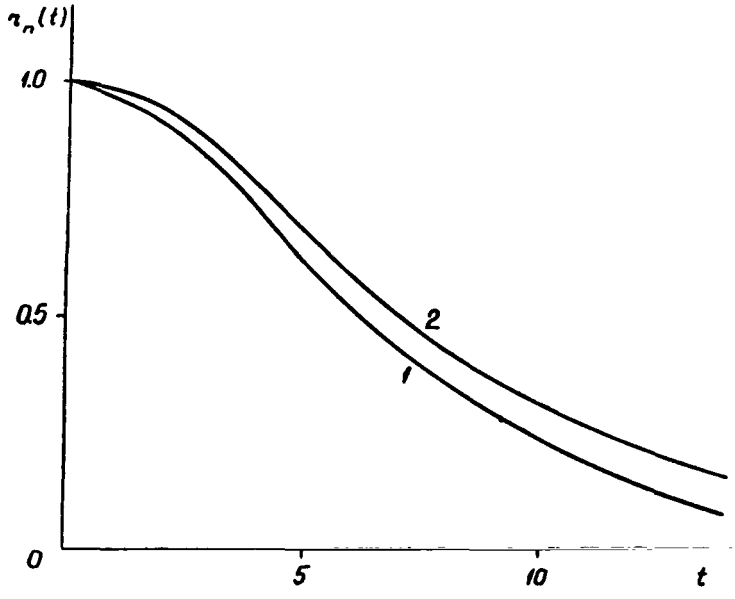

/132

Figure 61. Autocorrelation Functions of Amount of Relative Cloudiness Versus t in min: 1, n(0) = 0.1; 2, n(0) = 0.4-0.6.

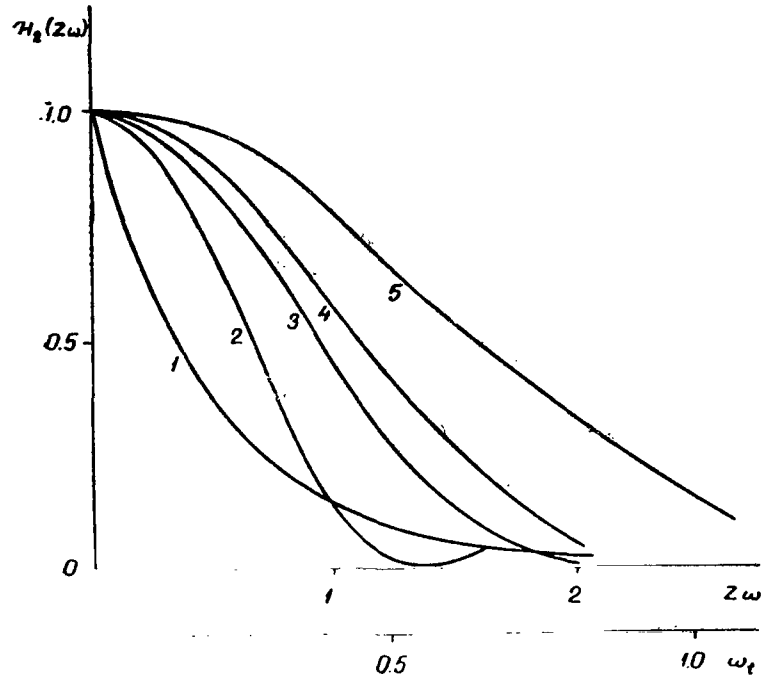

Figure 62. Two-Dimensional Spectral Characteristics of Filters for Averaging of Amount of Clouds Versus ω in Min^{-1} or Versus Z_ω: 1, Over Hemisphere; 2, Over Circumference at $\vartheta = 60°$; 3, Over Circle at $\vartheta = 60°$; 4, Over Circumference at $\vartheta = 45°$; 5, Over Circle at $\vartheta = 45°$.

·/133

Let us consider the simplest model of distribution of the velocities of vertical air motion near the lower boundary of cumulus clouds. For this purpose we assume that flows of constant speed directed upward are observed within the limits of the visible bases of the clouds, and flows directed downward between the clouds. It can easily be seen that for this model the correlation functions and spectral densities of the vertical wind speed components fully coincide with the corresponding characteristics of the presence or absence of clouds at the zenith (see Section 2 of this chapter). The description provided by such a model as this of the vertical turbulence component is of course very approximate.

The few studies conducted up to the present time of the structure of turbulence in the case of cumulus clouds [67-72] have shown that the vertical speeds of turbulent flows are very chaotic in distribution both within clouds and outside them. Ascending and descending vertical flows are observed in this instance both in the clouds and in the gaps between them. On the average the cross-section of ascending flows in a cloud are always smaller than the area of the base of the cloud, representing only 50-80% of it. At the same time, descending flows outside a cloud are observed chiefly around a cloud with a cross-section approximately equalling the area of the base of the cloud. The

maximum of the vertical flow speeds in a cloud is only slightly correlated with the dimensions of the base of the latter [70]. High vertical flow speeds are observed both in small and in large cumulus clouds.

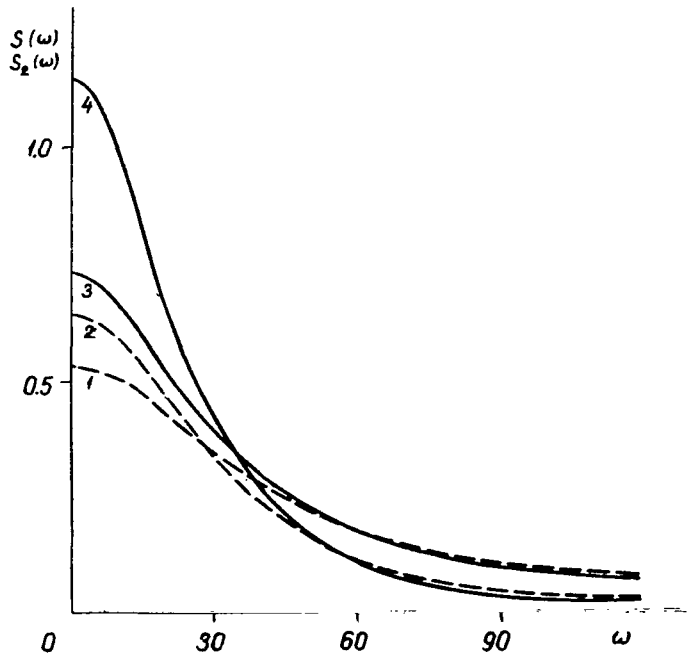

Figure 63. Spectral Densities of the Presence of Clouds at the Zenith Calculated with Formulas (3.55) and (3.56) Versus Circular Frequency ω in min^{-1}. One-dimensional spectral densities: 1, when n(0) = 0.1; 3, when n(0) = 0.4-0.6. Two--dimensional spectral densities: 2, n(0) = 0.1; 4, when n(0) = 0.4-0.6.

Analysis of the experimental studies of turbulent structure reveals that in order to obtain more plausible information on turbulence it is necessary in the proposed problem to abandon the assumption that the vertical flows are constant inside and outside clouds. The experimental measurements made by us of the presence of clouds unfortunately contain no information on the vertical speeds at the level of the clouds. Hence we employ as the next approximation a /137 model in which the vertical turbulence component over the cross-section of the cloud field is yielded by a continuous random function by the restriction of which a relay signal is obtained describing the presence of clouds at the zenith (see Chapter I, Section 6). Transition from the statistical characteristics of the presence of clouds at the zenith to statistical characteristics of the vertical turbulence speed is accomplished by means of the algorithms derived in Section 2 of this chapter, on the assumption that the continuous random process is a normal one. But it follows from what has been said that the distribution of vertical velocities must be normal. The conversion employed by us of the relay signal to a continuous function contains insignificant errors even when the continuous process differs greatly from a normal one [28-30].

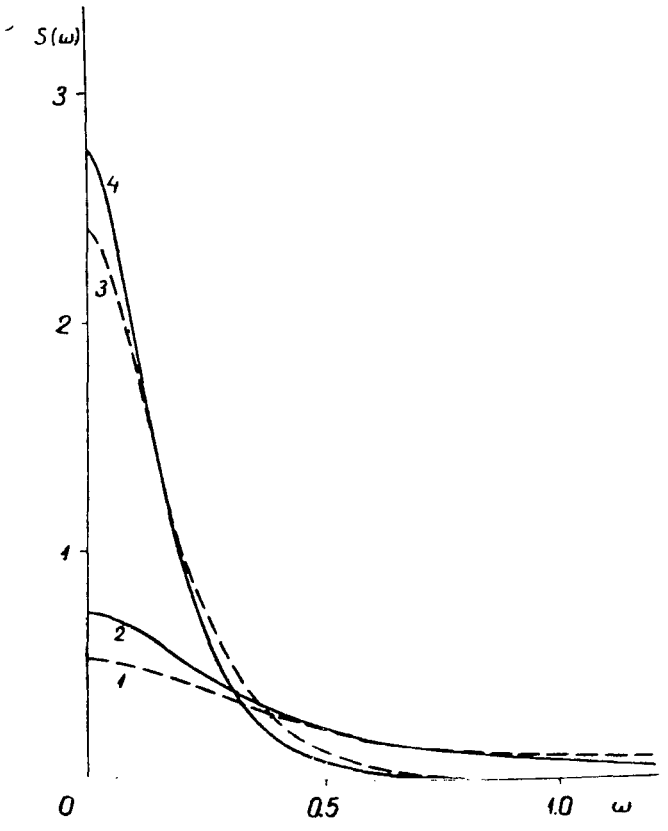

/135

Figure 64. One-Dimensional Spectral Densities of the Presence of Clouds at the Zenith: 1, When n(0) = 0.1; 2, when n(0) = 0.4-0.6 and with Relative Cloudiness; 3, When n(0) = 0.1; 4, When n(0) = 0.4-0.6, as a Function of Circular Velocity ω in Min^{-1}.

By approximating the correlation functions of the presence of clouds at the zenith with formula (3.12) we find that the exponent of the spectral density of the continuous process is 0.57 larger than the exponent of the spectral density of the presence of clouds (see Chapter III, Section 2). The exponent for the spectral density of the vertical turbulence speed is consequently larger than 5/3 according to our indirect measurements and ranges from 1.97 to 2.17. This agrees closely with the results of empirical study of the structure of vertical flow speeds over the cross-section of a cloud cover [70], according to which the exponent equals 2.04, with a root mean square error of 0.15.

It also follows from the results of [70] that the low-frequency component accounts for a large part of the energy in the spectral density of the vertical speeds, and the periods corresponding to it are comparable to the linear dimensions of the clouds. This latter circumstance is apparently due to generation of vertical flow speeds by the release of latent heat.

The predominance of low frequencies in this speed spectrum also explains the close agreement between our results and those of [70].

According to the rule established by A. M. Obukhov, departure of the exponent for the spectral density of the vertical wind speed component from the value of 5/3 indicates arrival of energy from outside [27], for example, through the release of latent heat. For this reason the stage of development, that is, the rates of growth or disintegration of cumulus cloud fields, may be determined on the basis of this departure value. /138

It is to be noted that the results of this section are highly tentative and hypothetical in nature. For the purpose of comprehensive study of the possibilities of extracting from measurements of the optical properties of the cloud cover information on turbulence at the cloud level it is necessary to conduct combined simultaneous experimental studies of the optical properties of the cloud cover itself and of turbulence and its altitude.

CHAPTER IV. STOCHASTIC STRUCTURE OF SHORTWAVE RADIATION FIELDS OF THE CLOUD ATMOSPHERE

/139

Section 1. Relationship Between the Statistical Characteristics of the Cumulus Cloud Field and the Radiation Field of the Atmosphere

The radiation conditions of the atmosphere when cumulus clouds are present are determined in the first approximation by the distribution of clouds over the sky, the coverage of the Sun by clouds, and the mean relationship of cloud and sky brightness between clouds to the zenith angle. By use of the information on the statistical structure of cumulus clouds, to the study of which Chapter III was devoted, it is possible to ascertain the basic patterns of variation in radiation fluxes.

At zenith distances of the sun smaller than 50°, at which the apparent coalescence of clouds is small, the variability of direct solar radiation in time is similar to the variability of cloud coverage of the zenith. However, the comparison of the recordings of direct radiation and of the presence of clouds obtained respectively in measurement with an actinometer and with a low-inertia narrow-angle detector show that the variability of direct solar radiation can be described only in approximation by a train of rectangular pulses. Aside from the cases of absence of direct radiation (when the Sun is covered with clouds) and of total radiation flux (there being no clouds in the vicinity of the Sun), a situation is also observed (over 12-15% of the duration of observation) in which the direct radiation flux has an intermediate value. The intermediate gradations of the direct radiation flux are due to various factors. Firstly, the Sun may be partly covered with clouds or covered by optically thin parts of clouds; secondly, the considerable inertia of the actinometer smooths out the /140
abrupt changes in radiation; and thirdly, bright edges of clouds may enter the field of view of the instrument. The variability of the direct radiation flux measured by the actinometer is studied in detail in [73]. Taking into account the inertia of the actinometer (see Chapter I, Section 3), the frequency of appearance of clouds in its field of view (see Chapter III, Section 3), the viewing angle of the actinometer [74], and the probability density of direct radiation [73], we find that approximately 12% of the intermediate values of direct radiation is accounted for by the transparency of the optically thin parts of clouds, 10% by partial coverage of the Sun's disc with clouds, 42% by actinometer inertia, and 36% by the edges of clouds entering the field of view of the actinometer.

Of the estimates made the greatest error characterizes the role of optically thin edges of clouds, which are the most variable and depend on the variability of cloudiness from observation to observation. This requires further more detailed empirical studies.

The analysis made in the foregoing indicates that of the differences between the results of measurements performed by means of narrow-angle detectors and actinometers about 20% are accounted for by the transparency of clouds and 80% by other factors. On the basis of measurements of the presence of clouds made with narrow-angle detectors it is consequently possible to determine the

structure of the variability of direct radiation with smaller error than by measurement of direct radiation with the actinometer. As has also been demonstrated in [73], the fictitious transparence may be eliminated from the results of measurements with the actinometer in the course of processing by skillful choice of the cutoff level. This also substantiates the use of the results of direct radiation measurements for indication of cloud coverage of the sky in the direction of the Sun (Chapter III, Section 2).

The structure of scattered radiation variability, as with the relationships among cloud characteristics (Chapter III, Section 5), is linearly related to the variability in brightness at the zenith. In this case as well we assume the brightness fields to be isotropic in space. We also assume that with fluctuation in brightness its indicatrix does not vary either for clouds or for the clear sky between clouds. /141

On transition from the brightness of the zenith to scattered radiation the weighting function assumes the form

$$u(\vartheta)=\frac{1}{\bar{D}\downarrow}[n(\vartheta)I_n(\vartheta)+c(\vartheta)I_c(\vartheta)]\cos\vartheta\sin\vartheta, \tag{4.1}$$

in which $\bar{D}\downarrow$ is the mean descending flux of scattered radiation and $I_n(\vartheta)$, $I_c(\vartheta)$ is the relationship of the mean cloud brightnesses and clear sky to the zenith angle. In the first approximation we assume weighting function (4.1) to be isotropic, that is, we disregard the relationship of brightness to the azimuth. It is to be noted that, on the one hand, there is at the present time no information, either empirical or theoretical, with which to allow for the relationship of sky brightness to the azimuth in the presence of cumulus clouds. On the other hand, the flux of scattered radiation as a value averaged over the sky does not contain the fine structure of brightness variability for individual zenith directions. Hence to ascertain the basic patterns of scattered radiation weighting function (4.1) may be applied to the statistical characteristics of cloud coverage of the zenith, for which the most complete array of empirical studies is available at the present time (see Chapter III). This latter circumstance means that for all zenith directions of sighting within the limits of clouds, as well as in the gaps between them, the brightness is constant and its variability in time or in space may be simulated by means of a "rect" signal. We effect transition from the statistics of the brightness at the zenith to the statistics of the scattered radiation flux by deriving the spectral characteristics of filters for three forms of relationship of mean brightness to the zenith angle.

If the sky brightness does not depend on the zenith angle the spectral characteristics of the filter for transition from zenith brightness to scattered radiation flux is expressed by

$$H_2(\omega)=\frac{\pi^2}{4}(\omega Z)^2[H_1^{(1)}(j\omega Z)]^2, \tag{4.2}$$

in which $H_1^{(1)}(j\omega Z)$ is the third-order Bessel function of the fictitious argument (Hankel function).

Formula (4.2) was obtained by means of the Hankel transform from the weighting function in polar coordinates /142

$$u(R)=\frac{Z^2}{\pi(Z^2+R^2)^2}, \tag{4.3}$$

in which Z is the distance between the lower boundary of the cloud cover and the level of observation, and R is the radius on the cloud field, which is related to zenith angle ϑ by the equation tg ϑ = R/Z.

If the mean sky brightness decreases in the direction of the horizon in proportion to cos ϑ, the weighting function for the transition from zenith brightness to scattered radiation flux is of the form

$$u(R)=\frac{3Z^3}{2\pi(Z^2+R^2)^{2.5}}. \tag{4.4}$$

There corresponds to the latter filter spectral characteristic

$$H_2(\omega)=(\omega Z+1)^2e^{-2\omega Z}. \tag{4.5}$$

According to the formulas of G. V. Rozenberg [32], the course of sky brightness for optically thick cloud layers is proportional to (1/3 + cos ϑ).

The weighting function is in this case expressed by

$$u(R)=\frac{Z^2}{3\pi(Z^2+R^2)^2}+\frac{Z^3}{\pi(Z^2+R^2)^{2.5}}, \tag{4.6}$$

and the spectral characteristic of the filter corresponding to it by

$$H_2(\omega)=\left[-\frac{\pi\omega Z}{6}H_1^{(1)}(j\omega Z)+\frac{2}{3}e^{-\omega Z}(1+\omega Z)\right]^2 \tag{4.7}$$

On increase in brightness toward the horizon in proportion to sec ϑ the weighting function and the spectral characteristic of the filter for transition from zenith brightness to scattered radiation flux coincide with the corresponding functions of the transition from presence of clouds at the zenith to relative cloudiness (see formulas (3.52) and (3.53)). The filter spectral characteristics obtained are presented in Figure 65, which also illustrates the course of the filter characteristic for transition from the presence of clouds at the zenith to relative cloudiness. The trace of the characteristics of the first three /143 filters is virtually the same. It is to be observed that the increase in cloudiness toward the horizon was disregarded in derivation of formulas (4.2)--(4.7), as in analysis of the relationships among the statistical cloudiness characteristics (Chapter III, Section 5). In the majority of cases the weighting functions for transition from zenith brightness to scattered radiation flux decrease with the zenith angle more than cos ϑ times faster than does the weighting function for transition from cloud coverage of the zenith to relative cloudiness. Thus because of the relatively low weight of the zone around the /144 horizon disregard of the increase in the amount of clouds toward the horizon has no appreciable effect on the accuracy of determination of the dispersion, correlation function, and spectral density.

If the brightness decreases with increase in the zenith angle in proportion to cos ϑ, the simple form of filter characteristic (4.5) permits derivation of a

formula for the dispersion of scattered radiation in analytical form. By using the two-dimensional spectral density of the presence of clouds at the zenith in the form of (3.55), we can express the required dispersion as the sum of the integrals

$$\sigma^2_D = 2\pi a \sum_i \int_0^\infty \frac{C_i \omega e^{-2\omega Z}}{(a^2 i^2 + \omega^2)^{3/2}} (\omega Z + 1)^2 \, d\omega, \tag{4.8}$$

in which

$$C_i = \frac{2[\Phi^{(i)}(0)]^2}{\pi (i-1)!}.$$

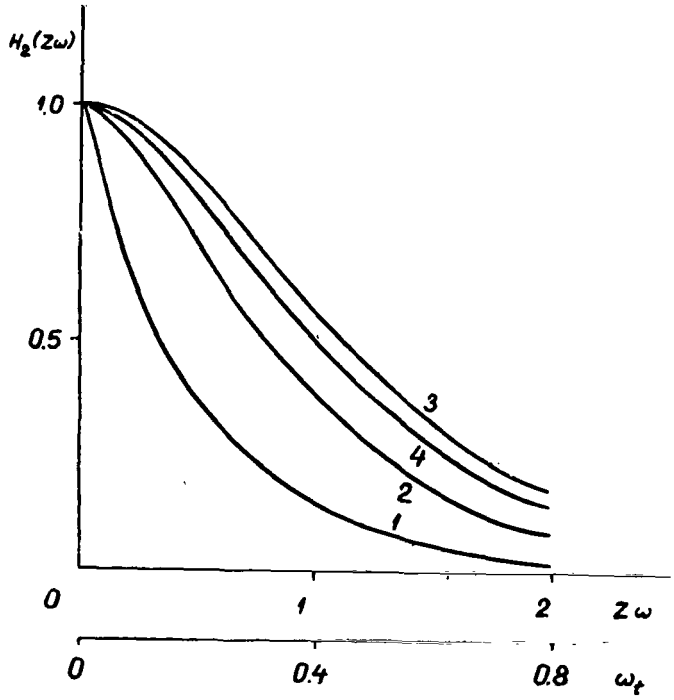

/143

Figure 65. Two-Dimensional Spectral Characteristics of Filters Versus Circular Frequency ω in Min^{-1} or Z_ω for Transition from Presence of Clouds at the Zenith to Relative Cloudiness 1 and from Zenith Brightness to Scattered Radiation Flux, if 2, $I(\vartheta)$ = = const; 3, $I(\vartheta) \sim \cos \vartheta$; 4, $I(\vartheta) \sim (1/3 + \cos \vartheta)$.

After the integration, having set $w = \alpha Z$, it is convenient to write out the dispersion in three parts:

$$\sigma^2_D = \sigma^2_1 + \sigma^2_2 + \sigma^2_3, \tag{4.9}$$

in which

$$\sigma^2_i = 2\pi \sum_{i=1,3,5,\ldots} C_i \left\{ \frac{1}{i} - \pi w [S_0(2iw) - N_0(2iw)] \right\}, \tag{4.10}$$

$$\sigma^2_2 = 4\pi w \sum_{i=1,3,5,\ldots} C_i \left\{ 2iw - \pi iw [S_1(2iw) - N_1(2iw)] + \right.$$
$$\left. + \frac{\pi}{2} [S_0(2iw) - N_0(2iw)] \right\}, \tag{4.11}$$

$$\sigma^2_3 = 2\pi w^2 \sum_{i=1,3,5,\ldots} C_i \left\{ 2i \left(\frac{i^2 w^2}{3} - 1 \right) + \frac{\pi}{2} i^2 w [S_0(2iw) - N_0(2iw)] + \right.$$
$$\left. + i\pi [S_1(2iw) - N_1(2iw)] - \frac{\pi}{2} i^2 w [S_2(2iw) - N_2(2iw)] \right\}, \tag{4.12}$$

and S_0, S_1, S_2 are the Struve functions and N_0, N_1, N_2 the Neumann functions.

The relationship of the dispersion of scattered radiation in zenith brightness dispersion units to the altitude of the cloud cover Z, with α = 0.3, 0.4, as calculated from formulas (4.9)-(4.12), is illustrated in Figure 66. /145

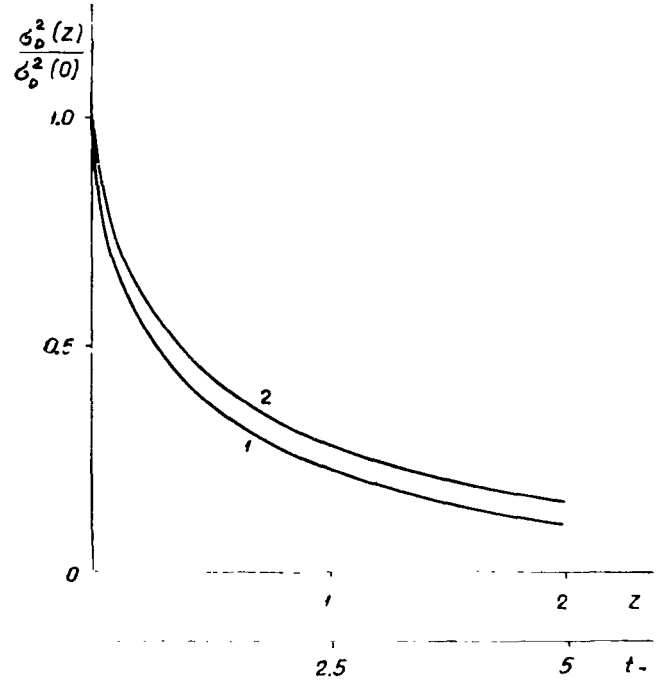

Figure 66. Relative Dispersion of Scattered Radiation Versus Altitude of Cloud Cover (Z in km, t_Z in Min), as Calculated with Formulas (4.9)-(4.12): 1, α = 0.4; 2, α = 0.3.

We must point out that α = 0.3, 0.4 corresponds to a zenith coverage of n(0) = 0.4 or 0.6 and 0.1 or 0.9 (see Chapter III, Section 2). It is to be seen that the dispersion of scattered radiation depends but little on the mean coverage of the zenith. In addition, the course of this relationship with increase in the distance between the observer and the cloud cover is similar to the course of dispersion for relative cloudiness.

The correlation function of the total radiation as the sums of the fluxes of direct and scattered radiation may be represented in the form

$$r_Q(t) = \frac{\sigma_S^2 r_S(t) + \sigma_D^2 r_D(t) + \sigma_S \sigma_D [r_{S,D}(t) + r_{D,S}(t)]}{\sigma_Q^2}, \quad (4.13)$$ /146

in which $\sigma_Q^2 = \sigma_S^2 + \sigma_D^2 + 2\sigma_S\sigma_D r_{S,D}$ is the dispersion of the total radiation, σ_S^2 is the dispersion of direct radiation onto the horizontal surface, and $r_{S,D}$ and $r_{D,S}$ are the reciprocal calculation functions for direct and scattered radiation.

It is to be noted that the statistics of the total radiation may also be expressed by spectral densities $S_S(\omega)$, $S_D(\omega)$ and reciprocal spectral densities $S_{S,D}(\omega)$, $S_{D,S}(\omega)$ of direct and scattered radiation

$$S_Q(\omega) = \frac{\sigma_S^2 S_S(\omega) + \sigma_D^2 S_D(\omega) + \sigma_S \sigma_D [S_{S,D}(\omega) + S_{D,S}(\omega)]}{\sigma_Q^2} \quad (4.14)$$

or, since the random processes representing variability S and D are substantial,

$$S_Q(\omega) = \frac{\sigma_S^2 S_S(\omega) + \sigma_D^2 S_D(\omega) + \sigma_S \sigma_D [S_{S,D}(\omega) + S_{S,D}(-\omega)]}{\sigma_Q^2}. \quad (4.15)$$

The reciprocal correlation functions and spectral densities entering into formulas (4.13)-(4.15) may either be derived from direct experiments or may be obtained by theoretical calculations (see the following section).

The scattered radiation dispersion appearing in formulas (4.13)-(4.15) is generally relatively small (see Section 4 of this chapter). Hence the correlation function and spectral density of the total radiation is determined chiefly by the correlation function or spectral density of the direct radiation and the reciprocal correlation function or spectral density of the direct and the scattered radiation.

Examination has been made in the foregoing of the relationships between the statistical characteristics of the presence of clouds at the zenith and the statistical characteristics of fluxes of direct, scattered, and total radiation, but for the energetics of the atmosphere, and in particular for calculations based on formulas (4.13)-(4.15), it is important to know the relationships among the statistical characteristics of direct, scattered, and total radiation, and these we will now undertake to analyze.

Section 2. Theoretical Analysis of Relationships Among Statistical Characteristics of Fluxes of Direct, Scattered, and Total Radiation /147

It was demonstrated in the preceding section that the statistical characteristics of direct, scattered, and total radiation are in the first approximation unambiguously related to the statistical characteristics of the presence of clouds at the zenith. Hence the reciprocal correlation functions of the fluxes can be obtained by using the relationships at the outputs of several linear conversion systems (direct, scattered, and total radiation), when the same random process (presence of clouds at the zenith) operates at the inputs [22].

This problem may be solved by two equally valid methods: firstly, averaging with the corresponding weighting functions of the correlation function of the presence of clouds at the zenith, and secondly, by filtration of the spectral density of the presence of clouds at the zenith by means of the appropriate filters.

In seeking the relationships between direct and scattered radiation we employ the second method, which reveals the essential nature of the transformation more clearly.

The reciprocal spectral density of direct and scattered radiation is obtained by filtration of the two-dimensional spectral density of the presence of clouds at the zenith. This filtration can be accomplished by means of the square root of the corresponding spectral characteristic of the filter for scattered radiation in (4.2), (4.5), and (4.7), that is, $S_{\xi,\eta}(f)=\sqrt{A^2(f)+B^2(f)}$.

The two-dimensional spectral densities of direct and scattered radiation are expressed by

$$S_{2,S,D}(\omega)=-\frac{\pi\sigma_S}{2\sigma_D}\omega Z H_1^{(1)}(j\omega Z)S_{2,n(0)}(\omega), \tag{4.16}$$

$$S_{2,S,D}(\omega)=\frac{\sigma_S}{\sigma_D}e^{-\omega Z}(1+\omega Z)S_{2,n(0)}(\omega), \tag{4.17}$$

$$S_{2,S,D}(\omega)=\frac{\sigma_S}{\sigma_D}\left[-\frac{\pi\omega Z}{6}H_1^{(1)}(j\omega Z)+\frac{2}{3}e^{-\omega Z}(1+\omega Z)\right]S_{2,n(0)}(\omega) \tag{4.18}$$

for isotropic brightness, if the brightness descreases in proportion to cos ϑ and 1/3 + cos ϑ with increase in the zenith angle.

The normalized reciprocal correlation function of direct and total radiation /148 is of the form

$$r_{S,Q}(t)=\frac{\sigma_S}{\sigma_Q}r_S(t)+\frac{\sigma_D}{\sigma_Q}r_{S,D}(t). \tag{4.19}$$

There correspond to the latter the one-dimensional and two-dimensional reciprocal spectral densities

$$S_{S,Q}(\omega)=\frac{\sigma_S}{\sigma_Q}S_S(\omega)+\frac{\sigma_D}{\sigma_Q}S_{S,D}(\omega), \tag{4.20}$$

and

$$S_{2,S,Q}(\omega)=\frac{\sigma_S}{\sigma_Q}S_{2,S}(\omega)+\frac{\sigma_D}{\sigma_Q}S_{2,S,D}(\omega). \tag{4.21}$$

On the analogy of formula (4.19) the reciprocal correlation function of scattered and total radiation is of the form

$$r_{D,Q}(t)=\frac{\sigma_S}{\sigma_Q}r_{S,D}(t)+\frac{\sigma_D}{\sigma_Q}r_D(t). \tag{4.22}$$

From the latter we obtain the one-dimensional and two-dimensional spectral densities

$$S_{D,Q}(\omega)=\frac{\sigma_S}{\sigma_Q}S_{S,D}(\omega)+\frac{\sigma_D}{\sigma_Q}S_D(\omega) \tag{4.23}$$

and

$$S_{2,D,Q}(\omega)=\frac{\sigma_S}{\sigma_Q}S_{2,S,D}(\omega)+\frac{\sigma_D}{\sigma_Q}S_{2,D}(\omega). \tag{4.24}$$

The root mean square deviation of total radiation, σ_Q appearing in formulas (4.19)-(4.24) is expressed by the dispersions and root mean square deviations of direct and scattered radiation with the formula

$$\sigma_Q=[\sigma^2_S+\sigma^2_D+2\sigma_S\sigma_D r_{SD}(0)]^{1/2}.$$

It is to be seen from formulas (4.14), (4.19)-(4.24) that the correlation function and the spectral density of the total radiation flux, as well as the reciprocal correlation functions and reciprocal spectral densities of the flux of direct and total radiation and of scattered and total radiation, may be determined if the correlation functions and spectral densities of direct and scattered radiation, the reciprocal correlation function and reciprocal spectral density of direct and scattered radiation, and the dispersions for direct, scattered, and total radiation are known.

Since in the derivation of formulas (4.16)-(4.18) it was assumed that the weighting function (distribution of brightness over the sky) does not depend on the azimuth, the reciprocal correlation functions obtained in theory are even. As a result the reciprocal spectral densities are real rather than complex functions. In this instance the spectral densities are symmetrical, that is, the relations /149

$$\begin{aligned} S_{S,D}(\omega)&=S_{D,S}(\omega),\\ S_{Q,D}(\omega)&=S_{D,Q}(\omega),\\ S_{S,Q}(\omega)&=S_{Q,S}(\omega). \end{aligned} \tag{4.25}$$

are valid for both one-dimensional and two-dimensional spectra. It follows that coherence $C(\omega)$ equals unity for all cases of reciprocal spectral density (see formula (1.12)). Under natural conditions the atmosphere is nonisotropic and the weighting function accordingly depends on the azimuth and in addition extends in the direction of the Sun. Hence the empirically determined reciprocal spectra are always complex, and the coefficient of coherence is always smaller than unity (see Section 4 of this chapter).

The significance of the imaginary part of the reciprocal spectra, as well as the difference between the measured coherence and unity, may be utilized for evaluation of the validity of the theoretical formulas for description of the statistical structure of radiation fluxes and the structure of clouds in the real atmosphere derived in Section 5, Chapter III, and in Sections 1 and 2 of this chapter. The derivation of formulas for quantitative evaluation remains a task for the future.

Let us now proceed to analysis of the results of the empirical studies.

Section 3. Empirical Data on Variability of Fluxes of Direct, Scattered, and Total Radiation

For the purposes of empirical study of the variability in time and space of radiation flux fields in the case of the cloud cover the fluxes of direct, scattered, and total radiation were recorded on the ground and the fluxes of total and reflected radiation from aircraft (see Chapter II). Up to the present /150 we have obtained 273 observations, of which 103 ground measurements and 23 aircraft measurements have been fully processed. In view of the fact that the variability of the direct radiation flux of the Sun is very near that of the presence of clouds on the line of sight (see Section 1 of this chapter and Chapter III), in this section we shall concern ourselves chiefly with discussion of the results of study of the fluxes of scattered and total radiation.

To eliminate the influence of the diurnal variation in the scattered radiation flux analysis was made of the dimensionless value $D^* = D/D_0$, in which D_0 is the mean diurnal variation in the scattered radiation of a cloudless sky as calculated from the empirical formula

$$D_0 = 0.190 m_{\odot}^{-0.36} - 0.033, \tag{4.26}$$

derived in [75] on the basis of data of the Tartu actinometric station. In this formula $m_{\odot}$ is the mass of atmosphere in the direction of the Sun.

The diurnal variation and total radiation were eliminated in a similar manner. Analysis was made of the dimensionless value $Q^* = Q/Q_0$ in which Q_0 is the mean diurnal variation in the possible total radiation of a cloudless sky for a given calendar day in Tartu, as calculated with the formula given in [76]

$$Q_0 = \frac{S_0 \cos \vartheta_{\odot}}{1 + g \sec \vartheta_{\odot}} \tag{4.27}$$

In this formula S_0 is the solar constant and g a coefficient depending on the optical thickness of the atmosphere in the direction of the Sun and on the albedo of the underlying surface. It is to be noted that formula (4.27) has been employed in many studies [17, 77] to eliminate the influence of the diurnal variation in analysis of the variability of total radiation.

The relative flux of total radiation Q^* over the interval n = 0.2 - 1.0 undergoes linear decrease with increase in relative cloudiness (Figure 67).

The dispersion of the relative flux of direct radiation is expressed by the /151 dispersion of the presence of clouds, by the relation

$$\sigma^2_{S^*} = (S^*)^2 \sigma^2_{n(\vartheta_{\odot})}. \tag{4.28}$$

Hence, as with the dispersion of the presence of clouds, the dispersion of relative direct radiation is at the maximum when $n(\vartheta_{\odot}) = 0.5$ and decreases with increase or decrease in cloud coverage in the direction of the Sun, coming to equal zero if $n(\vartheta_{\odot}) = 1$ or $n(\vartheta_{\odot} = 0)$.

The variability of total radiation is determined chiefly by the variability of the direct radiation in the case of cumulus clouds. This is to be seen from Table 5, in which the dispersions of direct, scattered, and total radiation are presented for 3 observations. The total radiation dispersion also has a maximum at $n(\vartheta_{\odot}) = 0.5$ and decreases with increase or decrease in the mean cloud coverage of the Sun. Figure 68 shows the root means square deviation of total radiation Q* plotted against the amount of relative cloudiness. As may be seen, its maximum is situated around n = 0.6. A mean coverage of the Sun (zenith) of n(0) = 0.5 corresponds approximately to the latter value (see Chapter III, Section 1). Unlike the direct radiation, the root mean square deviation of total radiation does not approach zero on transition from variable to unbroken clouds. /153 When n = n(0) = 1 the root mean square deviation of total radiation is determined by the variability of scattered radiation. This circumstance explains the asymmetrical course of σ_{Q^*} as a function of the amount of clouds relative to n(0) = 0.5.

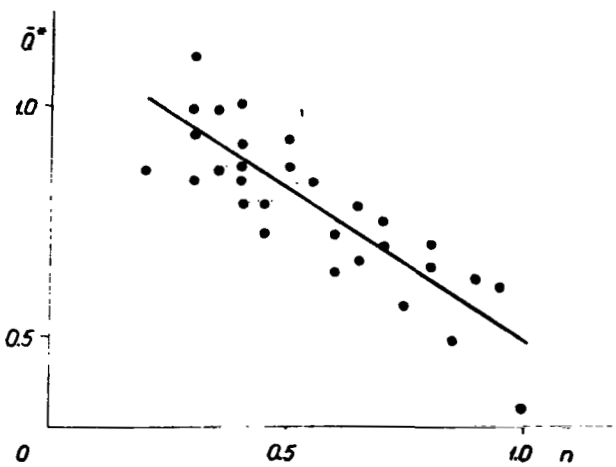

/151

Figure 67. Mean Relative Flux of Total Radiation Versus Mean Amount of Cumulus Clouds (Ground Measurements).

TABLE 5. RELATIVE DISPERSION OF RADIATION FLUXES. /152

	3—4 Cu	4—6 Cu	7—8 Cu
σ^2_S/σ^2_Q	$8.31 \cdot 10^{-1}$	$7.66 \cdot 10^{-1}$	$6.80 \cdot 10^{-1}$
σ_S/σ_Q	$9.12 \cdot 10^{-1}$	$8.75 \cdot 10^{-1}$	$8.25 \cdot 10^{-1}$
σ^2_D/σ^2_Q	$7.90 \cdot 10^{-3}$	$1.71 \cdot 10^{-2}$	$3.12 \cdot 10^{-2}$
σ_D/σ_Q	$8.89 \cdot 10^{-2}$	$1.31 \cdot 10^{-1}$	$1.77 \cdot 10^{-1}$
$\sigma_S\sigma_D/\sigma^2_Q$	$8.12 \cdot 10^{-2}$	$1.13 \cdot 10^{-1}$	$1.45 \cdot 10^{-1}$
$2\sigma_S\sigma_D/\sigma^2_Q$	$1.62 \cdot 10^{-1}$	$2.26 \cdot 10^{-1}$	$2.90 \cdot 10^{-1}$
σ_S	$2.66 \cdot 10^{-1}$	$3.10 \cdot 10^{-1}$	$3.56 \cdot 10^{-1}$

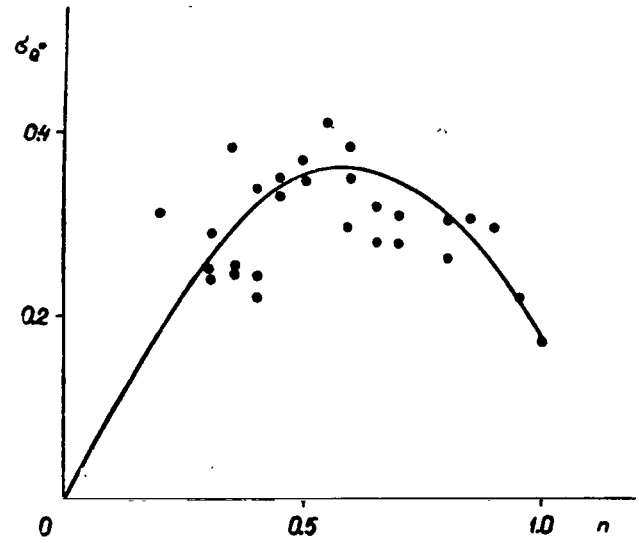

/152

Figure 68. Root Mean Square Deviation of Relative Total Radiation Versus Mean Amount of Cumulus Clouds (Ground Measurements).

The coefficient of variation in total radiation (Figure 69) undergoes linear increase with increase in the amount of relative cloudiness up to approximately n = 0.7, and then begins to decrease, at n = 1 coming to equal the corresponding coefficient of variation for a cloudy sky (scattered radiation with n = 1).

The distribution functions of the relative fluxes were calculated for the observations of direct, scattered, and total radiation in time. The probability distribution functions of direct radiation have been studied in detail in [73], and the probability density of total radiation is presented in [77]. Examples of the probability densities are given in Figures 70-72.

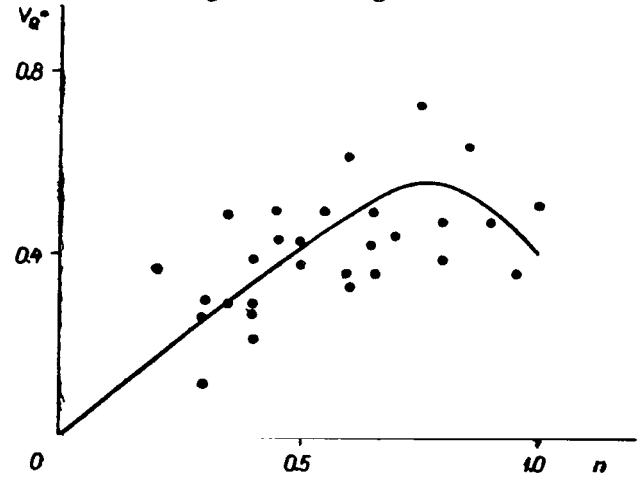

Figure 69. Coefficient of Variation in Mean Total Radiation Flux Versus Mean Amount of Cumulus Clouds (Ground Measurements).

As may be seen from Figure 70, the probability density of the flux of scattered radiation for cumulus clouds is monomodal and extends in the direction of large relative fluxes, the more so the greater is the amount of relative cloudiness. At the same time, the distribution function widens as the amount of cloudiness increases. The elongation of the probability density in the direction of large fluxes is apparently due to the nonlinearity of the relationship between the optical thickness and the cloud brightness (for further details see Sections 5, 6 of Chapter I and Section 6 of this chapter). /154

At the same time, the probability density of total radiation for cumulus clouds is generally bimodal in form [77] (Figures 71 and 72). In this instance the first mode corresponds to small values Q* (when the Sun is covered with clouds). The second mode is determined by the direct and scattered radiation (when the Sun is not covered with clouds). With increase in the amount of clouds the probability of the first mode increases and that of the second decreases. This circumstance is due to the decrease in the duration of sunshine with increase in the amount of clouds. /155

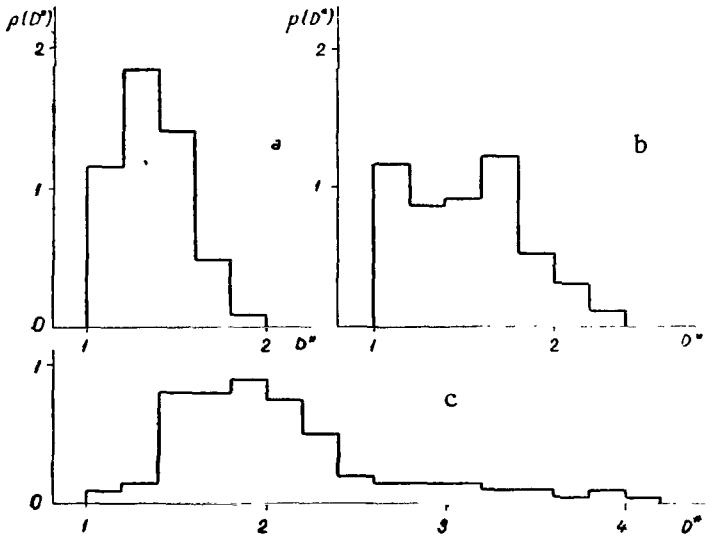

Figure 70. Examples of Probability Density of Relative Scattered Radiation for Cumulus Clouds (Ground Measurements): a, n = 0.3-0.4; b, n = 0.4-0.6; c, n = 0.7-0.8.

The influence of the direct radiation distribution function on the total radiation distribution function is clearly illustrated by Figure 72, which shows the probability densities of fluxes of direct and total radiation for the same observation.

It is further to be noted that the distribution functions of fluxes of scattered and total radiation coincide in the extreme case, that is, for unbroken clouds. This is confirmed by comparison of Figures 70 and 73, which show the probability densities of total radiation for unbroken Sc clouds. /156

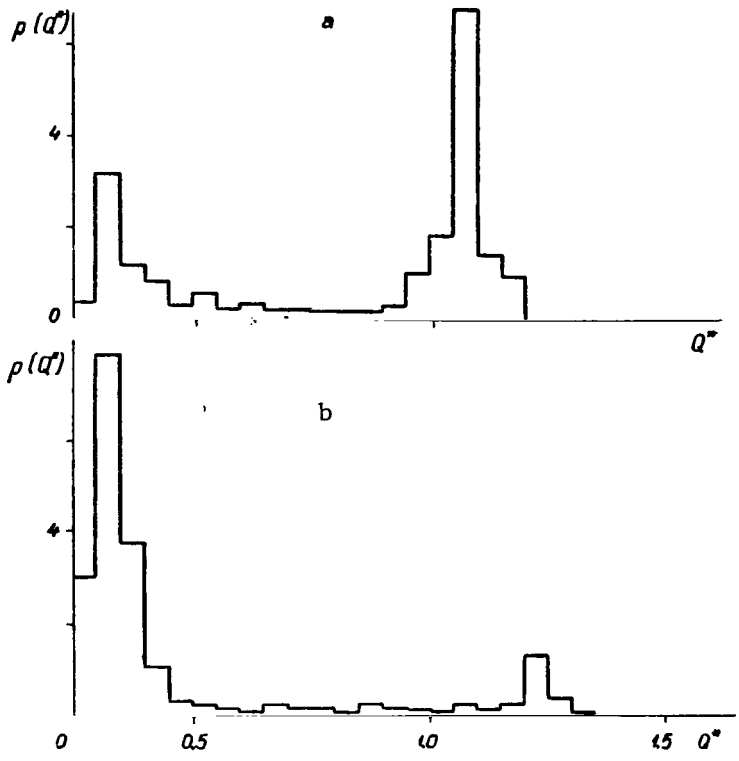

Figure 71. Examples of Probability Density of Relative Total Radiation for Cumulus Clouds (Ground Measurements): a, n = 0.2; b, n = 0.8--0.9.

In accordance with the theoretical arguments advanced in Sections 5 and 6 of Chapter 3 and in Section 1 of this chapter, the correlation function of the scattered radiation flux for cumulus clouds is similar to the correlation function of relative cloudiness, but decreases somewhat more rapidly with displacement in time. This is confirmed by Figure 74, in which the correlation function of relative cloudiness is presented along with the correlation functions of scattered radiation for individual observations. This correlation function of relative cloudiness was calculated with the formulas given in Section 5, Chapter III. The considerable dispersion of the empirically determined correlation functions of the scattered radiation flux is in all probability due, in addition to the errors in determination of this radiation, also to possible differences in brightness structure and to the variability from observation to observation in the mean amount of clouds and mean wind speed at the altitude of the clouds.

Examples of the correlation functions derived by us of the total radiation flux, averaged over the observations and grouped as a function of the amount of clouds in the sky, are presented in Figure 75. Comparison of Figures 75 and 36, in which the correlation functions for direct radiation (the presence of clouds) are given, reveals that the correlation functions are similar so long as the

amount of cumulus clouds $n \leqslant 0.7$, 0.8 ($n(0) \leqslant 0.6$-0.7). On increase in the amount of clouds ($n > 0.8$) the total radiation correlation function approaches the scattered radiation correlation function. This may be verified by comparing correlation function r_{Q^*} with n = 0.9 (Figure 75) with the correlation functions of the scattered radiation flux given in Figure 74. There are substantial differences between the correlation functions of the direct and the total /158
radiation despite the apparent similarity. While for the direct radiation flux the correlation radius is at the maximum at $n(0) = 0.5$ and decreases with increase or decrease in the amount of clouds, for total radiation the correlation radius shown in Figure 6 is at the minimum when $n(0) \approx 0.3$ ($n \approx 0.4$) and increases with increase or decrease in the amount of clouds. The correlation radius of the total radiation flux exceeds the direct radiation correlation radius by an insignificant amount so long as the amount of cumulus clouds $n \leqslant$ $\leqslant 0.6$-0.7 ($n(0) \leqslant 0.5$-0.6). On further increase in the amount of clouds it /159
approaches the scattered radiation correlation radius. This behavior of the total radiation correlation function is to be ascribed to the combined influence of the variability of the fluxes of direct and scattered radiation. As may be seen from examination of formula (4.13), the correlation function of total radiation is determined by the correlation functions of direct and scattered radiation, as well as by their reciprocal correlation. In this instance the relative weight of the correlation functions is determined by the weight of their dispersion in the total radiation dispersion. As is to be seen from Table 5, the dispersion of direct radiation predominates (70-90%) for mean amounts of clouds. At the same time, the weight of the scattered radiation dispersion is /160
negligibly small (1-3%). A more substantial contribution (15-30%) is made by the reciprocal correlation function of direct and scattered radiation, that is, the correlation function of the total radiation flux is influenced only by fluctuations in the scattered radiation operating in phase with the fluctuations in direct radiation. This is illustrated by Figure 77, which shows the correlation functions of the fluxes of direct, scattered, and total radiation for one specific observation when n = 0.5 ($n(0) = 0.4$). It may be seen that the total radiation correlation function repeats the course of the direct radiation correlation function and is situated somewhat above it. The weight of the fluctuation in direct radiation and that of the reciprocal correlation decrease with increase or decrease in the amount of clouds relative to $n(0) = 0.5$, owing chiefly to the decrease in dispersion of the direct radiation. As a result the /161
fluctuations in total radiation are largely influenced by the variability in scattered radiation, which in this instance depends only slightly on the amount of clouds. This circumstance increases the radius of correlation of the total radiation flux. Its spectral density is simultaneously contracted. Figure 78 shows the spectral density for standard radiation, Figure 79 the range of variability of the spectral densities of total radiation, and Figure 80 the spectral densities of total radiation for specific measurements. It is to be seen that the lower frequencies predominate in the spectral density of scattered radiation in comparison to the spectral density of total radiation.

The weight of the high frequencies in the spectral density of the total radiation flux is at the maximum when n = 0.4 ($n(0) = 0.3$) and decreases with increase or decrease in the amount of clouds.

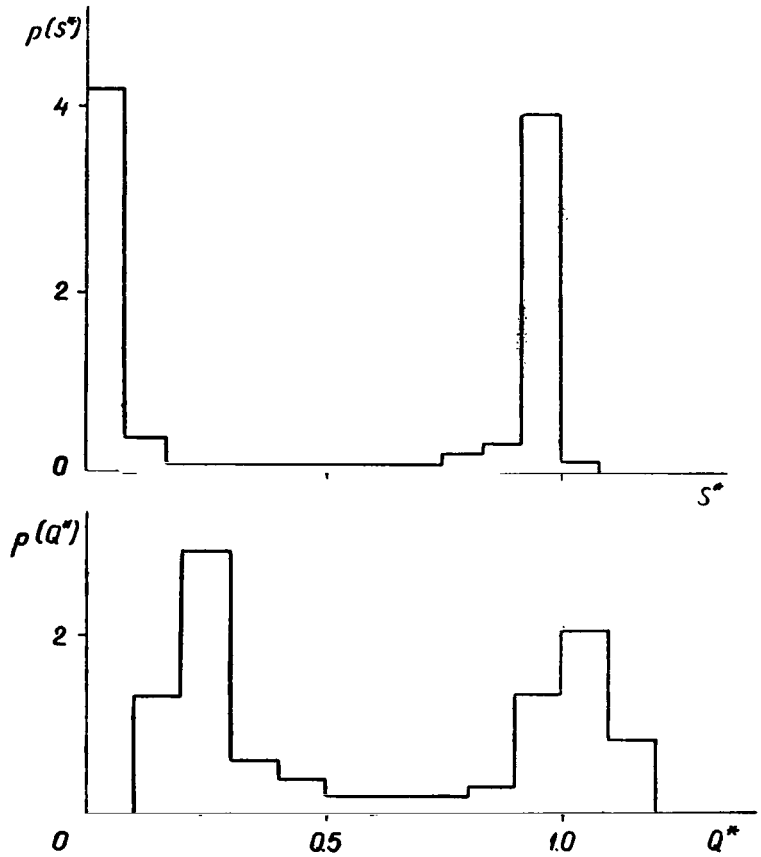

Figure 72. Examples of Probability Density of Relative Fluxes of Direct and Total Radiation for the Same Observation at n = 0.6 (Cu) (Ground Measurements).

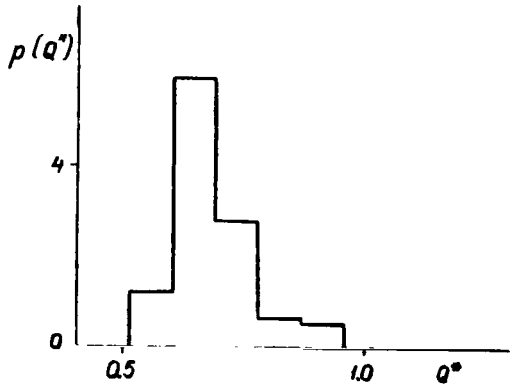

Figure 73. Examples of Probability Density of Relative Total Radiation for Unbroken Sc Clouds (Ground Measurements).

The spatial structure of fields of shortwave radiation has been studied experimentally for stratocumulus and cumulus clouds. Aircraft studies were conducted for this purpose above the Ukraine in 1967-1969 in collaboration with the Ukrainian Hydrometeorological Research Institute. In the case of stratocumulus clouds flights were flown both above and below the clouds, and in some instances inside the cloud layer as well, at a distance of approximately 100 m from the upper boundary. In the case of cumulus clouds within a mass all measurements were generally conducted below the clouds. /164

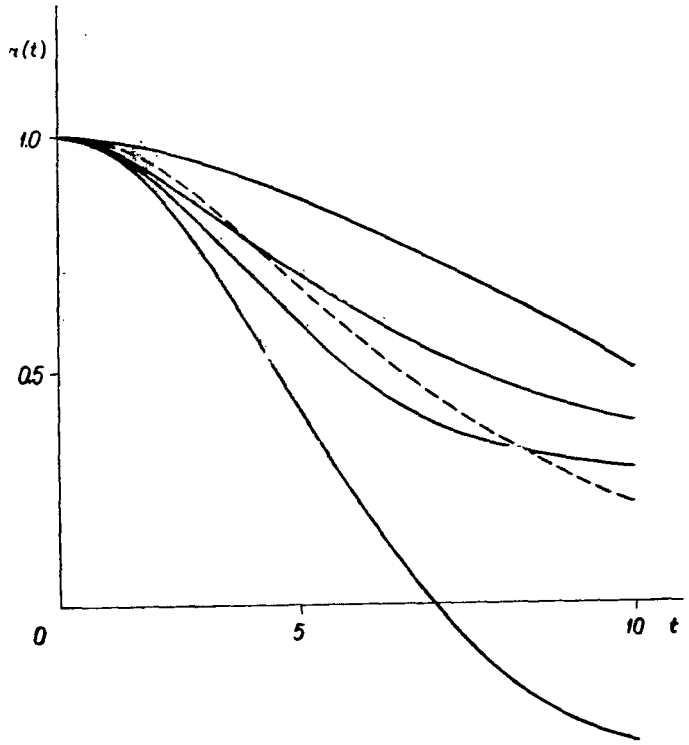

Figure 74. Examples of Autocorrelation Functions of Scattered Radiation Flux (Solid Line Curves) and of Relative Cloudiness (Broken Line Curves) for Cumulus Clouds n = 0.5 (Ground Measurements, t in min).

Figure 81 a shows the mean autocorrelation functions of fluxes of shortwave radiation and the albedo inside the layer, and Figure 81 b the mean correlation functions for fluxes of total and reflected radiation measured below stratocumulus and below cumulus clouds. Owing to the small number of observations it was not possible to make a study of the correlation as a function of the amount of clouds. The correlation functions of the descending flow and the albedo inside the layer are similar in the case of the stratocumulus clouds. There is a slight difference between them and the correlation function of the descending flow. The correlation radius of the ascending flow generally exceeds the /165
correlation radius of the descending flow and the albedo. The large correlation radius of the ascending flow is due to the considerable averaging over the brightness field of the underlying surface, which participates in formation of the ascending flow. In other words, the fluctuations in the descending flow are due chiefly to the variability in cloudiness above the aircraft, and the structure of the ascending flow depends largely on the variability of the albedo of the underlying surface as well as on the variability of the cloud cover both below and above the aircraft. This circumstance increases the correlation owing to the averaging over the area of the Earth's surface (the degree of averaging depends on the altitude of flight). This is clearly illustrated by Figure 81 b,

which shows the autocorrelation functions of descending and ascending flows for cumulus clouds measured immediately below the clouds. The correlation functions obtained under these conditions of the descending flow for cumulus clouds fully coincided with the correlation functions of the presence of clouds at the zenith. This is due to the slight averaging over space in flight at small distances from the lower boundaries of the clouds and confirms the correctness of the conclusions drawn in Sections 5 and 6 of Chapter III and in Sections 1 and 2 of this chapter regarding the similarity between the statistical characteristics of the zenith coverage and the corresponding characteristics of relative cloudiness and between the statistical characteristics of brightness and the corresponding characteristics of flows under these conditions. /166

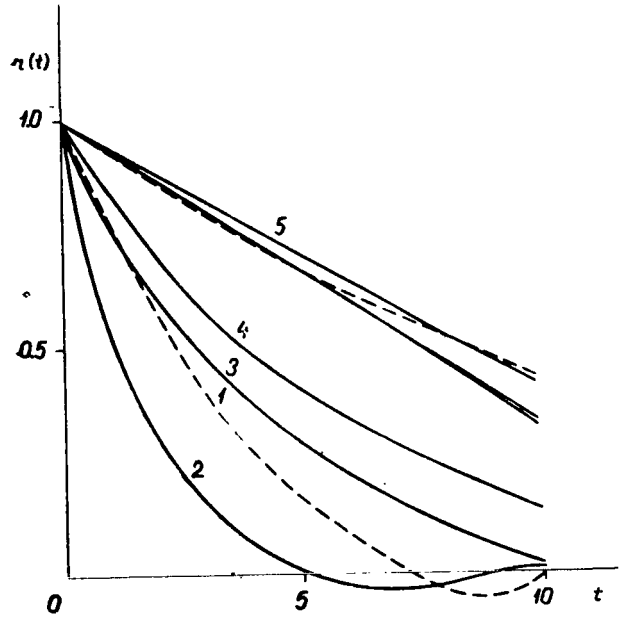

Figure 75. Autocorrelation Functions of Total Radiation Averaged Over Observations and Grouped According to Amount of Relative Cloudiness (Ground Measurements, t in min): 1, n = 0.2 (Cu); 2, n = 0.3-0.4 (Cu); 3, n = 0.5-0.6 (Cu); 4, n = 0.7-0.8 (Cu); 5, n = 0.9-1.0 (Cu, St, Sc, Ci).

It is also to be seen from Figure 81 b that the correlation radius of the descending flow below the cloud cover in the case of stratocumulus clouds is on the average twice as large as the correlation radius in the case of cumulus clouds. This circumstance indicates that there /167 are different inhomogeneity scales for individual cloud cover forms. It is to be noted that establishment of the quantitative relationships between the typical scales of individual cloud cover forms remains a task for future experimental studies. It is logical for this purpose to conduct studies with narrow-angle detectors, since in this instance the results will contain virtually no averaging over area, and this will permit direct comparison of ground and aircraft data.

Figure 82 shows the mean spectral densities of shortwave radiation fluxes in flights inside stratocumulus clouds (corresponding to the correlation functions in Figure 81 a) in the linear frequency range from 0.015 to 0.6 km^{-1}. Figure 83 shows the mean spectral densities of radiation fluxes for cumulus clouds corresponding to the correlation functions of Figure 81 b. The spectral densities in logarithmic coordinates for the /169 fluxes in the case of stratocumulus and cumulus clouds are presented in Figures 84 and 85 respectively. We see that the spectral densities of the descending fluxes may be described by relation $S(f) \sim f^{-k}$ with a constant exponent k = 1.3 for statocumulus clouds and k = 0.62 for cumulus clouds.

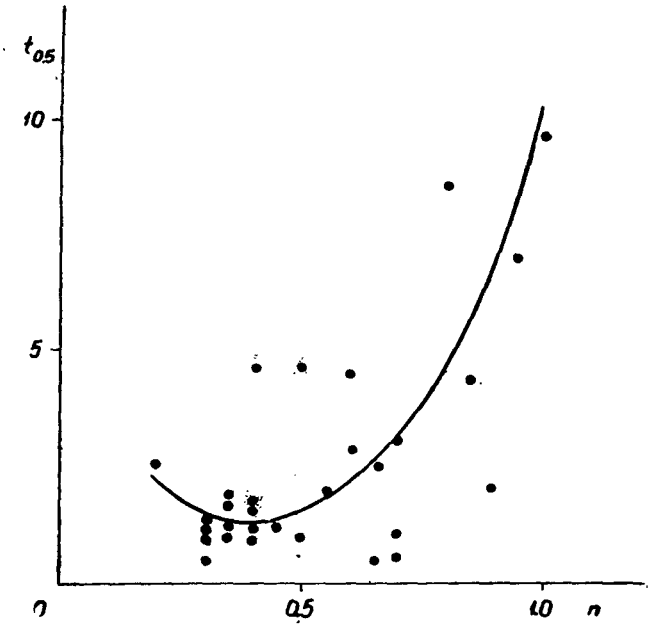

Figure 76. Correlation Radius ($t_{0.5}$ in Min) of Total Radiation Flux Versus Amount of Relative Cloudiness (Cu) (Ground Measurements).

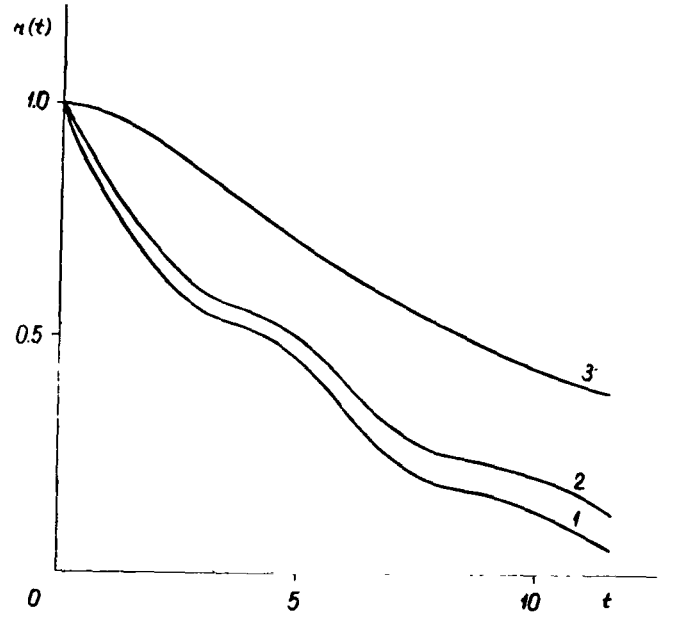

Figure 77. Autocorrelation Functions of Direct 1, Scattered 3, and Total 2 Radiation for One Specific Observation for Cumulus Clouds with n = 0.5, n(0) = = 0.4 (Ground Measurements, t in Min).

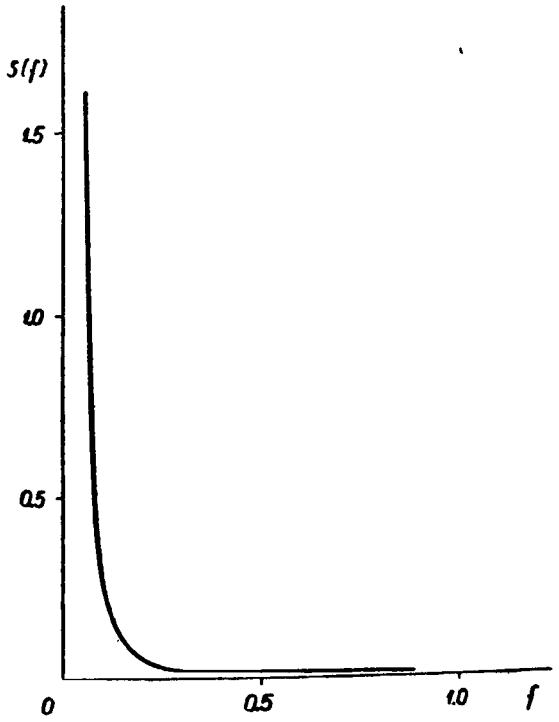

Figure 78. Spectral Density, Averaged over Observations, of Scattered Radiation for Cumulus Clouds Versus Linear Frequency f in Min^{-1} (Ground Measurements).

Section 4. Relationships Among Variability of Fluxes of Direct, Scattered, and Total Radiation

In what follows we present the results of ground and aircraft experimental studies of the relationships among direct, scattered, /170 and total radiation, information on which is necessary in the theoretical analysis made in Sections 1 and 2 of this chapter.

Examples of reciprocal correlation functions of fluxes of direct and scattered radiation are shown in Figure 86 a. The reciprocal correlation functions of scattered radiation and cloud coverage of the zenith for the same cases are presented in Figure 86 b. It is to be seen that the reciprocal correlation functions reach values of up to 0.5 and decrease more slowly with displacement in time than do the correlation functions of the fluxes of direct and total radiation (see Figures 36 and 75). In this instance the correlation between the fluxes of direct and scattered radiation somewhat exceeds the correlation between zenith coverage and scattered radiation. This latter circumstance is due to the in-phase fluctuations of direct and scattered radiation determined chiefly by the wide variability in the brightness of clouds in the vicinity of the Sun.

As we saw in the preceding section, in the case of mean amounts of cumulus clouds the contribution made by the mutual correlation of fluxes of direct and /171 scattered radiation in determination of the correlation function for total radiation is 15-30%. Since the normalized reciprocal correlation function of the fluxes of direct and scattered radiation reaches values of up to 0.5, it consequently accounts for up to 15% of the total radiation correlation function.

The similarity of the correlation functions of the fluxes of the direct and total radiation (see the preceding section) is also confirmed by the course of the reciprocal correlation functions of direct and total radiation, which are shown in Figures 87 and 88 respectively for $n(\vartheta_\odot) < 0.3$ and $0.3 < n(\vartheta_\odot) < 0.5$. As may be seen, the coefficient of reciprocal correlation reaches 0.9, decreasing somewhat with increase in the amount of clouds. At the same time, in the

majority of cases there is observed a slight displacement in time (of up to one minute) of the mutual correlation maximum, a displacement which may be due in part to the nonsynchronous plotting of the ordinates during the primary processing of the recording instrument tapes. Since up to the present reciprocal correlation functions have in the main been derived only for an amount of clouds $n(\vartheta_{\odot})$ ranging from 0.1 to 0.5, more detailed study of their behavior as a function of the amount of clouds remains a task for future experimental studies. The correlation between total radiation and cloud coverage of the zenith is small (Figure 89). This is due chiefly to the slight correlation between cloud coverage of the zenith and the Sun at $\vartheta_{\odot} \approx 40\text{-}50°$ (see Chapter III, Section 4). /172

This latter circumstance is also confirmed by experimental measurements of the reciprocal correlation functions of the flux of direct radiation and cloud coverage of the zenith (see Figure 90).

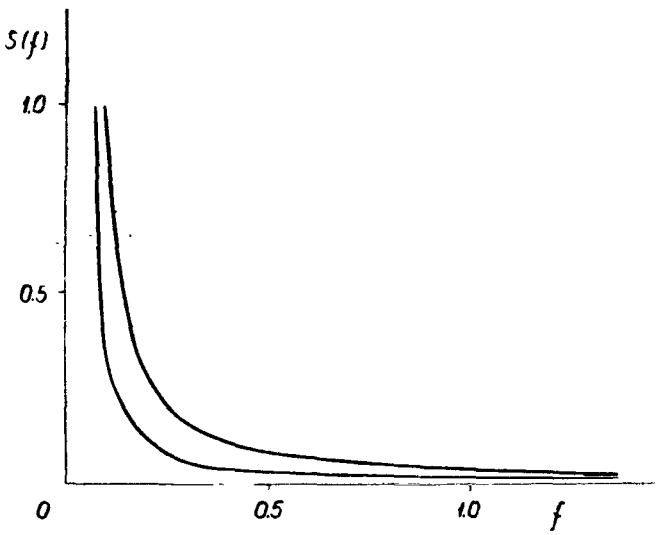

Figure 79. Range of Variability of Spectral Densities of Total Radiation Versus f in Min^{-1} (Ground Measurements).

The reciprocal correlation between the fluxes of scattered and total radiation (Figure 91) is also small. The correlation between scattered and total radiation improves with increase in the amount of clouds, this being due to increase in the weight of the flux of scattered radiation in the total radiation. This also follows from the theoretical considerations advanced in this chapter. /173

In the case of the aircraft studies reciprocal correlation functions were derived only for the fluxes of total and reflected radiation, which were measured in flights both above and below clouds and inside stratocumulus clouds. /174 As may be seen from Figure 92, which illustrates the reciprocal correlation functions obtained in flights respectively above clouds, through the summits of clouds at a distance of 100 m from the upper boundary, and below clouds over bare ground, considerable improvement is observed in the correlation with decrease in the altitude of flight. The correlation function becomes more

symmetrical in this instance. This is due to the symmetry of distribution of the brightnesses relative to the zenith under depth conditions (see Section 6 of this chapter, in which an analysis is made of radiation conditions in the case of stratified clouds).

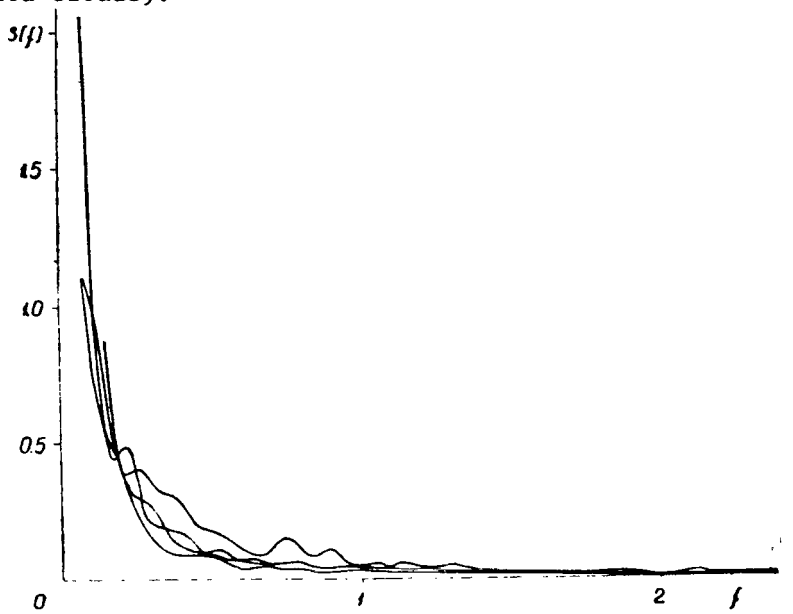

Figure 80. Spectral Densities of Total Radiation for Specific Observations for Cumulus Clouds n = 0.5 Versus f in Min^{-1} (Ground Measurements).

Reciprocal spectral analysis was also carried out for the purpose of more detailed study of the relationships among the radiation fluxes. Calculation was made of the moduli of complex reciprocal spectral densities /176

$$|S_{\xi,\eta}(f)| = \sqrt{A^2(f)+B^2(f)},$$

in which A(f) and B(f) are respectively the real and imaginary portions of the spectral density. The moduli of the reciprocal spectral densities for ground measurements are shown in Figures 93-98 for ground measurements and in Figure 99 for aircraft measurements. The low-frequency components predominate in all the reciprocal spectral densities. In addition, the spectral densities oscillate to a considerable extent in the case of the ground measurements, thus indicating the existence of a set of maxima which shift from observation to observation. The reciprocal spectral densities are more greatly smoothed in the case of the aircraft studies (Figure 99) and generally decrease more rapidly with /177 increase in the frequency, the lower is the altitude of flight, that is, the greater is the optical thickness of the cloud cover above the aircraft.

The coherence (see formula 1.12), that is, the correlation of the different frequencies of reciprocal spectral density, also decreases with increase in frequency. The coherence is substantial in the case of ground measurements only for direct and total radiation (Figures 100-105). We see that the coherence

changes abruptly in all instances with change in the frequency. The locations of the coherence maximi shift from observation to observation. In the case of the aircraft studies, as is to be seen from Figure 106, the coherence is at the minimum in flights above clouds and increases with decrease in the altitude of flight. The coherence reaches considerable values inside the cloud layer or /179
below it, decreasing much more slowly with increase in the frequency than in the case of the ground measurements.

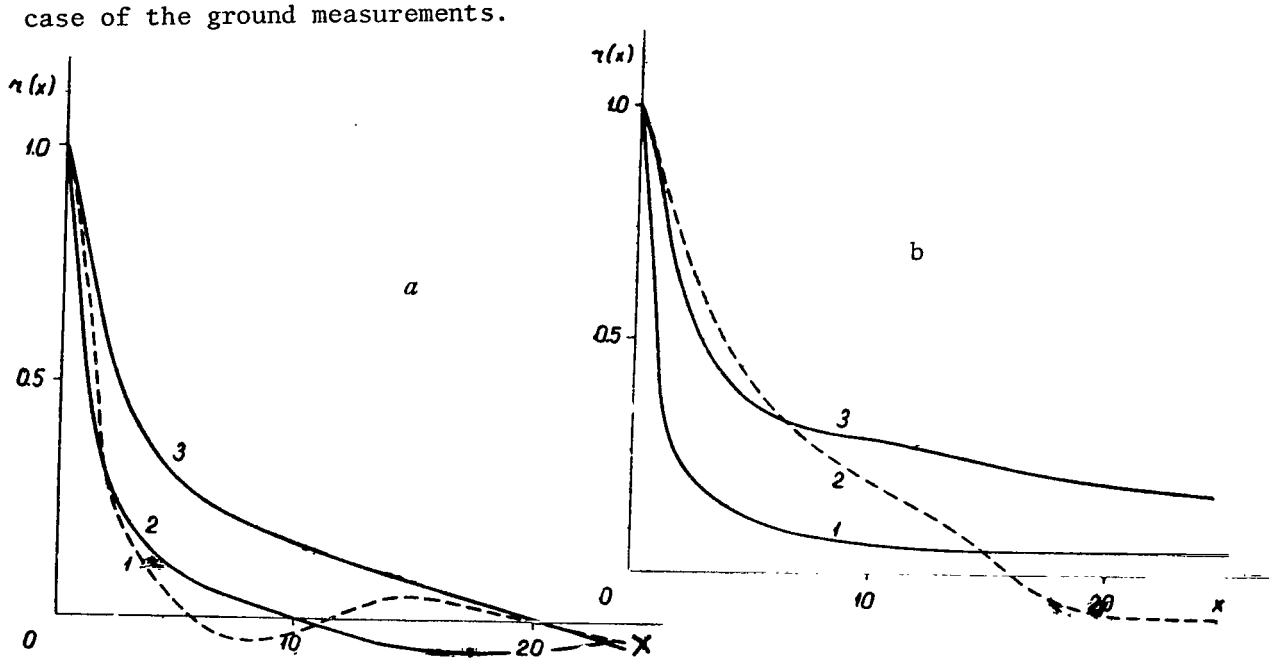

Figure 81. Autocorrelation Functions Averaged over Observations Versus x in km: a, Inside Cloud Layer (Sc) (1, Total Radiation; 2, Albedo; 3, Reflected Radiation); b, Below Clouds (1, Total Radiation with Cu; 2, Total Radiation with Sc; 3, Reflected Radiation with Cu).

The phase shift as expressed in units of time (length) also decreases with increase in the frequency. As may be seen from Figures 107-112, the phase shift is in the majority of cases smaller than 30 sec in the ground measurements. /180
It usually is less than 0.5 km in the case of the aircraft measurements (Figure 113).

It may be said in recapitulation that the phase shift and the shift of the reciprocal correlation function maximum are not essential for the majority of the problems we have considered.

Section 5. Representation of the Distribution of Brightness over the Sky by Means of Eigenfunctions

We have considered the statistical characteristics of radiation fields, and have also presented algorithms determining the interrelation between the statistical characteristics of brightness fields and radiation fluxes. However, owing to the absence of information on the structure of the distribution of

brightness over the sky when clouds are present, it would have been possible to solve the problem in theory only in the first approximation, by use of model distributions of brightness over the sky not verified by full-scale measurements. In order to fill this gap and to obtain the next approximation of the theoretical algorithms, measurement of the distribution of brightness over the sky at wavelengths of 707 and 723 nm has been conducted since 1970 at the Institute of Physics and Astronomy of the Academy of Sciences of the Estonian SSR. Up to the present we have obtained 18 zenith angle scannings, 16 of which have been fully processed. For the purpose of determining the parameters of the structure of brightness fields over the sky use is made of expansion on the basis of the optimum eigenvalues and eigenfunctions of the brightness correlation matrix [6, 7]. It is to be noted that a similar approach was adopted in order to determine the parameters of distribution of clouds over the sky, the results of this determination being presented in Chapter III, Section 4, in which the coefficients of correlation of the presence or absence of clouds at various zenith distances serve as the elements of the correlation matrix. /188

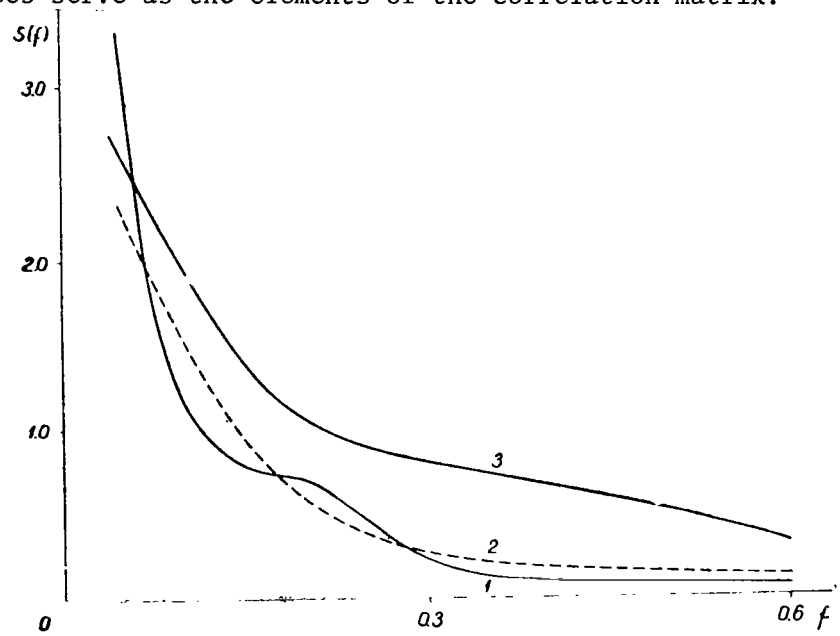

Figure 82. Spectral Densities, Averaged over Observations, of Shortwave Radiation in Flights Inside a Layer of Stratocumulus Clouds Versus Linear Frequency f in km^{-1}: 1, Ascending Flow; 2, Descending; 3, Albedo.

Up to the present scanning has been conducted only for cumulus clouds in the plane perpendicular to the solar vertical. The eigenfunctions and eigenvalues for brightness have consequently been obtained only as a function of the zenith angle of observation. The averaged relationships of brightness to zenith angle for individual specific observations of a duration of 60 to 200 minutes, normalized on the basis of the zenith brightness, are shown in Figure 114. The averaged brightness decreases slowly in the direction of the horizon in the case of large amounts of cumulus clouds. With mean amounts of clouds the brightness is virtually independent of the zenith angle of observation, and in /189

the case of small amounts of clouds increases with increase in the zenith angle approximately to 30-40°, and then decreases slowly or remains constant even with further increase in the zenith angle. This brightness behavior is due to the combined effect of the brightness of the clouds and the clear sky between the clouds. It has been established by theoretical calculations and experimental studies [32, 78-83] that the brightness of a cloudless sky increases considerably with increase in the zenith angle, while the brightness decreases somewhat in the case of an unbroken cloud cover. A brightness maximum is observed for /190
cumulus clouds in the vicinity of zenith angles $\vartheta \approx 30\text{-}40°$, this being used in all probability to reflection of sunshine by the illuminated sides of the clouds. It must be observed that enough experimental studies have not as yet been conducted to permit clearcut determination of the relationship between brightness distribution and amount of clouds. The relative root mean square deviations of brightness, normalized on the basis of the corresponding values at the zenith, are presented in Figure 115. It is to be seen that with increase in the zenith /191
angle the root mean square deviation first increases to reach a maximum at $\vartheta = 20\text{-}40°$, and then generally decreases. The maximum at the mean zenith angles is due to the high brightness of the sides of the clouds illuminated by the Sun and thereby confirms the conclusion drawn in the analysis of the behavior of mean brightness. The decrease in the root mean square deviation toward the horizon at $\vartheta > 50°$ is due to decrease in the variability of the cloud conditions owing to the influence of the sides of the clouds (see Chapter III, Section 1).

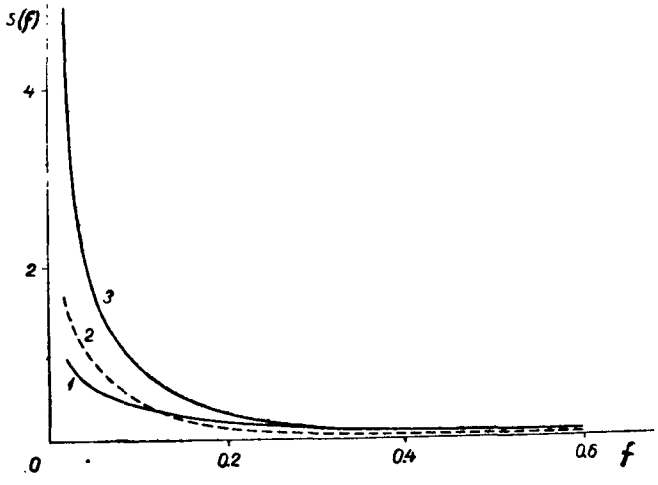

Figure 83. Spectral Densities, Averaged Over Observations of Shortwave Radiation Fluxes Under Cloud Cover Versus f in km: 1, Descending Flow (Cu); 2, Ascending (Cu); 3, Descending (Sc).

The normalized coefficients of correlation of brightness in directions $\vartheta = 5$, 35, and 65° with the brightnesses in other directions, $K_{5,\vartheta}$, $K_{35,\vartheta}$, and $K_{65,\vartheta}$ are shown in Figures 116-118 respectively. We see that the correlation coefficients of the individual observations, has in the discussion of cloud coverage of the direction of sighting (see Chapter III, Section 9), are similar, while the correlation radius decreases with increase in zenith angle ϑ. This latter circumstance is due to the increase in distance in space with increase in zenith angles ϑ with the difference between them the same.

Like the correlation coefficient, the eigenvalues of the correlation matrix as well do not vary appreciably from observation to observation. The eigenvalues and the relative accuracy in utilization of the first with components for brightness are presented in Table 6. As may be seem, the first eigenfunctions account for 38-68% of the dispersion, the second ones 14-25, and the third eigenfunctions 6-15%. On the average the first eigenvalues account for 55% of the dispersion,

the first two account for 74%, and the first three 84%, these values being somewhat smaller than the corresponding ones for the cloud cover structure. This is quite natural, since the cloud cover eigenvalues were obtained on the basis of coverages of the directions of sighting averaged over the azimuth (see Chapter III, Section 4). The first brightness eigenfunctions for individual observations are presented in Figure 119. We see that their trace is similar from case to case. The first eigenfunction generally has a maximum at mean zenith angle values ϑ = 20-40° and decreases both in the direction of the zenith and in that of the horizon to approach zero in the vicinity of the horizon. From the physical viewpoint this course of $X_1(\vartheta)$ means that the greatest deviations of one specific observation from the mean course of brightness are observed at zenith angles from 20-40°, owing to the relatively great brightness of the sides of the clouds and their substantial weight at ϑ = 20 to 40°. /194 Fluctuations from the mean are generally small on the horizon. The second eigenfunction provides information on distortions in the course of the first eigenfunctions. Increase or decrease in the brightness obtained in a specific measurement around the zenith (ϑ = 0-30°) is accompanied by simultaneous decrease or increase in the brightness at greater zenith distances (ϑ = 40-70°) (Figure 120). The third eigenfunctions provides information on the finer structure of deviation from the mean trace (Figure 121). /196 We see that increase in brightness around the zenith is accompanied by increase in brightness in the vicinity of the horizon and decrease in it at mean zenith distances, and vice versa. As may be seen from Figures 119-121, the similarity in eigenfunctions from case to case decreases with increase in their index number. The similarity of the second and third eigenfunctions for brightness and cloud coverage of the direction of sighting (see Figures 50 and 51) indicates that the finer structure /197 of deviations of brightness from the mean is determined basically by the structure of the cloud's presence. Only the first eigenfunctions differ in quality (see Figure 52). In this instance a substantial influence is exerted by the difference in the brightness of individual clouds, as well as by the circumstance that the course of brightness as a function of the zenith angle is not monotonic. The fine structure of brightness distribution within individual clouds is described by eigenfunctions starting with the fourth. They vary widely from case to case, however, and for this reason do not lend themselves well to physical interpretation. In addition, since their weight in the total dispersion is small, and the number of cases investigated is also small, we will not enter into a discussion of them at this point.

Section 6. Relationships Between the Statistical Characteristics of Radiation Fields and the Statistical Characteristics of Optical Cloud Structure Parameters

The variability in radiation fluxes in the case of cumulus clouds, as indicated by the results of Sections 1-4 of this chapter, broadly determines the variability in cloud coverage of the sky. However, study of the fine structure of brightness and radiation fluxes for cumulus clouds, as well as study of the variability of brightness and fluxes for stratified clouds, are inconceivable without study of the relationships between the statistical characteristics of brightness fields and the statistical characteristics of clouds. Together with the possibility of using these relationships to extract information on cloud structure, turbulence inside clouds, and so forth [84], studies of this kind are

important because of the nonlinearity of the relationships between radiation conditions and the optical parameters of the real atmosphere, and also because of the nonlinearity of the influence of light on such natural processes as photosynthesis, evaporation, melting of snow and ice, convection, etc. Thus it has of late become essential to study the optical properties of the cloud cover as a complete formation.

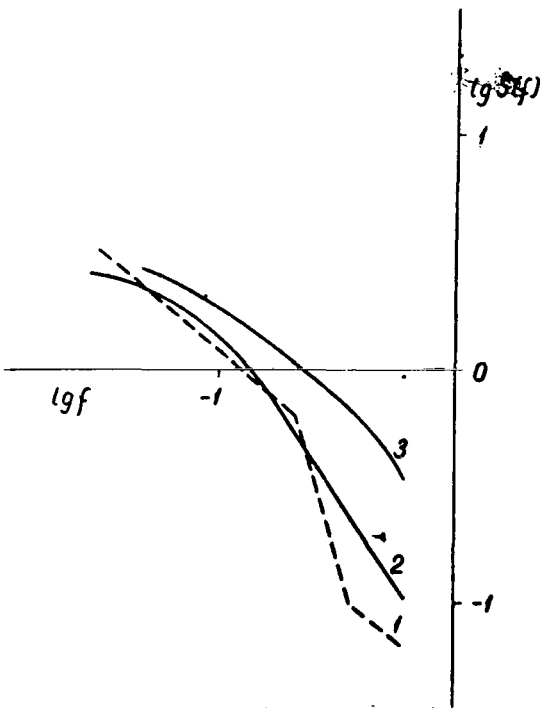

Figure 84. Spatial Spectral Densities, Averaged over Observations of Shortwave Radiation Fluxes Inside Layer of Stratocumulus Clouds Represented in Logarithmic Coordinates: 1, R_k; 2, Q; 3, A_k.

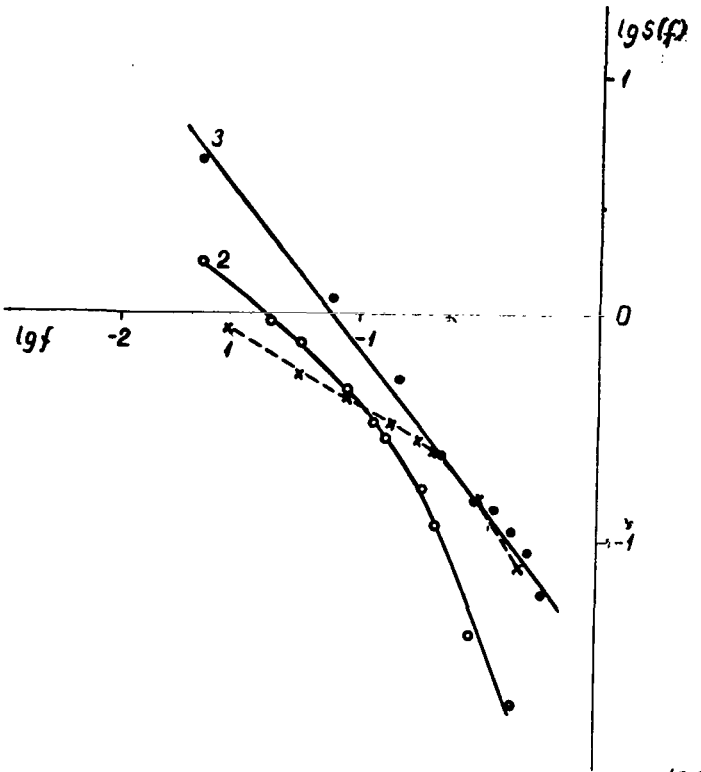

/168

Figure 85. Spatial Spectral Densities, Averaged over Observations of Shortwave Radiation Fluxes Below Cloud Layer Represented in Logarithmic Coordinates: 1, Q for Cu; 2, R_k for Cu; 3, Q for Sc.

As was pointed out in Chapter I, radiation conditions in a scattering medium are connected by a nonlinear relationship to the optical parameters of the medium usually employed in the transfer theory: the coefficient of scattering and absorption, the scattering indicatrix, and the optical thickness. /198 Description of the radiation conditions of heterogeneous media by means of the transfer equation with the mean parameters of a medium consequently entails a systematic error which often cannot be evaluated by the investigator. Although the need for extending the transfer theory to media having randomly distributed parameters was recognized several years ago [85], but only now is solution of this problem being approached [32, 39, 86-92]. Formulation of the radiation

transfer problem of clouds is not possible within the framework of the classical transfer theory. The chief obstacle is the absence of means for determining the microphysical cloud cover parameters entering into this theory and their variability for a specific observation, as well as the mathematical difficulties involved in solving the transfer equation for a medium with statistically distributed optical parameters. But even the possibility of solving the transfer equation for heterogeneous media would contribute little toward development of cloud cover optics, since, because of the considerable number of parameters of the process of propagation of light, the results in the forms of tables and graphs cannot be used to solve the problem. The best prospects are thus afforded by finding macrocharacteristics of the cloud cover such as define the general outline of the cloud brightness picture.

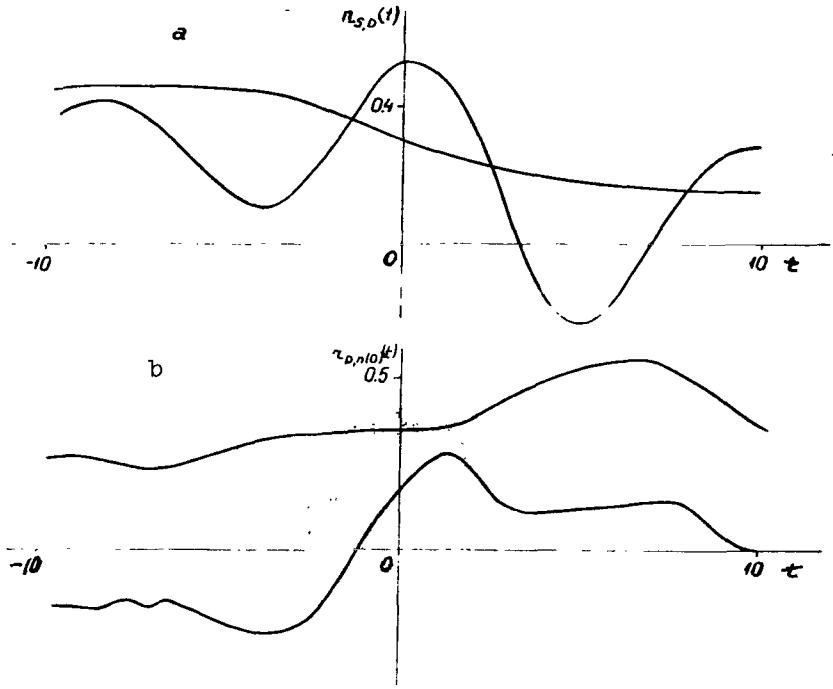

Figure 86. Examples of Reciprocal Correlation Functions for Cumulus Clouds n = 0.3-0.8 (t in min): a, for Direct and Scattered Radiation; b, for Scattered Radiation and Cloud Coverage of the Zenith.

Aside from the physical aspect, an approach such as this is at the present dictated by the mathematical difficulties, since statistical analysis in the general form (without numerical analysis in the form of tables and graphs) simply cannot be accomplished without a convenient and flexible mathematical apparatus.

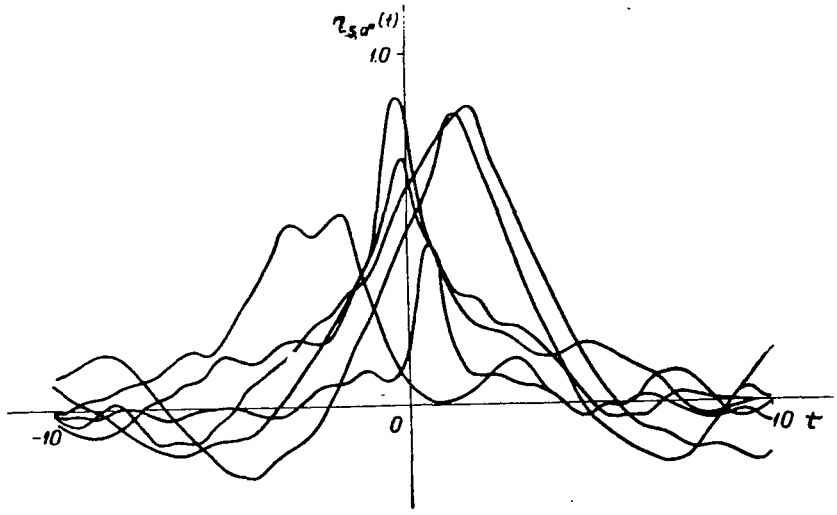

Figure 87. Examples of Reciprocal Correlation Functions of Direct and Total Radiation for Cumulus Clouds $n(\vartheta_{\odot}) = 0.3$ (t in min).

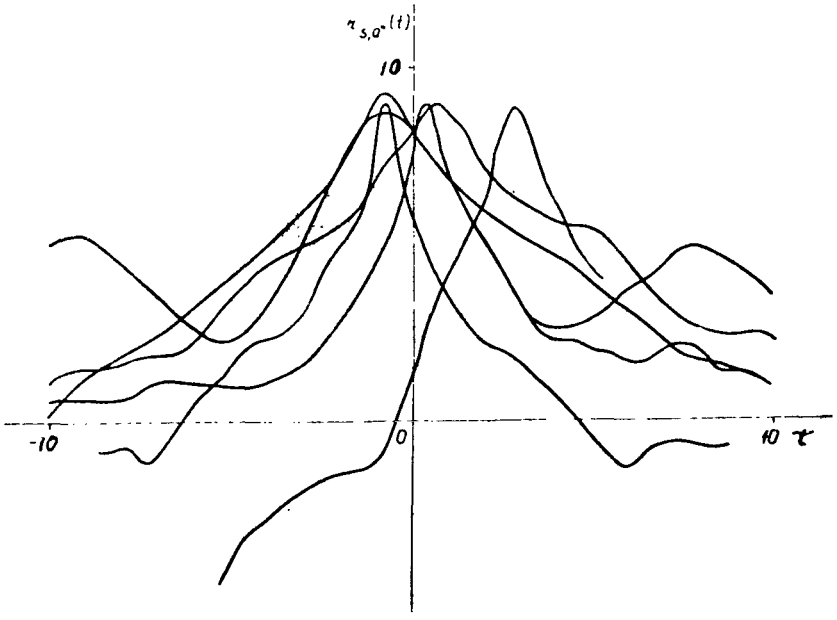

Figure 88. Examples of Reciprocal Correlation Functions of Direct and Total Radiation for Cumulus Clouds $n(\vartheta_{\odot}) > 0.3$ (t in min).

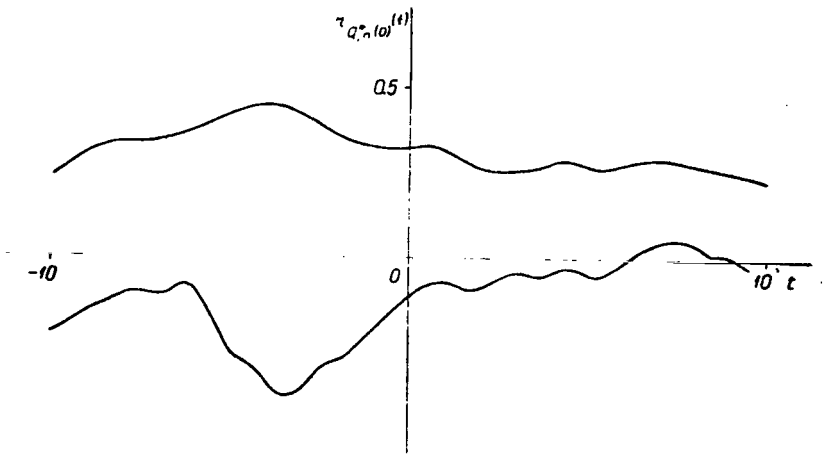

Figure 89. Examples of Reciprocal Correlation Functions of Total Radiation and Coverage of the Zenith by Cumulus Clouds (t in min).

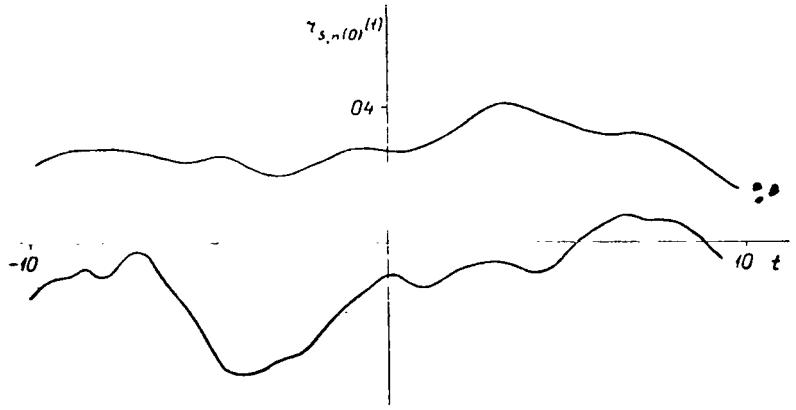

Figure 90. Examples of Reciprocal Correlation Functions of Direct Radiation and Coverage of the Zenith by Cumulus Clouds (t in min).

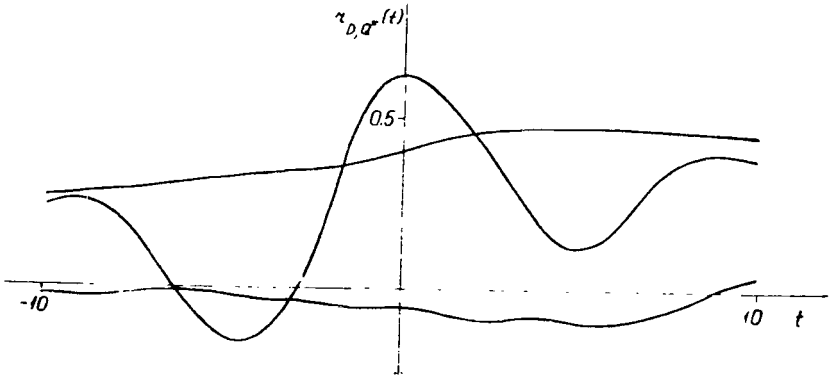

Figure 91. Examples of Reciprocal Correlation Functions of Scattered and Total Radiation for Cumulus Clouds (t in min).

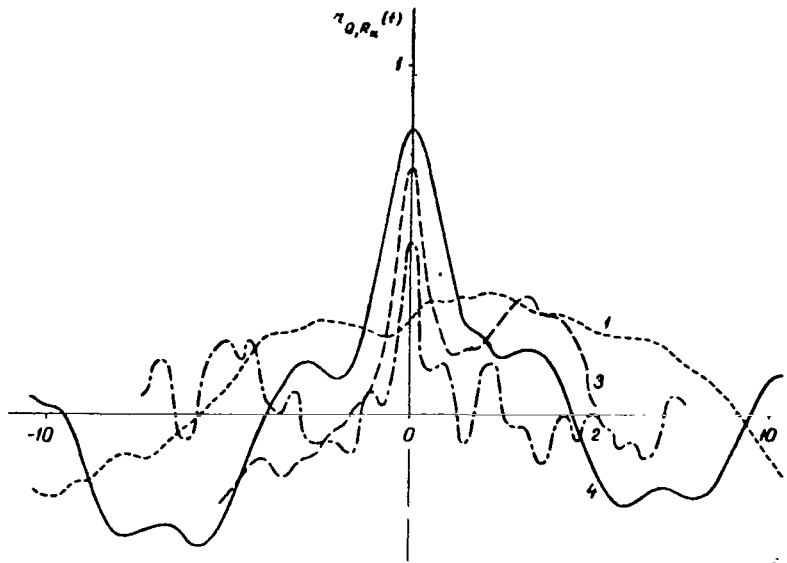

Figure 92. Examples of Reciprocal Correlation Functions of Ascending and Descending Fluxes of Shortwave Radiation (x in km): 1, Above Layer of Stratocumulus Clouds; 2, 3, Inside Cloud Layer (Sc); 4, Below Layer of Stratocumulus Clouds.

To illustrate the foregoing let us make an excursion into the field of molecular physics. As we know, thermodynamics, while it does not enter into microscopic examination of processes nevertheless permits the drawing of a large number of conclusions regarding the general progress of such processes, ones which are just as reliable as the fundamental laws underlying thermodynamics.

TABLE 6. EIGENVALUES OF SHORTWAVE RADIATION INTENSITY.

Cloudiness	m	$\lambda_{1,m}\%$	$\lambda_{2,m}\%$	$\lambda_{3,m}\%$	$\lambda_{4,m}\%$	$\lambda_{5,m}\%$
1Ci, Cs, 3Cu	18	45.6	64.5	79.6	86.6	91.2
1Ci, Cs, 3Cu	18	60.5	75.0	84.2	89.2	92.4
0Ci, Cc, 4Cu—0Ci, Cs, 2Cu	18	63.0	79.2	85.7	90.4	93.1
0Ci, Cc, 4Cu—0Ci, Cs, 2Cu	18	49.8	72.3	81.4	86.9	90.8
5Cu, Cb — 6Cu	18	64.8	79.2	87.3	91.3	94.2
5Cu, Cb — 6Cu	18	47.0	68.2	83.6	88.9	92.1
5Cu — 8Cu	18	38.2	63.2	73.9	84.8	91.2
5Cu — 8Cu	18	50.0	72.2	79.4	85.1	88.3
$\overline{10}$ Cu, Cb — 1Ci, 6Cu	9	67.7	88.0	94.1	96.7	97.9
$\overline{10}$ Cu, Cb — 1Ci, 6Cu	18	60.0	79.2	87.0	92.9	95.5

In translating the foregoing into the terms of cloud cover optics we note that cloud brightness parameters do not reflect many minute details of the macrooptical parameters of the elementary scattering and absorbing volume. /199
Hence it is advisable to exclude superfluous details in formulation of the problem. From the viewpoint of optical properties the cloud cover as a whole should be characterized by a small number of generalizing macroparameters. The

relationships between the cloud cover and radiation fluxes for cumulus clouds presented in Sections 1-4 of this chapter were derived in the first approximation precisely in this manner.

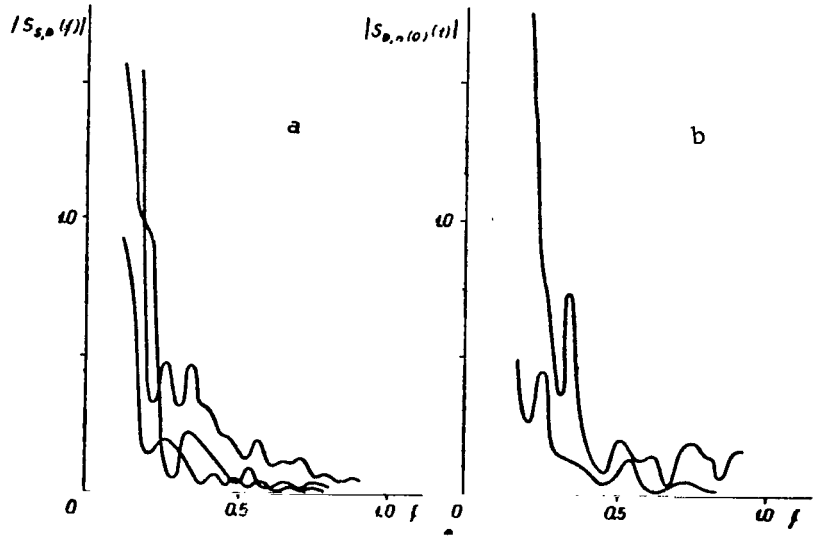

Figure 93. Examples of Moduli of Reciprocal Spectral Densities for Cumulus Clouds, n = = 0.3-0.8, Versus Linear Frequency (f in min^{-1}): a, for Direct and Scattered Radiation; b, for Scattered Radiation and Cloud Coverage of the Zenith.

In what follows we will consider the variability in the transmission and reflection of an optically dense cloud layer as a function of the variability of its optical thickness due to the variability of the altitude of the lower and upper boundaries, moisture content, and microstructure. It is here assumed that the variability in optical thickness may be described by a normal random process (see Chapter I, Section 6). This obviously is plausible, since the optical thickness is formed under the combined influence of several randomly varying parameters.

Approximate solutions of the transfer equation in the form of simple analytical formulas were used for studies of this kind. Of the great number of approximate formulas currently in existence the asymptotic formulas of G. V. Rozenberg for homogeneous layers of optically thick turbid media have been confirmed by extensive laboratory studies [80]. The relationship has been established in this case between the macrooptical parameters figuring in the theory and the microoptical parameters of clouds [32, 80].

If appreciable absorption takes place in the layer of the atmosphere below clouds, the transmission coefficient P of a plane-parallel cloud layer is described by the following formula:

$$T(\mu_0, \mu, \bar{\tau}+\tau) = \frac{\mu N(\mu_0, \mu, y)}{\pi \operatorname{sh}\left[\left(\frac{\tau+\bar{\tau}}{l}+1\right) y\right] - A \operatorname{sh}\left(\frac{\tau+\bar{\tau}}{l} y\right)}, \tag{4.29}$$

in which $\mu_0 = \cos \vartheta_\odot$, $\vartheta_\odot$ is the zenith distance of the Sun, $\mu = \cos \vartheta$, ϑ is the zenith distance of the direction of observation, $y = 2\sqrt{l\beta}$, l is a parameter characterizing the degree of extension of the scattering indicatrix, $\beta = \alpha/\sigma$ is the specific absorption by the cloud mass, α and σ are the coefficients of absorption and scattering, which we assume to be constant within the limits of a particular cloud layer, A is the albedo of the underlying surface, $\bar{\tau}$ and τ /200 are the mean optical thickness of the layer and its deviation from the mean, and $N(\mu_0, \mu, y)$ is a function introduced to simplify the notation (see [32]).

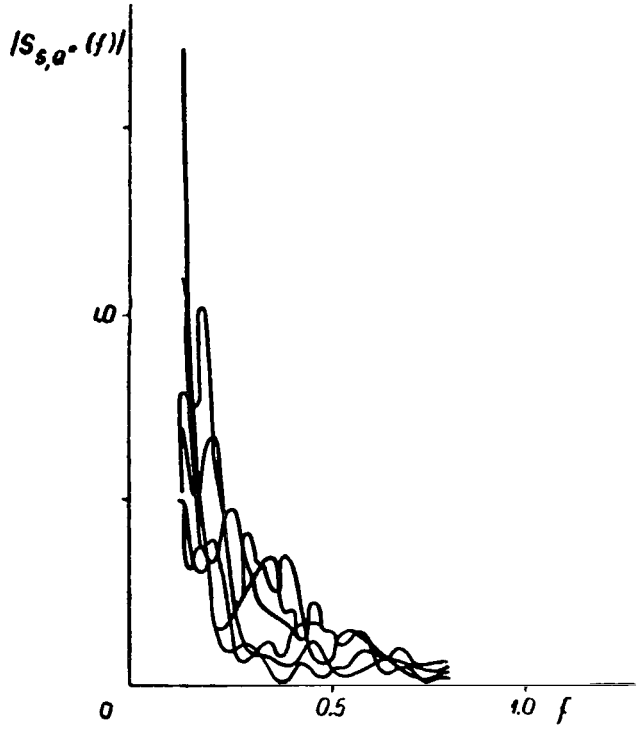

Figure 94. Examples od Moduli of Reciprocal Spectral Densities of Direct and Total Radiation for Cumulus Clouds $n(\vartheta_\odot) \geqslant 0.3$ (f in min^{-1}).

When $\beta \to 0$, that is, when absorption is entirely absent from the cloud layer, formula (4.29) is simplified and assumes the form

$$T(\mu_0, \mu, \bar{\tau}+\tau) = \frac{\mu c_1}{\pi[1+c_2(\bar{\tau}+\tau)]}, \tag{4.30}$$

in which $c_1 = \frac{1}{3} + \mu_0$ for the flux, or $c_1 = (\frac{1}{3} + \mu_0)\left[\frac{1 + 2A}{3} + (1 - A)\mu\right]$ for the intensity, and $c_2 = \frac{1 - A}{l}$ is constant. In this instance the reflecting power

of the cloud layer is expressed in the form of a simple relation by its transmission coefficient

$$|S_{\xi,\eta}(f)| = h\sqrt{A^2(f)+B^2(f)}, \tag{4.31}$$

in which $h(\mu_0, \mu)$ is a function independent of the optical thickness and differing but little from unity

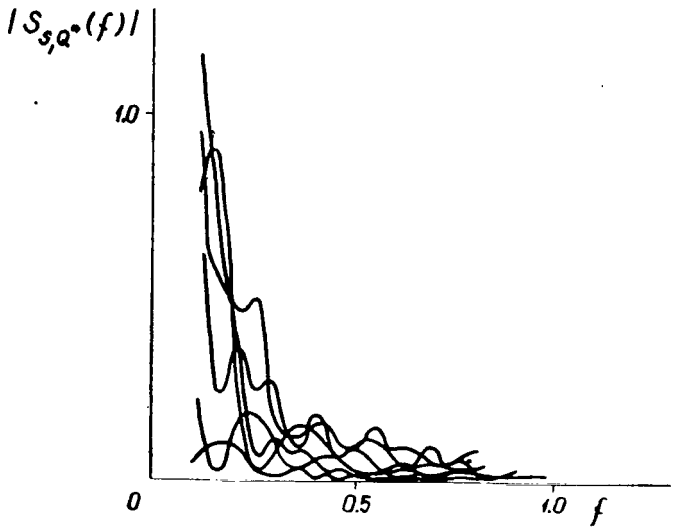

Figure 95. Examples of Moduli of Reciprocal Spectral Densities of Direct and Total Radiation for Cumulus Clouds, $n(\vartheta_\odot)$ = 0.4-0.5 (f in min^{-1}).

If the cloud layer is sufficiently thick ($y \ll 1$, $\bar{\tau} + \tau \gg l$), when absorption is present ($\beta \neq 0$) from formula (4.29) we obtain for the transmission coefficient

$$T(\mu_0, \mu, \bar{\tau}+\tau) = \frac{\mu}{\pi} N(\mu_0, \mu, y, A) e^{-\frac{\bar{\tau}+\tau}{l}\nu}, \tag{4.32}$$

in which $N(\mu_0, \mu, y, A)$ is a function introduced to simplify the notation (see [32]).

Formulas (4.29)-(4.31) are strictly speaking applicable to description of the propagation of light in plane-parallel horizontally homogeneous optically thick layers $\bar{\tau} + \tau \geqslant 5$, and since for clouds $l \approx 7$ to 10. Formula (4.32) is applicable when $\bar{\tau} + \tau \gg 10$. For study of the fluctuation in the brightness of real clouds by means of formulas (4.29)-(4.32) it is necessary for the scales of the heterogeneities of the cloud cover to be slightly larger than the mean free path of a photon in a cloud. As we know, under natural conditions the typical scale of the heterogeneities of the cloud cover are much greater than the mean / 201
free path of a photon in a cloud. The small-scale heterogeneities encountered in nature are smoothed out and averaged in such treatment it remains a problem of the future to take them into account.

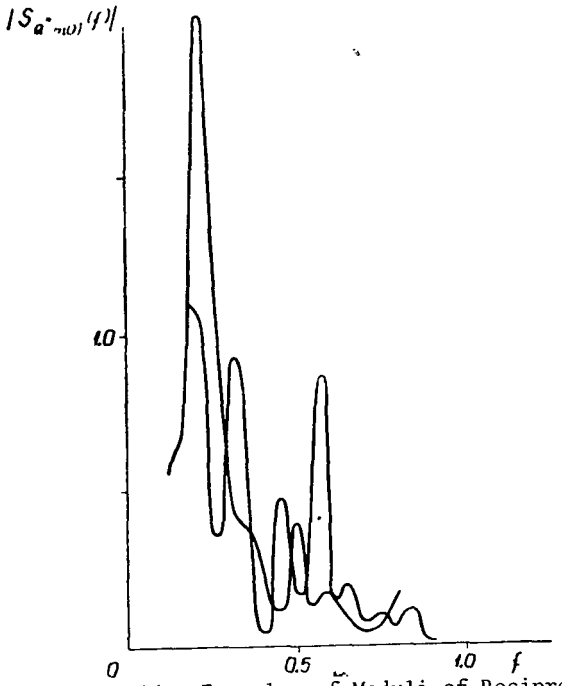

Figure 96. Examples of Moduli of Reciprocal Spectral Densities of Total Radiation and Coverage of the Zenith by Cumulus Clouds at n(0) = 0.2-0.4 (f in min^{-1}).

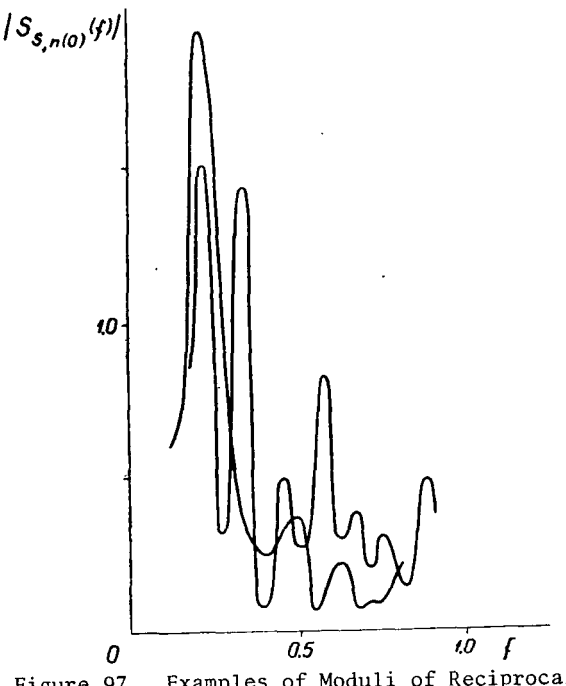

Figure 97. Examples of Moduli of Reciprocal Spectral Densities of Direct Radiation and Coverage of the Zenith by Cumulus Clouds at n(0) = 0.2-0.4 (f in min^{-1}).

Since formulas (4.29)-(4.32) describe similar situations, we will henceforth use formulas (4.30) and (4.31) for more detailed analysis, and on the basis of relations (4.29) and (4.32) present only formulas for the means, dispersions, and correlation functions of transmission as a function of the statistical characteristics of the optical thickness. /202

On the basis of formulas (1.38) and (4.30) we obtain for the transmission probability density

$$p(T)=\frac{c_1}{\sqrt{2\pi}\,c_2\sigma_\tau T^2}\exp\left[-\frac{1}{2\sigma_\tau^2}\left(\frac{c_1}{c_2T}-\frac{1}{c_2}-\bar{\tau}\right)^2\right], \tag{4.33}$$

in which σ^2_τ is the dispersion of the optical thickness.

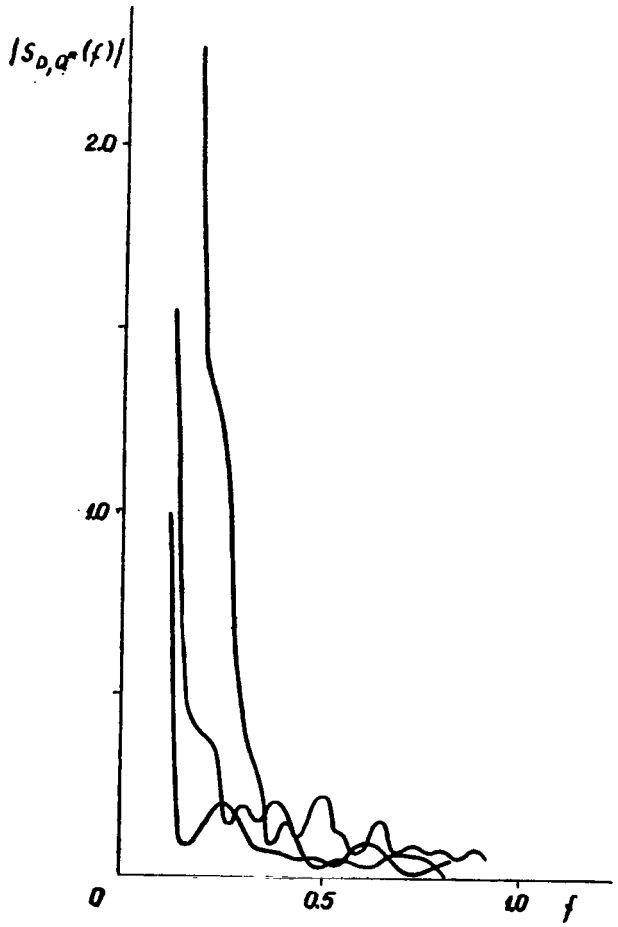

Figure 98. Examples of Moduli of Reciprocal Spectral Densities of Scattered and Total Radiation for Cumulus Clouds, n = 0.4-0.8 (f in min^{-1}).

The transmission coefficient probability distribution functions are shown in Figure 122 plotted against the mean optical thickness and its dispersion. $c_2 = 0.1$ and $\mu_0 = 0.5$ were adopted in the calculations. As is to be seen, the distribution function is the more asymmetrical the greater is the dispersion of the optical thickness. In addition, the distribution function extends in the direction of the higher transmissions. On the one hand, with increase in $\bar{\tau}$ the maximum in the transmission distribution is shifted toward smaller values of P and the maximum brightness probability increases. The modal transmission does not coincide with the transmission for the mean optical thickness but is displaced toward the greater optical thicknesses, the further the greater is the dispersion of the optical thickness and the smaller is the mean optical thickness of the layer, that is, $T_{mod} < T_{\bar{\tau}}$. On the other hand, the optical thickness corresponding to mean transmission $\bar{T}$ is smaller than the mean optical thickness $\tau(\bar{T}) < \bar{\tau}$. The empirical functions of distribution of zenith brightness and total

radiation flux probabilities for unbroken clouds are presented in Figure 123. The curves have been calculated theoretically on the basis of formula (4.33). It is to be seen from Figures 123, 70, and 73, as well as from [73, 77], that the empirically derived probability densities of brightness (transmission) are asymmetrical and always extend in the direction of the high brightnesses. This circumstance does not contradict the hypothesis advanced regarding the normal distribution of optical thickness.

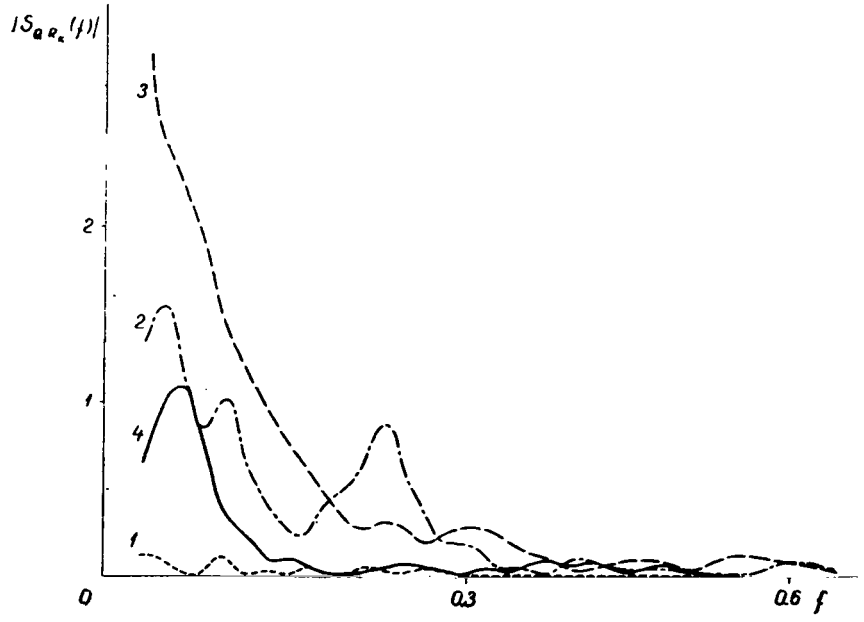

Figure 99. Examples of Moduli of Reciprocal Spectral Densities of Ascending and Descending Fluxes of Short-wave Radiation (f in km^{-1}): 1, Above Layer of Stratocumulus Clouds; 2, 3, Inside Cloud Layer (Sc); 4, Below Layer of Stratocumulus Clouds.

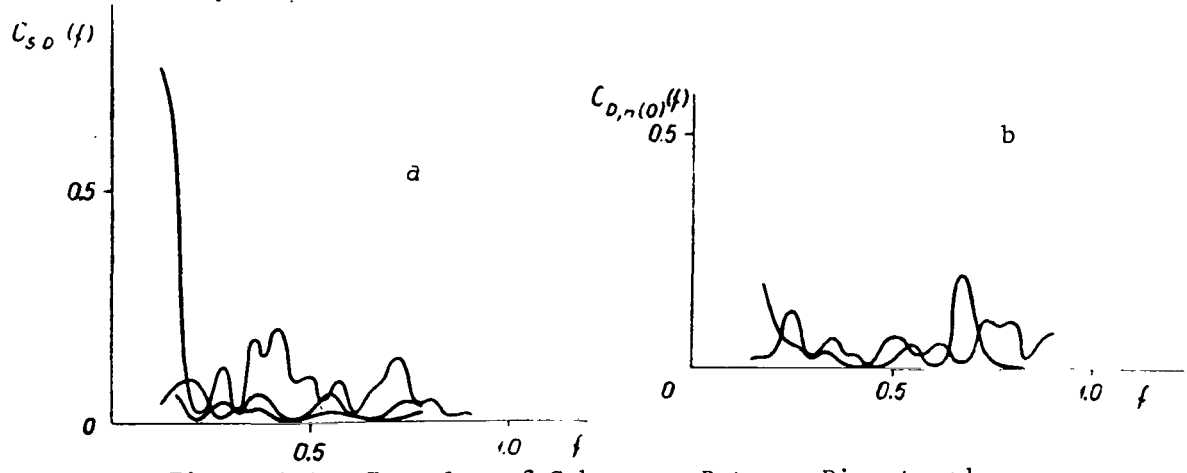

Figure 100. Examples of Coherence Between Direct and Scattered Radiation a, and Scattered Radiation and Cloud Coverage of the Zenith b with n = 0.3-0.8 (f in min^{-1}).

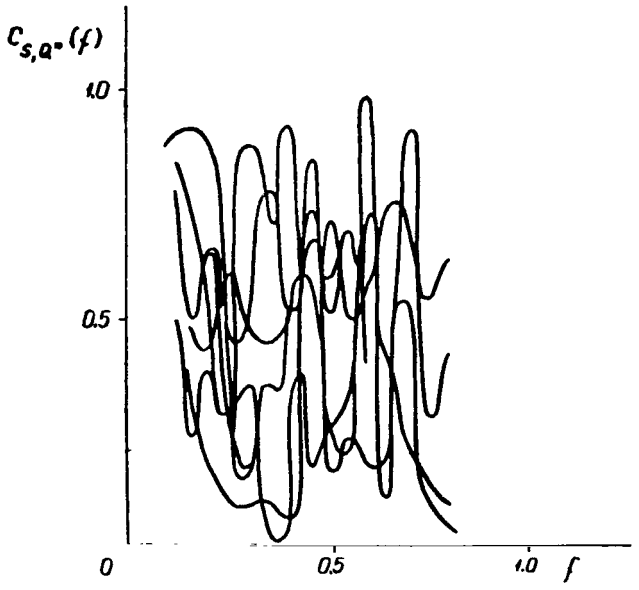

Figure 101. Examples of Coherence Between Direct and Total Radiation for Cumulus Clouds, $n(\vartheta_\odot) \geqslant 0.3$ (f in min^{-1}).

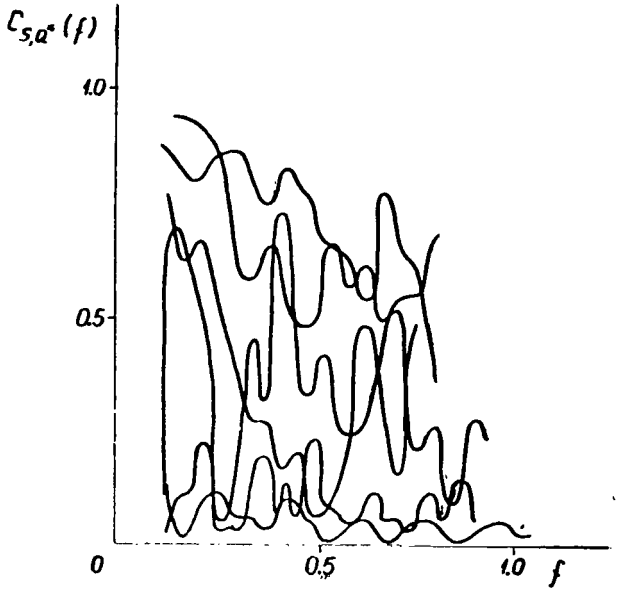

Figure 102. Examples of Coherence Between Direct and Total Radiation for Cumulus Clouds, $n(\vartheta_\odot) = 0.4\text{-}0.5$ (f in min^{-1}). /182

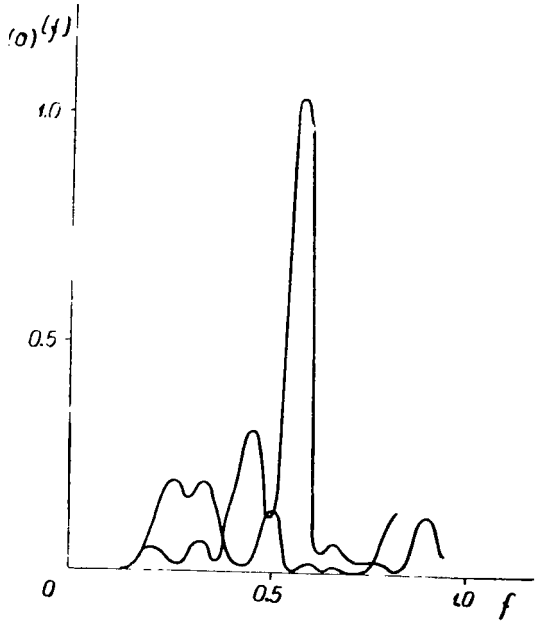

Figure 103. Examples of Coherence Between Total and Radiation amd Coverage of the Zenith by Cumulus Clouds (f in min^{-1}).

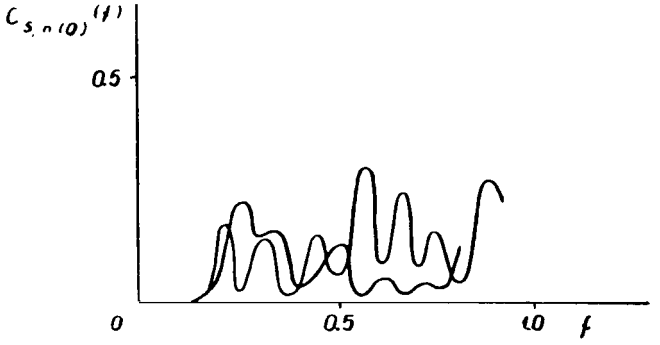

Figure 104. Examples of Coherence Between Direct Radiation and Coverage of the Zenith by Cumulus Clouds, with n(0) = 0.2-0.4 (f in min^{-1}).

/183

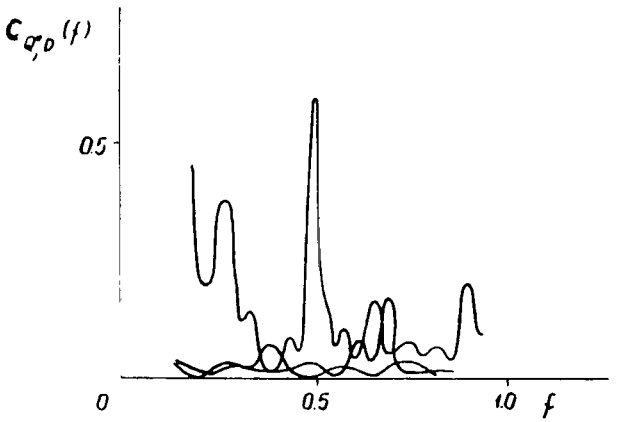

Figure 105. Examples of Coherence Between Total and Scattered Radiation for Cumulus Clouds, n = 0.4-0.5 (f in min^{-1}).

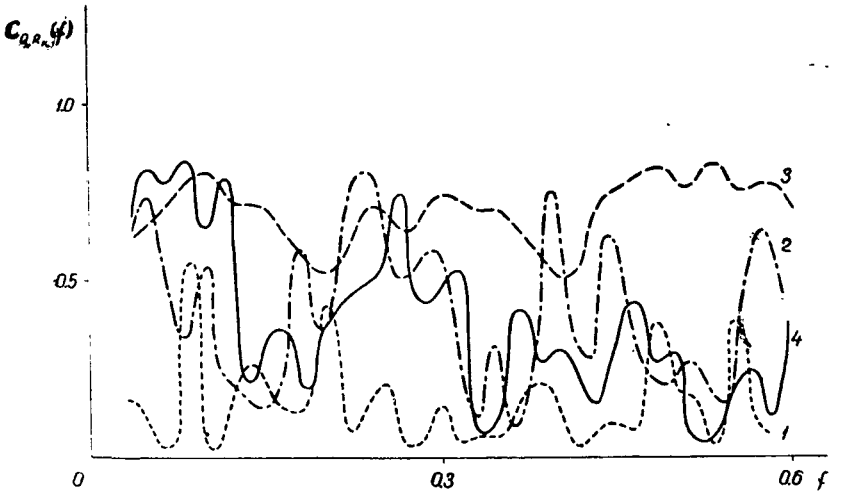

Figure 106. Examples of Coherence Between Ascending and Descending Fluxes of Shortwave Radiation (f in km^{-1}): 1, Above Layer of Stratocumulus Clouds; 2, 3, Inside Cloud Layer (Sc); 4, Below Layer of Stratocumulus Clouds.

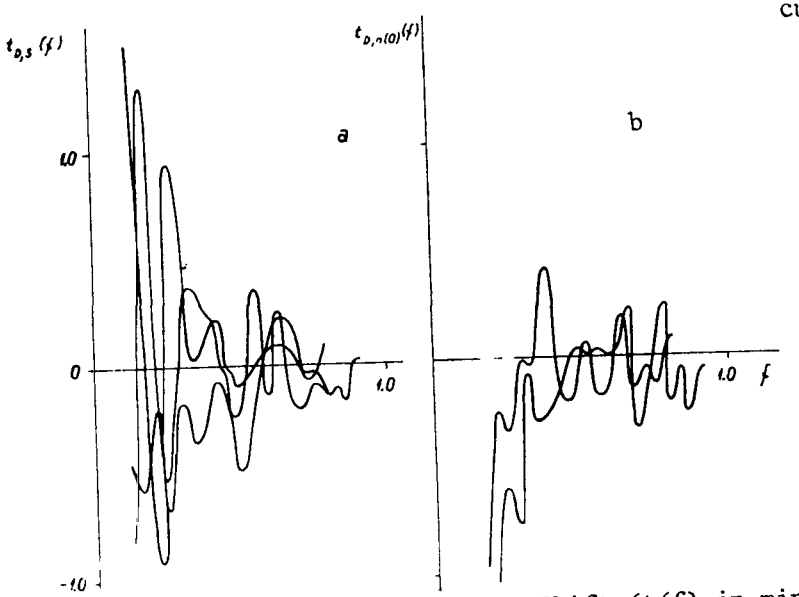

Figure 107. Examples of Phase Shift (t(f) in min) Between Scattered and Direct Radiation a, and Scattered Radiation and Cloud Coverage of the Zenith b, for Cumulus Clouds, n = 0.3-0.8, Versus Frequency f in min^{-1}.

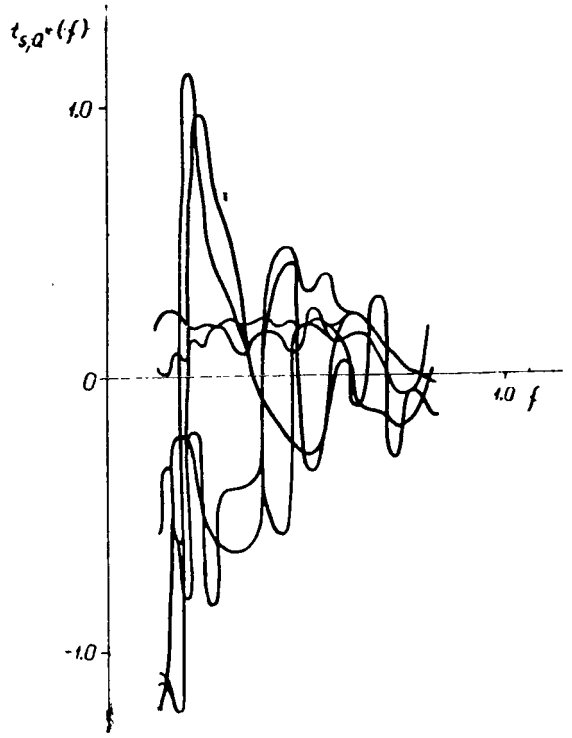

Figure 108. Examples of Phase Shift Between Direct and Total Radiation for Cumulus Clouds, $n(\vartheta_\odot) \geqslant 0.3$ (t (f) in min), f in min^{-1}).

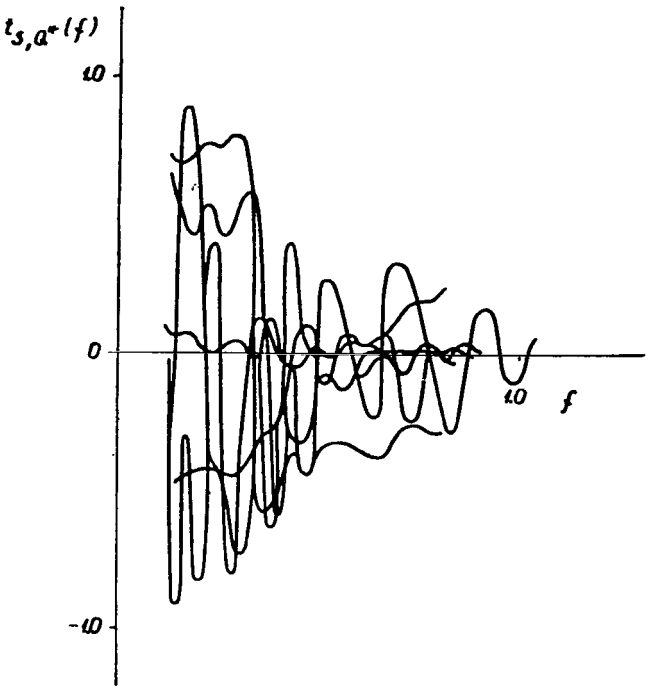

Figure 109. Examples of Phase Shift Between Direct and Total Radiation for Cumulus Clouds, $n(\vartheta_\odot) = 0.4\text{-}0.5$ (t(f) in min, f in min^{-1}).

The mean transmission coefficient (reflection factor), its dispersion, and its correlation function as a function of the variability of the optical thickness may be obtained by substituting in formulas (1.39)-(1.41) the transmission /203 coefficient expressed by relations (4.29)-(4.32). However, the expressions derived in analytical form cannot be integrated. We employ the moment method in order to obtain definitive results in the form of approximate analytical formulas. For this purpose we expand transmission coefficient $T(\mu_0, \mu, \bar{\tau} + \tau)$ into a Maclaurin series on the basis of the fluctuations in optical thickness and substitute them in formulas (1.42)-(1.44). As will be demonstrated later, a sufficiently high accuracy of approximation is ensured even by the first terms of the expansion.

The mean coefficients of transmission and reflection based on formulas (4.29)-(4.32) are expressed by

$$\overline{T(\mu_0, \mu, \bar{\tau}+\tau)} = T(\mu_0, \mu, \bar{\tau})\left[1+\frac{y^2}{2l^2}(2E^2-1)\sigma_\tau^2\right], \qquad (4.34)$$

in which

$$E=\frac{\operatorname{ch}\left(\frac{\bar{\tau}}{l}+1\right)y-A\operatorname{ch}\frac{\bar{\tau}}{l}y}{\operatorname{sh}\left(\frac{\bar{\tau}}{l}+1\right)y-A\left(\operatorname{sh}\frac{\bar{\tau}}{l}y\right)}, \tag{4.35}$$

$$\overline{T(\mu_0,\mu,\bar{\tau}+\tau)}=T(\mu_0,\mu,\bar{\tau})\left[1+c^2\sigma^2_\tau\right], \tag{4.36}$$

/204

in which

$$c=\frac{c_2}{1+c_2\bar{\tau}},$$

$$\overline{\varrho(\mu_0,\mu,\bar{\tau}+\tau)}=\frac{\mu_0}{\pi}h(\mu_0,\mu)-(1-A)\overline{T(\mu_0,\mu,\bar{\tau}+\tau)}= \tag{4.38}$$

$$=\varrho(\mu_0,\mu,\bar{\tau})-(1-A)T(\mu_0,\mu,\bar{\tau})c^2\sigma^2_\tau$$

and

$$\overline{T(\mu_0,\mu,\bar{\tau}+\tau)}=T(\mu_0,\mu,\bar{\tau})\left(1+\frac{y^2}{2l^2}\sigma^2_\tau\right) \tag{4.39}$$

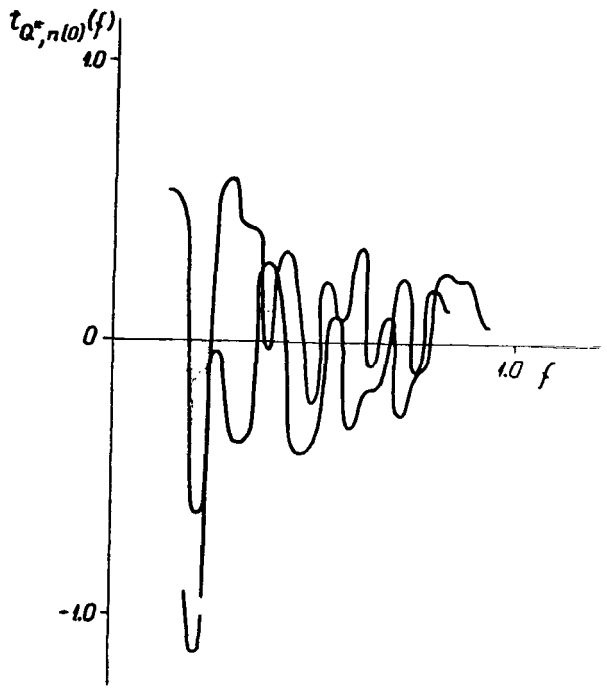

Figure 110. Examples of Phase Shift Between Total Radiation and Coverage of Zenith by Cumulus Clouds at n(0) = = 0.2-0.4 (t(f) in min, f in min^{-1}).

In formulas (4.34)-(4.39) $T(\mu_0, \mu, \bar{\tau})$ is the transmission coefficient and $\rho(\mu_0, \mu, \bar{\tau})$ is the reflecting power of the layer plane-parallel to mean optical thickness $\bar{\tau}$, which may be derived from formulas (4.29)-(4.32) when $\tau = 0$. It is to be seen that the mean transmission is expressed by the transmission at the mean optical thickness multiplied by a corresponding correction factor. It follows from formulas (4.34)--(4.37) and (4.39) that the mean transmission coincides with the transmission at the mean optical thickness $\bar{\tau}$ only in the limiting case, when the optical thickness dispersion approaches zero, that is, when there are no fluctuations in optical thickness. In all of the cases the mean transmission is greater than would be obtained from formulas (4.29)-(4.32) for the mean optical thickness. At the same time, the reflecting power of a layer of variable optical thickness (4.38) is always lower than the reflecting power of a plane-parallel layer of mean optical thickness $\bar{\tau}$.

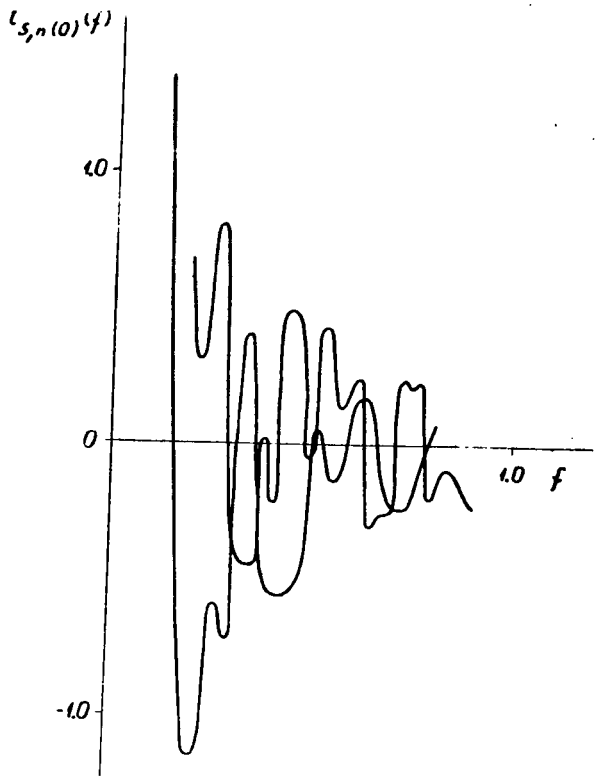

Figure 111. Examples of Phase Shift Between Direct Radiation and Coverage of Zenith by Cumulus Clouds at n(0) = = 0.2-0.4 (t(f) in min, f in min^{-1}).

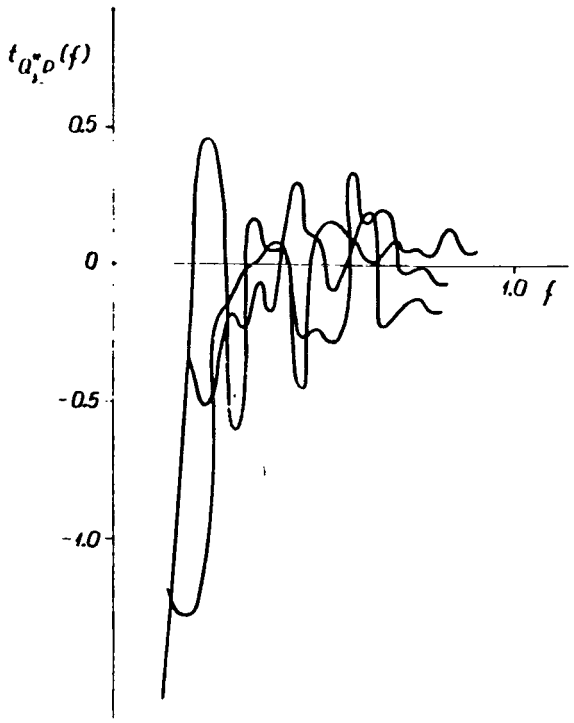

Figure 112. Examples of Phase Shift Between Total and Scattered Radiation for Cumulus Clouds, n = = 0.4-0.8 (t(f) in min, f in min^{-1}).

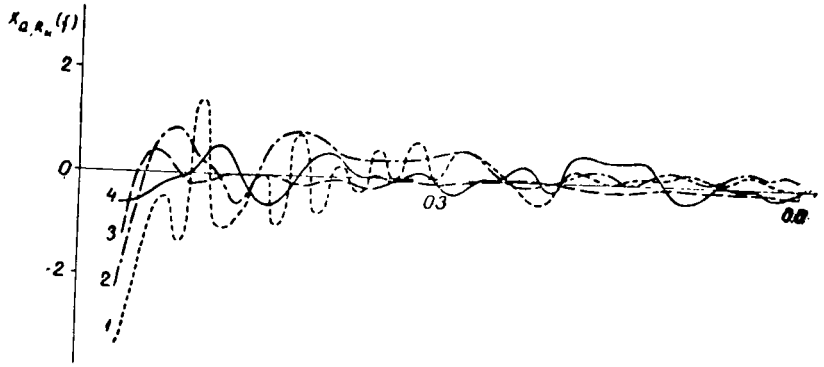

Figure 113. Examples of Phase Shift Between Descending and Ascending Fluxes of Shortwave Radiation: .1, for Stratocumulus Clouds; 2, 3, Inside Cloud Layer (Sc); 4, Below Sc Layer (x(f) in km; f in km^{-1}).

In observations, especially from a great distance (as from outer space), or in measurements of the scattered radiation flux averaging is performed over a certain surface Ω of the cloud layer. Let us carry out analysis of the influence of averaging for formulas (4.30) and (4.36). Substituting the value $\tau' = \tau + \bar{\tau} - \bar{\tau}^{\Omega}$ for τ in formula (4.30) and replacing dispersion σ_{τ}^2 in formula (4.36) with dispersion $\sigma_{\tau'}^2 = \sigma_{\tau}^2 - \sigma_{\bar{\tau}\Omega}^2$, we obtain the approximate relation between $\bar{T}_{\Omega}$ and $\bar{\tau}_{\Omega}$ at the average correction value $\sigma_{\tau'}^2$,

$$\bar{T}^{\Omega}(\mu_0, \mu, \bar{\tau}^{\Omega}+\tau') = T(\mu_0, \mu, \bar{\tau}^{\Omega})[1+c_{\Omega}^2(\sigma_{\tau}^2 - \sigma_{\bar{\tau}\Omega}^2)], \tag{4.40}$$

in which

$$c_{\Omega} = \frac{c_2}{1+c_2\bar{\tau}^{\Omega}},$$

and $\sigma_{\bar{\tau}\Omega}^2$ is the dispersion of τ values averaged over region Ω. If $\Omega \to 0$, then $\bar{\tau}^{\Omega} \to \tau$ and $\sigma_{\bar{\tau}\Omega}^2 \to \sigma_{\tau}^2$, that is, $\bar{T}_{\Omega} \to T$; if $\Omega \to \infty$, then $\bar{\tau}^{\Omega} \to \bar{\tau}$ and $\sigma_{\bar{\tau}\Omega}^2 \to 0$, this resulting in formula (4.36).

/205

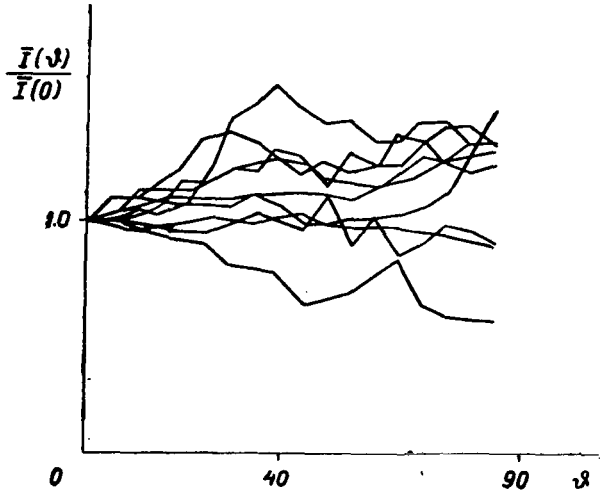

Figure 114. Relative Mean Sky Brightness Versus Zenith Angle of Direction of Sighting for Cumulus Clouds, n = 0.2--0.9.

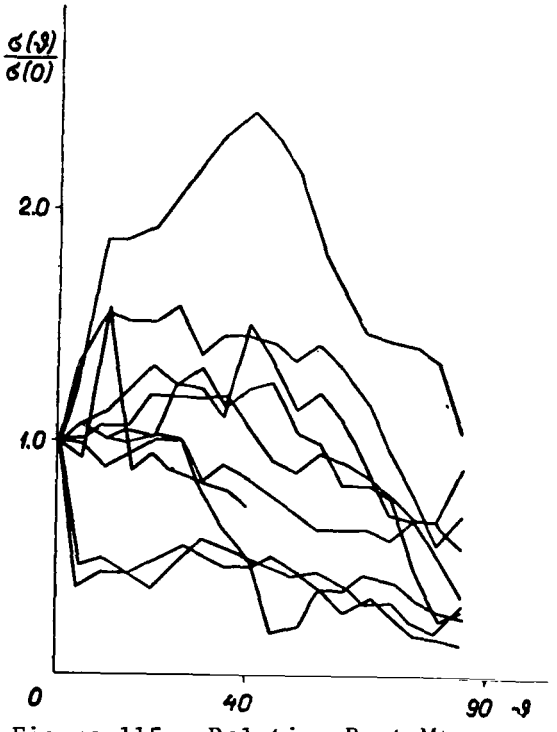

Figure 115. Relative Root Mean Square Deviations of Sky Brightness Versus Zenith Angle of Direction of Sighting for Cumulus Clouds, n = = 0.2-0.9.

If the averaging over space Ω is insufficient, the dispersion σ_{τ}^2, is a random value and the functional relationship (4.40) between $\bar{T}^{\Omega}$ and $\bar{\tau}^{\Omega}$ is random in nature.

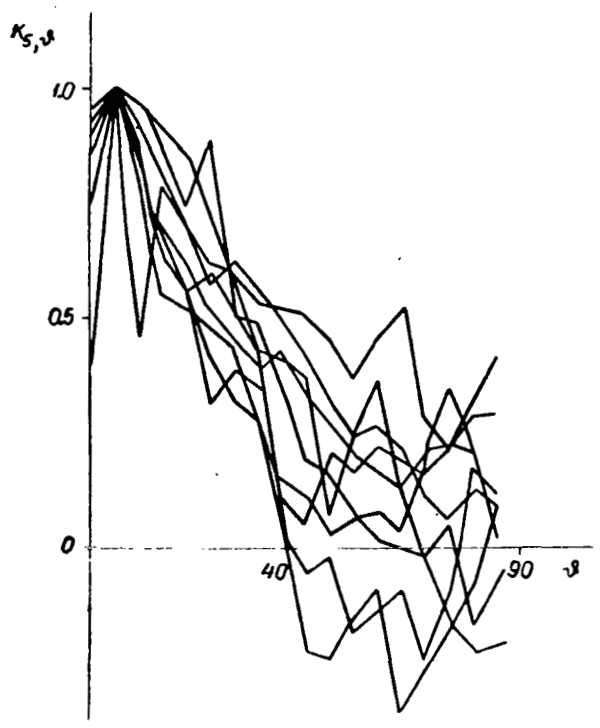

Figure 116. Normalized Coefficients of Sky Brightness Correlation (Cumulus Clouds) at ϑ = 5° with Brightness at ϑ = 0-85°.

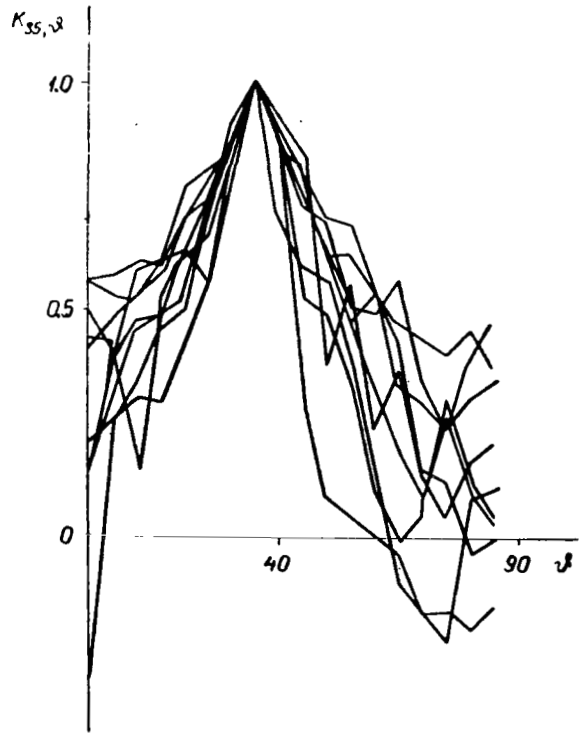

Figure 117. Normalized Coefficients of Sky Brightness Correlation (Cumulus Clouds) at ϑ = 35° with Brightness at ϑ = 0-85°.

The dispersion of dispersion σ^2_{τ}, has been calculated to evaluate the random nature of functional relationship (4.40). On the assumption that optical thickness τ has a correlation function of the form $r_{\tau}(t) = e^{-\alpha|t|}$, an approximate evaluation of the dispersion of dispersion $\sigma^2_{\sigma^2_{\tau}}$, has been obtained which is expressed as

$$\sigma^2_{\sigma^2_{\tau}} = \overline{\sigma^4_{\tau}} - (\overline{\sigma^2_{\tau}})^2 \leqslant \sigma^4_{\tau}\left[\frac{2}{1+a\Omega} - 2\left(\frac{2}{2+a\Omega}\right)^2\right] \tag{4.41}$$

or

$$\frac{\sigma^2_{\sigma^2_{\tau}}}{\sigma^2_{\tau} - \sigma^2_{\tau\Omega}} \leqslant \left(\frac{1}{1-\frac{2}{2+a\Omega}}\right)^2\left[\frac{2}{1+a\Omega} - 2\left(\frac{2}{2+a\Omega}\right)^2\right] \tag{4.42}$$

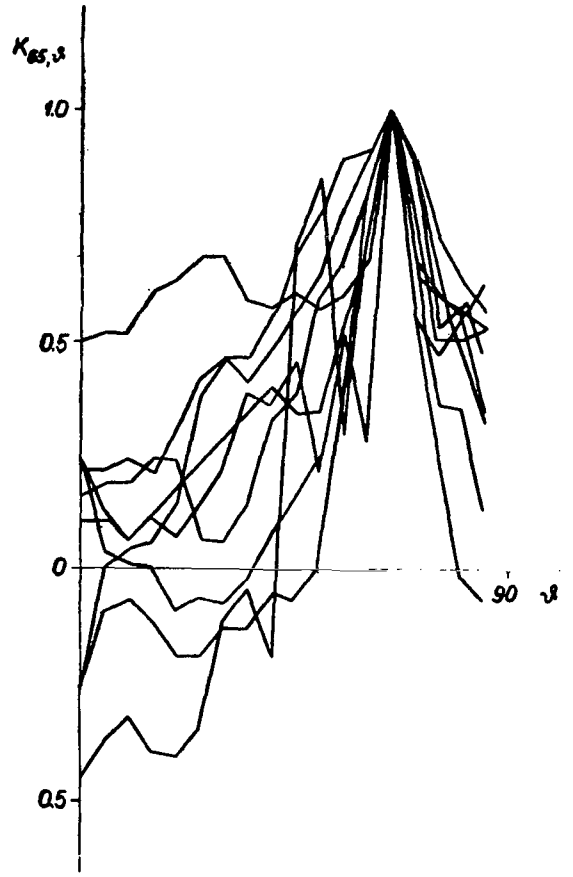

Figure 118. Normalized Coefficients of Sky Brightness Correlation (Cumulus Clouds) at $\vartheta = 65°$ with the Brightness at $\vartheta = 0\text{-}85°$.

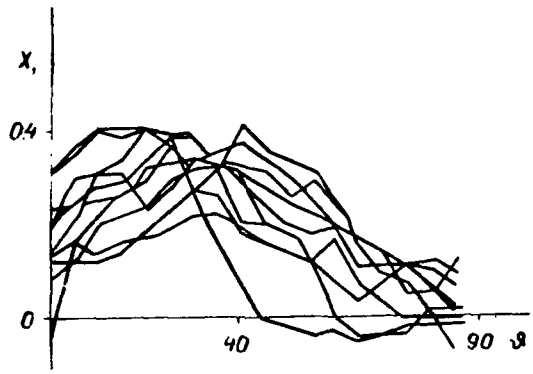

Figure 119. First Eigenfunctions of Sky Brightness (Cumulus Clouds) Versus Zenith Angle of Direction of Sighting.

Dispersion $\sigma^2_{\sigma^2_\tau}$ in σ^4_τ units and the root mean square deviations (Figures 1 and 2 and Figure 124) have been calculated from formulas (4.41) and (4.42), as well as the root mean square deviation for correction term $\sigma^2_{\tau'}$ in units of $\sigma^2_\tau - \sigma^2_{\frac{}{\tau}\Omega}$ (curve 3).

As may be seen from Figure 124, functional relationship (4.40) is the most random in averaging over a slightly smaller correlation radius $\alpha\Omega < 1$. On increase in the averaging scale relation (4.40)

becomes slowly less random, but becomes rapidly so when the scale is reduced.

It is to be noted that expressions similar to (4.40) may also be easily obtained for relations (4.29), (4.31), and (4.32). /206

The dispersions of the transmission and reflecting power based on formulas (4.29)-(4.32) are expressed respectively by

$$\sigma^2_T=[T(\mu_0,\mu,\bar{\tau})]^2\left[E^2+\frac{y^2}{l^2}\left(8E^4-7E^2+\frac{1}{2}\right)\sigma^2_\tau\right]\frac{y^2}{l^2}\sigma^2_\tau, \tag{4.43}$$

in which E is given by formula (4.35),

$$\sigma^2_T=[T(\mu_0,\mu,\bar{\tau})]^2c^2\sigma^2_\tau(1+8c^2\sigma^2_\tau), \tag{4.44}$$

in which c is given by formula (4.37),

$$\sigma^2_\rho=\frac{\mu_0^2}{\pi}(1-A)^2\sigma^2_T, \tag{4.45}$$

in which σ^2T is given by formula (4.44), and /207

$$\sigma^2_T=[T(\mu_0,\mu,\bar{\tau})]^2\left[1+\frac{3y^2}{4l^2}\sigma^2_\tau\right]\frac{y^2}{l^2}\sigma^2_\tau. \tag{4.46}$$

The expressions for the correlation functions in the same approximation for the same relations, (4.29)-(4.32), are more unwieldy and less easy to survey:

$$r_T(t)=\frac{1+\frac{y^2}{l^2}(6E^2-5)\sigma^2_\tau E^2 r_\tau(t)+\frac{y^2}{2l^2}(4E^4-4E^2+1)\sigma^2_\tau r^2_\tau(t)}{E^2+\frac{y^2}{l^2}\left(8E^4-7E^2+\frac{1}{2}\right)\sigma^2_\tau}, \tag{4.47}$$

$$r_T(t)=\frac{(1+6c^2\sigma^2_\tau)r_\tau(t)+2c^2\sigma^2_\tau r^2_\tau(t)}{1+8c^2\sigma^2_\tau}, \tag{4.48}$$

and the correlation functions for the radiation reflected from the layer and that passing through it coincide:

$$r_T(t)=r_\rho(t), \tag{4.49}$$

$$r_T(t)=\frac{\left(1+\frac{y^2\sigma^2_\tau}{l^2}\right)r_\tau(t)+\frac{1}{2}\frac{y^2}{l^2}\sigma^2_\tau r^2_\tau(t)}{1+\frac{3}{4}\frac{y^2}{l^2}\sigma^2_\tau}. \tag{4.50}$$

In the derivation of formulas (4.34)-(4.50) no allowance was made for the restriction $\bar{\tau}+\tau\geqslant 5$, or for the circumstance that the expansions into a series of formulas (4.30)-(4.31) coincide if $|c\tau|<1$. In this instance the first of the restrictions in our analysis should obviously be regarded as definition of the concept of an optically dense unbroken cloud cover, while there corresponds to the latter the circumstance that negative optical thicknesses are not observed in nature, that is, always $\bar{\tau}+\tau>0$, nor are infinitely large optical densities, that is, $\tau<\infty$.

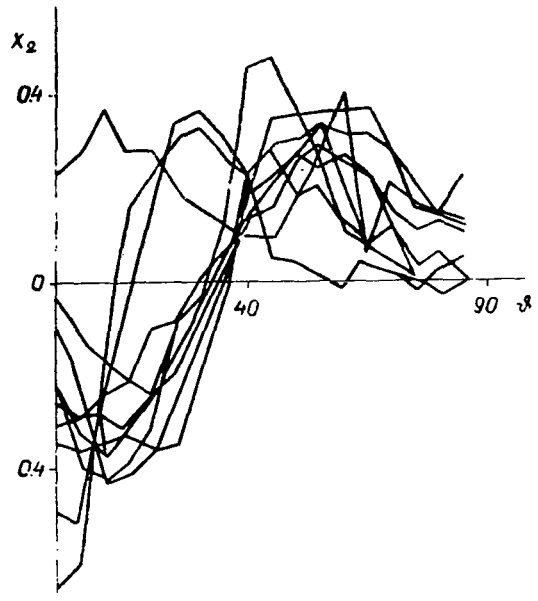

Figure 120. Second Eigenfunctions of Sky Brightness (Cumulus Clouds) Versus Zenith Angles of Direction of Sighting.

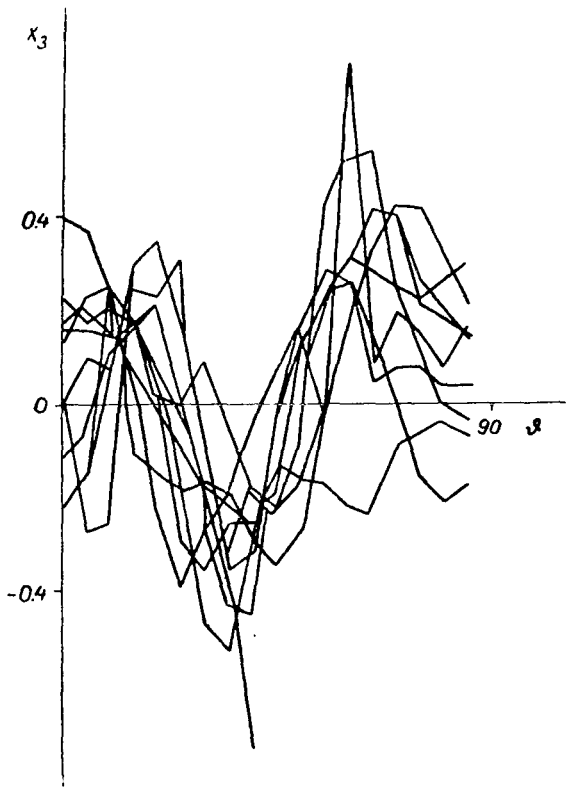

Figure 121. Third Eigenfunctions of Sky Brightness (Cumulus Clouds) Versus Zenith Angle of Direction of Sighting.

Let us analyze the applicability of formulas (4.34)-(4.50). In view of the similarity of initial formulas (4.29)-(4.32), we will confine ourselves to evaluation of the accuracy of the means, dispersions, and correlation functions of the transmission coefficient obtained on the basis of formula (4.30).

To allow for restrictions $\bar{\tau} + \tau \geqslant 5$, $|c\tau| < 1$, in place of the normal distribution function for optical thickness we use the normal distribution function bounded at a certain level a for both positive and negative fluctuations. This function is expressed by /208

$$p(\tau) = \frac{1}{\sqrt{2\pi}\,\sigma_\tau} \exp\left(-\frac{\tau^2}{2\sigma_\tau^2}\right) + \Phi\left(-\frac{\bar{\tau}-a}{\sigma_\tau}\right)[\delta(\tau+\bar{\tau}-a) + \delta(\tau-\bar{\tau}+a)], \tag{4.51}$$

if $|\tau| \leqslant \bar{\tau} - a$ and $p(\tau) = 0$, if $|\tau| > \bar{\tau} - a$, in which Φ is the probability integral, σ_τ^2 is the dispersion of the unbounded normal distribution of optical thickness, and $\delta(x)$ is the Dirac delta function. Thus the probability distribution function selected, (4.51), is normalized, and the symmetrical restriction, while not fundamental, greatly simplifies subsequent operations.

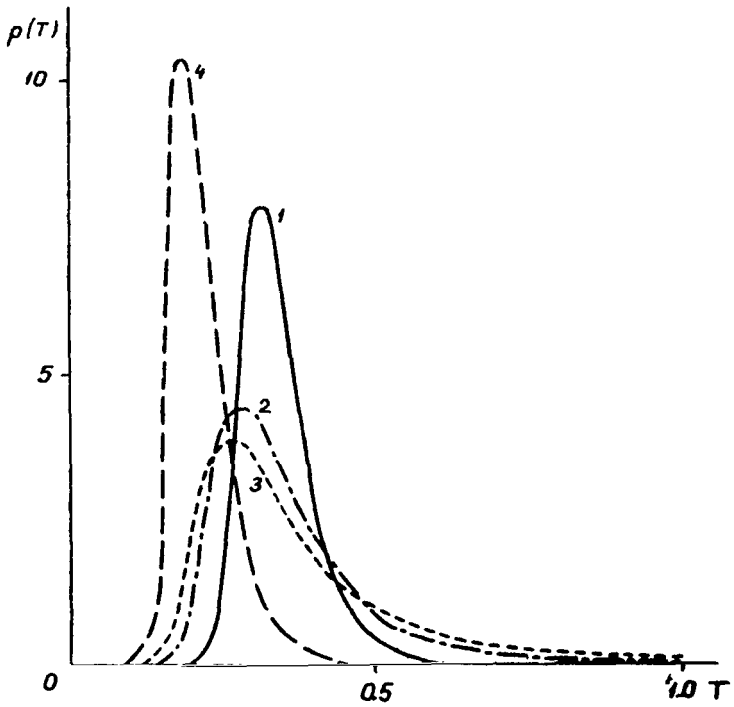

Figure 122. Transmission Probability Distribution Functions Calculated with Formula (4.33): 1, $\sigma_\tau^2 = 16$, $\bar{\tau} = 15$; 2, $\sigma_\tau^2 = 64$, $\bar{\tau} = 15$; 3, $\sigma_\tau^2 = 100$, $\bar{\tau} = 15$; 4, $\sigma_\tau^2 = 64$, $\bar{\tau} = 30$.

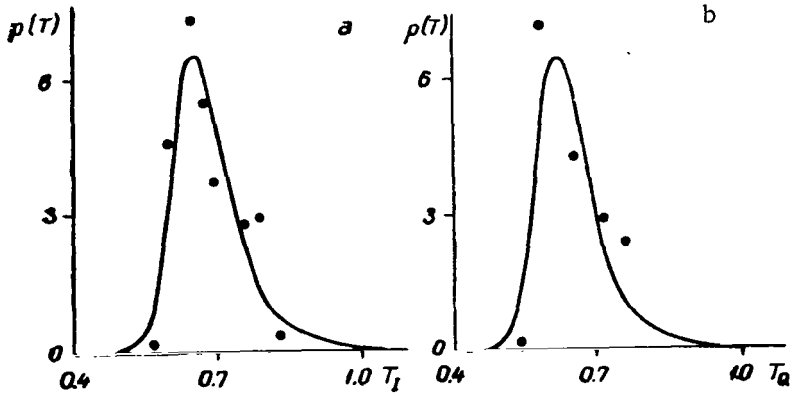

Figure 123. Probability Distribution Functions for Unbroken Clouds: a, for Brightness at the Zenith; b, for Total Radiation Flux. The dots represent empirical data and the curves data calculated on the basis of formula (4.33).

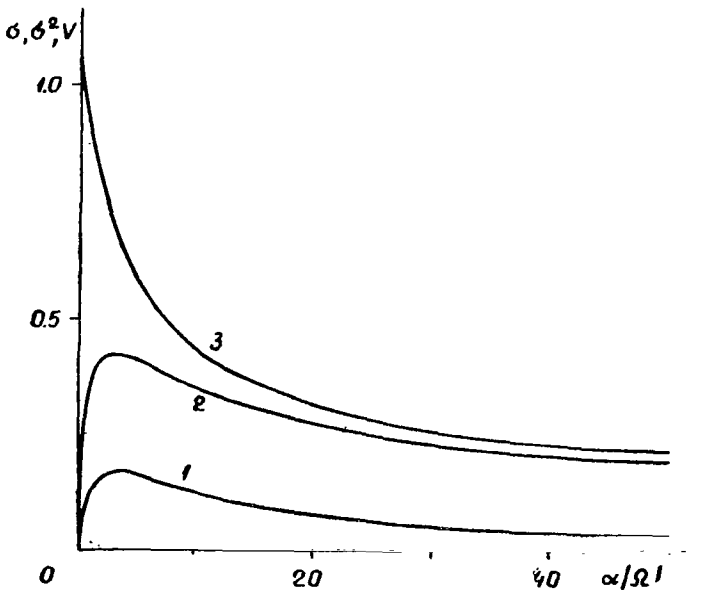

Figure 124. Dispersion of Dispersion of Cloud Layer Optical Thickness $\sigma^2_{\sigma^2_\tau}$ in Units of σ^4_τ (curve 1), Root Mean Square Deviation in Units of σ^2_τ Corresponding to It (Curve 2), and Variability Coefficient $\sigma_{\sigma^2_\tau}(\sigma^2_\tau - \sigma^2_{\bar{\tau}\Omega})^{-1}$ (Curve 3), as Calculated with Formulas (4.41)-(4.42).

Making use of the distribution function of (4.51) and the expansion into a series of formula (4.30), by means of the moment method we determine the mean transmission and its dispersion as a function of the values of parameters /210 c_2, a, $\bar{\tau}$, and σ^2_τ. In this instance we take the first ten terms of the expansion. The results obtained were utilized in calculation of correction factors g_1 and g_2 for formulas (4.36) and (4.44), which, with allowance made for the corrections, are respectively of the form

$$T(\mu_0, \mu, \bar{\tau}+\tau) = T(\mu_0, \mu, \bar{\tau})(1+g_1 c^2\sigma^2_\tau) \tag{4.52}$$

and

$$\sigma_T = [T(\mu_0, \mu, \bar{\tau})]^2 c^2\sigma^2_\tau(1+8g_2 c^2\sigma^2_\tau). \tag{4.53}$$

Correction factors g_1 are presented in Figures 125-127 for the mean transmission coefficient formula. It is to be seen from Figures 125-127 that correction factor g_1 may be disregarded if $\tau/\bar{\sigma}_\tau \geqslant 3$, this corresponding to unbroken clouds under natural conditions. At the same time, $g_1 > 0$ for all possible values of the parameters. It was determined from our experiments that $\tau/\sigma_\tau > 3$ for developed stratified and stratocumulus clouds. This ensures

applicability of approximate formulas (4.34)-(4.39). Evaluation of the accuracy of formulas such as (4.36) made in [38] has demonstrated that, with the restrictions stated above, the divergence yielded by precise calculations derived by numerical integration of the distribution function with the corresponding weighting function is only a few percent.

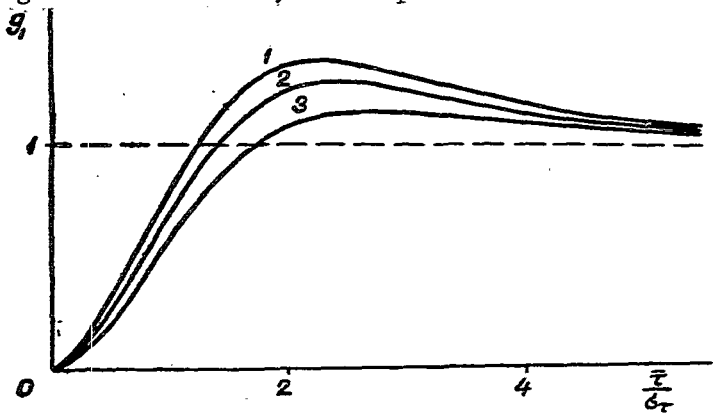

Figure 125. Correction Factor for Mean Transmission Coefficient Formula (4.52), with $\bar{\tau} = 20$, $c_2 = 0.1$; 1, a = 0; 2, a = 3; 3, a = 6.

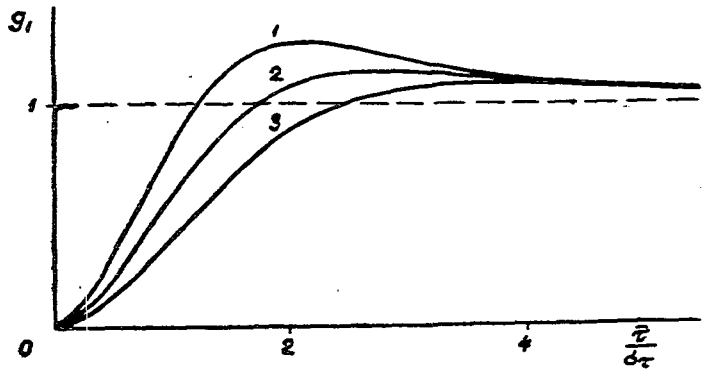

Figure 126. Correction Factor for Mean Transmission Coefficient Formula (4.52), with $\bar{\tau} = 20$, a = 3; 1, $c_2 = 0.3$; 2, $c_2 = 0.2$; 3, $c_2 = 0.1$.

The mean transmission is always greater than that obtained from formulas (1.39)-(1.41) for a homogeneous layer at the mean optical thickness. At the same time, the reflecting power is smaller than with a homogeneous layer of mean optical thickness. Our measurements reveal that the radiation transmission of stratified and stratocumulus clouds, because of their heterogeneity, increases from 5 to 15% in comparison to a homogeneous layer of optical thickness $\bar{\tau}$.

Similarly, the range of applicability of formulas (4.53)-(4.46) for calculation of dispersion is restricted by the condition that factor g_2 must

approach unity. As may be seen from Figures 128-130, which show factor g_2 as a function of the varying parameters, the approximate formulas for dispersion are less precise and thus the range of applicability is narrower in comparison to the formulas for mean transmission. Correction factor g_2 may be disregarded /212 if $\bar{\tau}/\sigma_\tau \geqslant 4$. It is this which determines the applicability of formulas (4.47)--(4.50) for derivation of the autocorrelation functions as second moments. The autocorrelation functions of optical thickness and transmission, and also of the reflecting power, do not differ substantially from each other. The correlation radius for optical thickness is in this case slightly larger than the correlation radius for transmission, as may be seen from Figure 131, which shows the autocorrelation functions calculated with formula (4.48).

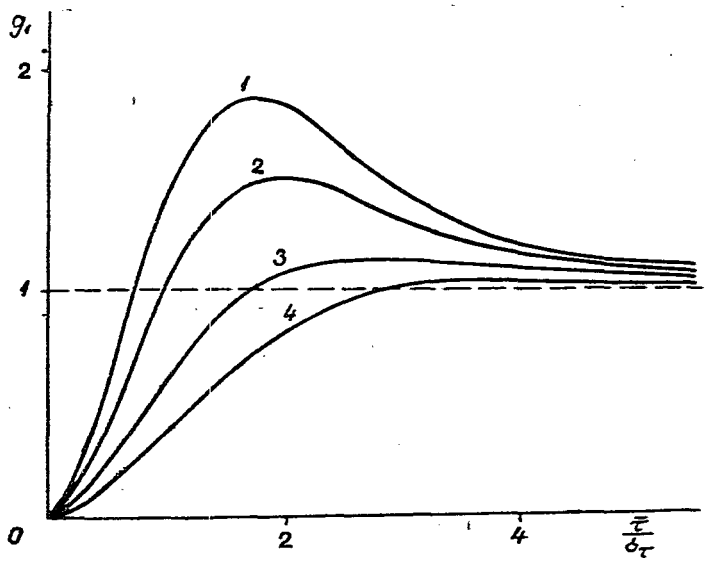

Figure 127. Correction Factor for Mean Transmission Coefficient Formula)4.52), with a = 3, c_2 = 0.1; 1, $\bar{\tau}$ = 100; 2, $\bar{\tau}$ = 50; 3, $\bar{\tau}$ = 20; 4, $\bar{\tau}$ = 10.

Solution of the inverse problem, that is, determination of the statistical /213 characteristics of optical thickness on the basis of the statistical characteristics of transmission is a more complex process. Utilization of the moment method entails certain difficulties, since the distribution of transmission may not be regarded as normal (see Figures 70, 73, and 123). Hence in processing the results of experiments use is made at the present time of the relations

$$\bar{\tau}=\tau(\bar{T})\frac{c_1}{c_2\bar{T}}\frac{\bar{T}^2-2\sigma_T^2\quad\sqrt{(\bar{T}^2-2\sigma_T^2)^2-4\sigma_T^2(\sigma_T^2-8\bar{T}^2)}}{2(\sigma_T^2-8\bar{T}^2)} \tag{4.54}$$

and

$$\sigma_\tau^2=\frac{\bar{T}}{c_1c_2}[\bar{\tau}-\tau(\bar{T})](1+c_2\bar{\tau})^2, \tag{4.55}$$

obtained by conversion of formulas (4.36) and (4.44). It is assumed in this instance that the autocorrelation functions of optical thickness and transmission coincide. /214

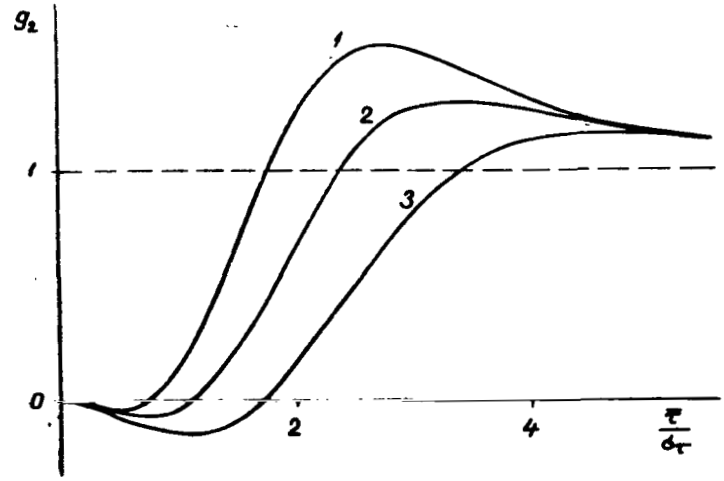

Figure 128. Correction Factor for Transmission Coefficient Dispersion Formula (4.53), with $\bar{\tau} = 20$, $c_2 = 0.1$; 1, a = 0; 2, a = 3; 3, a = 6.

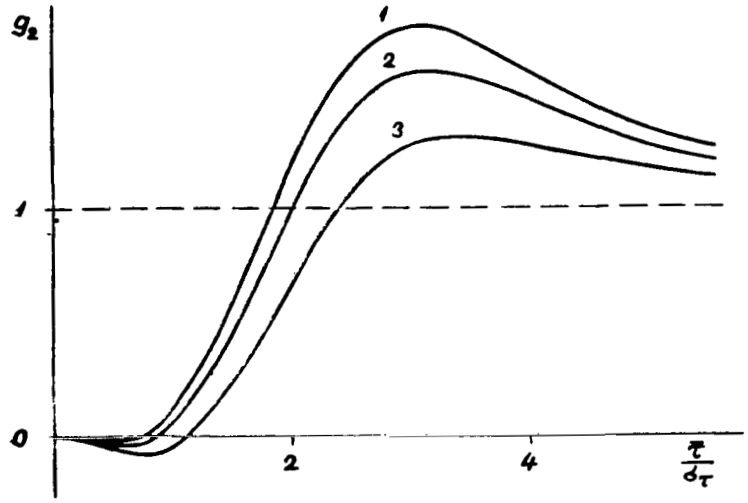

Figure 129. Correction Factor for Transmission Coefficient Dispersion Formula (4.53), with a = 3, $\bar{\tau} \neq 20$; 1, $c_2 = 0.3$; 2, $c_2 = 0.2$; 3, $c_2 = 0.1$.

By means of the moment method, in keeping with the foregoing, functional relations may also be derived for the case in which the albedo of the underlying surface fluctuates along with the optical thickness. If the albedo fluctuations described by a normal random process do not correlate with the fluctuations in

optical thickness, the mean transmission, its dispersion, and the correlation function, use being made of relation (4.30), assume the form

$$T(\mu_0, \mu, \tau+\tau, B+B) = T(\mu_0, \mu, \bar{\tau}, \bar{B})\,[1+c^2(\sigma^2_B\bar{\tau}^2+\sigma^2_\tau\bar{B}^2)], \tag{4.56}$$

$$\sigma^2_T = [T(\mu_0, \mu, \bar{\tau}, \bar{B})]^2[c^2(\bar{\tau}^2\sigma^2_B+\bar{B}^2\sigma^2_\tau)+$$
$$+(c^2+16c^4\bar{B}^2\bar{\tau}^2)\sigma^2_B\sigma^2_\tau+2c^4\bar{\tau}^4\sigma^4_B+2c^4\bar{B}^4\sigma^4_\tau], \tag{4.57}$$

$$r_T(t) = [T(\mu_0, \mu, \bar{\tau}, \bar{B})]^2\{\sigma^2_B[c^2\bar{\tau}^2+2c^4(3\bar{\tau}^4\sigma^4_B+3\bar{\tau}^2\bar{B}^2\sigma^2_\tau+$$
$$+9\bar{\tau}^2\sigma^2_\tau\sigma^2_B+2\bar{B}^2\sigma^4_\tau]r_B(t)+\sigma^2_\tau[c^2\bar{B}^2+2c^4(3\bar{B}^4\sigma^2_\tau+3\bar{B}^2\bar{\tau}^2\sigma^2_B+$$
$$+9\bar{B}^2\sigma^2_B\sigma^2_\tau+4\bar{\tau}^2\sigma^2_B]r_\tau(t)+\sigma^2_B\sigma^2_\tau[c^2+2c^4(9\bar{\tau}^2\sigma^2_B+9\bar{B}^2\sigma^2_\tau+ \tag{4.57}$$
$$+9\sigma^2_\tau\sigma^2_B+2\bar{B}^2\bar{\tau}^2)]r_B(t)r_\tau(t)+2c^4[\sigma^4_B(\bar{\tau}^4+2\bar{\tau}^2\sigma^2_\tau+\sigma^4_\tau)r^2_B(t)+$$
$$+\sigma^4_\tau(\bar{B}^4+2\bar{B}^2\sigma^2_B+\sigma^4_B)]r^2_\tau(t)\},$$

in which $c=\frac{c_3}{1+c_3\bar{\tau}\bar{B}}$, $c_3=\frac{1}{l}$, $B=1-A$ — is the absorption coefficient for the underlying surface. It is to be noted that $\sigma^2_B = \sigma^2_A$ and $r_B(t) = r_A(t)$. Experimental data on the variability of the albedo of the underlying surface are required for application of formulas (4.56)-(4.58), and this may constitute a task for future research.

The empirically determined autocorrelation and reciprocal correlation functions and spectral densities of zenith brightness and scattered radiation flux for stratified clouds (St) are presented in Figures 132-135. The autocorrelation functions for flux and brightness are generally similar and also decrease slowly with increase in the displacement in time (Figure 132). This indicates that low-frequency fluctuations predominate when stratified clouds /215
are present and are only slightly smoothed out by averaging over the sky. This is confirmed by Figure 133, which presents the spectral densities of zenith brightness and total radiation for the same observation. The reciprocal correlation functions are presented in Figure 134. They are not displaced and are symmetrical, while the correlation maximum is only slightly smaller than unity. The symmetry and absence of displacement of the reciprocal correlation function are indications that the cloud cover is opaque to direct rays of the Sun, that is, depth conditions are present. This indicates that the weighting function on transition from zenith brightness to total radiation flux for optically dense stratified clouds is symmetrical relative to the zenith and /216
does not depend on the azimuth (see the results of Section 1-4 of this chapter). The reciprocal correlation function is accordingly substantial. The reciprocal spectral density for the observation in question is presented in Figure 135. We see that it is near the spectral density of zenith brightness.

Whenever the cloud layer is of slight optical thickness or broken clouds /217
are observed, asymptotic formulas (4.29)-(4.32), which describe depth conditions, are not applicable. As a result approximate formulas (4.33)-(4.58) derived above, which describe the radiation conditions of an optically dense cloud layer with variable optical parameters, are also not applicable. In keeping

with the foregoing, however, by using the approximate solutions of the transfer equation describing the radiation conditions of strata of slight optical thickness it is possible to derive formulas characterizing the variability of the radiation parameters of the atmosphere when clouds of different shape are present.

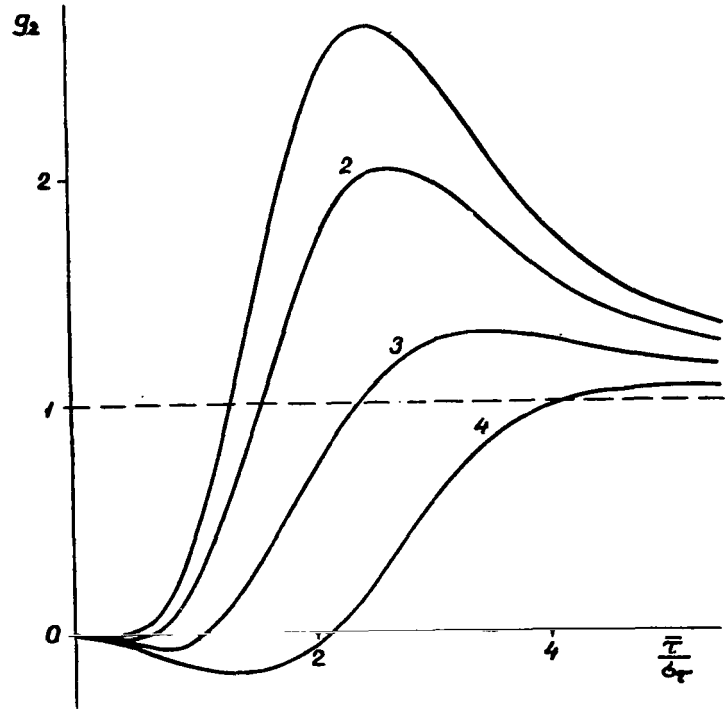

Figure 130. Correction Factor for Transmission Coefficient Dispersion Formula (4.53), with $a = 3$, $c_2 = 0.1$; 1, $\bar{\tau} = 100$; 2, $\bar{\tau} = 50$; 3, $\bar{\tau} = 20$; 4, $\bar{\tau} = 10$.

Use may be made for this purpose, for example, of the approximate formula of V. V. Sobolev [93]

$$T(\mu_0, \bar{\tau}+\tau) = \frac{2B_c(\mu_0, \bar{\tau}+\tau)}{4+(3-x_1)(1-A)(\bar{\tau}+\tau)}, \tag{4.59}$$

in which /219

$$B_c(\mu_0, \bar{\tau}+\tau) = 1+\frac{3}{2}\mu_0+\left(1-\frac{3}{2}\mu_0\right)e^{-\frac{\bar{\tau}+\tau}{\mu_0}}, \tag{4.60}$$

$$x_1 = \frac{3}{2}\int_0^\pi x(\gamma)\cos\gamma\sin\gamma\, d\gamma, \tag{4.61}$$

and $x(\gamma)$ is the scattering indicatrix and γ is the angle between the directions of the incident and the scattered radiation.

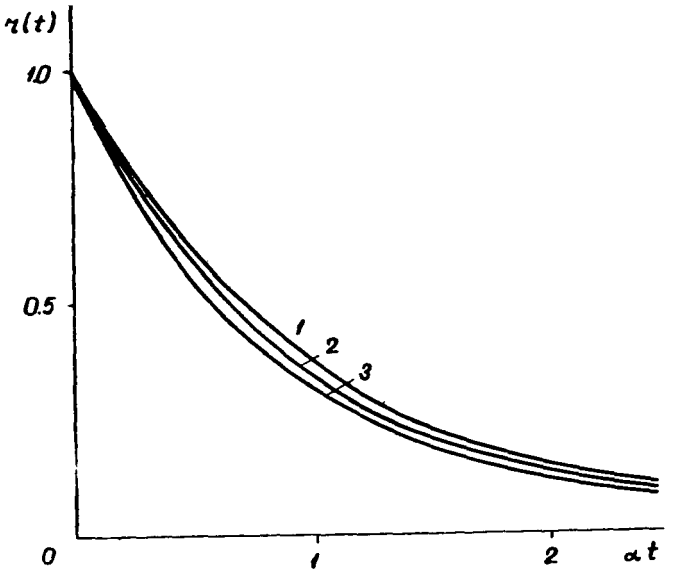

Figure 131. Correlation Functions of Optical Thickness (Curve 1) and Transmission Coefficient of Cloud Layer Calculated with Formula (4.48): 2, $c_2 = 0.1$, $\bar{\tau} = 20$, $\bar{\tau}/\sigma_\tau = 2$; 3, $c_2 = 0.1$, $\bar{\tau} = 20$; $\bar{\tau}/\sigma_\tau = 2/3$.

On the basis of formulas (4.59)-(4.61) and the procedure taken from [32], which was described earlier, an expression was derived in [39] for the mean transmission coefficient relative to the flux, which is of the form

$$T(\mu_0, \bar{\tau}+\tau) = [T_1(\mu_0, \bar{\tau}) + T_2(\mu_0, \bar{\tau})](1+c^2\sigma_\tau^2) + \\ + T_2(\mu_0, \bar{\tau})\left(\frac{c}{\mu_0} + \frac{1}{2\mu_0^2}\right)\sigma_\tau^2, \tag{4.62}$$

in which

$$c = \frac{(3-x_1)(1-A)}{4+(3-x_1)(1-A)\bar{\tau}}, \tag{4.63}$$

$$T_1(\mu_0, \bar{\tau}) = \frac{1+\frac{3}{2}\mu_0}{2+\frac{1}{2}(3-x_1)(1-A)\bar{\tau}}, \tag{4.64}$$

$$T_2(\mu_0, \bar{\tau}) = T_1(-\mu_0, \bar{\tau})e^{-\bar{\tau}/\mu_0}.$$

If the mean optical thickness $\bar{\tau} > 5$, then $T_2(\bar{\tau}) \to 0$ and formula (4.62) assumes a form similar to that of formula (4.36). The slight difference between them is due to the difference in the constants and parameters figuring in approximate formulas (4.30) and (4.59).

The transmission coefficient dispersion, when formula (4.59) is used, is expressed by

$$\sigma^2_T = [T_1(\mu_0, \bar{\tau}) + T_2(\mu_0, \bar{\tau})]^2 c^2 \sigma^2_\tau (1 + 8c^2\sigma^2_\tau) +$$
$$+ 2T_1(\mu_0, \bar{\tau}) T_2(\mu_0, \bar{\tau}) \left[\frac{c}{\mu_0} \sigma^2_\tau + \left(8\frac{c^3}{\mu_0} + \frac{5}{2}\frac{c^2}{\mu_0^2} + \frac{c}{2\mu_0^3} \right) \sigma^4_\tau + \right.$$
$$+ T^2_2(\mu_0, \bar{\tau}) \left[\left(\frac{2c}{\mu_0} + \frac{1}{\mu_0^2} \right) \sigma^2_\tau + \right. \qquad (4.65)$$
$$\left. \left. + \left(16\frac{c^3}{\mu_0} + 13\frac{c^2}{\mu_0^2} + 6\frac{c}{\mu_0^3} + \frac{3}{2\mu_0^4} \right) \sigma^4_\tau \right] .$$

Like formula (4.62), this expression for dispersion when $\bar{\tau} \geqslant 5$ is simplified and assumes a form similar to that of formula (4.44). /220

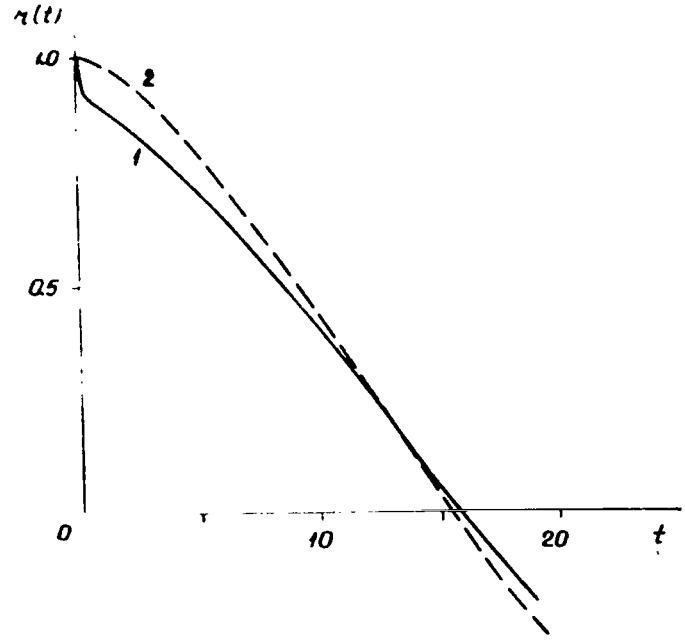

Figure 132. Examples of Measured Correlation Functions of Transmission Coefficient for Stratified Clouds: 1, for Zenith Brightness; 2, for Total Radiation Flux (t in min).

The formula for the correlation function of transmission in the same approximation is even more complex in form than dispersion expression (4.65). In view of the fact that the expression derived for the correlation function is difficult to survey and it is not advisable to apply it in calculations, we do not present it here.

When $\bar{\tau} \geqslant 5$, the approximate formula of the transmission correlation function for relation (4.59), like the corresponding formulas for the mean and dispersion, is simplified and assumes a form similar to that of formula (4.48).

As with formula (4.59), expressions (4.62)-(4.65) obtained above for description of radiation field structure are applicable with any optical thicknesses $0 \leqslant \bar{\tau} + \tau < \infty$. However, formula (4.59) is strictly speaking applicable only to plane-parallel strata of turbid media. Thus whenever the scales of horizontal heterogeneities is smaller than the vertical extent of the cloud cover formulas (4.62)-(4.65) presented in the foregoing may not be applied. Formulas (4.62)--(4.65) consequently may be used to study all forms of clouds except for cumulus and cumulonimbus ones, in which the vertical extent of individual clouds is of the same order of magnitude as the bases of the clouds.

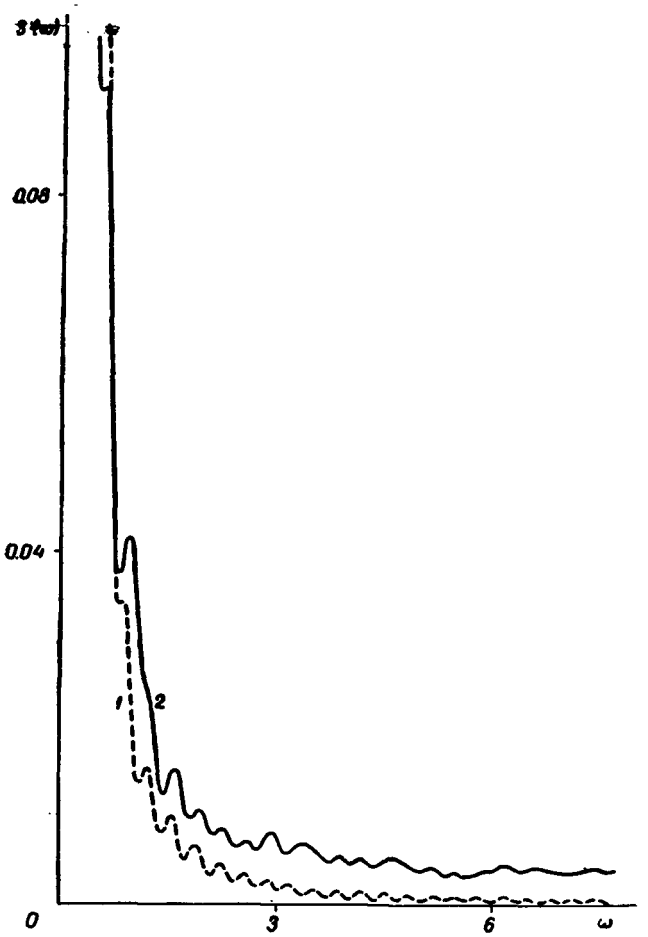

Figure 133. Examples of Spectral Densities of Total Radiation 1 and Zenith Brightness 2 for Stratified Clouds (ω in min^{-1}).

Section 7. Influence of Macroroughness of Upper Boundary of Layered Clouds on Brightness Coefficient and Albedo

Under natural conditions all natural light scattering surfaces or the interfaces of light scattering media, including the upper boundary of clouds,

are macrorough to a greater or lesser extent. We know that surface topography may exert a substantial influence on the reflection properties of the macrosurface. Such problems have been examined in general form for an arbitrary topography by A. S. Monin [94], and the characteristics of the urban radiation climate by means of geometric models by V. G. Kastrov [95] and W. Kaempfert [96, 97].

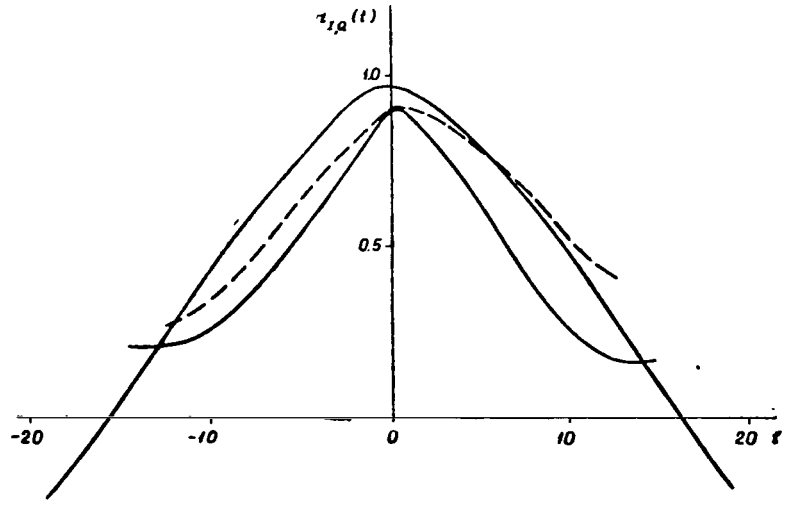

Figure 134. Examples of Reciprocal Correlation Functions of Zenith Brightness and Total Radiation Flux for Stratified Clouds (t in min).

In reality natural surfaces such as the upper boundaries of clouds, mountain /221
regions, forests, snowfields, the surface of a heavy sea, and so forth are irregular surfaces which it is advisable to characterize by random functions. To determine the average reflection properties of such surfaces it is sufficient to know the distribution function of the slopes relative to the angles, the optical properties of the elementary plane surfaces, and the direction of the incident radiation.

We adopted an approach such as this in calculations of the optical parameters of the surface of a heavy sea [98]. The same approximation is used in bioactinometry in analysis of reflection and transmission by the leaves of plants the orientation of which in space is uniform or conforms to a specific pattern [99].

Simulation by means of plane elementary surfaces involves a number of errors, which increase with increase in the steepness of the slopes of the surface and the zenith distance of the direction of incident and reflected radiation [98]. The major portion of the error is due to shading of some sections of the surface by others.

Design formulas were derived in [61] to allow for shading on the surface of the sea, ones which in principle may be applied to any light scattering

macrorough surfaces. But since many natural surfaces (mountain regions, the upper boundary of clouds, and so forth) are rougher than the surface of the sea, it is necessary to allow for shading over a wider range of solar altitudes than was done in [61]. Allowance for shading widens considerably the range of applicability of the model employed in calculations of the optical properties of the surface of the sea and renders such an approach suitable also for macrorough surfaces having steeper slopes.

In accordance with [98], we present below formulas the purpose of which it is to allow for reflection from an uneven surface when the reflection from the elements of the surface is diffuse. If the reflection from the elements of the surface is orthotropic, the design formulas are greatly simplified and permit the drawing of a number of conclusions.

Let us consider a light beam of intensity $I(\vartheta, \varphi)$ in solid angle $d\Omega$, which strikes the surface at an angle ϑ, φ. Diffusely scattered light of intensity $I_1(\vartheta_1, \varphi_1)$ is propagated in direction ϑ_1, φ_1. /222

It may be demonstrated that the angles between the normal of the surface element, ϑ_n, φ_n, and the directions of the incident and reflected beam are expressed respectively by

$$\cos\chi_1=\cos\vartheta_n\cos\vartheta+\sin\vartheta_n\sin\vartheta\cos(\varphi-\varphi_n),$$
$$\cos\chi_2=\cos\vartheta_n\cos\vartheta_1+\sin\vartheta_n\sin\vartheta_1\cos(\varphi_1-\varphi_n). \tag{4.66}$$

The brightness of one specific slope is expressed by

$$I(\vartheta_1, \varphi_1)=\cos\chi_1\rho(\chi_1, \chi_2)I(\vartheta, \varphi)d\Omega, \tag{4.67}$$

in which $\rho(\chi_1, \chi_2)$ is the brightness coefficient.

The portion of the unit section of surface formed by projections of all the elements of the real surface with a specific orientation of the normal within solid angle $d\Omega_n$ equals

$$p(\vartheta_n, \varphi_n)d\Omega_n, \tag{4.68}$$

in which $p(\vartheta_n, \varphi_n)$ is the distribution function.

The real area of the aggregate of correspondingly oriented sections per unit surface area will be

$$p(\vartheta_n, \varphi_n)\sec\vartheta_n d\Omega_n, \tag{4.69}$$

while the area of their projections onto the unit plane perpendicular to the direction of the scattered beam is defined as

$$p(\vartheta_n, \varphi_n)\sec\vartheta_1\sec\vartheta_n\cos\chi_2 d\Omega_n. \tag{4.70}$$

From expression (4.67) and (4.70) we derive the brightness formula for a beam scattered by statistically distributed sections over range $d\Omega_n$ in direction ϑ_1, φ_1

$$dI_1(\vartheta_1, \varphi_1) = I(\vartheta, \varphi)\, d\Omega \varrho(\chi_1, \chi_2)\, p(\vartheta_n, \varphi_n) \times \\ \times \sec\vartheta_1 \sec\vartheta_n \cos\chi_1 \cos\chi_2\, d\Omega_n. \tag{4.71}$$

The total intensity in a particular direction is obtained after integration relative to ϑ_n, φ_n within the range corresponding to all possible directions of incident radiation (χ_1, $\chi_2 \leqslant 90°$), in the form /223

$$I_1(\vartheta_1, \varphi_1) = \sec\vartheta_1 I(\vartheta, \varphi)\, d\Omega \int_{\Omega_n} \varrho(\chi_1, \chi_2)\, p(\vartheta_n, \varphi_n) \times \\ \times \sec\vartheta_n \cos\chi_1 \cos\chi_2\, d\Omega_n, \tag{4.72}$$

and the reflected flux in the form

$$F(\vartheta, \varphi) = \int_{(2\pi)} I_1(\vartheta_1, \varphi_1) \cos\vartheta_1\, d\Omega_1. \tag{4.73}$$

Formulas (4.72) and (4.73) are applicable whenever the brightness coefficient varies with altitude (mountain regions). Then in place of two-dimensional distribution functions $p(\vartheta_n, \varphi_n)$ we use three-dimensional functions $p(z, \vartheta_n, \varphi_n)$ and integrate additionally with respect to z.

When the reflection by the surface elements is orthotropic,

$$\varrho(\chi_1, \chi_2) = \frac{b}{\pi}, \tag{4.74}$$

in which $b \leqslant 1$ and the distribution function does not depend on azimuth φ_n, after simple conversions formula (4.72) assumes the form

$$I_1(\vartheta_1, \varphi_1) = \frac{b}{\pi} \sec\vartheta_1 I(\vartheta, \varphi)\, d\Omega \Big[\cos\vartheta \cos\vartheta_1 \int_{\Omega_n} p(\vartheta_n, \varphi_n) \times \\ \times \cos\vartheta_n\, d\Omega_n + \frac{1}{2} \sin\vartheta \sin\vartheta_1 \times \\ \times \cos(\varphi - \varphi_1) \int_{\Omega_n} p(\vartheta_n, \varphi_n) \frac{\sin^2\vartheta_n}{\cos\vartheta_n} d\Omega_n \Big]. \tag{4.75}$$

Thus we obtain the brightness coefficient for surface macroroughness:

$$\varrho(\vartheta, \vartheta_1) = \frac{b}{\pi} \Big[\int_{\Omega_n} p(\vartheta_n, \varphi_n) \cos\vartheta_n\, d\Omega_n + \\ + \frac{1}{2} \operatorname{tg}\vartheta_1 \operatorname{tg}\vartheta \cos(\varphi - \varphi_1) \int_{\Omega_n} p(\vartheta_n, \varphi_n) \frac{\sin^2\vartheta_n}{\cos\vartheta_n} d\Omega_n \Big]. \tag{4.76}$$

Provided that /224

$$\chi_1, \chi_2 \leqslant 90°, \\ \vartheta + \vartheta_{n,max} \leqslant 90°, \\ \vartheta_1 + \vartheta_{n,max} \leqslant 90° \tag{4.77}$$

the albedo equals

$$F(\vartheta_1) = b \int_{\Omega_n} p(\vartheta_n, \varphi_n) \cos \vartheta_n \, d\Omega_n, \tag{4.78}$$

this being approximately equal to the albedo for a smooth surface, b, if the roughness is not too great. It follows that the albedo of a rough surface is always smaller than the albedo of a smooth surface, since

$$\int_{\Omega_n} p(\vartheta_n, \varphi_n) \cos \vartheta_n \, d\Omega_n < 1. \tag{4.79}$$

If the restrictions of (4.77) are adhered to:

1. The brightness of a rough surface in the plane $|\varphi - \varphi_1| = \pi/2$ is constant and is always smaller than the brightness of a smooth Lambert surface.

2. In the fourth sphere, $|\varphi - \varphi_1| < \pi/2$, the brightness is greater than in the fourth sphere $|\varphi - \varphi_1| > \pi/2$, and in the latter case may under the same conditions exceed the brightness of a smooth Lambert surface. The intensity of backscattered radiation is greater than the intensity of radiation scattered forward, the more so the larger are ϑ and ϑ_1 and the smaller is $|\varphi - \varphi|$.

In comparison with a smooth surface the macroroughness of a surface consequently determines the redistribution of brightness by angles.

For real reflection indicatrices surface roughness reduces extension in the direction of the mirror reflection, the more so the greater is the roughness and the greater is the zenith distance of the Sun. The albedo decreases with increase both in surface roughness and in the zenith angle of the Sun.

The albedo decreases greatly owing to shading in the region in which $\vartheta + \vartheta_{n,max} \gg 90°$. This latter circumstance substantially reduces the mean albedo of clouds and the albedo of mountain regions, as well as that of rough snow fields in the high latitudes, in which the altitude of the Sun is low.

The unevennesses of the upper boundary of the cloud cover consequently affect the albedo of the surface as with the variability of optical thickness (see Section 6 of this chapter); they reduce the reflecting power and increase the radiation transmission of stratified clouds. More detailed experimental and theoretical analysis of the relationships of these two effects remains a task for future research. /225

CHAPTER V. STOCHASTIC STRUCTURE OF LONGWAVE RADIATION FIELDS OF THE CLOUD ATMOSPHERE

Section 1. Averaged Thermal Radiation Flux Values of the Atmosphere for Cumulus Clouds

The flux of longwave radiation of the atmosphere averaged over a certain territory, $\overline{F}\downarrow(x, y, z)$, is in the general case calculated with the following formula taken from [76]:

$$\overline{F}\downarrow(S, z) = \frac{\int_S F\downarrow(x, y, z)\,dS}{\int_S dS} = \frac{\int_S \int_0^{2\pi} \int_0^{\pi/2} I\downarrow(x, y, z, \vartheta, \varphi) \sin\vartheta \cos\vartheta\, d\vartheta\, d\varphi\, dS}{\int_S dS}. \tag{5.1}$$

In this formula S is the area of the territory in question; dS = dxdy; x, y are horizontal coordinates; z is the vertical coordinate; and $I\downarrow(x, y, z, \vartheta, \varphi)$ is the intensity of radiation at point (x, y, z) at azimuth φ and zenith angle ϑ.

On the one hand, in the case of broken clouds the value of $F\downarrow(x, y, z)$ in formula (5.1) varies greatly with change in x, y [76, 100]. On the other hand, we note that within the limits of a territory over which clouds of one form are present (i.e., there is a specific air mass above the region in question and there are no frontal zones) the temperature, pressure, and moisture content of the air undergo relatively little variation in the horizontal direction. Hence the horizontal variability of the flux of longwave radiation of the atmosphere, /227
$F\downarrow(x, y, z)$, is determined chiefly by the amount and distribution of clouds over the sky.

For a statistically isotropic plane-parallel atmosphere in which the values of the meteorological parameters do not vary in the horizontal direction and the lower boundary of all clouds remains at the same altitude, the mean value of the longwave radiation of the atmosphere is calculated with the formula taken from [101]:

$$\overline{F}\downarrow = \int_0^{\pi/2} c(\vartheta) I_c\downarrow(\vartheta) \sin\vartheta \cos\vartheta\, d\vartheta + \int_0^{\pi/2} [1 - c(\vartheta)] I_n\downarrow(\vartheta) \sin\vartheta \cos\vartheta\, d\vartheta. \tag{5.2}$$

In this formula $c(\vartheta)$ is the probability, averaged over the territory in question, of a free line of sight, i.e., the probability that the radiation at zenith angle ϑ will arrive from clear parts of the sky; $1 - c(\vartheta)$ is the probability that the radiation at angle ϑ will come from parts of the sky covered by clouds; and $I_c\downarrow(\vartheta)$ and $I_n\downarrow(\vartheta)$ are the values of the intensity of thermal radiation arriving respectively from clear and cloud covered parts of the sky.

Calculation of $\bar{F}\downarrow$ from formula (5.2) is extremely laborious and requires information on the angular distribution of $c(\vartheta)$, $I_c\downarrow(\vartheta)$, and $I_n\downarrow(\vartheta)$. Thus it is of value to derive simplified approximate formulas for calculation of the mean values of the longwave radiation of the atmosphere. It is demonstrated in [102] that, if a cumulus cloud field is simulated by a set of randomly arranged plates situated at the same level, the mean flux of descending thermal radiation is defined by the following formula:

$$\bar{F}\downarrow=[1-n(0)]\bar{F}_c\downarrow+n(0)\bar{F}_n\downarrow. \tag{5.3}$$

Formula (5.3) may be derived directly from formula (5.2), in which the probability of a free line of sight $c(\vartheta)$ does not depend on the zenith angle and equation $c(\vartheta) = 1 - n(0)$ is satisfied, on the assumption that the clouds represent absolute black plates. /228

The principal errors of formula (5.3) have been analyzed in [102]. It has been demonstrated that the error arising in determination of the mean value of the longwave radiation of the atmosphere, $\bar{F}\downarrow$, for real, bounded territories is insignificant if the area of the region in question is greater than 100×100 km^2. The assumptions we have made regarding constant temperature, moisture content, and pressure in the horizontal directions are valid only in approximation in the real atmosphere. If the range of variability of the meteorological parameters in the horizontal direction is narrow in the region of territory S, calculation of $F_c\downarrow$ and $F_n\downarrow$ on the basis of the mean vertical temperature, pressure, and moisture content distributions for the particular region introduces virtually no additional errors into the value of $\bar{F}\downarrow$, but in the case of meteorological parameters in the atmosphere with large horizontal gradients, it is advisable to use the following approximate formula taken from [102]:

$$\bar{F}\downarrow=\frac{1}{S}\sum_i \bar{F}_i\downarrow(S_i)S_i. \tag{5.4}$$

In this formula S is divided into sections S_i in such a way that the range of horizontal variability of the meteorological parameters of the atmosphere is sufficiently narrow within each section; $\bar{F}_i\downarrow(S_i)$ is the longwave radiation flux calculated in accordance with formula (5.3) on the basis of the mean meteorological parameters for section S_i. It has been demonstrated in [102] that the errors resulting from use of the temperature, moisture content, and pressure values averaged over sections S_i are more or less compensated when averaging is performed over the entire territory (formula (5.4)). One of the reasons for this is represented by the strong radiation (and absorption) of the lower dense layers of the atmosphere, owing to which the role of the radiation from parts of the atmosphere distant from the point of observation is slight in creation of the flux of thermal radiation at the point in question. In the general case, in the event of considerable random variability of the meteorological parameters, it is necessary for calculations of the mean values of the thermal radiation flux, as with the calculations of the mean shortwave

radiation values (see Chapter IV, Section 6), to know the characteristics of variability of these parameters at least within the framework of correlation--dispersion analysis. It is found, however, that in the majority of cases the main source of errors resulting from formula (5.3) will be represented by the fact that we do not allow for the radiation of the sides of clouds. The contribution of this additional radiation depends on the vertical thickness and temperature of the clouds, and to a great extent also on the nature of distribution of the clouds over the sky. If the clouds were to be concentrated in one large mass, the role of the radiation of the sides of the mass would be insignificant, but with broken clouds of great vertical thickness (Cu) the radiation contribution made by the sides of the clouds to the radiation flux $\overline{F}\downarrow$ may be appreciable. To allow for the radiation of the sides of the clouds [102] proposes introduction into formula (5.3) of a correction factor by the amount of which the values of n(0) in this formula are to be increased. According to the tentative estimates of [102], in the case of one cloud the value of this correction factor equals $\overline{h}/2$, while for a cloud field with mean cloud frequency $\varkappa$ it will be $1/2\ \varkappa\overline{h}$ (in which $\overline{h}$ is the mean vertical thickness of the clouds and $\varkappa$ is the cloud frequency, i.e., the mean number of clouds per unit length). /229

It may additionally be assumed that formula (5.3) can also be refined by using the corresponding averaged relative cloudiness values in it in place of absolute cloudiness values (n(0)). This method is recommended, for example, in [103], but without any quantitative estimates.

In [101] the averaged values of the back radiation of the atmosphere calculated with formula (5.3) for the free cloud models indicated above are compared with the corresponding results obtained with more precise formula (5.2). (Back radiation is understood to mean the thermal radiation of the atmosphere at the level of the Earth's surface.) The statistical characteristics of clouds required in radiation calculations ($c(\vartheta)$, n(0), $\overline{h}$, $\varkappa$, n) have been determined for a real cloud system on the basis of the results of an experiment conducted by V. G. Plank [104]. In this study cumulus cloud systems were photographed from aircraft and studied for a period of 19 days at intervals of 1-2 hours (in the vicinity of Tampa, Florida, 28° north latitude). The most typical cases were selected and subjected to the most thorough analysis possible. As a result analytical formulas were derived in [104] for determination of the various statistical characteristics of cumulus clouds. The parameters appearing in these formulas were also determined experimentally as a function of the intensity of the ascending air flows and as a function of time. A description is given of the diurnal variation in the statistical characteristics of clouds as a function of the amount of clouds. It is to be noted that the results of the studies cited in [104] are in good qualitative agreement with the results of our studies presented in Chapter III. To ascertain the patterns of variation in the averaged values of atmospheric back radiation as a function of the amount of clouds it is preferable to use the experimental data of [104] for two reasons: firstly, more clearcut detection of the typical features of back radiation is fostered by the relatively great vertical thickness of the tropical cumulus clouds within masses, and secondly, the statistical characteristics of the thickness of cumulus clouds have not as yet been studied in sufficient detail in our experiments. /230

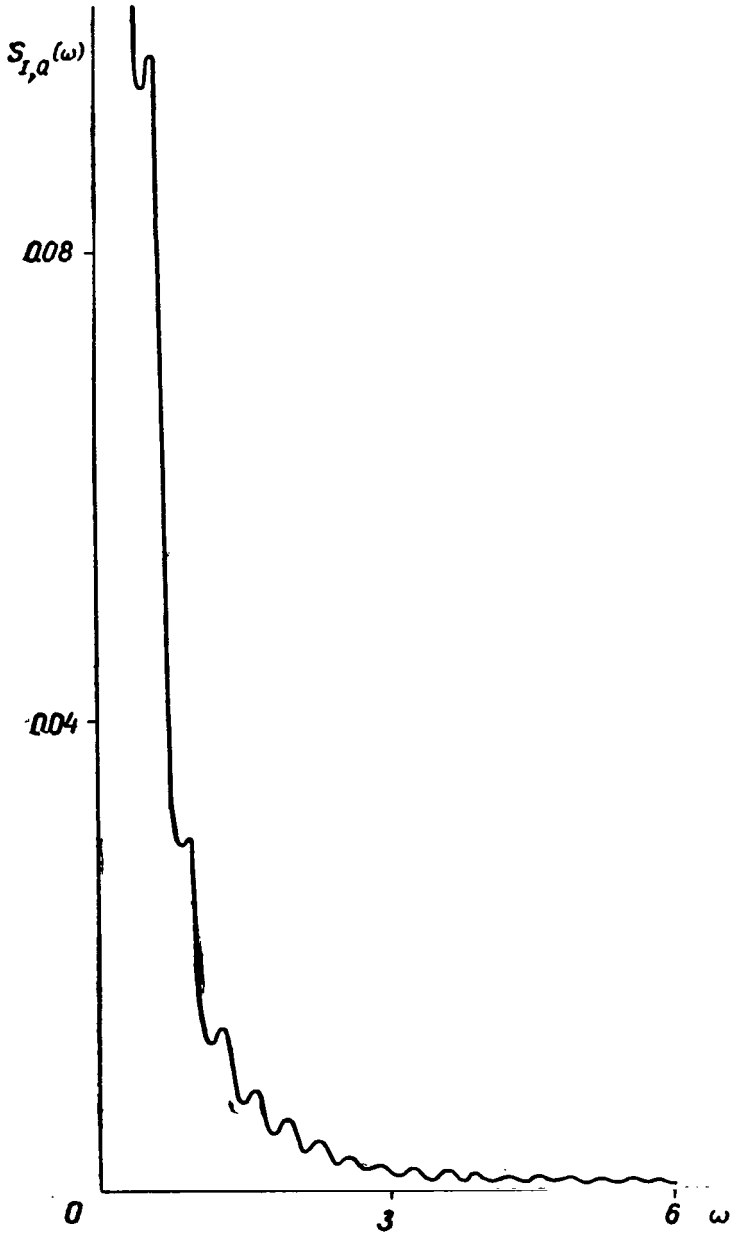

Figure 135. Reciprocal Spectral Density of Zenith Brightness and Total Radiation Flux for Stratified Clouds (ω in min^{-1}).

The so-called "typical cloud cover" alternative, which characterizes the picture of cumulus cloud field development most often encountered from 0800 to 1700 hours (Figure 136) was selected from the materials in [104]. In addition, use was made of 3 observations of particularly thick cumulus clouds.

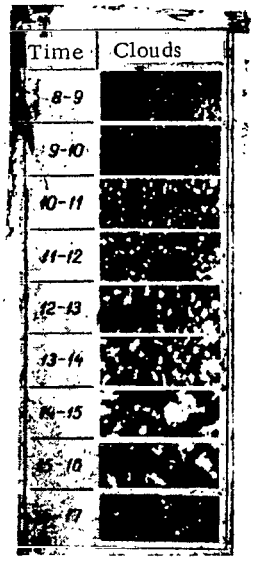

Figure 136. Example of Typical Diurnal Variation in Cumulus Clouds (Based on [104]).

The data resulting from V. G. Plank's experiment [104] unfortunately do not contain the information on temperature, pressure, and moisture content of the atmosphere necessary for calculations of back radiation. It was necessary for this reason to perform calculations based on a "model" stratification of the atmosphere which met the requirements of labile stratification and corresponded to the cumulus cloud season and to the climatic conditions of Florida [101]. /231

The design model proposed and analyzed in [64, 101, 105] was used to calculate the values of $c(\vartheta)$ and n (see Chapter III, Section 1).

As was noted earlier, the diurnal variation in the back radiation of the atmosphere at the level of the Earth's surface is determined from formulas (5.2) and (5.3), as well as from the following formulas analogous to (5.3):

$$\overline{F}\downarrow = [1 - n(45°)]\overline{F}_c\downarrow + n(45°)\overline{F}_n\downarrow, \tag{5.5}$$

$$\overline{F}\downarrow = (1 - n)\overline{F}_c\downarrow + n\overline{F}_n\downarrow. \tag{5.6}$$

In this instance

$$n(45°) = n(0) + \frac{1}{2}\varkappa\overline{h}. \tag{5.7}$$

The values of $\overline{F}_c\downarrow$ and $\overline{F}_n\downarrow$ required for these calculations were calculated by the universally known method by use of the integral transmission function [106, 108].

The results of these calculations are presented in Table 7. The values of n(0), n, n(45°), $\overline{h}$, $\varkappa$, $\overline{F}_c\downarrow$, and $\overline{F}_n\downarrow$ are also given in the Table. The data in Table 7 confirm the well-known fact [76, 103] that the dense absorbing layers of the atmosphere near the ground greatly attenuate the influence of clouds on back radiation. Thus the diurnal variation in the back radiation flux is much less pronounced than the diurnal variation in the cloud cover. The cloud cover is in the cases in question nevertheless an important factor causing variability in radiation: the amplitude of the diurnal variation in $\overline{F}\downarrow$ is appreciably greater than the amplitude of the diurnal variation in $\overline{F}_c\downarrow$ and $\overline{F}_n\downarrow$. The natural cause is in this instance represented by the nature of variation in the amount of clouds during the day: the maximum amount of clouds virtually coincides with the maximum air temperature.

The shielding effect of the air layer below the clouds is unquestionably one of the factors guaranteeing close agreement of the results of back radiation calculation based on different methods of allowing for the influence of the cloud cover. When the humidity values are large enough all 3 simplified methods (those based on n(0), n(45°) and n) apparently permit calculation of the average back radiation flux values with errors of less than 3%. The values of $\bar{F}\downarrow$ obtained on the basis of n(0) are consistently understated, the results obtained by use of n are consistently exaggerated, and the results based on n(45°) in all the cases investigated by us yielded the best agreement with the refined back radiation values (those obtained with formula (5.2)). In the last-named case the absolute back radiation error does not exceed ±0.1 $mw \cdot cm^{-2}$, this representing only about 0.3% of the values of $\bar{F}\downarrow$. /233

TABLE 7. COMPARISON OF VARIOUS METHODS OF CALCULATING AVERAGED VALUES OF ATMOSPHERIC BACK RADIATION FLUXES

No.	Time	n(0)	n(45°)	n	$\bar{h}$(km)	$\frac{1}{2}\varkappa(km^{-1})$	$\bar{F}\downarrow$ ($mwt \cdot cm^{-2}$) Based on formula (5.2)	Based on n(0)	Based on n(45°)	Based on n	$F_c\downarrow$ ($mw \cdot cm^{-2}$)	$F_n\downarrow$ ($mw \cdot cm^{-2}$)
						Typical cloud cover						
1	08—09	0.062	0.075	0.147	0.146	0.181	36.5	36.5	36.6	37.1	36.1	43.1
2	09—10	0.180	0.218	0.337	0.276	0.277	38.4	38.0	38.3	39.1	36.8	43.6
3	10—11	0.262	0.318	0.454	0.513	0.217	39.1	38.8	39.1	40.0	37.0	43.7
4	11—12	0.309	0.375	0.516	0.466	0.281	39.9	39.3	40.0	40.7	37.3	43.9
5	12—13	0.349	0.423	0.566	0.603	0.246	40.0	39.4	39.9	40.9	37.1	43.8
6	13—14	0.477	0.579	0.710	0.854	0.238	41.4	40.6	41.3	42.1	37.6	44.0
7	14—15	0.309	0.375	0.517	0.935	0.141	39.5	39.0	39.4	40.4	36.9	43.7
8	15—16	0.185	0.224	0.344	0.856	0.092	38.0	37.6	37.9	38.7	36.3	43.4
9	16—17	0.072	0.087	0.161	0.522	0.059	36.0	35.9	36.0	36.6	35.4	42.9
						Very thick clouds						
10	9—10	0.421	0.511	0.650	0.326	0.519	40.4	39.9	40.5	41.5	37.1	43.8
11	12—13	0.642	0.778	0.851	0.892	0.305	42.1	41.7	42.5	42.9	38.0	43.8
12	15—16	0.290	0.351	0.492	0.857	0.143	39.0	38.4	38.8	39.8	36.4	43.4

Analysis of the possibilities of obtaining initial information on the various cloud cover parameters shows that it is the easiest to determine the amount of absolute cloudiness (by means of satellite photographs, for example). Determination of the initial data for calculation of n and n(45°) requires the organization of a special experiment in each specific case [101, 105]. For this reason it is of interest to arrive at empirical formulas permitting calculation of n and n(45°) solely on the basis of absolute cloudiness data. It is demonstrated in [101] that on the basis of the materials in question (numbers 1-12) the relationship between n(0) and n is described well by the empirical formula

$$n = n(0) + 0.8[1 - n(0)][n(0)]^{0.8}, \quad (5.8)$$

and the relationship between n(0) and n(45°) by the formula

$$n(45^\circ) = 1.2n(0). \qquad (5.9)$$

Comparison of formula (5.8) with approximation formula (3.8) obtained on the basis of our measurements shows that the contribution made by the lateral surfaces of clouds under tropical climatic conditions is twice as great as in the temperature latitudes. This apparently is largely due to the relatively great thickness of the cumulus clouds of the tropics.

Curves plotted on the basis of formulas (5.8) and (5.9) are presented in Figure 137, in which circles and dots designate respectively the values of n and n(45°) taken from Table 7. We see that there is very close agreement between the results of the experimental materials and formulas (5.8) and (5.9). It should be observed, however, that formulas (5.8) and (5.9) should be regarded as merely approximate, since they were derived on the basis of experimental materials for only one geographic point (Tampa, Florida). /234

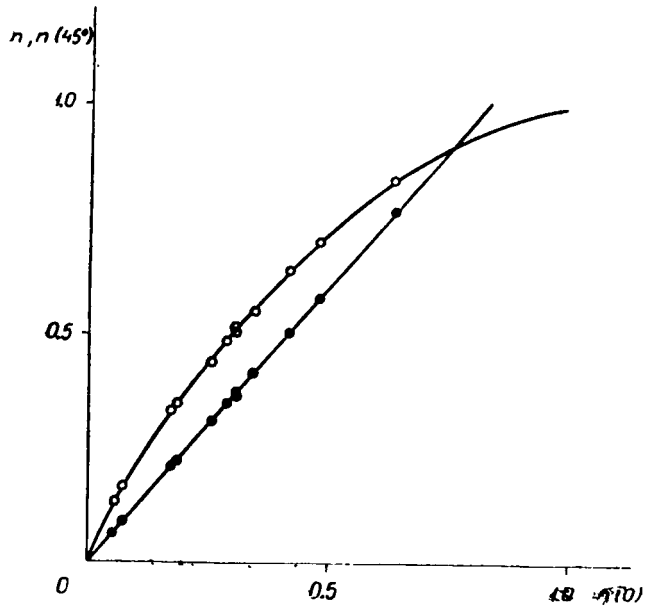

Figure 137. Values of n and n(45°) Versus Corresponding Absolute Cloudiness Values. Circles: relative cloudiness calculated on the basis of V. G. Plank's data (cases numbers 1-12); dots: n(45°) calculated on the basis of V. G. Plank's data; curve: calculation with formula (5.8); straight line: calculation with formula (5.9).

The data of [101, 104, 105] permit both calculation of the averaged radiation flux values and determination of the mean angular distribution of the intensity of thermal radiation as a function of the amount and form of clouds and the meteorological parameters. The mean intensity, $\bar{I}\downarrow(\vartheta)$ is calculated from the formula

$2 - \bar{I}\downarrow(\vartheta)$, $3 - I_c\downarrow(\vartheta)$.

$$\bar{I}\downarrow(\vartheta)=c(\vartheta)I_c\downarrow(\vartheta)+[1-c(\vartheta)]I_n\downarrow(\vartheta), \qquad (5.10)$$ /235

in which $I_c\downarrow(\vartheta)$ and $I_n\downarrow(\vartheta)$ are the intensities with clear and overcast skies respectively. As an example Figure 138 presents curves of the angular distribution of $\bar{I}\downarrow(\vartheta)$, $I_c\downarrow(\vartheta)$ and $I_n\downarrow(\vartheta)$ for cases number 11 and 12 obtained in [104] by averaging over individual observations. As was to be expected, the cloud cover reduces the angular dependence of radiation intensity. For example, in the case of an unbroken cloud cover the values of $I_n\downarrow(\vartheta)$ are virtually independent of ϑ over the range ϑ = 0-70°.

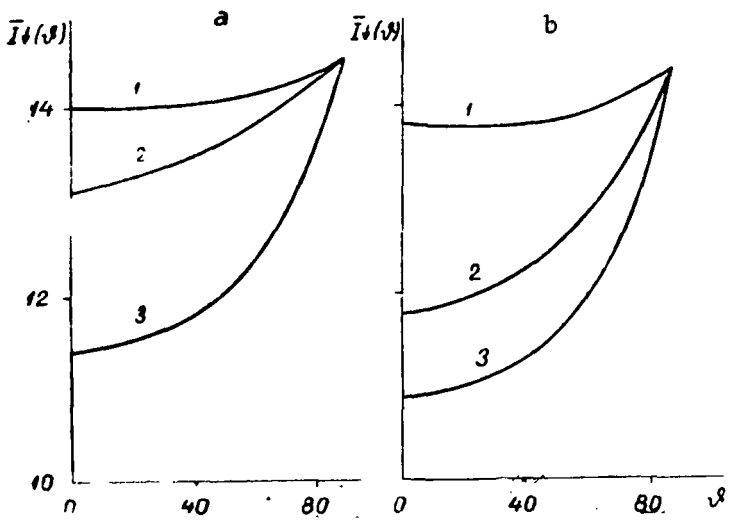

Figure 138. Angular Dependence of Descending Intensity of Thermal Radiation (in mw·cm^{-2}·ster^{-1}) for Cases a, no. 11 (in n(0) = 0.642) and b, 12 (n(0) = 0.290) Calculated with Formula (5.10): 1, $I_n\downarrow(\vartheta)$; 2, $\bar{I}\downarrow(\vartheta)$; 3, $I_c\downarrow(\vartheta)$.

Proper selection of cloud cover characteristics and obtaining the initial information for their determination are thus of substantial importance in solving problems relating to the energetics of the atmosphere. For example, to determine the duration of sunshine it is necessary to have data on the diurnal variation in $c(\vartheta_\odot)$ ($\vartheta_\odot$ in this instance being the zenith angle of the Sun), and to determine the mean values of thermal radiation intensity data are required on the variation in $c(\vartheta)$ with variation in the zenith angle. Data on absolute cloudiness, n(0), are of fundamental importance in determination of the mean values of the radiation fluxes of the atmosphere. It must be emphasized that it is necessary to conduct additional experimental studies under different climatic conditions for the purpose of definitive establishment of the possibilities of determining the values of n and n(45°) on the basis of data on absolute cloudiness alone. /236

Since the calculations presented in the foregoing on the mean back radiation values were performed on the basis of approximate models of the vertical distributions of the meteorological parameters, the results obtained should be regarded as being merely approximate. To obtain information on radiation fluxes in the case of cumulus clouds it is essential to conduct studies for the purpose of accumulating dependable data on the variability of temperature and humidity in time and space.

Section 2. Variability of Intensity and Fluxes of Longwave Radiation

When cumulus clouds are present the brightness of thermal radiation between clouds is virtually constant; it fluctuates slightly within individual clouds and changes abruptly on transition from cloud to clear sky. Hence, as with the statistical characteristics of shortwave radiation (see Chapter IV), the statistical characteristics of the brightness and flux of atmospheric back radiation are in the first approximation determined by the distribution of clouds over the sky and the mean dependence of the brightness of clouds and the sky between them on the zenith angle in the region of thermal radiation. Information on the distribution of the intensity of atmospheric thermal radiation as a function of the zenith angle was presented in the preceding section. By making additional use of information on the statistical characteristics of cumulus clouds, which were studied in Chapter III, let us ascertain the basic patterns of variability in thermal radiation.

Up to zenith distances of the Sun $\vartheta \leqslant 50°$, at which the influence of the lateral portions of clouds is slight, the variability of the intensity of longwave radiation up to frequencies the periods of which are comparable to the dimensions of the clouds approaches the variability of cloud coverage of the zenith (Sun). A correlation-spectral analysis of cloud coverage of the sky in the direction of the zenith and Sun was presented in Chapter III, Section 2, and for this reason will not be dealt with here. /237

The statistical characteristics of the back radiation flux, as with the relationships between the parameters of clouds (Chapter III, Section 5) and shortwave radiation (Chapter IV, Section 3), are connected by a linear relationship to the statistical characteristics of brightness at the zenith. We assume the brightness field to be isotropic in space. We additionally assume that the indicatrix both for clouds and for gaps does not vary with fluctuations in brightness. The indicatrices for clouds and clear sky may differ from each other in this instance. Owing to the greater optical thickness of clouds in the region of thermal radiation, the assumption regarding constant indicatrices agrees much more closely with the actual conditions than in the visible region of the spectrum.

The weighting function for transition from zenith brightness to back radiation flux is similar to the weighting function for transition from zenith brightness to scattered radiation (4.1) and is of the form

$$n(\vartheta) = \frac{1}{\bar{F}\downarrow}[n(\vartheta) I_n\downarrow(\vartheta) + c(\vartheta) I_c\downarrow(\vartheta)] \cos\vartheta \sin\vartheta, \tag{5.11}$$

in which $\bar{F}\downarrow$ is the mean flux of atmospheric back radiation, and $I_n\downarrow(\vartheta)$ and $I_c\downarrow(\vartheta)$ are the mean cloud brightness and clear sky brightness in the longwave region of the spectrum.

The climatic conditions of Estonia were taken into account in the calculations of the thermal radiation intensity for "model" stratification. The temperature at the Earth's surface is assumed to equal 20°C, and its vertical distribution is determined by the labile stratification of the atmosphere in the case of cumulus clouds. Thus the temperature gradient from the Earth's surface to the condensation level equals -10°/km and -6°/km above this level. It was here assumed that the lower boundary of the cloud cover is situated at the level of 1 km. The relative humidity value at the level of the Earth's surface calculated on the basis of these data in accordance with [109] is 66%. It is assumed that the relative humidity increases slightly starting at the Earth's surface, becomes constant in the cloud layer, and decreases at a relatively rapid rate above the clouds. The atmospheric pressure was calculated from the barometric formula $p_{z=0}$ = 1,000 mb. /238

The angular distribution of the mean brightness, normalized with the brightness at the zenith with mean cloud coverages of the zenith of 0.1, 0.3, 0.5, and 0.8, is shown in Figure 139. We see that the brightness always increases toward the horizon, the more rapidly the smaller is the mean amount of cloudiness at the zenith.

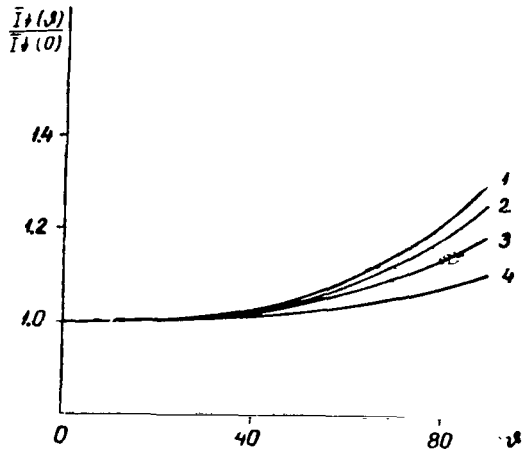

Figure 139. Angular Dependence of Mean Relative Descending Intensity of Thermal Radiation Calculated with Formula (5.10): 1, n(0) = 0.1; 2, n(0) = 0.3; 3, n(0) = = 0.5; 4, n(0) = 0.8.

The increase in brightness toward the horizon is due chiefly to the increase in the contribution by the natural radiation of the atmosphere between the clouds and the observer. It is advisable to disregard the dependence of brightness on the zenith angle for effecting the transition from the statistical characteristics of zenith brightness to the back radiation characteristics, also in view of the smoothing of the fluctuation in cloud brightness on passage of radiation through the layer of the atmosphere below the clouds. The spectral characteristic of the filter for such a transition was presented in Chapter IV, Section 1, in the form of formula (4.2). The results of correlation-spectral analysis of the flux of longwave radiation of the atmosphere must fully coincide with the corresponding characteristics for scattered radiation obtained on the assumption that the mean brightness of shortwave radiation does not depend on the zenith angle of observation (see Chapter IV, Sections 1 and 3). /239

As we saw in Chapter IV, Section 5, in which the results of experimental studies of sky brightness in the shortwave region of the spectrum were presented, in the majority of cases the brightness increases slightly toward the horizon (Figure 114). Hence correlation-spectral analysis of the results of measurements of the scattered radiation flux for cumulus clouds (see Chapter IV, Section 3) in the first approximation also describes the variability of longwave atmospheric radiation.

Let us proceed to analysis of theoretical studies of the longwave radiation field above cumulus clouds. The cloud field is simulated by means of a normal random process (see Chapter I, Section 6) the parameters of which were determined by way of experiment and were presented in Chapter III. Since no experimental data were available on the meteorological parameters of the atmosphere in the case of cumulus clouds, use was made of a model of labile stratification for summertime conditions. We assume that the lower boundary of the clouds is situated at an altitude of 1 km.

The means, dispersions, variation coefficients, and correlation functions of the intensity and flux of ascending longwave radiation above cumulus clouds have been calculated for the model of the atmosphere in question as a function of the amount of clouds at the zenith.

The mean intensity of ascending radiation is expressed by

$$\bar{I}\uparrow=\bar{I}_n\uparrow n(0)+\bar{I}_c\uparrow[1-n(0)]=\bar{I}_n\uparrow n(0)+\bar{I}_c\uparrow c(0), \tag{5.12}$$

in which the nonaveraged brightness of the clouds is calculated with the formula

$$I_n\uparrow=\sigma(T_n-\nabla Th)^4. \tag{5.13}$$

In this instance h is the height from the base of the cloud, T_n is the temperature of the lower boundary of the cloud, σ is the Stefan-Boltzmann constant, and ∇T is the temperature gradient of the cloud surface, assumed in our calculations to equal $\nabla T = 6.5^\circ\ km^{-1}$. /240

To simplify the calculations we linearize relation (5.13) relative to h. As a result of the simplifications we obtain

$$I_n\uparrow=\sigma T_n^4-4\sigma T_n^3\nabla Th. \tag{5.14}$$

The error of formula (5.14) of course increases with increase in height h. When h = 1 km the intensity of the ascending radiation is exaggerated by 6%.

Making use of the function of probability density distribution of the surface of cumulus clouds in altitude (3.20) and formula (5.14) we obtain for mean brightness $\bar{I}_n\uparrow$ the expression

$$\bar{I}_n\uparrow=\sigma T_n^4-\frac{0.4T_n^3\nabla T}{\sqrt{2\pi}\,n(0)}e^{-\frac{v^2}{2\cdot 0.4^2}}, \tag{5.15}$$

in which

$$w = \arg\operatorname{erf}[1 - 2n(0)], \quad \text{if} \quad n(0) \leqslant 0.5$$

and

$$w = -\arg\operatorname{erf}[1 - 2n(0)], \quad \text{if} \quad n(0) \geqslant 0.5.$$

Substituting (5.15) in expression (5.12), we obtain the design formula for the mean intensity of ascending radiation. The dispersion and autocorrelation function are, in accordance with [28], expressed approximately by /242

$$\sigma^2_{I\uparrow} = (0.16\nabla T \sigma T_n^3)^2 \left\{ \Phi^2\left(-\frac{w}{0.4}\right) + \sum_{k=2}^{10} \frac{1}{k!}\left[\Phi^{(k-1)}\left(\frac{w}{0.4}\right)\right]^2 \right\} \tag{5.16}$$

and

$$r_{I\uparrow}(t) = \frac{(0.16\nabla T \sigma T_n^3)^2}{\sigma^2_{I\uparrow}} \left\{ \Phi^2\left(-\frac{w}{0.4}\right) r_z(t) + \sum_{k=2}^{10} \frac{1}{k!}\left[\Phi^{(k-1)}\left(\frac{w}{0.4}\right)\right]^2 r_z^k(t) \right\}, \tag{5.17}$$

in which Φ is the probability integral, $\Phi^{(k)}$ is the k-order derivative of the probability interval, and $r_2(t) = e^{-0.3|t|}$ is the correlation function of a continuous random process (see Chapter III).

Let us now present the results of numerical calculations for the model of /243 the atmosphere described above, which were obtained by means of formulas (5.12)--(5.17). Figure 140 shows the angular distribution of the mean radiation intensity for zenith cloudiness of 0.2, 0.5, and 0.8. It is to be seen that the radiation intensity decreases with increase in the zenith angle of observation, the more rapidly the smaller is the zenith cloudiness. Figure 141 illustrates the mean ascending flux of radiation and its dispersion as a function of coverage of the zenith. The mean radiation flux decreases slowly with increase in the amount of clouds. The dispersion of the flux is small and undergoes virtually linear increase with increase in cloudiness. This is clearly to be seen from Figure 142, which shows the coefficient of variation in the ascending flux of thermal radiation. With mean amounts of clouds the root mean /244 square deviation is approximately 2-3% of the mean.

The normalized correlation functions for a normal random process and for the brightness of thermal radiation with amounts of clouds at the zenith of 0.1, 0.3, 0.5, and 0.7 are presented in Figure 143. We see that the correlation radius decreases with decrease in the amount of clouds.

Comparison of the correlation functions presented in Figure 143 with the correlation functions of zenith coverage presented in Figures 35 and 36 reveals that they differ but little from each other in the first approximation. The correlation functions for the ascending flux of thermal radiation coincide in the first approximation with the correlation functions of scattered radiation and, as we saw earlier, also with the correlation functions of the descending flux of thermal radiation of the atmosphere (see Chapter IV, Section 1).

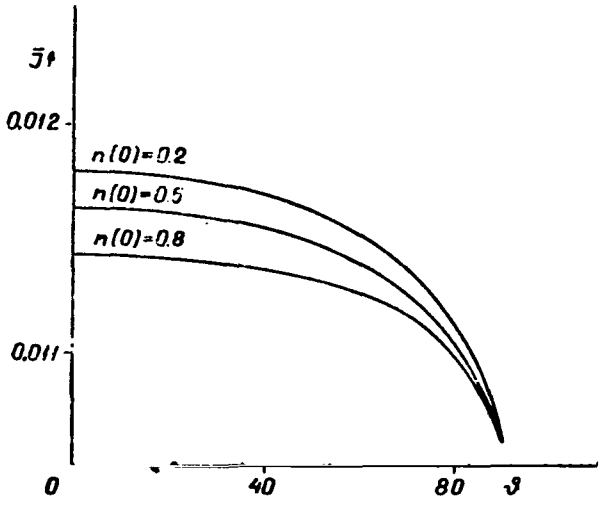

Figure 140. Angular Distribution of Mean Ascending Intensity of Thermal Radiation (in $mw \cdot cm^{-2} \cdot ster^{-1}$) with Cloudiness at the Zenith of 0.2, 0.5, and 0.8, as Calculated with Formula (5.12).

Section 3. Representation of Distribution of Brightness of Longwave Radiation over the Sky by Means of Eigenfunctions

Theoretical calculations were made of the eigenfunctions and eigenvalues of the intensity of thermal radiation averaged over the azimuth and of the zonal flux. The initial data used were represented by the results of experimental studies of the distribution of cumulus clouds over the sky (Chapter III) and the mean distributions calculated in the preceding section of the intensity of thermal radiation for clear and cloudy skies as a function of the zenith angle for model stratification.

The intensity of thermal radiation as a function of zenith angle ϑ was calculated with formula (5.10), which may easily be reduced to the form

$$I\downarrow(\vartheta) = I_c\downarrow(\vartheta) + n(\vartheta)[I_n\downarrow(\vartheta) - I_c\downarrow(\vartheta)] \qquad (5.18)$$

Only a part of this formula — $[I_n\downarrow(\vartheta) - I_c\downarrow(\vartheta)]$ is the weighting function for the experimental data on the distribution of clouds over the sky in calculations of the eigenvalues and of the eigenfunctions of the intensity of thermal radiation. This greatly simplifies numerical calculations. The weighting function and the intensity of back radiation for clear and cloudy skies as a function of the zenith angle are presented in Figure 144. /245

On the assumption that the brightness of clouds and of the clear sky is constant in time for individual zenith directions, the normalized correlation matrix of brightness coincides with the correlation matrix of the presence of clouds (see Chapter III, Section 4). The first three eigenfunctions for radiation intensity, averaged over the azimuth, are presented in Figures 145-147. /246 Comparison of these eigenfunctions with the eigenfunctions for the presence of clouds (Figures 49-51) reveals that they are similar. The eigenfunctions for the intensity of thermal radiation at the horizon decrease somewhat more rapidly than do the eigenfunctions for the presence of clouds. The dispersion of radiation intensity eigenfunctions from observation to observation is smaller than that of the corresponding functions for the presence of clouds. Comparison of the first eigenfunctions of the intensity of shortwave (see Figure 119) and longwave (Figure 145) radiation shows that the latter have no maximum but undergo almost linear decrease with increase in the zenith angle. The second and third

eigenfunctions are similar in this instance. This indicates that, as with the presence of clouds, the fluctuations in thermal radiation are the most extensive around the zenith and decrease monotonically with increase in the zenith angle.

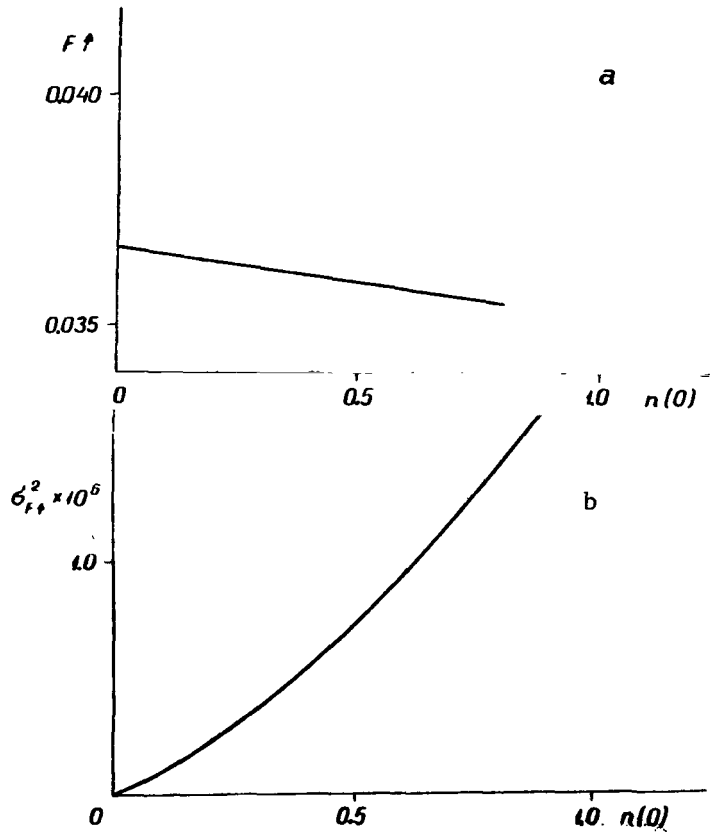

Figure 141. Relationships Calculated with Formulas (5.15) and (5.16): a, Ascending Flux of Thermal Radiation (in $mw^2 \cdot cm^{-2}$) and b, its Dispersion (in $mw^2 \cdot cm^{-4}$) Versus Coverage of the Zenith by Cumulus Clouds.

The eigenvalues and the relative accuracy of expansion when the first ith components are used for the thermal radiation intensity averaged over the azimuth are presented in Table 8. The first eigenfunctions account for 81-85% of the dispersion, and the first three eigenfunctions cover 94-96% of the dispersion. Comparison of these data with Table 3 reveals that the thermal radiation intensity is described more accurately by means of the first or first three eigenfunctions than is the distribution of clouds. /251

Similarly calculated eigenfunctions for zonal thermal radiation are presented in Table 9, and the first three eigenfunctions in Figures 148-150. It is to be seen that the first eigenfunctions account for 70-83% of the dispersion and the first three around 95%.

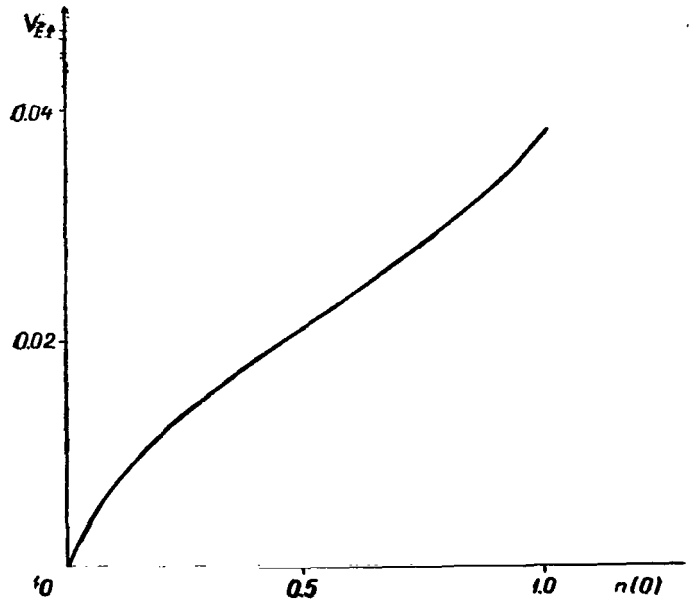

Figure 142. Coefficient of Variation in Ascending Flux of Thermal Radiation Versus Coverage of the Zenith by Cumulus Clouds.

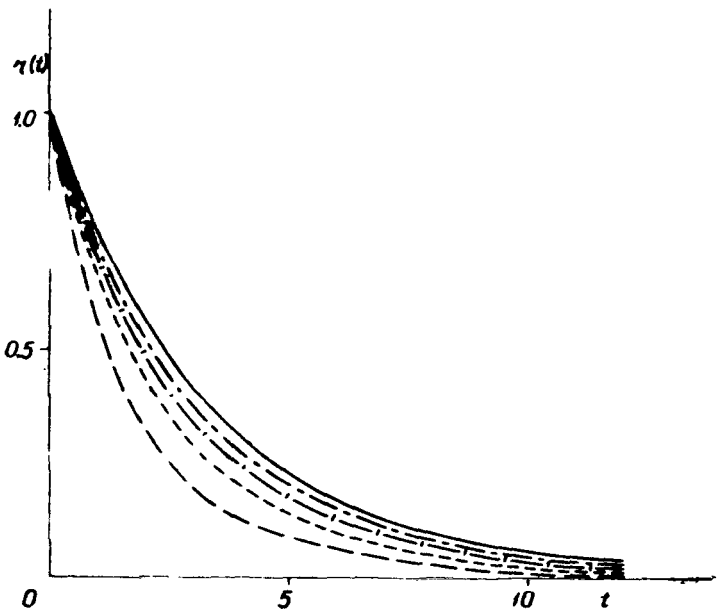

Figure 143. Autocorrelation Functions of Normal Random Process (——) and of Ascending Intensity of Thermal Radiation Calculated with Formula (5.17), with Cumulus Clouds Present: — — —, n(0) = = 0.7; —•—•, n(0) = 0.5; ---, n(0) = 0.3; — --, n(0) = 0.1.

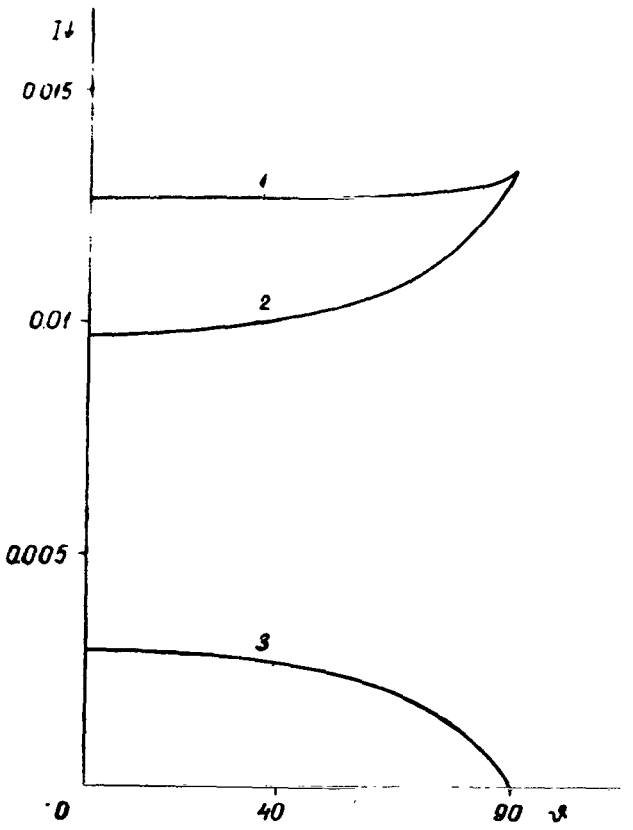

Figure 144. Intensity of Back Radiation for Cloudy 1 and Clear 2 Skies and Weighting Function for Cumulus Clouds 3 Versus Zenith Angle, as Calculated with Formula (5.18).

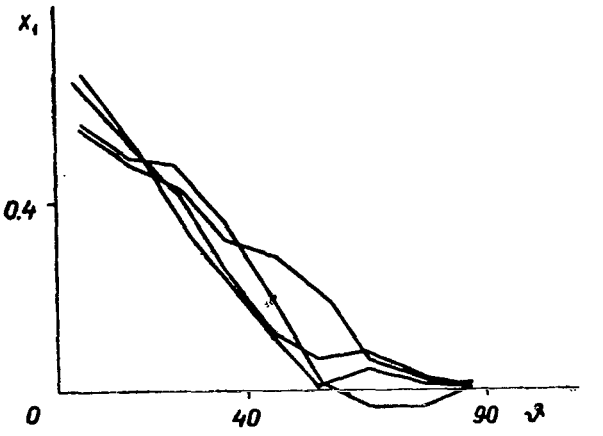

Figure 145. First Eigenfunctions of Back Radiation Intensity Averaged over the Azimuth Versus Zenith Angle of Direction of Sighting.

The eigenfunctions of the thermal radiation flux by zones are similar to the eigenfunctions for the relative zonal cloudiness (Figures 52-54). The eigenfunctions for the flux by zones at the horizon decrease more rapidly in this instance and their dispersion is smaller in comparison with the eigenfunctions for the relative zonal cloudiness. /252

Section 4. Experimental Studies of the Fine Structure of Cloud Brightness Fields in the 8-13 μ Spectral Region[1]

In the experimental research on the brightness fields of shortwave radiation the results of which were presented in Chapter IV, no study was made of the fine structure of brightness fields, and thus of the fine structure of cloud formations. Study of the fine structure of brightness fields in the visible region of the spectrum proved to be impossible owing chiefly to the low resolving power of the narrow angle radiation detectors (with a viewing angle of the order of one degree; see Chapter II), and also to the considerable inertia

[1]The authors wish to thank Yu. A. Shub for his valuable advice and the attention he bestowed on the work, as well as G. F. Asyakin, N. Ye. Vystavkin, and V. V. Mikhaylov for their assistance in the measurements and processing of the results presented in this section.

of the detectors and of the recording system as a whole (see Chapter I, Section 3). At the same time, study of the fine structure of cloud formations by optical methods in the shortwave region of the spectrum is basically impossible because of the averaging of the radiation scattered by cloud particles over the considerable volume participating in formation of the light scattered by the clouds.

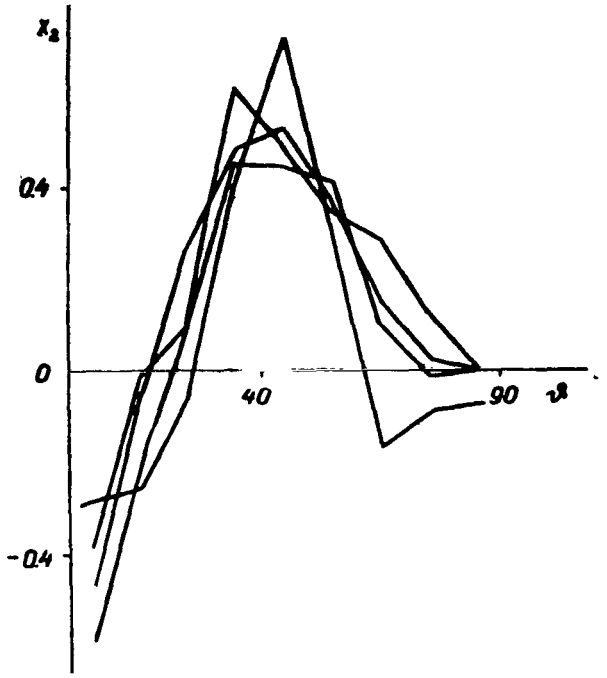

Figure 146. Second Eigenfunctions of Back Radiation Intensity Averaged over the Azimuth Versus Zenith Angle.

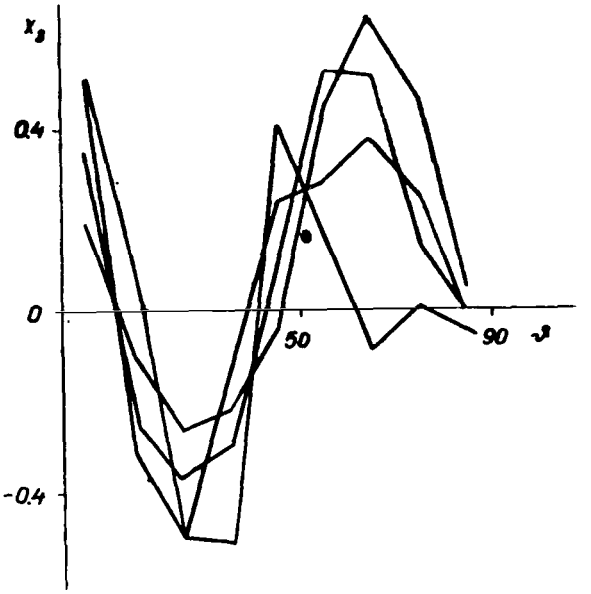

Figure 147. Third Eigenfunctions of Back Radiation Intensity Averaged over the Azimuth Versus Zenith Angle.

The finer structure of cloud formations is accessible to study by optical methods in the infrared radiation region of the spectrum, in which the brightness properties of clouds are determined chiefly by their surface layer. This means, however, that only the structure of the surface layers of the clouds are accessible to study.

The importance of research of this kind to determine the relations between the radiation and the physical parameters of clouds has been pointed out in many works [84, 110-112]. To establish these relationships it is necessary to know the various parameters of the cloud cover: form, optical thickness, albedo, moisture content, cloud brightness, and so forth, as well as their variation in time and in space. One of the parameters determining the conditions chiefly of the surface layers of the cloud cover, and accordingly the one the most closely associated with their radiation properties, is the temperature heterogeneity of cloud fields. /253

TABLE 8. EIGENVALUES OF THERMAL RADIATION INTENSITY AVERAGED OVER THE AZIMUTH /248

	$n(0) = 0.2$, $n = 0.5$, $N = 34$		$n(0) = 0.3$, $n = 0.4$, $N = 15$		$n(0) = 0.3$, $n = 0.5$, $N = 21$		$n(0) = 0.5$, $n = 0.7$, $N = 28$	
i	$S(X_i) \cdot 10^{-5}$	λ_{i9}	$S(X_i) \cdot 10^{-5}$	λ_{i9}	$S(X_i) \cdot 10^{-5}$	λ_{i9}	$S(X_i) \cdot 10^{-5}$	λ_{i9}
1	0.2845	73.5	0.3719	85.6	0.2345	83.4	0.3820	81.3
2	0.0630	89.8	0.0311	92.8	0.0192	90.2	0.0508	92.1
3	0.0212	95.3	0.0172	96.8	0.0097	93.7	0.0177	96.0
4	0.0090	97.7	0.0070	98.4	0.0085	96.7	0.0081	97.7
5	0.0041	98.8	0.0032	99.1	0.0041	98.2	0.0049	98.7
6	0.0027	99.5	0.0022	99.6	0.0033	99.4	0.0032	99.4
7	0.0013	99.8	0.0012	99.9	0.0011	99.8	0.0020	99.8
8	0.0010	100.0	0.0004	100.0	0.0005	100.0	0.0010	100.0
9	0.0001	100.0	0.0002	100.0	0.0000	100.0	0.0001	100.0

TABLE 9. EIGENVALUES OF ZONAL FLUX OF ATMOSPHERIC THERMAL BACK RADIATION AVERAGED OVER THE AZIMUTH /249

	$n(0) = 0.2$, $n = 0.5$, $N = 34$		$n(0) = 0.3$, $n = 0.4$, $N = 15$		$n(0) = 0.3$, $n = 0.5$, $N = 21$		$n(0) = 0.5$, $n = 0.7$, $N = 28$	
	$S(X_i) \cdot 10^{-6}$	λ_{i9}	$S(X_i) \cdot 10^{-6}$	λ_{i9}	$S(X_i) \cdot 10^{-6}$	λ_{i9}	$S(X_i) \cdot 10^{-6}$	λ_{i9}
1	0.3049	70.4	0.4370	80.3	0.1875	72 3	0.5164	83.3
2	0.0756	87.8	0.0686	92 9	0.0363	86 3	0.0542	92.1
3	0.0339	95.6	0.0180	96.2	0.0176	93 1	0.0265	96.4
4	0.0071	97.2	0.0107	98.2	0.0084	96.1	0.0107	98.1
5	0.0056	98.5	0.0065	99.4	0.0054	98.2	0.0064	99.1
6	0.0035	99.4	0.0019	99.7	0.0022	99.1	0.0030	99.6
7	0.0014	99.7	0.0013	99.9	0.0017	99.8	0.0018	99.9
8	0.0011	100.0	0.0017	100.0	0.0004	100.0	0.0010	100 0
9	0.0000	100.0	0.0000	100 0	0.0000	100.0	0.0000	100.0

Problems of this nature relating to study of the spatial structure as one determining the characteristics of the cloud cover have also been discussed in [17, 114-116].

In what follows we present the results of experimental study of the fine structure of cloud formations of various forms obtained by means of a high speed instrument characterized by fairly high spatial resolution (4' x 4') in the 8-13 μ water vapor window. The instrument employed is described in Chapter II, Section 4, and some of the results obtained are presented in [59, 117]. A report was made in [115] on investigation of the spatial structure of the brightness fields of the clouds of the upper and lower tier in the 8-12 μ region of the spectrum. The correlation functions of cloud brightness presented in this work were obtained with an instrument possessing a fairly high spatial resolution (10' × 30'). The results of these studies may not be regarded as complete, however, since they were obtained for a specific cloud field situation (at the zenith) over a short time interval (5 hours) with equipment characterized by relatively low sensitivity and considerable inertia.

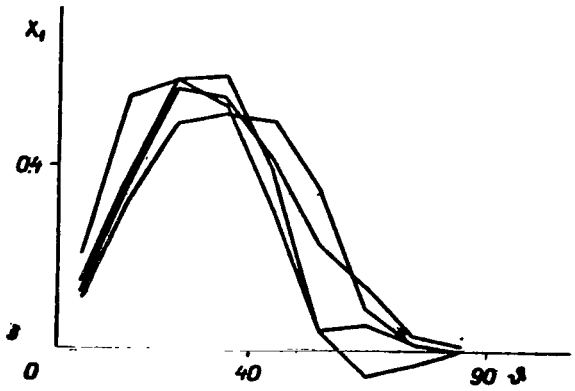

Figure 148. First Eigenfunctions of Zonal Back Radiation Versus Zenith Angle.

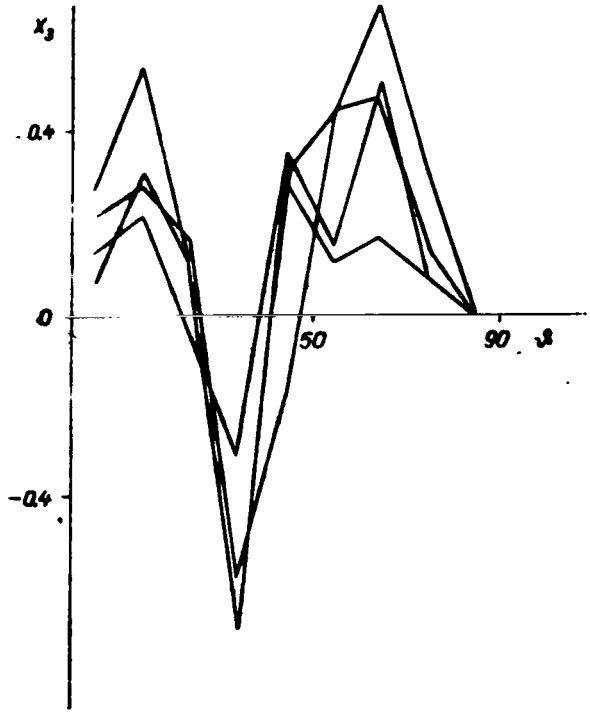

Figure 150. Third Eigenfunctions of Zonal Back Radiation Versus Zenith Angle.

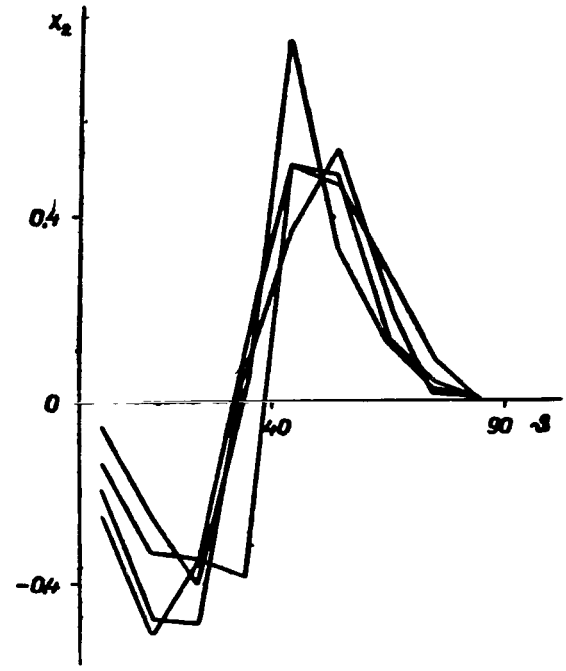

Figure 149. Second Eigenfunctions of Zonal Back Radiation Versus Zenith Angle.

In the process of study of cloud radiation processes we are faced with the problem of determining the form of the cloud cover, this at the present time being accomplished exclusively by visual means in keeping with the classification of clouds [118]. As we know, however, this method of determination is to some extent subjective and is not in keeping with the capabilities of the equipment employed (see Chapter II, Section 4, and [117]). In addition, visual determination of the form of the cloud cover at night is virtually impossible. Hence to determine the form of clouds for purposes of identification in daytime and especially at night it is desirable to develop equipment methods the application of which would eliminate observer error. At the present /254 time the region of natural cloud radiation (8-13 μ) appears to be the most promising one for the application of equipment methods.

The number of parameters determining the radiation properties of clouds is fairly large in the case of ground measurements, and for this reason simultaneous measurement of all of them is not possible at the present time. In the process of the work measurement was made, along with the brightness structure in the water vapor window, also of the air temperature of the ground layer, the coordinates of the section of sky studied, and the altitude of the Sun. The use of high speed equipment for brightness measurements permits the assumption that these parameters are constant for individual specific observations.

In the following study of the radiation characteristics of cloud formations the latter have been classified in accordance with [118]. In this case as well, as in study of the structure of the cloud cover in the visible region of the spectrum and the structure of shortwave radiation (see Chapters III and IV), we assume it to be permissible to use the hypothesis regarding the statistical isotropicity of the radiation fields and cloud cover of the forms of clouds investigated, and also to apply the normal law of distribution to fluctuation of the brightness fields of longwave radiation (see Chapter I, Section 6). In studies of the fine structure of intensity it is more justifiable to apply the hypothesis regarding isotropicity, since, according to the theory of turbulence, the departures from isotropicity increase with increase in the scales in space.

The results of many years of research make it possible to gain an idea of the variability in space of the brightness of cumulus, altocumulus, and cirrus clouds. Chiefly the results of measurement of a single-tier cloud cover were subjected to processing. The research program called for the following:

1) Determination of the influence of the Sun on the variability in space of fluctuations in the radiation of various clouds;

2) investigation of the angular distribution of the radiation of a cloudless sky;

3) comparison of the variability in space of the brightness of daytime and nighttime clouds;

4) investigation of the fluctuations in radiation on the illuminated and shaded sides of cumulus clouds of great thickness; /255

5) investigation of the isotropicity of the radiation of cirrus clouds.

The correlation function was calculated on the basis of the values of the signal obtained from the output of the radiometer-pyrometer during operation of the latter in the second mode: scanning at a frequency of 7 Hz over a circumference with an angular radius of 5°. To automate the calculations the signal obtained in one scanning period (one observation) is represented as a sequence of readings following each other at an interval corresponding to the spatial resolution of the instrument.

The calculations were performed by a BESM-4 computer in accordance with the formula

$$r(k\Delta t)=\frac{1}{N-k}\sum_{i=1}^{N-k}\xi(i\Delta t)\xi[(i+k)\Delta t], \tag{5.19}$$

in which r(kΔt) are the values of the function sought; ξ(iΔt) are the values of the signal; Δt is the reading interval, which equals $3\cdot10^{-4}$sec; and N is the total number of readings over the period of observation.

To increase the accuracy averaging was performed over the aggregate of the various observations in study of the same form of cloud cover.

Under the assumptions made in the foregoing regarding the spatial structure of clouds the argument of the correlation function is represented by only one variable, the distance between the points of the section investigated. However, the value of r(kΔt) found by the method described above is the correlation function obtained over the circumference, and its argument is angle ψ expressed in kΔt. In order to effect transition to the correlation function whose argument is the distance between points it is necessary to switch to the variable

$$\Delta\vartheta=2R\sin\frac{k\Delta t}{2}, \tag{5.20}$$

in which R is the scanning radius, which equals 5°, and to express the correlation function through this variable Δϑ.

Typical correlation functions of the brightness of cumulus clouds measured in the spectral regions of 8-13 and 10.2-11.5 μ are presented in Figure 151 as a function of scanning angle ψ and angular distances in the sky ϑ, φ. We see that the correlation radius of small-scale heterogeneities is ψ = 2°. /256

In our case, in which ψ < 4°, expression (5.20) may be linearized to Δϑ ≈ ψ without substantial error. This means that the correlation function of brightness as a function of angular distance in the sky is in form near that of the correlation function of Figure 151. The correlation radius in this instance is $\Delta\vartheta \lesssim 2°$, to which a linear distance on the cloud of the order of 100 m corresponds.

We use the spatial spectral density of longwave cloud brightness as the basic characteristic of spatial variability of cloud formations. High-speed radiometry equipment permits measurement of the spectral components over such short time intervals that the brightness variations of the section investigated in time may be disregarded. In this case the signal from the radiometer output is periodic and a standard spectrum analyzer may be used for frequency analysis. An S5-3 analyzer with a passband of Δf = 6 Hz was used in our work. The spectral density was determined by squaring spectrum for brightness and averaging the values obtained over the observations (usually over 10-15). /257 /258

If the length of the scanning line in space is known, the number of harmonics may be expressed as the number of periods per radian, but it must be remembered that the scanning trajectory is curvilinear in space. The first harmonic

corresponds to a scanning line length equaling 31 angular degrees, and the hundredth harmonic to one of 0.31°.

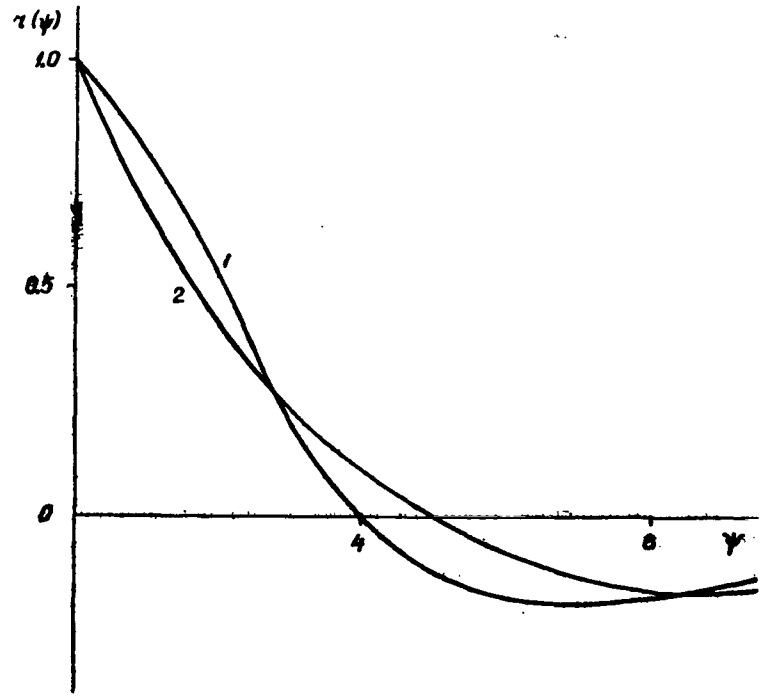

Figure 151. Correlation Functions of Cumulus Cloud Brightness, Averaged over Observations, Versus Circular Scanning Angle ψ: 1, $\Delta\lambda$ = 8.5-12.5 μ, ϑ = 65°, φ = 50°; 2, $\Delta\lambda$ = 10.2-11.5 μ, ϑ = 80°, φ = 75°.

The specific nature of the scanning has a particularly heavy impact on the first harmonics, the values of which depend both on the fluctuation in radiation and on the temperature gradient, which depends on the zenith angle of sighting of the instrument and on the curvilinearity of the scanning trajectory. /259

Spectral densities S(k) of the brightness of cumulus clouds for zenith angle ϑ = 60-70° at azimuths φ = 0-360° are shown in Figure 152. As may be seen from the Figure, the spectra are virtually independent of the azimuth. The dispersion of the spectral density is slight (shaded areas) and may be ascribed to the slight change in zenith angle $\Delta\vartheta$ = 10°, as well as to experimental errors determined by the errors of the S5-3 analyzer.

The results of study of the variability of the brightness of various clouds in space as a function of zenith angle ϑ for azimuths φ = 20-40° are shown in Figure 153. It is to be seen that the spectral density of the brightness of altocumulus clouds has a greater abundance of small spatial heterogeneities than that of the cumulus clouds and depends on the zenith angle. It is to be noted that the heavy dependence of the spectral density for the low frequencies on the zenith angle is due to the considerable contribution made by the radiation

of the atmospheric column and the variability in the amount of clouds along the circular scanning trajectory, especially at small angles to the horizon [31, 105, 119]. This relationship is manifested in operation of the instrument in the second mode, it being confirmed by the results of measurement of the brightness of a cloudless sky. These results are presented in Figure 154, which reveals a sharp increase in brightness at small angles to the horizon. For this reason the signal differentials increase with decrease in the zenith angle in circular scanning. This figure also shows the brightness of a cloudless sky as a function of the zenith angle for various azimuths measured at intervals of 10-20° over the range from 0 to 360°. The slight dispersion of brightness over the azimuth may be explained by the varying degree of turbidity of the atmosphere in the area of measurement. The results of many studies are in agreement with the theoretical calculations [120, 121].

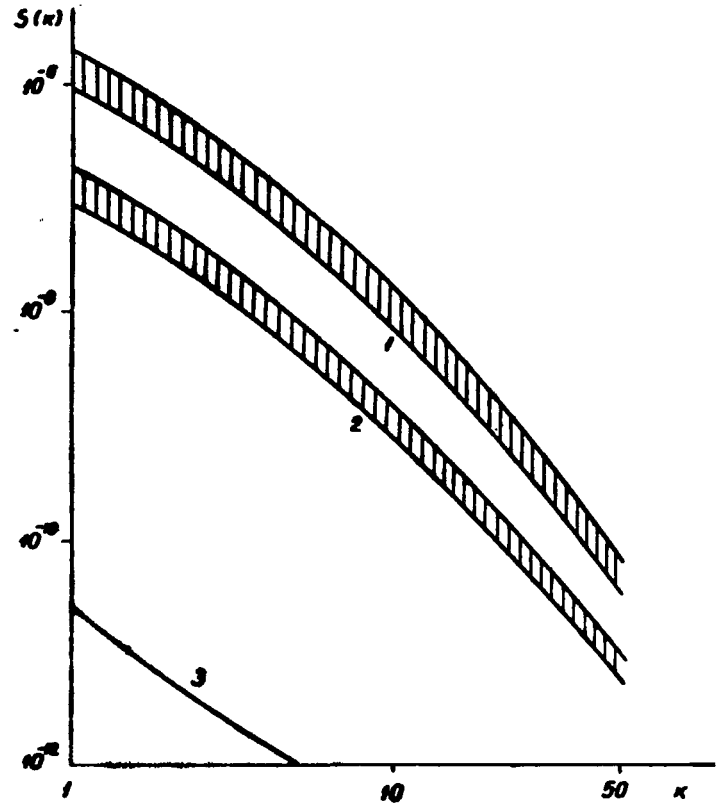

Figure 152. Spectral Densities of Cumulus Cloud Brightness (in $(w \cdot cm^{-2} \cdot ster^{-1})^2$) Versus Number of Harmonics k: 1, $\Delta\lambda$ = 8.4-12.5 μ; 2, $\Delta\lambda$ = 10.2--11.5 μ; 3, Equipment Noise.

On the one hand, attention must be called to the fact that in the case of the measured spectral densities of the brightness of cumulus clouds of great thickness in the direction of the zenith (Figure 153, curve 1 (dot-and-dash line)) the low-frequency component is smaller in value than in the case of the spectra for clouds of the same form situated at the horizon. On the other /260

hand, we know [122] that the coefficient of radiation blackness of cumulus clouds is near unity, and the contrast between clouds and cloudless sky is at the maximum at the zenith. It is to be noted that the temperature of cumulus clouds differs by 10-15° from the temperature of the layer of atmospheric air near the ground. This conclusion may not be drawn, however, on the basis of the value of the low-frequency components of spectral density.

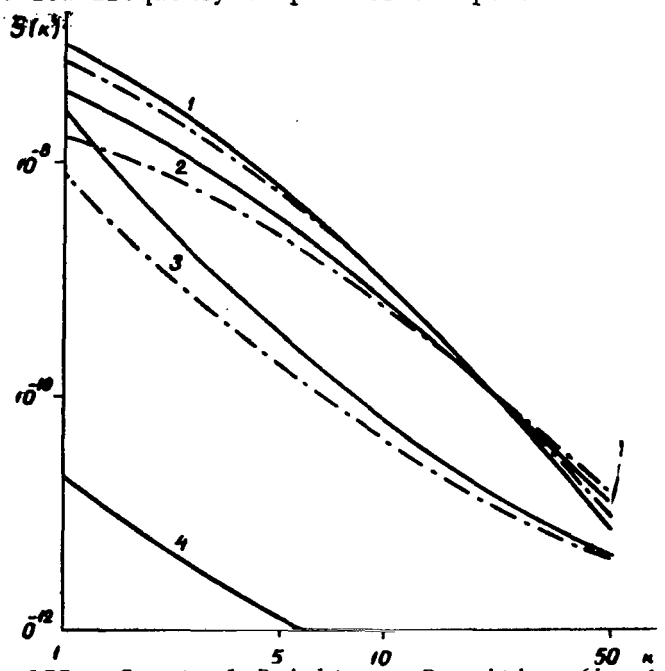

Figure 153. Spectral Brightness Densities (in $(w \cdot cm^{-2} \cdot ster^{-1})^2$) of Clouds of Different Form Versus Number of Harmonics k at $\Delta\lambda$ = 10.2-11.5 μ, φ = 20-40°. Curve ——, ϑ = 80-85°, —•—•, ϑ = 0-5°; 1, Cumulus Clouds; 2, Altocumulus; 3, Cirrus; 4, Equipment Noise.

This behavior of the spectral density may be ascribed to the fact that, owing to the small turning angle of the field of view of the instrument in space for individual observations, the scanning was performed cloud by cloud, that is, high-frequency components were present in the spectral density of the signal, ones due chiefly to fluctuations in brightness on the surface of a cloud. As a matter of fact, the greatest dispersion of the values of the low-frequency component in the spectral density of the signal are manifested precisely for angles near the zenith angle. It follows that with the form of scanning adopted determination of the spectral density of the brightness of cumulus clouds of great thickness requires a greater number of observations than for clouds such as altocumulus ones. As was to be expected, the high frequency components of the spectrum are somewhat less pronounced than, for example, for clouds of the same form measured at angles near the zenith angle. This is due to the finite resolution of the instrument, that is, the linear dimensions of the field of view in measurement of clouds on the horizon are much larger than in measurements at the zenith. As a result, averaging by the detector varies over the surface of the clouds and increases with the zenith angle of observation (see Chapter I, Section 4).

/ 261

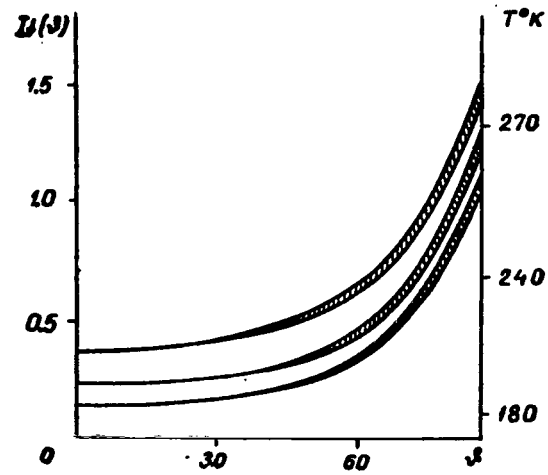

Figure 154. Examples of Dependence of Brightness (in $w \cdot cm^{-2} \cdot ster^{-1} \cdot 10^{-3}$) of a Cloudless Sky on the Zenith Angle at $\Delta\lambda$ = 8.5-12.5 μ.

Account must also be taken of the fact that small brightness or temperature heterogeneities at large zenith angles are filtered out more extensively in view of the scattering and absorption in the atmosphere [10].

The layer of the atmosphere between the clouds and the Earth's surface has virtually no effect on the spectral density at angles ϑ = 0-40°. The spectral densities for these angles coincide.

The spatial structure of the brightness of cirrus clouds does not lend itself well to dependable description. The spectral densities are fairly variable, as may be seen from Figure 153, in which the most typical cases for cirrus clouds are presented.

In the processing of the materials it was observed, for example, that for certain observations the spectral densities of the brightness of cirrus clouds Ci differ little from the spectral densities of the brightness of altocumulus clouds.

The dispersion in the spectral densities may be ascribed to failure to allow for the various forms of cirrus clouds and to certain characteristics of their structure. For example, the nature of the spatial structure of brightness varies in linear scanning along and across Ci cloud banks (Figure 155). As may be seen from this figure (curve 2), the signal is very jagged in scanning across the banks, small spatial heterogeneities are present, and the fluctuations in radiation are damped out on passage from bank to bank. There is little variation in the brightness of cirrus clouds along the banks (curve 1) and between them (curve 3), and small unevennesses are absent from the signal. The great variability of the S(k) of individual observations of the brightness of cirrus clouds is apparently determined by the fact that spatial heterogeneities of small dimensions are present in some observations, while their weight is relatively low in others. For example, for more precise determination of S(k) for Cu the averaging for circular scanning should be carried out on the basis of a larger number of observations in comparison with the more homogeneous Ac clouds. /262

The measurement procedure also provided for investigation of the effect of the Sun on the spatial structure of the longwave brightness of clouds. For this purpose study was made of the nature of fluctuations in brightness on the illuminated and the shaded sides of clouds. Single-tier thick cumulus clouds several dozen angular degrees in dimensions with clearcut boundaries and well /263

illuminated and shaded sides were selected for observation. The instrument was aimed at a cloud by means of an optical system integrated with the field of view of the radiometer. It was noted that in individual instances the fluctuations in radiation are more pronounced on the illuminated side, while on the shaded side they are faint or altogether absent [59]. Figure 156 shows the distinctive features of fluctuations in radiation on the illuminated and the shaded sides of clouds. It is to be observed that the clouds with clearcut borders and appreciably illuminated and shaded sides, which are convenient for observation, were rather seldom encountered during the period of investigations and for this reason relatively few such studies were conducted.

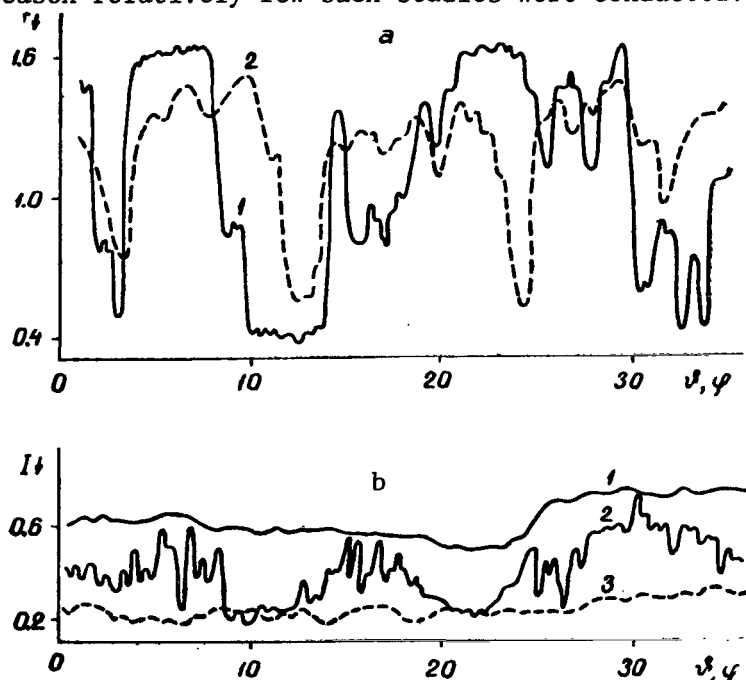

Figure 155. Examples of Variability of Cloud Brightness (in $w \cdot cm^{-2} \cdot ster^{-1} \cdot 10^{-3}$) at $\Delta\lambda$ = 8.5-12.5 μ; a, Thick Cumulus Clouds; 1, $\vartheta = 45°$, $\varphi = 305\text{-}340°$, Daytime; 2, $\vartheta = 45°$, $\varphi = 23\text{-}58°$, Nighttime; b, Cirrus Clouds: 1, Along Banks, $\vartheta = 15\text{-}90°$; $\varphi = 300°$; 2, Across Banks; $\vartheta = 20°$, $\varphi = 290\text{-}325°$; 3, Between Banks, $\vartheta = 15\text{-}90\text{-}15°$, $\varphi = 305°$.

Corresponding measurements were performed for the purpose of comparison of the spatial structures of nighttime and daytime clouds; the results are presented in Figure 157. The clouds could be classified as cumulus during the day and at sunset. The measurements were conducted between 2200 and 2330 hours. It unfortunately cannot be stated that the clouds observed were also of this form in the case of the nighttime observations. As may be seen from Figure 157, the averaged spectral densities of the brightness of nighttime and daytime clouds, which were studied with approximately the same spatial coordinates, differ only slightly from each other. However, in view of the /264 cooling of the clouds at night the curves of the spectral densities of

brightness for the nighttime clouds are situated lower than the curves of the spectral densities obtained for the daytime clouds.

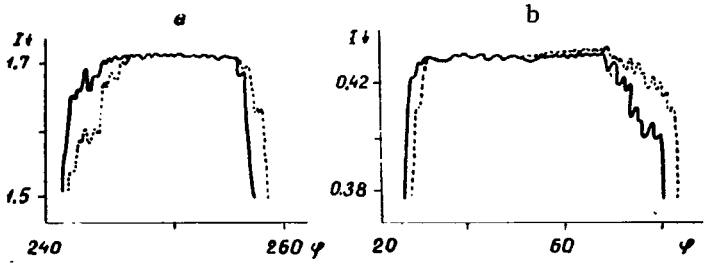

Figure 156. Examples of Variability in Brightness (in $w \cdot cm^{-2} \cdot ster^{-1} \cdot 10^{-3}$) of Thick Cumulus Clouds at $\vartheta = 55°$. a, $\Delta\lambda$ = 8.5-12.5 μ; b, $\Delta\lambda$ = 10.2-11.5 μ.

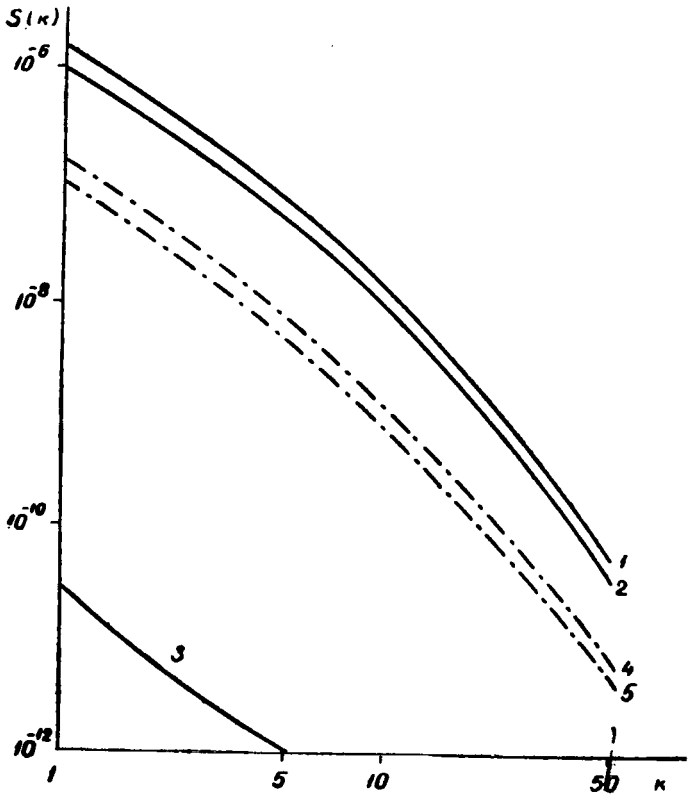

Figure 157. Spectral Densities of Brightness (in $wt \cdot cm^{-2} \cdot ster^{-1})^2$) of Thick Cumulus Clouds Versus Number of Harmonics k: Solid lines, $\Delta\lambda$ = 8.5-12.5 μ, Dot-and-Dash Lines, $\Delta\lambda$ = 10.2--11.5 μ; 1, 4, Daytime; 2, 5, Nighttime; 3, Equipment Noise.

The nature of the variability of brightness is also illustrated by Figure 155, from which it is to be seen that the small heterogeneities of brightness

in the case of daytime clouds are somewhat more pronounced than for the nighttime clouds. Should the fact ascertained in the foregoing of more extensive fluctuation of radiation on the illuminated sides be ascribed to reflection of solar radiation by the unevennesses of the sides of the clouds? Theoretical estimates have been made that show that, owing to reflection of solar radiation, brightness fluctuations in the spectral range of 8-12 μ may at the maximum reach values corresponding to variations in the radiation temperature of up to 0.1°. Thus the more intensive fluctuations on the illuminated side of clouds are apparently caused chiefly by the temperature heterogeneities of the latter. These heterogeneities are probably due to absorption of the radiant energy of the Sun at all wavelengths and to more vigorous turbulent mixing on the illuminated sides of the clouds. /265

The results obtained in investigation of the spatial structure of cloud brightness may be utilized, for example, to determine the form of clouds both in daytime and at night. Determination of the form of clouds by equipment methods with sufficient dependability can be achieved by measurement of the intrinsic radiation of clouds in the water vapor window.

REFERENCES

1. "Program for the Minsk-2 Computer," No. 3, *Institut Kibernetikh AN EstSSSR Publishers*, Tallin, 1966. /266
2. Tatarskiy, V. I., *Rasprostraneniye Voln v Turbulentnoy Atmosfere* [Propagation of Waves in a Turbulent Atmosphere], "Nauka" Press, Moscow, 1967.
3. Jenkins, G. M., "General Considerations in the Analysis of Spectra," *Technometrics*, Vol. 3, No. 2, 1961.
4. Homan, C. T. and J. W. Tierney, "Determination of Dynamic Characteristics of Processes in the Presence of Random Disturbances," *Chemical Engineering Sci.*, Vol. 12, No. 3, 1960.
5. Livshits, N. A. and V. N. Pugachev, *Veroyatnostnyy Analiz Sistem Avtomaticheskogo Upravleniya* [Probability Analysis of Automatic Control Systems], "Sovetskoye Radio" Press, Moscow, 1963.
6. Bagrov, N. A., "Analytical Representation of a Sequence of Meteorological Fields by Means of Natural Orthogonal Components," *Tr. TsIP*, No. 74, 1959.
7. Obukhov, A. M., "Statistically Orthogonal Expansions of Empirical Functions," *Izv. AN SSSR*, No. 3, 1960.
8. Rukhovets, L. B., "Optimum Representation of Vertical Distributions of Certain Meteorological Elements," *Izv. AN SSSR*, No. 4, 1963.
9. Koprova, L. I. and M. S. Malkevich, "Empirical Orthogonal Functions for Optimum Parametrization of Temperature and Humidity Profiles," *Izv. AN SSSR*, Vol. 1, No. 1, 1965.
10. Malkevich, M. S., "The Spatial Structure of the Long Wave Radiation Field of the Earth," *Izv. AN SSSR*, Vol. 2, No. 4, 1966.
11. Malkevich, M. S. and V. I. Tatarskiy, "Determination of the Vertical Temperature and Humidity Profiles of the Earth's Atmosphere on the Basis of Measurements of the Earth's Radiation from Satellites," in: *Issledovaniya Kosmicheskogo Prostranstva* [Space Research], "Nauka" Press, Moscow, 1965.
12. Boldyrev, V. G., L. I. Koprova and M. S. Malkevich, "Allowance for Variations in the Vertical Temperature and Humidity Profiles in Determination of the Temperature of the Underlying Surface on the Basis of Escaping Radiation," *Izv. AN SSSR*, Vol. 2, No. 7, 1966.
13. Istomina, L. G., M. S. Malkevich and V. I. Syachinov, "The Spatial Structure of the Brightness Field of the Earth on the Basis of Measurements from the 'Kosmos-149' Satellite," *Izv. AN SSSR*, Vol. 6, No. 5, 1970. /267
14. Gorchakova, I. A., M. S. Malkevich and V. F. Turchin, "Determination of the Vertical Humidity Profile of the Atmosphere on the Basis of Measurements of the Intrinsic Radiation of the Earth," *Izv. AN SSSR*, Vol. 6, No. 6, 1970.
15. Rukhovets, L. V., "Statistically Optimum Representations of the Vertical Distributions of Meteorological Elements in the Troposphere and Lower Stratosphere," *Tr. GGO*, No. 165, 1964.
16. Holmstroem, I., "On a Method for Parametric Representation of the State of the Atmosphere," *Tellus*, Vol. 15, No. 2, 1963.

17. Mullamaa, Yu. A., M. Sulev and V. O. Pyldmaa, "The Statistical Characteristics of the Radiation Field of a Cloudy Sky," in: *Radiatsiya i Oblachnost', IFA AN EstSSR*, Tartu, 1969.
18. Vilenkin, S. Ya., *Statisticheskiye Metody Issledovaniya Sistem Avtomaticheskogo Regulirovaniya* [Statistical Methods of Investigating Automatic Control Systems], "Sovetskoye Radio" Press, Moscow, 1967.
19. Lamin, D. Zh. and G. A. Panovskiy, *Struktura Atmosfernoy Turbulentnosti* [The Structure of Atmospheric Turbulence], "Mir" Press, Moscow, 1966.
20. Perov, V. P., *Statisticheskiy Sintez Impulsnykh Sistem* [Statistical Synthesis of Pulse Systems], "Sovetskoye Radio" Press, Moscow, 1959.
21. Tsypkin, Ya. Z., *Teoriya Lineynykh Impul'snykh Sistem* [The Theory of Linear Pulse Systems], *Izd. Fiz.-Mat. Lit.*, Moscow, 1963.
22. Levin, B. R., *Teoreticheskiye Osnovy Statisticheskoy Radiotekhniki* [The Theoretical Principles of Statistical Radio Engineering], Vol. 1, "Sovetskoye Radio" Press, Moscow, 1969.
23. Levin, B. R., *Teoreticheskiye Osnovy Statisticheskoy Radiotekhniki* [The Theoretical Principles of Statistical Radio Engineering], Vol. 2, "Sovetskoye Radio" Press, Moscow, 1968.
24. Rytov, S. M., *Vvedeniye v Statisticheskuyu Radiofiziku* [Introduction to Statistical Radio Physics], "Nauka" Press, Moscow, 1966.
25. Sveshnikov, A. A., *Prikladnyye Metody Teorii Sluchaynykh Funktsiy* [Applied Methods of the Theory of Random Functions], "Nauka" Press, Moscow, 1968.
26. O'Neyl, E., *Vvedeniye v Statisticheskuyu Optiku* [Introduction to Statistical Optics], "Mir" Press, Moscow, 1966.
27. Monin, A. S. and A. M. Yaglom, *Statisticheskaya Gidromekhanika* [Statistical Hydromechanics], Part II, "Nauka" Press, Moscow, 1967.
28. Tikhonov, V. I., *Statisticheskaya Radiotekhnika* [Statistical Radio Engineering], "Sovetskoye Radio" Press, Moscow, 1966.
29. Tikhonov, V. I., *Vybrosy Sluchaynykh Protsessov* [Excursions of Random Processes], "Nauka" Press, Moscow, 1970.
30. Kramer, G. and M. Lidbetter, *Statsionarnyye Sluchaynyye Protsessy (Svoystva Vybrosnykh Funktsiy i Ikh Prilozheniya)* [Stationary Random Processes (Properties of Excursion Functions and Their Applications)], "Mir" Press, Moscow, 1969.
31. Mullamaa, Yu. A., "Coverage of the Sky by Cumulus Clouds," in: *Radiatsiya i Oblachnost', IFA AN EstSSR Press*, Tartu, 1969.
32. Rozenberg, G. V., G. K. Ilvich, S. A. Makarevich and Yu. R. Mullamaa, "Cloud Brightness (Results of Comprehensive Study)," *Izv. AN SSSR*, Vol. 6, No. 5, /268 1970.
33. Mullamaa, Yu. R., "The Transmission of Radiation by Stratified Clouds as a Function of the Statistical Characteristics of the Cloud Structure," in: *Teploobmen v Atmosfere*, "Nauka" Press, Moscow, 1972.
34. Mullamaa, Yu. R., V. K. Pyldmaa and M. A. Sulev, "The Structure of the Cumulus Cloud Field," in: *Teploobmen v Atmosfere*, "Nauka" Press, 1972.
35. Avaste, O. A., "Increase in Cloudiness at the Horizon in the Case of Ground Observations," in: *Teploobmen v Atmosfere, IFA AN EstSSR*, Tartu, 1969.

36. Avaste, O. A., "A Method of Calculating Sky Coverage by the Lateral Portions of Cloud Elements," in: *Teploobmen v Atmosfere, IFA AN EstSSR*, Tartu, 1969.
37. Likhterov, Ya. M. and L. S. Gurin, "The Probability of Coverage of a System Segment by Random Segments," *Izv. AN SSSR*, No. 4, 1966.
38. Avaste, O. A., "Transfer of Shortwave Radiation in the Case of Broken Clouds," *Tezisy Dokladov VIII Nauchnogo Soveshchaniya Po Optike Atmosfery i Aktinometrii* [Theses of the Proceedings of the VIII Scientific Conference on Atmospheric Optics and Actinometry], Tomsk, June, 1970.
39. Avaste, O. and G. Vainikko, "Calculation of the Mean Values of the Intensities and Fluxes in Broken Clouds," *IAMAP/IAGA International Union of Geodesy and Geophysics, XV General Assembly*, Moscow, 1971.
40. Bibikova, T. N., "An Experiment in Observation of Clouds by the Photographic Method Using a Spherical Mirror," *Vestnik MGU*, No. 2, 1960.
41. Yudich, M. Z., *Skhemy Tranzistornoy Elektroniki* [Transistor Electronic Circuits], "Energiya" Press, Moscow-Leningrad, 1966.
42. Davydov, V. S., V. N. Osipov and G. A. Fratini, "The Effect of Unmodulated Radiation on the Parameters of Pb:Te Photoresistors," *Optiko-Mekhanicheskaya Promyshlennost'*, No. 12, 1963.
43. Koshchavtsev, N. F., A. A. Semenov and G. K. Kirchevskaya, "The Exposure Characteristics of Certain Semiconductor Detectors," *Svetotekhnika*, No. 5, 1968.
44. Alekseev, A. M., "The Effect of Unmodulated Exposure on the Sensitivity of Pb:Te Photoresistors," *Optiko-Mekhanicheskaya Promyshlennost'*, No. 11, 1968.
45. Astaf'ev, A. I. and G. K. Kholopov, "The Voltage Sensitivity of Sulfur-Lead Photoresistors as a Function of Background Exposure," *Optiko-Mekhanicheskaya Promyshlennost'*, No. 10, 1969.
46. Allenov, M. I. and B. M. Rogov, "The Effect of Unmodulated Radiation on the Parameters of a Ge:Hg Photoresistor," *Optiko-Mekhanicheskaya Promyshlennost'*, No. 1, 1971.
47. Kruz, P., L. Makgloumin and R. Makkvistan, *Osnovy Infrakrasnoy Tekhniki* [The Principles of Infrared Engineering], Voyennoye Izd-vo, Moscow, 1964.
48. Lennard, J. K., *Proceedings of the National Electronics Conference*, Vol. 18, /269 1962.
49. Gorodetskiy, A. K. and A. M. Kasatkin, "A Radiometer for Determination of the Temperature of the Earth's Surface and Clouds. Actinometry and Atmospheric Optics," *Tr. VI Mezhvedomstvennogo Soveshchaniya Po Aktinometrii i Optike Atmosfery* [Proceedings of the Sixth Interdepartmental Conference on Actinometry and Atmospheric Optics], Tartu, June, 1966. "Valgus" Press, Tallin, 1968.
50. Angerer, E., *Tekhnika Fizicheskogo Eksperimenta* [The Technique of Physical Experimentation], *Izdat. Fiz.-Mat. Lit.*, Moscow, 1962.
51. Kholopov, G. K. and V. S. Strunov, "Calculation of the Radiation Coefficient of Absolute Black Body Models," *Optiko-Mekhanicheskaya Promyshlennost'*, No. 7, 1963.
52. Bramson, M. A., *Spravochnyye Tablitsy Po Infrakrasnomy Izlucheniyu Nagretykh Tel.* [Reference Tables on the Infrared Radiation of Heated Bodies], "Nauka" Press, Moscow, 1964.

53. Allenov, M. I. and Yu. N. Shuba, "A Radiometer-Pyrometer for Measurement of the Microstructure of Cloud Radiation," *Izv. AN SSSR*, Vol. 8, No. 6, 1972.
54. Vladimirov, V. I. and S. S. Shchegolev, "A Method of Noncontact Measurement of the Temperature of Slightly Heated Bodies," *Promyshlennyye Obraztsy, Tovarnyye Znaki*, No. 11, 1968.
55. Kelton, I., "Infrared Target and Background Radiometric Measurements — Concepts Units and Techniques," *Infrared Physics*, Vol. 3, No. 3, 1963.
56. Aksyutov, L. N., V. I. Tevyashov, G. K. Kholopov, Ye. K. Sharabrin and Yu. A. Shuba, "Methods of Radiometer Graduation," *Optiko-Mekhanicheskaya Promyshlennost'*, No. 3, 1969.
57. Aksyutov, L. N., D. K. Selezneva, V. I. Tevyashov, G. K. Khelopov and Yu. A. Shuba, "The Graduation of Radiometers in Absolute Radiation Values," *Optiko-Mekhanicheskaya Promyshlennost'*, No. 11, 1968.
58. Allenov, M. I., Yu. A. Shuba and V. I. Sagadeyev, "Study of the Microstructure of Clouds in the 8-14 μ Region of the Spectrum," *X Vsesoyuznaya Konferentsiya Po Aktual'nym Voprosam Isparenіya, Goreniya i Gazovoy Dinamiki Dispersnykh Sistem. Materialy Konferentsii* [Tenth All-Union Conference on Current Questions of Evaporation, Combustion, and Gas Dynamics of Disperse Systems. Conference Materials], Odessa, 1970.
59. Allenov, M. I., V. D. Bokiy and Yu. A. Shuba, "The Characteristics of Radiation of Clouds in the 8-14 μ Region of the Spectrum," *Tr. Vsesoyuznogo Soveshchaniya po Svetorasseyaniyu* [Proceedings of the All-Union Conference on Light Scattering], Alma-Ata, 1969.
60. Dreyer, A. A., "Semiautomatic Reading of Graphic Information," *Meteorologiya i Gidrologiya*, No. 5, 1968.
61. Mullamaa, Yu. A. P., Wind Waves and the Effectively Reflecting Area of the Surface of the Sea," *Izv. AN SSSR*, Vol. 4, No. 7, 1968.
62. "Symposium on Wind Waves," (edited by Yu. M. Krylov), "IL" Press, Moscow, 1962.
63. Belyayev, Yu. I., "The Number of Intersections of a Level by a Random Gaussian Process," *Teoriya Veroyatnostey i Yeye Primeneniye*, Vol. 11, No. 1, 1966.
64. Niylisk Khel'gi, Yu. Mullamaa and M. Sulev, "Cloud Coverage of the Sky," in: *Radiatsiya v Atmosfere* [Radiation in the Atmosphere], *IFA AN EstSSR*, Tartu, 1969. /270
65. Stratonovich, R. L., *Uslovnyye Markovskiye Protsessy i Ikh Primeneniye k Teorii Optimal'nogo Upravleniya* [Conventional Markovian Process and Their Application to the Theory of Optimum Control], Izd. MGU, 1966.
66. Stratonovich, R. L., *Izbrannyye Voprosy Teorii Flyuktuatsiy v Radiotekhnike* [Problems of the Theory of Fluctuations in Radio], "Sovetskoye Radio" Press, Moscow, 1961.
67. Vul'fson, N. I., "Convection Movements in Cumulus Clouds," *DAN SSSR*, Vol. 97, No. 1, 1954.
68. Vul'fson, N. I., "Compensatory Downdrafts Due to the Development of Cumulus Clous," *Izv. AN SSSR*, No. 1, 1957.
69. Vul'fson, N. I., "A Method of Studying Compensatory Downdrafts in the Vicinity of Developing Cumulus Clouds," *DAN SSSR*, Vol. 112, No. 4, 1957.
70. Warner, J., "The Microstructure of Cumulus Clouds. Part III. The Nature of the Updraft," *J. Atm. Sciences*, Vol. 27, No. 4, 1970.

71. Vul'fson, N. I., *Issledovaniye Konvektivnykh Dvizheniy v Svobodnoy Atmosfere* [Study of Convective Movements in the Free Atmosphere], "Nauka" Press, Moscow, 1961.
72. "Symposium on Dynamics of Cumulus Clouds," "Mir" Press, Moscow, 1964.
73. Timanovskaya, R. G. and Ye. M. Feygel'son, "Solar Radiation Fluxes at the Surface of the Earth in the Case of Cumulus Clouds," *Meteorologiya i Gidrologiya*, No. 11, 1970.
74. Yanishevskiy, Yu. D., *Aktinometricheskiye Pribory i Metody Nablyudeniya* [Actinometric Instruments and Observation Methods], "Gidrometeoizdat", Leningrad, 1957.
75. Kallis, A., "Scattered Radiation Versus Cloudiness (Based on the Data of the Tartu Actinometric Station)," *Diplomnaya Rabota, TGU* [Diploma Project, TGU], 1966 (in Estonian).
76. Kondrat'ev, K. Ya., *Aktinometriya* [Actinometry], "Gidrometeoizdat", Leningrad, 1965.
77. Pyldmaa, V. K. and R. G. Timanovskaya, "Certain Statistical Characteristics of Total Radiation Under Cloud Conditions," *Izv. AN SSSR*, Vol. 5, No. 5, 1969.
78. Feygel'son, Ye. M. and M. S. Malkevich, et al., "Calculation of the Brightness of Light in the Atmosphere in the Case of Anisotropic Scattering," *Tr. IFA AN SSSR*, No. 1, 1958.
79. Coulson, K. L., J. V. Dave and Z. Sekera, *Tables Related to Radiation Emerging from a Planetary Atmosphere with Rayleigh Scattering*, Univ. of California Press, Berkley, Los Angeles, 1960.
80. Ivanov, A. P., *Optika Rasseivayushchikh Sred.* [The Optics of Scattering Media], "Nauka i Tekhnika", Minsk, 1969.
81. Feygel'son, Ye. M., *Radiatsionnyye Protsessy v Sloistoobraznykh Oblakakh* [Radiation Processes in Stratified Clouds], "Nauka" Press, 1964.
82. Feygel'son, Ye. M., *Luchistyy Teploobmen i Oblaka* [Radiative Heat Transfer and Clouds], "Gidrometeoizdat", Leningrad, 1970.
83. Pyldmaa, V., "The Distribution of Scattered Radiation Over the Sky," *Issledovaniya Po Fizike Atmosfery*, No. 4, *IFA AN EstSSR*, Tartu, 1963.
84. Malkevich, M. S., A. S. Monin and G. V. Rozenberg, "The Spatial Structure of /271 the Radiation Field as a Source of Meteorological Information," *Izv. AN SSSR*, No. 3, 1964.
85. Rozenberg, G. V., "The Urgent Tasks of Atmospheric Optics," in: *Aktinometriya i Optika Atmosfery* [Actinometry and Atmospheric Optics], "Nauka" Press, Moscow, 1964.
86. Giovanelli, R. G., *Progress in Optics*, Vol. 4, North Holland, 1964.
87. Poss, Yu. K. and T. A. Nil'son, "A Mathematical Model of the Radiation Regime of the Vegetation Cover," in: *Aktinometriya i Optika Atmosfery* [Actinometry and Atmospheric Optics], "Valgus" Press, Tallin, 1968.
88. Drobyshevich, V. I., "The Relationship of the Statistical Characteristics of Cloud Fields and Departing Shortwave Radiation," in: *Aktinometriya i Optika Atmosfery* [Actinometry and Atmospheric Optics], "Valgus" Press, Tallin, 1968.
89. Keyevallik, S. Kh. and A. Kh. Laysk, "The Propagation of Radiation in a Scattering Medium Accompanied by Uneven Absorption," *Izv. AN SSSR*, Vol. 5, No. 12, 1969.

90. Keyevallik, S. Kh., "The Propagation of Radiation in Extensively Absorbing Heterogeneous Turbid Layers," *Izv. AN SSSR*, Vol. 6, No. 6, 1970.
91. Keyevallik, S. Kh., "The Propagation of Radiation in One Possible Model of a Scattering Medium Accompanied by Uneven Absorption," *YeNSV TA Toimetised. Fueuesika Matematika*, No. 2, 1970.
92. Keyevallik, S. Kh., "The Propagation of Radiation in a Turbid Medium Accompanied by Uneven Scattering," *Izv. AN SSSR*, Vol. 6, No. 10, 1970.
93. Sobolev, V. V., *Perenos Luchistoy Energii v Atmosferakh Zveyed i Planet* [The Transfer of Radiant Energy in the Atmospheres of Stars and Planets], Gosizdat Tekhn.-Teor. Lit., Moscow, 1956.
94. Monin, A. S., "A Model of Wind on Slopes," *Tr. TsIP*, No. 8, p. 35, 1948.
95. Kastrov, V. G., "The Reflection of Radiation by an Urban Area," *Meteorologiya i Gidrologiya*, No. 4, 1940.
96. Kaempfert, W., "On the Question of Solar Irradiation of Narrow Streets," *Rundschau*, Vol. 2, No. 7/8, 1949.
97. Kaempfert W., "A Phase Diagram of Solar Irradiation," *Meteorol. Rundschau*, Vol. 4, No. 7/8, 1951.
98. Mullamaa, Yu. A. P., *Atlas Opticheskikh Kharakteristik Vzvolnovannoy Poverkhnosti Morya* [Atlas of the Optical Characteristics of the Agitated Surface of the Sea], *IFA AN EstSSR*, Tartu, 1964.
99. Poss, Yu. and T. Nil'son, "Calculation of the Photosynthetically Active Radiation in the Vegetation Cover," in: *Rezhim Solnechnoy Radiatsii v Rastitel'nom Pokrove* [Solar Radiation Conditions in the Vegetation Cover], *IFA AN EstSSR*,Tartu, 1968.
100. Niylisk, Kh. Yu., "Calculations of the Thermal Radiation of the Atmosphere Under Partial Cloudiness Conditions," *Izv. AN SSSR*, Vol. 4, No. 4, 1968.
101. Niylisk, Kh. Yu., "The Characteristics of the Cloud Cover in Problems Relating to Radiation Energetics in the Earth's Atmosphere," *Izv. AN SSSR*, Vol. 8, No. 3, 1972.
102. Niylisk, Kh. Yu., "Calculation of the Values of the Back Radiation Fluxes of the Atmosphere Averaged Over Large Territories," *Izv. AN SSSR*, Vol. 4, No. 5, 1968.
103. Niylisk, Kh. Yu., "Calculations of the Thermal Radiation of the Atmosphere in the Case of Broken Clouds," in: *Teploobmen v Atmosfere* [Heat Exchange in the Atmosphere], "Nauka" Press, No. 9, 1972. /272
104. Plank, V. G., "The Size Distribution of Cumulus Clouds in Representative Florida Populations," *Journ. Meteorol.*, Vol. 8, No. 1, 1969.
105. Niylisk, Kh. Yu., "Certain Characteristics of Clouds," in: *Radiatsiya i Oblachnost'* [Radiation and Clouds], *IFA AN EstSSR*, Tartu, 1969.
106. Kondrat'yev, K. Ya., *Luchistyy Teploobmen v Atmosfere* [Radiant Heat Exchange in the Atmosphere], "Gidrometeoizdat", Leningrad, 1956.
107. Niylisk, Kh. Yu., "On the Question of the Thermal Radiation of the Atmosphere," *Tr. Vsesoyuznogo Nauchnogo Meteorologicheskogo Soveshchaniya* [Proceedings of the All-Union Scientific Meteorology Conference], 1961, Vol. 6, Gidrometeoizdat Press, Leningrad, 1963.
108. Kondrat'yev, K. Ya., Kh. Yu. Niylisk and R. Yu. Noorma, "The Spectral Distribution of the Thermal Radiation of the Atmosphere Under Stratified Cloud Conditions," *Tr. GGO*, No. 275, 1971.
109. Borovikov, A. M., I. I. Gayvoronskiy, Ye. G. Zak, V. V. Kostarev, I. P. Mazin, V. Ye. Minervin, A. Kh. Khrgian and S. M. Shmeter, *Fizika Oblakov* [The Physics of Clouds], "Gidrometeoizdat", Leningrad, 1961.

110. Malkevich, M. S., I. P. Malkov, L. A. Pakhomova, G. V. Rozenberg and G. P. Faraponova, "Determination of the Statistical Characteristics of Radiation Fields Above Clouds," *Kosmicheskiye Issledovaniya*, Vol. 2, No. 2, 1964.
111. Malkevich, M. S., "Methods of Interpreting Radiation Measurements from Satellites. Actinometry and Atmospheric Optics," *Tr. VI Mezhvedomstvennogo Soveshchaniya Po Aktinometrii i Optike Atmosfery* [Proceedings of the Sixth Interdepartmental Conference on Actinometry and Atmospheric Optics], June 1966, Tartu, "Valgus" Press, Tallin, 1968.
112. Shvets, M. Ye., "The Need for Radiation Data in Modern Hydrodynamic Forecasting. Actinometry and Atmospheric Optics," *Tr. VI Mezhvedomstvennogo Soveshchaniya Po Aktinometrii i Optike Atmosfery* [Proceedings of the Sixth Interdepartmental Conference on Actinometry and Atmospheric Optics], June, 1966, Tartu, "Valgus" Press, Tallin, 1968.
113. Feygel'son, Ye. M., "The Contemporary Status of Data on Radiation Influx and Methods of Allowing for Radiation in Forecasting. Actinometry and Atmospheric Optics," *Tr. VI Mezhvedomstvennogo Soveshchaniya Po Aktinometrii i Optike Atmosfery* [Proceedings of the Sixth Interdepartmental Conference on Actinometry and Atmospheric Optics], June 1966, Tartu, "Valgus" Press, Tallin, 1968.
114. Istomina, L. G., "Determination of the Statistical Characteristics of the Spatial Structure of Cloud Fields On the Basis of Aerial Photographs," *Izv. AN SSSR*, Vol. 2, No. 3, 1966.
115. Gorodetskiy, A. K. and G. F. Filippov, "Ground Measurements of the Radiation of the Atmosphere and Underlying Surface in the 8-12 μ Region of the Spectrum," *Izv. AN SSSR*, Vol. 6, No. 2, 1968.
116. Kasatkina, O. I., L. B. Krasil'shchikov, I. V. Morosova and L. B. Pudneva, "Experimental Studies of Cloud Radiation in the 8-12 μ Region," *Tezisy Doklada VIII Nauchnogo-Soveshchaniya Po Optike Atmosfery i Aktinometrii* [Theses of the Report of the Eighth Scientific Conference on Atmospheric Optics and Actinometry], Tomsk, June, 1970.
117. Allenov, M. I. and Yu. A. Shuba, "Investigation of the Structure of Cloud Radiation in the 8-13 μ Range by Means of a High Speed Radiometer-Pyrometer," *Izv. AN SSSR*, Vol. 7, No. 9, 1971. /273
118. *Atlas Oblakov* [Cloud Atlas], "Gidrometeoizdat", Leningrad, 1957.
119. Grishchenko, Z. I., "The Relationship of Radiation Conditions to Clouds. Actinometry, Atmospheric Optics, and Ozonometry," *Tr. GGO*, No. 223, 1968.
120. Niylisk, Kh. Yu. and R. Noorma, "The Spectral Distribution of Intensity and Fluxes of Thermal Radiation in the Free Atmosphere," *Issledovaniya Po Fizike Atmosfery*, No. 8, *IFA AN EstSSR*, Tartu, 1967.
121. Ashcheulov, S. V., K. Ya. Kondrat'yev and D. B. Styro, "Investigation of the Emission Spectra of Atmospheric Back Radiation. Actinometry and Atmospheric Optics," *Tr. VI Mezhvedomstvennogo Soveshchaniya Po Aktinometrii i Optike Atmosfery* [Proceedings of the Sixth Interdepartmental Conference on Actinometry and Atmospheric Optics], June, 1966, Tartu, "Valgus" Press, Tallin, 1968.
122. Novosel'tsev, Ye. P., "The Emission Power of Clouds of Different Tiers. Actinometry and Atmospheric Optics," *Tr. VI Mezhvedomstvennogo Soveshchaniya Po Aktinometrii i Optike Atmosfery* [Proceedings of the Sixth Interdepartmental Conference on Actinometry and Atmospheric Optics], June, 1966, Tartu, "Valgus" Press, Tallin, 1968.

Translated for the National Aeronautics and Space Administration under Contract No. NASw-2485 by Techtran Corporation, P.O. Box 729, Glen Burnie, Maryland, 21061; translator, William L. Hutcheson.

*U.S. GOVERNMENT PRINTING OFFICE: 1975 - 635-275/35

"The aeronautical and space activities of the United States shall be conducted so as to contribute . . . to the expansion of human knowledge of phenomena in the atmosphere and space. The Administration shall provide for the widest practicable and appropriate dissemination of information concerning its activities and the results thereof."

—NATIONAL AERONAUTICS AND SPACE ACT OF 1958

NASA SCIENTIFIC AND TECHNICAL PUBLICATIONS

TECHNICAL REPORTS: Scientific and technical information considered important, complete, and a lasting contribution to existing knowledge.

TECHNICAL NOTES: Information less broad in scope but nevertheless of importance as a contribution to existing knowledge.

TECHNICAL MEMORANDUMS: Information receiving limited distribution because of preliminary data, security classification, or other reasons. Also includes conference proceedings with either limited or unlimited distribution.

CONTRACTOR REPORTS: Scientific and technical information generated under a NASA contract or grant and considered an important contribution to existing knowledge.

TECHNICAL TRANSLATIONS: Information published in a foreign language considered to merit NASA distribution in English.

SPECIAL PUBLICATIONS: Information derived from or of value to NASA activities. Publications include final reports of major projects, monographs, data compilations, handbooks, sourcebooks, and special bibliographies.

TECHNOLOGY UTILIZATION PUBLICATIONS: Information on technology used by NASA that may be of particular interest in commercial and other non-aerospace applications. Publications include Tech Briefs, Technology Utilization Reports and Technology Surveys.

Details on the availability of these publications may be obtained from:

SCIENTIFIC AND TECHNICAL INFORMATION OFFICE

NATIONAL AERONAUTICS AND SPACE ADMINISTRATION

Washington, D.C. 20546